EJA

European Journal of Anatomy

Volume 27 - Number 1 January 2023

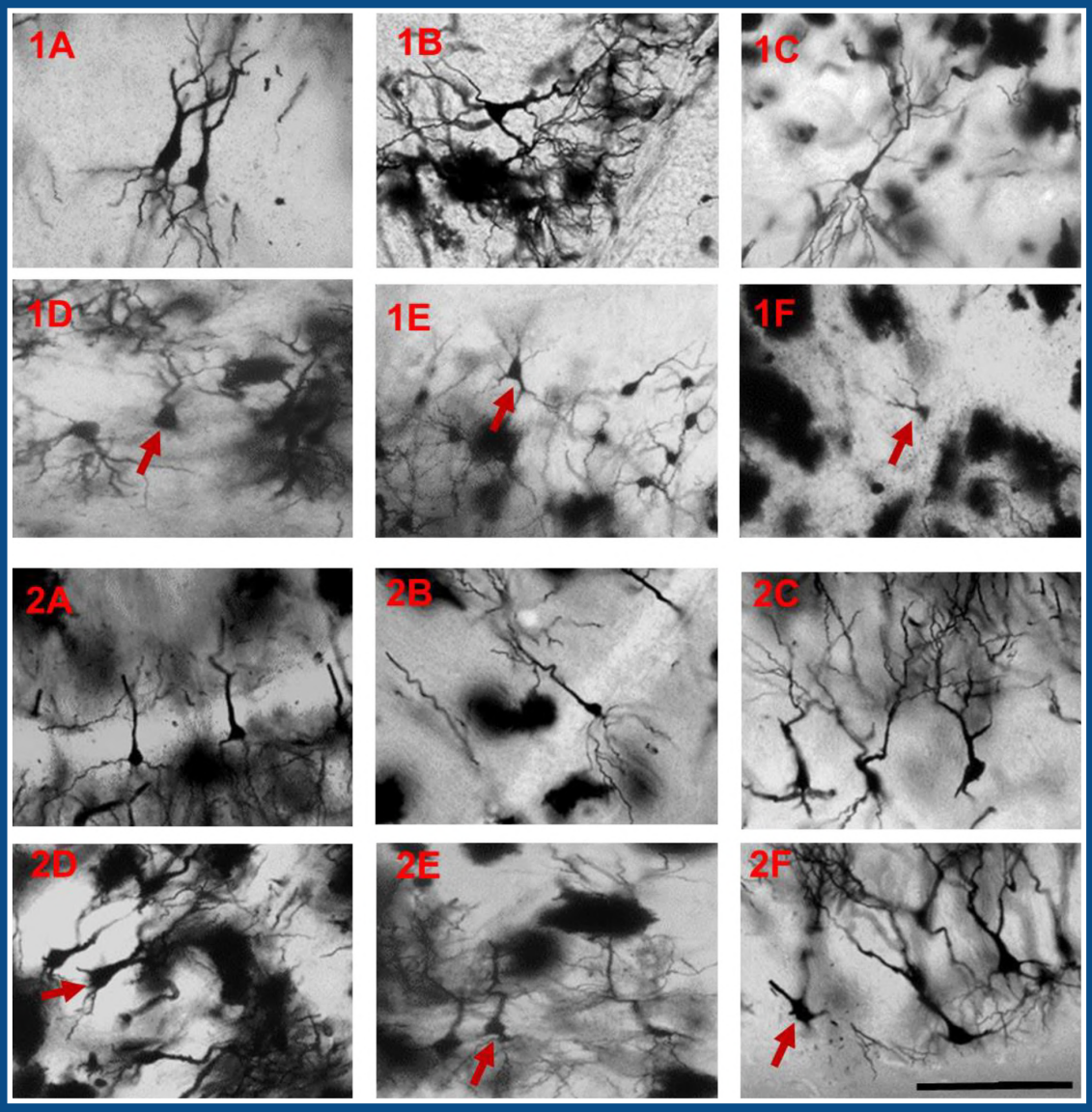

Indexed in:

CLARIVATE
- JCR:2020
- Q4 (21/23)
- I.F. J.C.I.: 0.19

DIALNET

EMBASE / Excerpta Medica

SCOPUS
- SJCR: 2020
- Q4 (31/39)
- I.F.: 0.162

Emerging Sources Citation Index

LATINDEX. Catálogo v1.0 (2002-2017)

Official Journal of the Spanish Society of Anatomy

www.eurjanat.com

EJA
European Journal of Anatomy

Volume 27 - Number 1 January 2023

Histomorphological and histomorphometric changes in the testes of male Wistar rats following prepubertal exposure to caffeine

David O. Adeyemi[1], Paul O. Awoniran[2], Ogheneyoma M. Orumana[1], Kehinde A. Jolayemi[2]

[1] Department of Anatomy and Cell Biology, Faculty of Basic Medical Sciences, College of Health Science, Obafemi Awolowo University, Ile-Ife, Nigeria

[2] Department of Human Anatomy, Faculty of Basic Medical Sciences, Redeemer's University, Ede, Osun State, Nigeria

SUMMARY

This experiment was designed to study the effects of caffeine on the histomorphology of the testes of prepubertal male Wistar rats. Prepubertal Wistar rats (25-28 days old), weighing between 50-60 g were randomly divided into three treatment groups (B, C and D) and control (A) of ten rats each. Group A rats received distilled water while Groups B, C, and D rats were respectively given daily dose of 50 mg/kg, 100 mg/kg, and 200 mg/kg of caffeine dissolved in distilled water for 14 days by gavage. Five rats from each group were sacrificed 24 hours after the last caffeine administration while the remaining rats were monitored for another three weeks for them to attain sexual maturity. The rats were sacrificed under diethyl ether anesthesia and the testes were fixed by immersion in Bouin's fluid. The tissues were processed for histomorphological and histomorphometric assessment. Data obtained were analyzed using one way ANOVA followed by Dunnett post hoc test for comparison with control. Alpha level was set at 0.05. Results showed that treatment with caffeine caused a significant decrease in testicular weight and a marked cellular degeneration and depletion of germ cells in the testes of rats in group D. The height of the germinal epithelium was significantly reduced when compared with control. This study concluded that prepubertal exposure of Wistar rats to caffeine reduced testicular growth and deleteriously alters testicular morphology.

Key words: Caffeine – Testes – Germinal epithelium – Histomorphology – Histomorphometry – Prepubertal Wistar rats

INTRODUCTION

Caffeine is a pharmacologically active component of many foods, beverages, dietary supplements and drugs (Wikoff et al., 2017). Being the most widely consumed psychoactive drug in the world, its consumption remains largely unregulated and legal in nearly all parts of the world unlike most other psychoactive substances. Consumption of high caffeine-containing energy drinks by the adolescent population has increased markedly in recent years due to the risk-taking behavior of adolescents and their lack of education on the negative effects of caffeine (Reissig et al.,

Corresponding author:
Dr. David Olawale Adeyemi (PhD). Department of Anatomy and Cell Biology, Faculty of Basic Medical Sciences, College of Health Science, Obafemi Awolowo University, Ile-Ife, Nigeria. Phone: +2348028101028. E-mail: david.adeyemi@oauife.edu.ng

Submitted: July 16, 2022. **Accepted:** September 3, 2022

https://doi.org/10.52083/KRMN9443

2009; Seifert et al., 2011; Dorostghoal et al., 2012). There is growing concern about a decrease in male reproductive health, because a number of laboratory animal studies and human cases have pointed to toxic effects of caffeine on the male reproductive system (Weinberger et al., 1978; Pollard et al., 1990; Ramlau-Hansen et al., 2008; Dorostghoal et al., 2012; Tinwell et al., 2013). For instance, several studies on effects of caffeine on testicular morphology and function in men and adult animals have been documented (Weinberger et al., 1978; Nawrot et al., 2003; Park et al., 2015; Bae et al., 2017). In addition, a number of studies suggest that prenatal and lactational caffeine exposure impairs male gonadal development and thus later gonadal function (Ramlau-Hansen et al., 2008; Dorostghoal et al., 2012). Since the adolescent gonad is not fully mature either anatomically or histochemically (August, 1972), it would not be surprising if chronic exposure to caffeine during this vulnerable period were to interfere with normal gonad maturation. Although detrimental effects of caffeine on the development of the reproductive system during prenatal period have been widely demonstrated, data on the effect on the reproductive system during the prepubertal period are relatively sparse and conflicting. Considering that puberty is a period of rapid development of reproductive capacity, its vulnerability to insults seems to be greater than that in adults (Sharpe, 1988). This study therefore aimed to investigate the effects of caffeine on morphology, morphometry as well as the parameters of growth and maturation of the testis in prepubertal male rats throughout most of their rapid growth period.

MATERIALS AND METHODS

Animals and Treatment

Prepubertal male (4 weeks) Wistar rats (50 - 65 g) were obtained from the Animal House of the College of Health Sciences, Obafemi Awolowo University, Ile–Ife, Nigeria. They were maintained under the condition of natural light and dark cycles, temperature and humidity. Standard laboratory rat chow (Ace feed, Osogbo) and clean water were provided daily to the rats throughout the period of experiment. Ethical clearance was obtained from Health Research and Ethics Committee (HREC) of Institute of Public Health, Obafemi Awolowo University and the guidelines for care and use of animals were strictly followed.

Experimental Design

The rats were randomly assigned into four groups of ten rats each (n = 10). The four groups are groups A, B, C and D. Rats in Group A were the normal control and they received distilled water orally for 14 days while Groups B, C, and D received 50 mg/kg, 100 mg/kg and 200 mg/kg graded doses of caffeine (Sigma-Aldrich, USA) respectively, administered orally for a period of 14 days. Twenty-four hours after the last administration, five rats from each group were anaesthetized under diethyl ether and their testes were excised. The remaining rats were monitored for another three weeks to attain sexual maturity after which they were also sacrificed.

Organ weight

At the end of the experiment, testes from each rat were excised, trimmed free of fats and weighed on a top loader digital weighing balance (Camry). Relative testicular weight was defined as percentage ratio of testes weight to final body weight. The formula below was used to calculate the organ weight.

$$\text{Relative organ weight} = \frac{\text{organ weight}}{\text{final body weight}} \times 100\%$$

Histological procedure

The testes were fixed in fresh Bouin's fluid and tissue processing was done via paraffin wax embedding method of Drury and Wallington (1980). The embedded tissues were sectioned on a rotary microtome (Leica RM 2125 RTS) and 5 µm thick sections were obtained and stained with Hematoxylin and Eosin for the demonstration of general histoarchitecture. The stained sections were examined under a Leica DM 750 microscope connected to a computerized digital camera system (Leica ICC50) and digital photomicrographs were taken.

Histomorphometry

All histomorphometric evaluations were performed by the same trained, calibrated, and blinded examiner using an image analysis system (Image J Version 1.4.3.67) to analyze digital photomicrograph taken at a final magnification of 100x. Four serial sections were traced for each testis, and eight measurements per section were made of the number of seminiferous tubules within two defined regions at 100-fold magnification; these measurements were computed to obtain a mean value per animal. The seminiferous tubular epithelia height, seminiferous tubular diameter and seminiferous luminal diameter were measured while the cross-sectional area and volume of the seminiferous tubules were calculated. For analyzing the diameters of the seminiferous tubules, we defined regions that had round or nearly round cross sections of tubules as possible. Then, the longest diameter (D_1) and the perpendicular diameter (D_2) of each cross section of tubules were measured; each seminiferous tubular diameter D was calculated as $\sqrt{D_1D_2}$.

Statistical Analysis

Results were expressed as Mean ± S.E.M and data were analyzed using one-way analysis of variance (ANOVA) followed by Dunnett post hoc test for comparison with control. Alpha level was set at 0.05. All statistical analysis was done using GraphPad Prism5 (5.0.3.0, GraphPad Inc.).

RESULTS

Organ Weight

There was a significant decrease in relative testicular weight of treated rats in group D ($p < 0.05$) when compared with control (Fig. 1). There was no difference in testicular weight between groups A, B, C and D after the recovery period (Fig. 2).

Histopathological results

Histological examination of haematoxylin-eosin-stained sections revealed that the rats which received the highest dose (group D), had morphological features of histopathological damages, and these are presented by cellular degeneration resulting in depleted germ cells, a disorganized seminiferous tubular epithelium and presence of pyknotic nuclei (Figs. 3 and 4). However, these features observed in group D rats were reversed after the 3-week recovery period (Figs. 5 and 6). Histological examination of the testes of treated groups B and C rats showed no obvious injury to the seminiferous tubules, spermatogonia cells and the Leydig cells scattered in-between them in the interstitial spaces. They reveal instead seminiferous tubules having normal testicular morphology, primary spermatocytes showing no degenerative changes which showed spermatogenesis was not disturbed (Figs. 5 and 6).

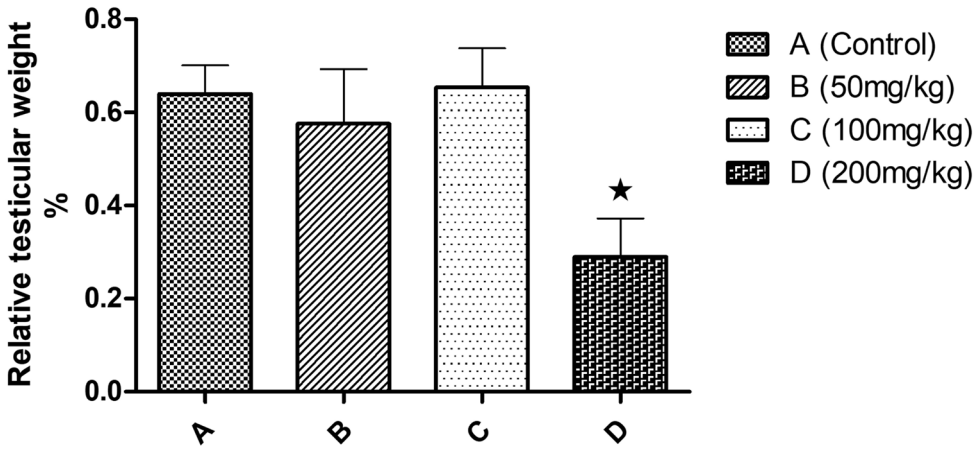

Fig. 1.- Effects of caffeine on the relative weights of the testes. Values are expressed as the mean ± SEM. * P<0.05 vs control.

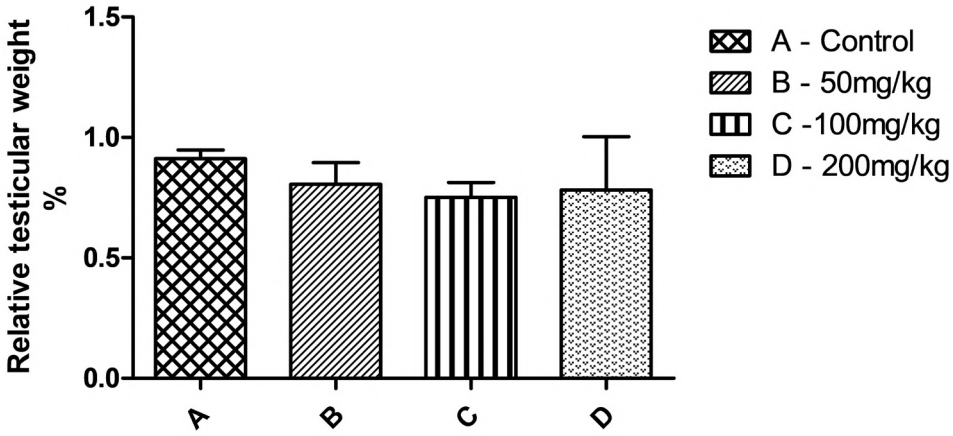

Fig. 2.- Effects of caffeine on the relative weights of the testes after 21 days recovery. Values are expressed as the mean ± SEM.

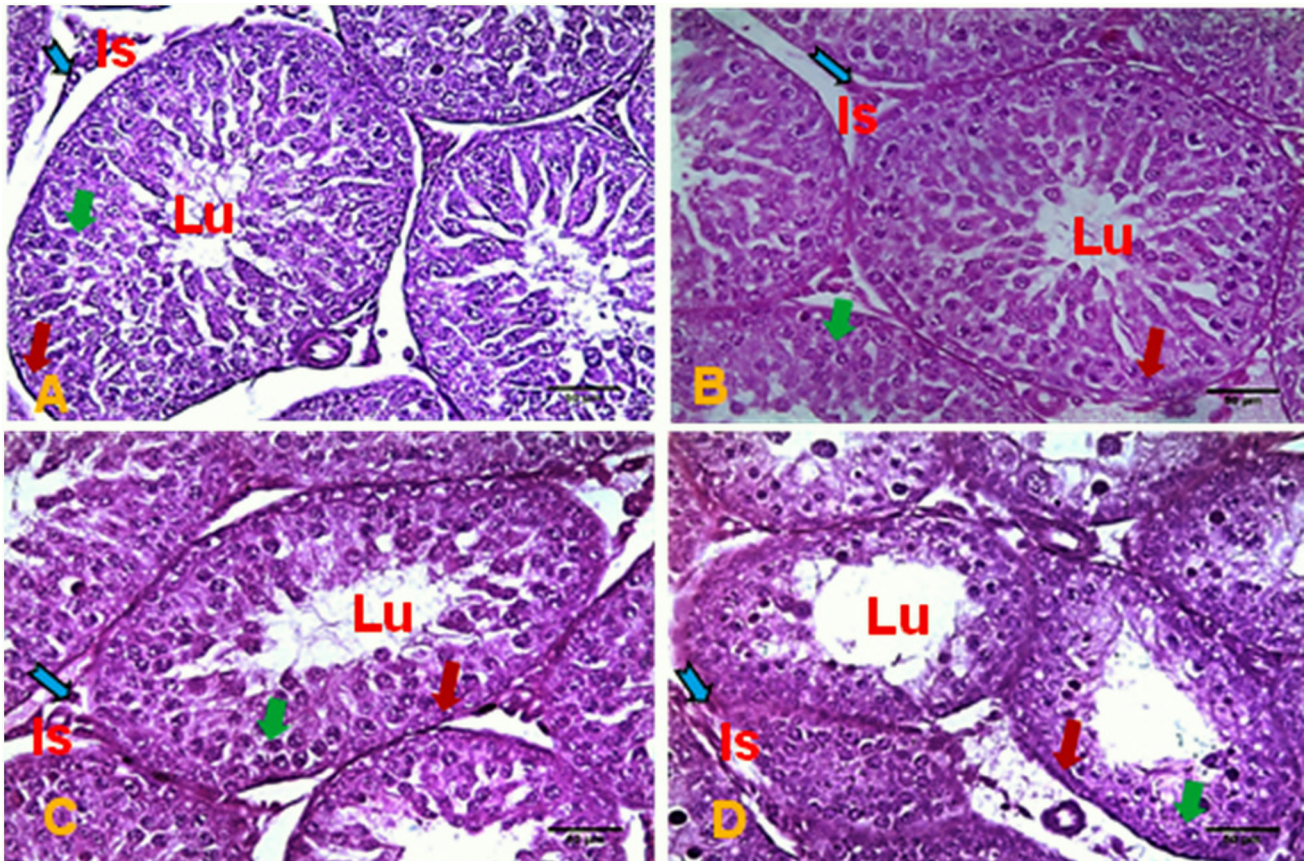

Fig. 3.- Sections of testes of prepubertal Wistar rats subjected to H&E stain after treatment. Note in slides A, B, C intact seminiferous tubules showing its lumen (Lu), interstitial cells of Leydig (blue arrows) within the interstitial space (Is) spermatogonia (red arrows), primary spermatocytes (green arrows). Also note D with smaller sizes of seminiferous tubules. Scale bars = 50 µm.

Histomorphometry

Histomorphometric analysis of the seminiferous tubular diameter presented nearly no differences ($p > 0.05$) between control group (A) and each of the other treated groups (B and C), while group D showed a significant reduction ($p < 0.05$) in seminiferous tubular diameter in comparison to group A and a significant reduction ($p < 0.05$) in seminiferous epithelial height in comparison to groups A and B (Table 1). The seminiferous luminal diameter was significantly increased in group D when compared with the other groups (Table 1). At recovery, significant decrease was observed in seminiferous epithelia height of

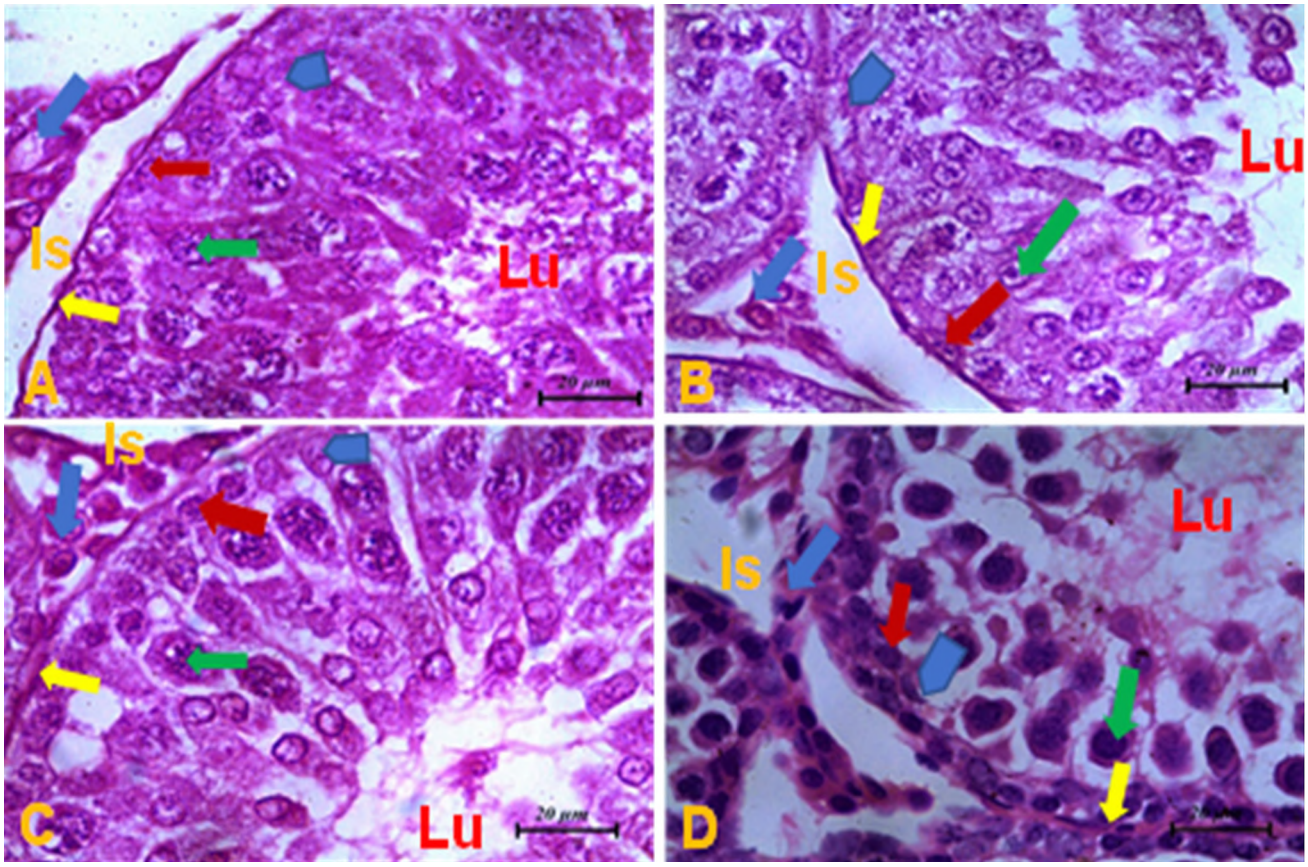

Fig. 4.- Sections of testes of prepubertal Wistar rats subjected to H&E stain. In slides A, B, and C, note the seminiferous tubule with a regular and thin basement membrane (yellow arrow), lumen (Lu), interstitial spaces (Is) containing interstitial cells (blue arrows), spermatogonia (red arrows), primary spermatocytes (green arrows), Sertoli cells (block arrows). Also note in D germinal epithelium with scanty immature spermatogenic cells. Scale bar = 20 µm.

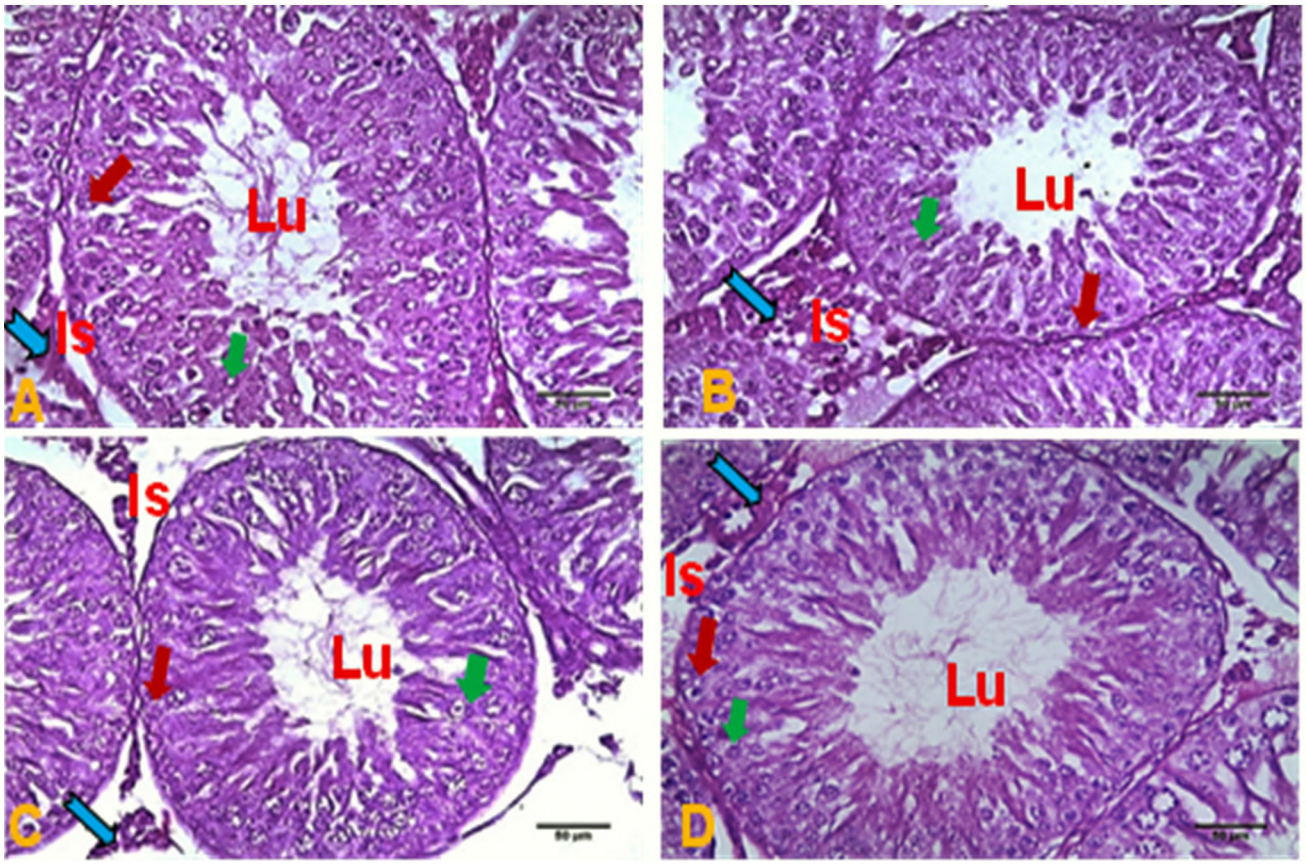

Fig. 5.- Sections of testes of prepubertal Wistar rats subjected to H&E stain following recovery. In slides A, B, C, D note the seminiferous tubules showing lumen (Lu), Interstitial cells of Leydig (blue arrows) within the interstitial space (Is), spermatogonia (red arrows) and primary spermatocytes (green arrows). Also note the marked recovery in D. Scale bars = 50 µm.

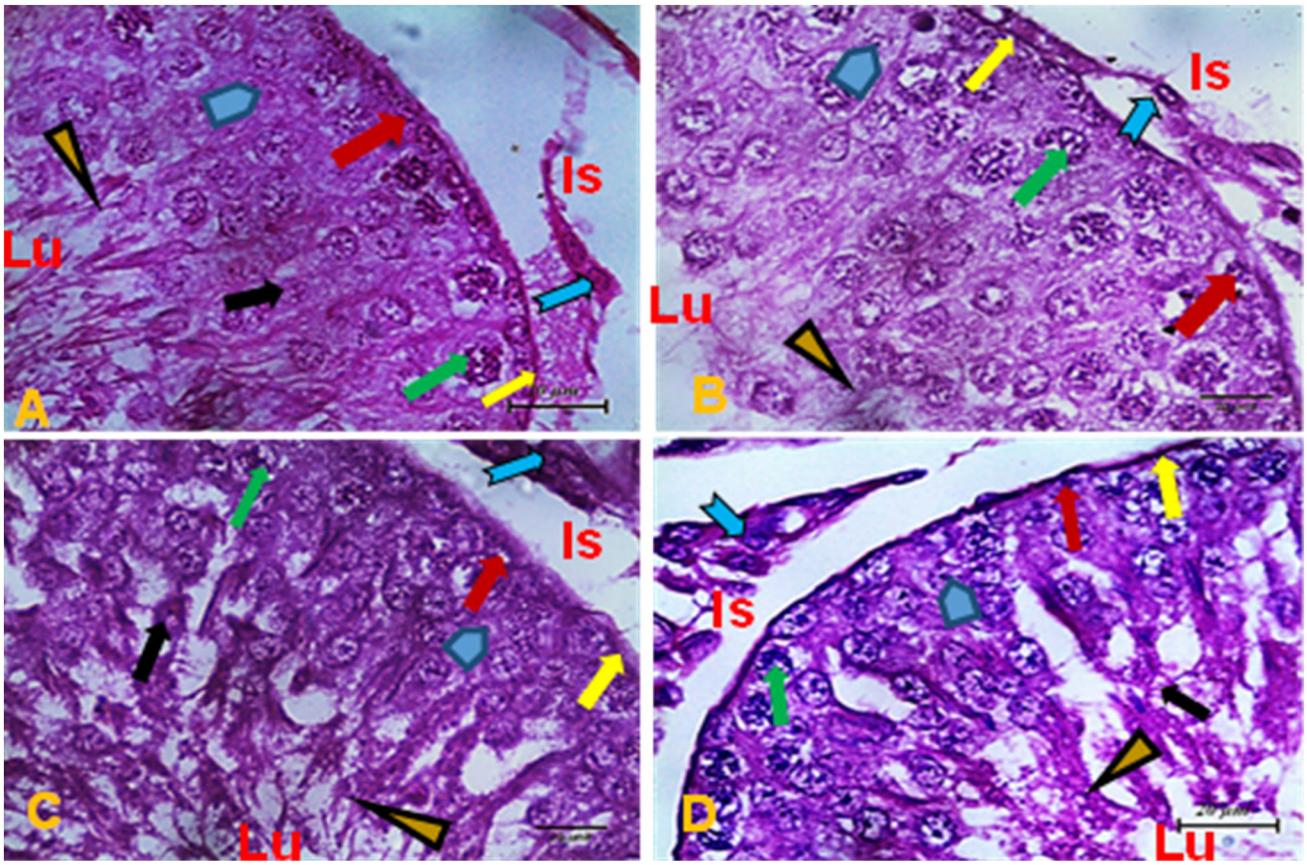

Fig. 6.- Sections of testes of prepubertal Wistar rats subjected to H&E stain following recovery. In slides A, B, C, and D note the seminiferous tubule with regular and thin basement membrane (yellow arrow), lumen (Lu) containing mature spermatozoa, interstitial spaces (Is) consisting of interstitial cells of Leydig (blue arrows), spermatogonia (red arrows), spermatocytes (green arrows), Sertoli cells (block arrows), round spermatids (black arrows), flagellum of elongated spermatids within the lumen (arrow heads). Scale bar = 20 µm.

Table 1. Effects of caffeine on the morphometry of the testis following treatment with caffeine.

Groups	Seminiferous tubular diameter (µm)	Seminiferous tubular epithelia height (µm)	Seminiferous luminal diameter (µm)	Cross-sectional area of seminiferous tubule (mm^2)	Volume of seminiferous tubules (μm^3)
Gp $1A_1$	249.8 ± 10.92	0.229 ± 0.019	76.02 ± 3.377	$49.02 \times 10^3 \pm 9.4 \times 10^1$	$8.16 \times 10^6 \pm 6.8 \times 10^3$
Gp $1B_1$	222.8 ± 19.62	0.179 ± 0.013	90.6 ± 9.027	$38.99 \times 10^3 \pm 30.2 \times 10^1$	$5.79 \times 10^6 \pm 3.9 \times 10^4$
Gp $1C_1$	221.1 ±11.13	0.180 ± 0.003	86.6 ± 5.086	$34.58 \times 10^3 \pm 30.5 \times 10^1$	$4.84 \times 10^6 \pm 4.0 \times 10^4$
Gp $1D_1$	209.8 ± 19.72*	0.155 ± 0.025*	102.3 ± 8.421*	$38.40 \times 10^3 \pm 9.7 \times 10^1$	$5.66 \times 10^6 \pm 7.2 \times 10^3$

Values are presented as Mean ± SEM (n=5).* = Significantly different from Control ($p<0.05$)

groups C and D when compared with control. A significant decrease in the seminiferous tubular diameter of groups B, C and D was also observed when compared with control while seminiferous luminal diameter of group D increased significantly ($p < 0.05$) when compared with control (Table 2). In addition, the cross-sectional area of the seminiferous tubule and the volume of the seminiferous tubules significantly decreased ($p < 0.05$) in groups B, C, and D compared to the control group A.

Table 2. Effects of caffeine on the morphometry of the testis following recovery from treatment with caffeine.

Groups	Seminiferous tubular diameter (µm)	Seminiferous tubular epithelia height (µm)	Seminiferous luminal diameter (µm)	Cross-sectional area of seminiferous tubule (mm^2)	Volume of seminiferous tubules (μm^3)
Gp $1A_2$	320.8 ± 22.43	0.281 ± 0.009	122.2 ± 5.975	$80.84 \times 10^3 \pm 4.0 \times 10^2$	$17.29 \times 10^6 \pm 5.9 \times 10^4$
Gp $1B_2$	274.0 ± 10.89*	0.239 ± 0.005	115.8 ± 4.102	$58.97 \times 10^3 \pm 9.3 \times 10^{1*}$	$10.77 \times 10^6 \pm 6.8 \times 10^{3*}$
Gp $1C_2$	250.1 ± 6.912*	0.194 ± 0.007*	121.7 ± 4.344	$49.13 \times 10^3 \pm 3.8 \times 10^{1*}$	$8.19 \times 10^6 \pm 1.7 \times 10^{3*}$
Gp $1D_2$	252.5 ± 13.41*	0.157 ± 0.028*	144.6 ± 12.820*	$50.08 \times 10^3 \pm 1.4 \times 10^{2*}$	$8.43 \times 10^6 \pm 1.3 \times 10^{4*}$

Values are presented as mean ± SEM (n=5). * = Significantly different from Control ($p<0.05$)

DISCUSSION

Morphological assessment of the testes of rats exposed to caffeine in this study revealed that caffeine intake caused a significant reduction on in testicular weight, a marked cellular degeneration and depletion of germ cells, a significant decrease in height of the germinal epithelium, seminiferous luminal diameter, seminiferous tubular diameter, cross sectional area and volume of seminiferous tubules of Wistar rats. This observation is in line with results of previous studies in which caffeine toxicity was reported to be associated with a decrease in germ cell proliferation, hence a reduced number of differentiating germ cells (Bae et al., 2017), as the weight of the testis is directly proportional to the mass of the differentiated spermatogenic cells (Boockfor and Blake, 1997). However, this morphological disruption appears to be reversible after the period of recovery. Oluwole et al., (2016) opined that the decrease in organ weight caused by caffeine could be due to the ability of caffeine to cause lipolysis. This resulted from inhibition of cyclic nucleotide phosphodiesterase that leads to accumulation of cyclic AMP in tissues which then activates hormone-sensitive lipase to promotes lypolysis (Hursel and Wester-Plantega, 2010). The decrease in organ weight, may have also resulted from diuresis which hinders reabsorption of salts and water, or increased metabolism (Huang et al., 2005). This study is also in line with the observations of Dorostghoal et al. (2012), who reported that prenatal caffeine exposure brought about a dose-related reduction in the testis weight of male offspring.

The examination of the histological sections of group D showed that caffeine induced deleterious effects on testicular architecture which could have resulted from interference with the testicular micro-environment thereby resulting in the disruption of the initiation and maintenance of the spermatogenesis. A reduction was observed in seminiferous tubular epithelia height of the group administered with the highest dose reveals shows caffeine has negative effect on testicular morphology. Pollard et al. (1990) had earlier reported that exposure of male Wistar rats to 30 mg/kg per day of caffeine, given by gavage for 15 to 38 consecutive days led to breakdown of the germinal epithelium. The seminiferous tubular diameter was observed to be decreased in all the animals after the recovery period. The decrease in seminiferous tubular diameter may be due to the fact that caffeine interferes with cell division which leads to a reduced number of spermatogenic cells. Dorostghoal et al. (2012), reported a decrease in the diameter of seminiferous tubules of the offspring of rats given caffeine during the prepubertal, postpubertal and adulthood periods. Pollard et al. (1990) also showed that caffeine when given prenatally, inhibited differentiation of the seminiferous cords. Daily administration of 30 or 60 mg/kg caffeine to mature male rabbits for four consecutive weeks caused a decrease in the sizes of the seminiferous tubules and inhibited spermatogenesis (Ezzat and el-Gohary, 1994).

CONCLUSION

This study concluded that prepubertal exposure of Wistar rats to caffeine reduced testicular growth and predisposed the seminiferous tubules of growing male Wistar rats to deleterious structural changes which were reversible over a recovery period.

REFERENCES

AUGUST GP, GRUMBACH MM, KAPLAN SL (1972) Hormonal changes in puberty: III. Correlation of plasma testosterone, LH, FSH, Testicular size, and bone age with male pubertal development. *J Clin Endocrinol Metab*, 34(2): 319-326.

BAE J, CHOI H, CHOI Y, ROH J (2015) Dose- and time-related effects of caffeine on the testis in immature male rats. *Exp Anim,* 66: 29-39.

BOOCKFOR FR, BLAKE CA (1997) Chronic administration of 4-tert-octylphenol to adult male rats causes shrinkage of the testes and male accessory sex organs, disrupts spermatogenesis, and increases the incidence of sperm deformities. *Biol Reprod,* 57: 267-277.

DOROSTGHOAL M, ERFANI-MAJD N, NOORAEI P (2012) Maternal caffeine consumption has irreversible effects on reproductive parameters and fertility in male offspring rats. *Clin Exp Reprod Med,* 39: 144-152.

DRURY RA, WALLINGTON EA (1980) *Carleton's Histological Techniques*. 5th edition. Oxford University Press, New York, pp 44-134.

EZZAT AR, EL-GOHARY ZM (1994) Hormonal and histological effects of chronic caffeine administration on the pituitary-gonadal and pituitary-adrenocortical axes in male rabbits. *Functional Develop Morphol*, 4: 45-50.

HUANG ZL, QU WM, EGUCHI N, CHEN JN, SCHWARZSCHILD MA, FREDHOLM BB (2005) Adenosine A2A, but not A1, receptors mediate the arousal effect of caffeine. *Nat Neurosci,* 8: 858-859.

HURSEL R, WESTERTERP-PLANTENGA MS (2010) Thermogenic ingredients and body weight regulation. *Int J Obes*, 34: 659-669.

NAWROT P, JORDAN S, EASTWOOD J, ROTSTEIN J, HUGENHOLTZ A, FEELEY M (2003) Effects of caffeine on human health. *Food Addit Contam,* 20: 1-30.

OLUWOLE OF, SALAMI SA, OGUNWOLE E, RAJI Y (2016) Implication of caffeine consumption and recovery on the reproductive functions of adult male Wistar rats. *J Basic Clin Physiol Pharmacol*, 27(5): 483-491.

PARK M, CHOI Y, CHOI H, YIM JY, ROH J (2015) High doses of caffeine during the peripubertal period in the rat impair the growth and function of the testis. *Int J Endocrinol,* 2015: 368475.

POLLARD I, WILLIAMSON S, MAGRE S (1990) Influence of caffeine administered during pregnancy on the early differentiation of fetal rat ovaries and testes. *J Development Physiol*, 13(2): 59-65.

RAMLAU-HANSEN CH, THULSTRUP AM, BONDE JP, OLSEN J, BECH BH (2008) Semen quality according to prenatal coffee and present caffeine exposure: two decades of follow-up of a pregnancy cohort. *Human Reprod*, 23(12): 2799-2805.

REISSIG CJ, STRAIN EC, GRIFFITHS RR (2009) Caffeinated energy drinks—a growing problem. *Drug Alcohol Dependence,* 99(1-3): 1-10.

SEIFERT SM, SCHAECHTER JL, HERSHORIN ER, LIPSHULTZ SE (2011) Health effects of energy drinks on children, adolescents, and young adults. *Pediatrics*, 127(3): 511-528.

SHARPE RM (1988). Endocrinology and paracrinology of the testis. In: Lamb JC, Foster PMD (eds). *Physiol Toxicol Male Reprod*. Academic Press, San Diego, pp. 71-99.

TINWELL H, COLOMBEL S, BLANCK O, BARS R (2013) The screening of everyday life chemicals in validated assays targeting the pituitary-gonadal axis. *Regul Toxicol Pharmacol*, 66(2): 184-196.

WEINBERGER MA, FRIEDMAN L, FARBER TM, MORELAND FM, PETERS EL, GILMORE CE, KHAN MA (1978) Testicular atrophy and impaired spermatogenesis in rats fed high levels of the methylxanthines caffeine, theobromine, or theophylline. *J Environ Pathol Toxicol,* 1(5): 669-688.

WIKOFF D, WELSH BT, HENDERSON R, BRORBY GP, BRITT J, MYERS E, GOLDBERGER J, LIEBERMAN HR, O'BRIEN C, PECK J, TENENBEIN M, WEAVER C, HARVEY S, URBAN J, DOEPKER C (2017) Systematic review of the potential adverse effects of caffeine consumption in healthy adults, pregnant women, adolescents, and children. *Food Chem Toxicol,* 109(1): 585-648.

Evaluation of mandibular incisive canal and mental foramen in Turkish population by conical beam computed tomography

Neslihan Yuzbasıoglu[1], Selva Sen[1], H. Emir Yuzbasioglu[2,3], B. Ufuk Sakul[1]

[1] İstanbul Medipol University, School of Medicine, Department of Anatomy, İstanbul, Turkey

[2] Bahcesehir University, Faculty of Dentistry, İstanbul, Turkey

[3] BAU International University, Department of Dentistry, Faculty of Medicine, Batumi, Georgia

SUMMARY

Surgical complications may occur in the interforaminal area when course and morphological features of anatomical structures, which includes neurovascular structures in the mandible, cannot be defined correctly. The aim of this study is to determine the course and morphological characteristics of the mental foramen (MF) and the mandibular incisive canal (MIC) in Turkish society. Cone Beam Computed Tomography (CBCT) is considered the gold standard for dental imaging; therefore, in this study 96 CBCT images were examined retrospectively. The width and the length of the MF, distance from the MF to the alveolar bone crest, lower border of the mandible, angulation of mental canal to buccal bone surface, the length of the MIC, the angle among mental foramen-incisive canal and a horizontal plane parallel to the inferior border of the mandible, and the height of the angle were measured. At the endmost point of the MIC, the distance between the canal and inferior, labial, and lingual borders of the mandible was measured. The most common locations of MF were along the second premolar (23.4%). MIC was absent in 24.4% of the cases. The most common locations of the endmost point of MIC were along the first incisive (35.8%), MIC length was significantly longer in males. Although the structures show variation among individuals, the mean values in Turkish society are similar to the mean values in the literature.

Key words: Mandibular incisive canal – Mental foramen – Anatomy – CBCT – Surgery

INTRODUCTION

The mandible is an important anatomical structure which is associated with dental anesthesia, implant treatment, and reconstructive procedures in dentistry. The mandible is the only movable bone of the facial skeleton and houses inferior teeth. Neurovascular structures course within the canals and foramina of the mandible and reach the target structure or area. Because of this, the anatomical structures of the mandible itself and related to the mandible must be taken into consideration during dental and surgical procedures.

Corresponding author:
Neslihan Yüzbasıoglu. Department of Anatomy, İstanbul Medipol University, Göztepe Neighborhood, Ataturk Street. No. 40, Beykoz- Kavacık, İstanbul, Turkey. Phone: 00 90 212 4534854; Fax: 00 90 212 5317555. E-mail: ncankara@medipol.edu.tr

Submitted: June 29, 2022. **Accepted:** September 3, 2022

https://doi.org/10.52083/LBPJ5041

The inferior alveolar nerve (IAN) which innervates the inferior teeth is within the mandibular canal. It begins from the mandibular foramen, which is located on the medial surface of the mandibular ramus, then it travels downwards obliquely within the ramus and finally courses anteriorly through the mental foramen (MF) (Haas et al., 2016; Juodzbalys et al., 2010). The mandibular canal bifurcates into the mental canal and the mandibular incisive canal (MIC) after just passing the mental foramen. These canals contain the terminal branches of the inferior alveolar nerve and accompanying vessels (Polland et al., 2001). MIC is the continuation of the mandibular canal within the body of the mandible towards the median plane or mesially (Polland et al., 2001). It begins from the MF, and the incisive nerve and vessels which travel within the MIC reach the anteriorly located teeth (2 incisives and 1 canine) (Pereira-Maciel et al., 2015; Polland et al., 2001). As to the mental canal, it provides the mental nerve and accompanying vessels passing through the superficially located mental area on the face via the mental foramen of the mandible (Polland et al., 2001). The prevalence, size and location of the MIC may be different between races (Apostolakis and Brown, 2012; Kuzmanovic et al., 2003; Li et al., 2013; Ramesh et al., 2015).

The area between two mental foramina is known as the interforaminal area. And this region is accepted as a safe zone for surgical procedures. Also, this region is an ideal site for chin block bone grafting, due to its ideal bone quality and distance from the IAN in comparison to the posterior mandible. The precise location of the bifurcation of the IAN is variational (Caughey et al., n.d.). Any edema, hematoma, infection, traction or compression of the nerve that may occur in this region may cause damage. And the damage of the inferior alveolar nerve and accompanying vessels may cause pain and loss of sensation on the anterior teeth, lips, skin and mucosa (Alyami et al., 2021; Khan et al., 2011; Worthington, 2004). Therefore, the presence, location, dimensions, and direction of the MIC should be elicited when placing implants, planning for the biopsy or removal of any pathology present in the anterior mandible (Caughey et al., n.d.).

Radiological imaging methods guide physicians in determining locations of anatomical structures and density of bone mass. Today, cone beam computed tomography (CBCT) images are frequently referenced by dentists and surgeons in the evaluation of pre-op structures (Phillips et al., 1990; Zhang et al., 2017). Studies in the literature report that the canals within the mandible on CBCT images show high visibility (de Brito et al., 2016).

A detailed anatomical study of the interforaminal region is significant to avoid complications (Tejada et al., 2022). Also, MF has been used as an important landmark for implant surgery, and many variations in these area have been reported (Alshamrani et al., 2021; Wong and Patil, 2018). Surgical complications related to implant surgery in the interforaminal area are likely to be related to failure of the anatomical identification of MF and MIC (Choi et al., 2019). Knowing variation, course and distances between dental roots and morphological features related to canals within the mandible is very important to prevent complications and achieve success during surgery. Because of this, this study aimed to determine the detailed features of these abovementioned canals in the Turkish population.

MATERIALS AND METHODS

This study was approved by the institutional ethics committee. The study was designed as a retrospective analysis of 346 CBCT images taken in a private clinic. All images were taken by the same technician, following a standardized protocol for patient positioning and exposure parameter setting. Some of the cases were eliminated. 185 of the images were not in the proper format, 40 images were poor in quality and 25 images were not in the appropriate age range. In the remaining 96 images (46 female, 50 males, 21-80 ages), the following measurements were performed on a total of 192 hemi-mandible with the Osirix MD software:

1. The visibility of mental foramen was noted as poor, medium, good
2. In the axial view, the width of MF (MF width) (Fig. 1).
3. In the sagittal view, the position of the MF related to the long axis of the adjacent teeth was de-

Fig. 1.- In the axial view, the width of mental foramen (MF width).

termined and the longitudinal length of mental foramen (MF length) was measured (Fig. 2).

4. In the coronal view, as in the study of Von Arx et al. (2013), distance from the superior margin of MF to the alveolar bone crest (MF alveolar crest), distance from the inferior margin of MF to lower border of the mandible (MF mand. border), angulation of mental canal to buccal bone surface (MF-MC angle) were measured (Fig. 3).
5. The visibility of the MIC was noted as none, poor, medium, good.
6. The length of mandibular incisive canal (MIC length) was measured (Fig. 4).
7. A line was drawn from the mental foramen to the endmost point of the MIC. Another line was drawn parallel to the inferior border of the mandible from the endmost point of the MIC. The angle (MF-MIC angle) and distance between these two lines (Angle height) were measured (Fig 5).
8. As in the study of Panjnoush et al. (2016) at the endmost point of the MIC in the last cross-sectional plane, the distance between the canal and inferior (MIC-mand border), labial (MIC-labial) and lingual (MIC-lingual) borders of mandible was measured (Fig. 6). And tooth root where the MIC was ended noted.

The data were presented as mean ± SD, and the prevalence in percentages was calculated for MF and MIC. The groups were compared using the chi-square test for categorical variables. T-test and One-Way ANOVA tests were used to compare quantitative variables. The significance level was accepted as $p < 0.05$ for all tests.

RESULTS

In this study, the average age of individuals was 47.65 ± 15.83 (21-80). Table 1 illustrates the gender and dental status distribution of the individuals.

Table 1. Gender and dental status distribution.

	Female	Male	Total
Edentulous	21 (45.7%)	32 (64%)	53 (55.2%)
Dentulous	19 (41.3%)	10 (20%)	29 (30.2%)
Partial dentulous	6 (13%)	8 (16%)	14 (14.6%)
Total	46 (47.9%)	50 (52.1%)	96

Fig. 2.- In the sagittal view, the position of the MF related to the long axis of adjacent teeth, the length of mental foramen (MF length).

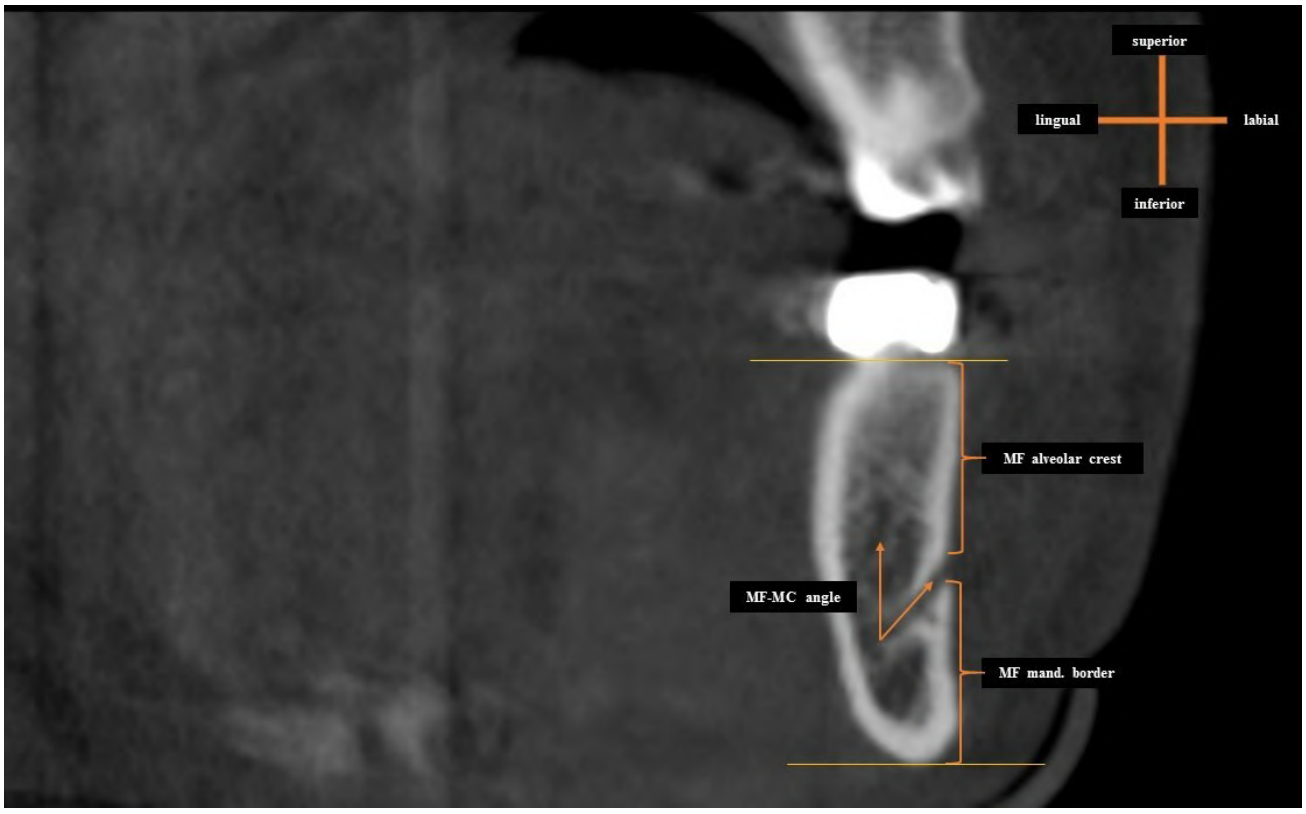

Fig. 3.- Distance from the superior margin of MF to the alveolar bone crest (MF alveolar crest), distance from the inferior margin of MF to lower border of the mandible (MF mand. border), angulation of mental canal to buccal bone surface (MF-MC Angle).

Fig. 4.- The length of mandibular incisive canal (MIC length).

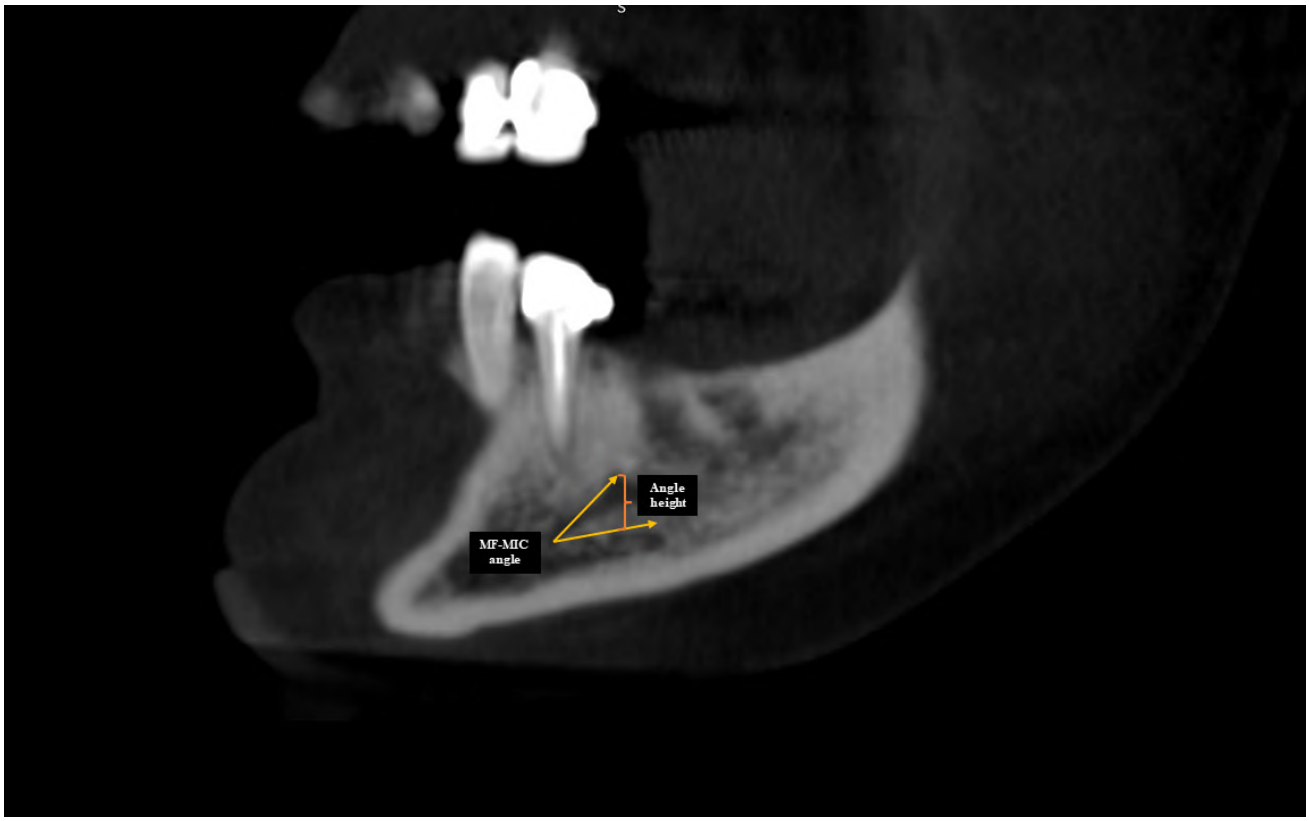

Fig. 5.- Angle among mental foramen- mandibular incisive canal and a horizontal plane parallel to the inferior border of the mandible (MF-MIC angle) and the height of the angle (Angle height).

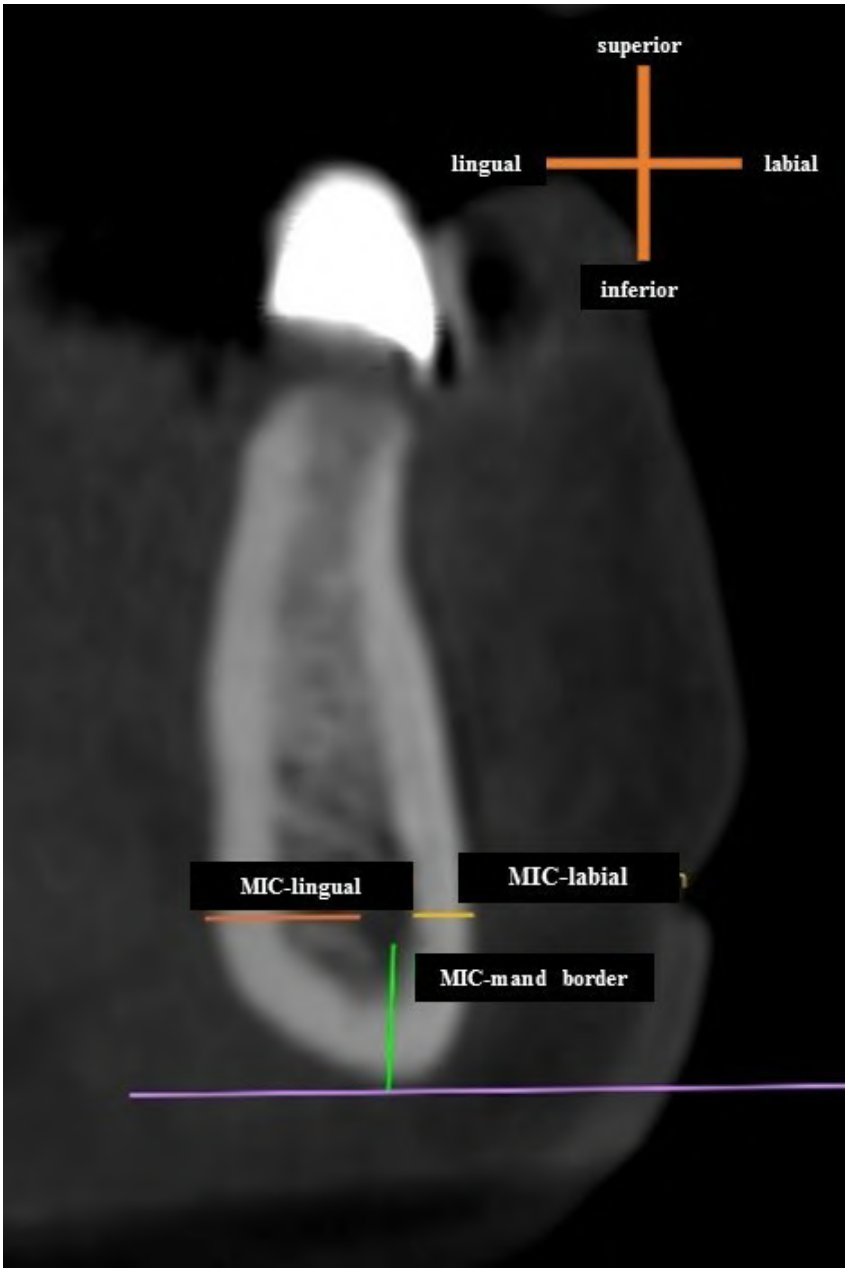

Fig. 6.- At the end most point of the MIC the distance between the canal and inferior (MIC-mand border), labial (MIC-labial) and lingual (MIC-lingual) borders of mandible.

Mandibular Incisive Canal

The visibility of the MIC is shown in Table 2. There was no statistically significant difference between the genders and sides in the presence of the mandibular incisive canal.

The location of the endmost point of the MIC with reference to the adjacent teeth are shown in Table 3. There was no statistically significant difference between the location of the endmost point of right and left MIC according to gender. As regards sides, there was no significant difference; the most common locations of MIC were first incisive on both sides for total cases.

Table 4 shows the mean values and standard deviations of the MIC length, MIC-mand border, MIC-labial and MIC-lingual borders of mandible and MF-MIC angle, and the angle height. There was no statistically significant difference in all parameters between the left and right sides. However, when compared with males and females, a statistically significant difference was found for the length of the left MIC ($p<0.05$): it was longer in males.

There was no statistically significant difference in other parameters according to gender or sides.

Mental Foramen (MF)

The visibility of MF is shown in Table 5. There was no statistically significant difference between the visibility of MF both genders and sides (p>0.05).

The location of MF regarding the long axis of adjacent teeth is shown in Table 6. There was no statistically significant difference between the location of right and left MF with reference to the adjacent teeth according to gender (p>0.05).

Table 7 shows the mean values and standard deviations of the MF width and MF length, MF alveolar crest, MF mand. border, MF-MC angle. A

Table 2. Visibility of mandibular incisive canal (MIC: Mandibular incisive canal).

	Right MIC					Left MIC					Total				
	None	Poor	Medium	Good	Total	None	Poor	Medium	Good	Total	None	Poor	Medium	Good	Total
Female	11 (24.4%)	22 (48.9%)	6 (13.3%)	6 (13.3%)	34 (75.6%)	10 (24.7%)	21 (45.7%)	9 (19.6%)	6 (13%)	36 (75.3%)	22.8%	47.8%	16.3%	13.1%	77.2%
Male	14 (28%)	22 (44%)	6 (12%)	8 (16%)	36 (72%)	12 (24.5%)	17 (34.7%)	12 (24.5%)	8 (16.3%)	37 (75.5%)	26%	40%	18%	16%	74%
Total	25 (26.3%)	44 (46.3%)	12 (12.6%)	14 (14.7%)	70 (73.7%)	22 (23.2%)	38 (40%)	21 (22.1%)	14 (14.7%)	73 (76.8%)	24.4%	43.8%	17.2%	14.6%	75.6%

Table 3. Location of the end point of the mandibular incisive canal with reference to the adjacent teeth.

	Right MIC				Left MIC				All MIC			
	1st incisive	2nd incisive	Canine	1st premolar	1st incisive	2nd incisive	Canine	1st premolar	1st incisive	2nd incisive	Canine	1st premolar
Female	19	6	6	0	19	7	7	0	38	13	13	0
	42.2%	13.3%	13.3%	0%	41.3%	15.2%	15.2%	0%	41.8%	14.3%	14.3%	0%
Male	17	5	9	0	13	10	7	1	30	15	17	1
	34.7%	10.2%	18.4%	0%	26.5%	20.4%	14.3%	2%	30.3%	15.2	17.2%	2%
Total	36	11	15	0	32	17	14	1	68	28	30	1
	37.9%	11.0%	15.8%	0.0%	33.7%	17.9%	14.8%	1%	35.8	14.7	15.8%	1%

Table 4. Measurement parameters of the mandibular incisive canal (MIC: Mandibular incisive canal).

	Right MIC			Left MIC			All MIC (n=147)
	Female (n=35)	Male (n=38)	Total (n=73)	Female (n=36)	Male (n=38)	Total (n=74)	
MIC length	11.39±3.15	12.91±4.09	12.18±3.72	10.10±3.19*	12.85±4.84*	11.51±4.32	11.76±4.14
MIC-mand border	11.43±10.83	12.07±9.48	11.76±10.09	9.57±3.36	12.39±14.26	11.02±10.51	11.31±10.28
MIC-labial	3.10±1.64	3.98±2.13	3.56±1.95	3.32±1.13	3.98±1.51	3.66±1.37	3.58±1.70
MIC-lingual	4.12±1.79	4.56±2.26	4.35±2.04	4.07±1.34	4.96±3.09	4.52±2.43	4.41±2.26
MF-MIC angle	24.92±11.80	23.01±11.77	23.93±11.74*	25.12±12.66	25.70±11.27	25.41±11.89*	24.51±11.93
Angle height	4.62±2.07	4.95±1.98	4.79±2.02	4.33±1.71	5.25±1.99	4.80±1.90	4.76±1.98

* statistically ssignificant difference between the length of the left mandibular incisive canal according to gender (p<0.05)

Table 5. Visibility of mental foramen (MF: Mental Foramen).

	Right MF			Left MF			All MF		
	Poor	**Medium**	**Good**	**Poor**	**Medium**	**Good**	**Poor**	**Medium**	**Good**
Female	16 (35.6%)	17 (37.8%)	12 (26.7%)	15 (32.6%)	17 (37%)	14 (30%)	31 (47.7%)	35 (49.9%)	26 (53.1%)
Male	17 (34%)	19 (38%)	14 (28%)	17 (34%)	24 (48%)	9 (18%)	34 (52.3%)	43 (55.1%)	23 (49.9%)
Total	33 (34.7%)	36 (37.9%)	26 (27.4%)	32 (33.3%)	41 (42.7%)	23 (24%)	65 (33.9%)	78 (40.6%)	49 (25.5%)

Table 6. Location of mental foramen (MF: Mental Foramen).

	Right MF			Left MF			Total MF		
	Between 1st and 2nd premolar	**1st premolar**	**2nd premolar**	**Between 1st and 2nd premolar**	**1st premolar**	**2nd premolar**	**Between 1st and 2nd premolar**	**1st premolar**	**2nd premolar**
Female	7 (15.2%)	3 (6.5%)	10 (21.7%)	7 (15.2%)	2 (4.3%)	15 (32.6%)	14 (73.7%)	5 (62.5%)	25 (55.6%)
Male	2 (4%)	1 (2%)	12 (24%)	3 (6%)	2 (4%)	8 (16%)	5 (26.3%)	3 (37.5%)	20 (44.4%)
Total	9 (9.4%)	4 (4.2%)	22 (22.9%)	10 (10.4%)	4 (4.2%)	23 (24%)	19 (9.9%)	8 (4.2%)	45 (23.4%)

Table 7. Measurement parameters of mental foramen (MF: Mental Foramen).

	FEMALE		MALE		ALL		Total
	Right	**Left**	**Right**	**Left**	**Right**	**Left**	
MF width	2.56±1.04	2.61±0.89	2.74±0.68	2.71±0.82	2.65±0.87	2.66±0.85	2.66±0.86
MF length	2.66±0.85	2.65±0.88	2.91±0.83	2.79±0.79	2.79±0.84	2.72±0.83	2.76±0.84
MF alveolar crest	11.78±4.51	12.83±4.29	11.82 ±3.78	11.99±5.11	11.80±4.13	12.39±4.73	12.10±4.44
MF mand. border	11.97±2.97*	13.09±4.12*	14.92±7.69*	14.93±3.59*	13.51±6.07	14.05±3.95	13.78±5.11
MF-MC angle	63.7 ±12.71	66.87±18.95	66.37±16.53	70.41±16.85	65.10±14.81	68.71±17.88	68.71±17.83

* statistically significant difference between the right and left sides for both genders ($p<0.05$)

statistically significant difference was only found between the right and left sides for both genders at this distance from the inferior margin of MF to the lower border of the mandible ($p<0.05$). This distance was longer in males. The mean values of the other parameters were also higher in males, but not statistically significant ($p>0.05$).

Dental Status

Visibility of MF, and presence and visibility of MIC according to dental status are shown in Table 8. There was a statistically significant difference between the visibility of MF in edentulous and dentulous patients ($p<0.05$). No statistically significant difference was found between the presence and visibility of the MIC according to the dental status.

Table 9 shows the parameters of the MF and MIC according to the dental status. There was a statistically significant difference right MF-alveolar crest and left MF-MC angle between dentulous and edentulous individuals ($p<0.05$). The right MF-alveolar crest was lower in edentulous subjects, and it was observed that left MF-MC angle increased to approximately 90 degrees.

There was also a statistically significant difference between MF-MIC angle on both sides and the right MIC-lingual between the dentulous and edentulous individuals ($p<0.05$). The right MIC-lingual was shorter in dentulous cases.

Table 8. Visibility of mental foramen and mandibular incisive canal according to dental status.

	MF			MIC			
	Poor	**Medium**	**Good**	**None**	**poor**	**Medium**	**Good**
Edentulous	45* 42.5%	44 41.5%	17 16.0%	24 22.6%	44 41.5%	20 18.9%	18 17.0%
Dentulous	11 19.0%	22 37.9%	25* 43.1%	13 22.4%	30 51.7%	9 15.5%	6 10.3%
Partial dentulous	9 32.1%	12 42.9%	7 25.0%	10 35.7%	10 35.7%	4 14.3%	4 14.3%
Total	65 33.9%	78 40.6%	49 25.5%	47 24.5%	84 43.8%	33 17.2%	28 14.6%

* statistically significant difference between the visibility of mental foramen in edentulous and dentulous patients ($p<0.05$)

Table 9. Parameters of the mental foramen and mandibular incisive canal according to dental status.

Dental Status	**Edentulous (n=53)**		**Dentulous (n=29)**		**Partial dentulous (n=14)**	
	Right	**Left**	**Right**	**Left**	**Right**	**Left**
MF width	2.63±0.75	2.66±0.85	2.76±0.98	2.74±0.97	2.52±1.10	2.49±0.61
MF length	2.87±1.22	2.74±0.82	2.97±1.02	2.78±0.92	2.57±0.81	2.57±0.77
MF alveolar crest	11.72±8.52*	11.52±4.83	13.91±4.30*	13.6.3±2.83	11.46±2.73	13.14±6.77
MF-mand. border	13.83±7.83	14.11±3.91	12.45±2.73	14.18±4.80	14.47±2.13	13.54±1.53
MF-MC angle	68.90±15.30	75.03±14.22**	58.82±12.71	56.87±16.26**	63.76±12.98	69.33±21.93
MF- MIC angle	16.33±11.90***	17.69±13.08***	28.11±17.66***	28.00±16.633***	15.51±16.40	15.84±15.09
Angle height	3.58±2.55	3.80±2.64	44.68±2.87	4.10±2.19	2.99±2.65	3.09±3.04
MIC length	10.35±6.09	10.17±6.61	8.23±5.88	7.42±4.78	7.26±6.44	6.97±6.15
MIC-mand border	8.68±9.17	7.88±5.10	9.83±13.06	10.37±16.99	08.07±6.52	6.89±6.33
MIC-labial	2.95±2.47	2.97±1.88	2.42±1.12	2.88±2.10	2.34±2.01	2.10±1.86
MIC-lingual	3.97±2.72****	3.87±3.21	2.54±2.06****	3.11±2.35	2.35±2.47	2.79±2.28

Significant difference among with the dentulous and edentulous between:
* right MF to alveolar bone crest distance($p<0.05$).
** left angulation of mental canal to buccal bone surface ($p<0.05$).
*** mental foramen- incisive canal and a horizontal plane parallel to the inferior border of the mandible in both sides($p<0.05$).
****right mandibular incisive canal distance to the lingual border of mandible (MIC-Lingual)

DISCUSSION

Mandibular Incisive Canal (MIC)

Visibility of MIC: Kabak et al. (2017) reported that the overall visibility of MIC on CBCT images was 92%. Panjnoush et al. (2016) reported that it appeared bilaterally in 94% and unilaterally in 3.5%. Brito et al. (2016) reported that in CBCT, MIC is displayed more frequently than panoramic images. Sahman et al. (2014) indicated that CBCT is the gold standard for MIC imaging. In this study, MIC visibility was lower than the literature, approximately 75-77%.

Location of the end point of MIC: Kabak et al. reported that MIC extends to the level of the first incisive root at a rate of 21% and neurovascular structures enter to the tooth root from the MIC through the spaces in the trabecular bone (Kabak et al., 2017). On the other hand, Sahman et al. reported that MIC most frequently terminates between the canine and first premolars (25.1% on the right, 24.6% on the left, 22.6% in women, 27.5% in men) (Sahman et al., 2014). In this study, it was found that the MIC mostly terminated at the level of the first incisive root in Turkish population similar with results of Kabak et al. (2017).

MIC distances: In the literature, MIC length was measured 9.11 mm by Rosa et al. (2013), measured 9.74 mm by Pereira-Maciel et al. (2015), measured an average of 10.48 mm on the right and 10.40 mm on the left by Panjnoush et al. (2016). Pereira-Maciel et al. (2015) measured MIC-mand border 10.25 mm, MIC-labial 4.62 mm, MIC-lingual 6.25 mm and stated that the terminal part of MIC was significantly closer to the buccal face. Panjnoush et al. (2016) reported that MIC-mand. border, MIC-labial and MIC-lingual average distances on the right side were 8.98 mm, 3.63 mm and 3.89 mm, respectively; on the left, 8.62 mm, 3.66 mm, and 4.13 mm, respectively. Both researchers reported that there was no statistically significant difference between gender and sides (Panjnoush et al., 2016; Pereira-Maciel et al., 2015). Similar results were found in our study as well, and there was no significant difference between genders and sides in MIC distances.

Mental foramen (MF)

Visibility of MF: In this study, the localization and dimensions of MF on CBCT images were evaluated, and MF was visualized in all cases. There was no difference between genders and sides (p>0,05).

Localization of MF: In this study, MF was mostly seen at the level of the second premolar root. There was no significant difference between genders and sides (p>0,05).

Variation of additional foramina in the mandible, such as accessory mental foramen (AMF) has been reported in previous studies. The AMF is a smaller foramen that appears in addition to the MF and is continuous with the mandibular canal. Presence of AMF may affect the location of MF and length of the nerve branches. Incidence of AMF is reported as 2.0-13.0%, but we did not observe AMF in our cases (Iwanaga et al., 2015, 2016; Lam et al., 2019).

In a comprehensive study on 663 patients in the literature, it was reported that MF was located between the first and second premolar root mostly (49.2%), and then at the level of the second premolar root at a rate of 39.7% (Goyushov et al., 2018). On the other hand, some researchers report that MF is most commonly found at the second premolar level (Carruth et al., 2015; Panjnoush et al., 2016; Valdec et al., 2019; Von Arx et al., 2013). Direk et al. reported that, unlike the rest of the literature, it was at the level of the first premolar root in all cases (Direk et al., 2018).

In the studies according to the races in the literature, the place of MF has been reported as follows: among the most common first and second premolar roots in the Saudi (Al-Shayyab et al., 2019; Aldosimani et al., 2019; Bello et al., 2018; Velasco-Torres et al., 2017; Zmyslowska-Polakowska et al., 2019), Leh, Jordanian populations and Caucasians; at the level of the second premolar root in Iranian, Lebanese populations and black race (Aoun et al., 2017; Bello et al., 2018; Khojastepour et al., 2015). Kalender et al. reported that it was at the level of the second premolar root, similar to our study, in their study on the Turkish population (Kalender et al., 2012). Carlson et al. reported that the distance of the MF to the premolar teeth differed between the sexes and was closer to the second premolar in women (Gungor et al., 2017). As a result, MF is mostly found at the second premolar root or between the first and second premolar roots in Turkish and other races.

MF dimensions: The studies in the literature have found that the mean length of MF was 2.16-3.55 mm, and the mean width was 3.15-4.42 mm (Bello et al., 2018; Chen et al., 2015; Direk et al., 2018; Dos Santos Oliveira et al., 2018; Goyushov et al., 2018; Gungor et al., 2017; Kalender et al., 2012; Prados-Frutos et al., 2017; Von Arx et al., 2013; Zmyslowska-Polakowska et al., 2019). In the studies according to race, the mean height was 2.87 mm, and the mean width was 3.56 mm in black race (Modi and Arsiwalla, 2019); average measurement was 3.11 mm in height (more in males) in Brazilian population, 3.15 mm in width (Dos Santos Oliveira et al., 2018); the mean height was 3.55 mm in Polish population (more in males on right), and the mean width has been reported to be 4.24 mm (more in males on both sides) (Zmyslowska-Polakowska et al., 2019). Kalender et al. (2012) reported the mean height of MF as 3.7 mm and its mean width as 3.4 mm, and stated that the dimensions of MF were higher in males

than females in the study with 3D reconstruction of the mandible in the Turkish race. In our study, however, no statistically significant difference was found between genders and right-left sides in MF dimensions ($p>0.05$).

The difference between the study by Kalender et al. and ours is due to the method used. Direk et al. found that the height of MF was higher on the right side in both genders (Direk et al., 2018); in all cases Gungor et al. (2017) reported that its width was greater on the right, and Goyushov et al. (2018) reported that MF width was greater only in males.

Distance of MF to upper and lower edge of mandible: The study by Direk et al. (2018) compared the difference between genders according to the age groups; it was found that MF alveolar crest and MF mand. border parameters were higher on right and left sides in men. Gungor et al. (2017) similarly reported that these two distances were lower in women than in men, and they were lower on the right than on the left. In our study, MF mand. border was found greater in men. It is thought that the difference between these values may be due to the skeletal difference between the genders.

Kalender et al. (2012) reported that the MF mand. border parameter varied between 7.9-18.6 mm, with an average value of 12.4 mm in Turkish population. Al-Mahalay et al. (2017) reported mean MF alveolar crest and MF mand. border distance as 14.3 mm and 13.8 mm, respectively.

Dos Santos Oliveira et al. (2018) found the MF alveolar crest distance to be 11.21 mm on average, and reported that there was no difference between genders and sides. In the same study, MF mand. border distance was found to be 12.31 mm on average and there was a significant difference between the genders. Von Arx et al. (2013) reported MF alveolar crest distance as 12.6 mm, MF mand. border distance as 13.2 mm. As a result, considering the data in the literature, MF alveolar crest and MF mand. border distances vary widely among individuals, with average values around 12-13 mm. In our study, these distances were also found in a similar range.

MF-MC angle: In our study, we evaluated the angulation of the MC with the buccal bone face. With the same method used in our study, Von Arx et al. (2013) reported the mean value of this angle as 46.8º (24.2º–81.3º). As stated in the study of Von Arx et al. (2013), we also found that the mental canal is upward oriented since the mean value in our study was also below 90°. We hypothesize that the higher values in our study may be due to racial differences.

Dental Status

In this study, MF was observed in all individuals. There was no significant difference between the right and left sides and genders in MF visibility according to dental status ($p>0.05$). A significant difference was found between dentulous and endentulous patients in terms of right MF-alveolar crest and left MF-MC angle. It was determined that the MF-alveolar crest distance decreased significantly on the right-side of endentulous patients, and the MF-MC angle parameter was significantly increased, almost 90° on the left side of endentulous patients.

Charalampakis et al. (2017) reported that MF was closer to the alveolar crest than the lower edge of the mandible (mean MF alveolar crest 6.4 mm, mean MF mand. border 12.6 mm) in their study on the edentulous bone mandible. It was also reported that the crest distance was significantly reduced by 0.01 level when the dentulous and edentulous mandibles were compared. Because the differences in the distances in our study were found only unilaterally, new studies should be needed on a larger number of samples in the future.

In this study, there was no significant difference between the right and left sides and genders in MIC visibility according to dental condition. MF-MIC angle on right and left sides was found to be significantly higher in dentulous patients than in endentulous. This suggests that the MIC is more vertically oriented in dentulous individuals. Significant differences were found between dentulous and endentulous patients' right MIC-lingual. This distance was lower in dentulous patients. In the literature, it has been reported that the MIC is larger and more superficial in the alveolar crest in edentulous patients (Caughey et al., n.d.). No study was found in the literature

that evaluated the same parameters in our study according to dental condition.

CONCLUSION

As a result, in this study, when we look at the course and morphological features of the MF and MIC, which includes neurovascular structures in the mandible in Turkish society, although these anatomical structures vary among individuals, it has been observed that the mean values in the Turkish population are similar to the mean values in the literature.

In this study, the most common locations of MF were along the second premolar: the total presence of the MIC was 75.6% in all cases. The most common locations of the endmost point of the MIC were along the first incisive. The length of the left MIC was significantly longer in males.

According to the dental status, visibility of MF was the weakest in edentulous, and MIC presence was similar to MF. The right MF alveolar crest was significantly lower and the left MF-MC angle significantly increased to approximately 90 degrees in edentulous.

ACKNOWLEDGEMENTS

This work was supported by the Istanbul Medipol University Medical Research Council (grant number 2016/12).

REFERENCES

AL-MAHALAWY H, AL-AITHAN H, AL-KARI B, AL-JANDAN B, SHUJAAT S (2017) Determination of the position of mental foramen and frequency of anterior loop in Saudi population. A retrospective CBCT study. *Saudi Dental J*, 29(1): 29-35.

AL-SHAYYAB MH, QABBA'AH K, ALSOLEIHAT F, BAQAIN ZH (2019) Age and gender variations in the cone-beam computed tomographic location of mandibular canal: Implications for mandibular sagittal split osteotomy. *Med Oral Patol Oral Cir Bucal*, 24(4): e545-e554.

ALDOSIMANI MA, ALJARBOU FA, ALTHUMAIRY RI, ALHEZAM AA, ALDAWSARI AI (2019) Analysis of mandibular premolar root position in relation to adjacent cortical plates and mental foramen using cone beam computed tomography in the Saudi population. *Saudi Med J*, 40(3): 298-301.

ALSHAMRANI AS, TOKHTAH RA, AL-OMAR A (2021) Cone-beam computed tomography evaluation of prevalence and location of mandibular incisive canal in patients attending King Saud University Dental Hospital. *J Orthod Sci*, 1-6.

ALYAMI OS, ALOTAIBI MS, KOPPOLU P, ALOSAIMY A, ABDULGHANI A, SWAPNA LA, ALOTAIBI DH, ALQERBAN A, SHEETHI KV (2021) Anterior loop of the mental nerve in Saudi sample in Riyadh, KSA. A cone beam computerized tomography study. *Saudi Dental J*, 33(3): 124-130.

AOUN G, EL-OUTA A, KAFROUNY N, BERBERI A (2017) Assessment of the mental foramen location in a sample of fully dentate lebanese adults using cone-beam computed tomography technology. *Acta Inform Med*, 25(4): 259-262.

APOSTOLAKIS D, BROWN JE (2012) The anterior loop of the inferior alveolar nerve: prevalence, measurement of its length and a recommendation for interforaminal implant installation based on cone beam CT imaging. *Clin Oral Implants Res*, 23(9): 1022-1030.

BELLO SA, ADEOYE JA, IGHILE N, IKIMI NU (2018) Mental foramen size, position and symmetry in a multi-ethnic, urban black population: radiographic evidence. *J Oral Maxillofac Res*, 9(4): e2.

CARRUTH P, HE J, BENSON BW, SCHNEIDERMAN ED (2015) Analysis of the size and position of the mental foramen using the cs 9000 cone-beam computed tomographic unit. *J Endodont*, 41(7): 1032-1036.

CAUGHEY J, DO Q, SHEN D, ... HO-A & C (2021) undefined. (n.d.). Comprehensive review of the incisive branch of the inferior alveolar nerve. *Synapse Koreamed Org*. Retrieved June 15, 2022, from https://synapse.koreamed.org/articles/1148594

CHARALAMPAKIS A, KOURKOUMELIS G, PSARI C, ANTONIOU V, PIAGKOU M, DEMESTICHA T, KOTSIOMITIS E, TROUPIS T (2017) The position of the mental foramen in dentate and edentulous mandibles: Clinical and surgical relevance. *Folia Morphol (Poland)*, 76(4): 709-714.

CHEN Z, CHEN D, TANG L, WANG F (2015) Relationship between the position of the mental foramen and the anterior loop of the inferior alveolar nerve as determined by cone beam computed tomography combined with mimics. *J Comput Assist Tomogr*, 39(1): 86-93.

CHOI DJ, KIM KD, JUNG BY (2019) Location of the mandibular incisive canal related to the placement of dental implants: a case report. *J Oral Implant*, 45(6): 474-482.

DE BRITO ACR, NEJAIM Y, DE FREITAS DQ, SANTOS C DE O (2016) Panoramic radiographs underestimate extensions of the anterior loop and mandibular incisive canal. *Imaging Sci Dentist*, 46(4): 297.

DIREK F, UYSAL II, KIVRAK AS, FAZLIOGULLARI Z, UNVER DOGAN N, KARABULUT AK (2018) Mental foramen and lingual vascular canals of mandible on MDCT images: anatomical study and review of the literature. *Anat Sci Int*, 93(2): 244-253.

DOS SANTOS OLIVEIRA R, RODRIGUES COUTINHO M, KÜHL PANZARELLA F (2018) Morphometric analysis of the mental foramen using cone-beam computed tomography. *Int J Dent*, . 2018: 4571895.

GOYUSHOV S, TÖZÜM MD, TÖZÜM TF (2018) Assessment of morphological and anatomical characteristics of mental foramen using cone beam computed tomography. *Surg Radiol Anat*, 40(10): 1133-1139.

GUNGOR E, AGLARCI OS, UNAL M, DOGAN MS, GUVEN S (2017) Evaluation of mental foramen location in the 10-70 years age range using cone-beam computed tomography. *Niger J Clin Pract*, 20(1): 88-92.

HAAS LF, DUTRA K, PORPORATTI AL, MEZZOMO LA, DE LUCA CANTO G, FLORES-MIR C, CORRÊA M (2016) Anatomical variations of mandibular canal detected by panoramic radiography and CT: a systematic review and meta-analysis. *Dentomaxillofacial Radiol*, 45(2): 20150310.

IWANAGA J, SAGA T, TABIRA Y, NAKAMURA M, KITASHIMA S, WATANABE K, KUSUKAWA J, YAMAKI K-I (2015) The clinical anatomy of accessory mental nerves and foramina. *Wiley Online Library*, 28(7): 848-856.

IWANAGA J, WATANABE K, SAGA T, TABIRA Y, KITASHIMA S, KUSUKAWA J, YAMAKI KI (2016) Accessory mental foramina and nerves: Application to periodontal, periapical, and implant surgery. *Clin Anat*, 29(4): 493-501.

JUODZBALYS G, WANG H-L, SABALYS G (2010) Anatomy of mandibular vital structures. Part I: Mandibular canal and inferior alveolar neurovascular bundle in relation with dental implantology. *J Oral Maxillofac Res*, 1(1): e2.

KABAK SL, ZHURAVLEVA NV, MELNICHENKO YM, SAVRASOVA NA (2017) Study of the mandibular incisive canal anatomy using cone beam computed tomography. *Surg Radiol Anat*, 39(6): 647-655.

KALENDER A, ORHAN K, AKSOY U (2012) Evaluation of the mental foramen and accessory mental foramen in Turkish patients using cone-beam computed tomography images reconstructed from a volumetric rendering program. *Clin Anat*, 25(5): 584-592.

KHAN I, HALLI R, GADRE P, GADRE KS (2011) Correlation of panoramic radiographs and spiral CT scan in the preoperative assessment of intimacy of the inferior alveolar canal to impacted mandibular third molars. *J Craniofac Surg*, 22(2): 566-570.

KHOJASTEPOUR L, MIRBEIGI S, MIRHADI S, SAFAEE A (2015) Location of mental foramen in a selected Iranian population: A CBCT assessment. *Iran Endod J*, 10(2): 117-121.

KUZMANOVIC DV, PAYNE AGT, KIESER JA, DIAS GJ (2003) Anterior loop of the mental nerve: a morphological and radiographic study. *Clin Oral Implants Res*, 14(4): 464-471.

LAM M, KOONG C, KRUGER E, TENNANT M (2019) Prevalence of accessory mental foramina: a study of 4,000 CBCT scans. *Clin Anat*, 32(8):1048-1052.

LI X, JIN Z-K, ZHAO H, YANG K, DUAN J-M, WANG W-J (2013) The prevalence, length and position of the anterior loop of the inferior alveolar nerve in Chinese, assessed by spiral computed tomography. *Surg Radiol Anat*, 35(9): 823-830.

MODI P, ARSIWALLA T (2019) Crocodile tears syndrome. *StatPearls*, 26(2): 167.

PANJNOUSH M, RABIEE ZS, KHEIRANDISH Y (2016) Assessment of location and anatomical characteristics of mental foramen, anterior loop and mandibular incisive canal using cone beam computed tomography. *J Dent (Tehran, Iran)*, 13(2): 126-132.

PEREIRA-MACIEL P, TAVARES-DE-SOUSA E, OLIVEIRA-SALES MA (2015) The mandibular incisive canal and its anatomical relationships: A cone beam computed tomography study. *Med Oral Patol Oral Cir Bucal*, 20(6): e723-e728.

PHILLIPS JL, WELLER RN, KULILD JC (1990) The mental foramen: Part I. Size, orientation, and positional relationship to the mandibular second premolar. *J Endod*, 16(5): 221-223.

POLLAND KE, MUNRO S, REFORD G, LOCKHART A, LOGAN G, BROCKLEBANK L, MCDONALD SW (2001) The mandibular canal of the edentulous jaw. *Clin Anat*, 14(6): 445-452.

PRADOS-FRUTOS JC, SALINAS-GOODIER C, MANCHÓN Á, ROJO R (2017) Anterior loop of the mental nerve, mental foramen and incisive nerve emergency: tridimensional assessment and surgical applications. *Surg Radiol Anat*, 39(2): 169-175.

RAMESH AS, RIJESH K, SHARMA A, PRAKASH R, KUMAR A, et al. (2015) The prevalence of mandibular incisive nerve canal and to evaluate its average location and dimension in Indian population. *J Pharm Bioallied Sci*, *7*(Suppl 2): S594.

ROSA MB, SOTTO-MAIOR BS, DE CARVALHO MACHADO V, FRANCISCHONE CE (2013) Retrospective study of the anterior loop of the inferior alveolar nerve and the incisive canal using cone beam computed tomography. *Int J Oral Maxillofac Implants*, 28(2): 388-392.

SAHMAN H, ERCAN SEKERCI A, SISMAN Y, PAYVEREN M (2014) Assessment of the visibility and characteristics of the mandibular incisive canal: cone beam computed tomography versus panoramic radiography. *Int J Oral Maxillofac Implants*, 29(1): 71-78.

TEJADA CML, CLAUDINO M, AZEVEDO ALANIS LR, MANFRINATO JPL, BERNARDES SR, THOMÉ G, FONTÃO FNGK (2022) Tomographic evaluation of the mandibular nerve in the mental region and its surgical implications: a cross-sectional study. *Int J Oral Maxillofac Surg*, 51(3): 398-404.

VALDEC S, BORM JM, CASPARIS S, DAMERAU G, LOCHER M, STADLINGER B (2019) Vestibular bone thickness of the mandible in relation to the mandibular canal - a retrospective CBCT-based study. *Int J Implant Dent*, 5(1): 37.

VELASCO-TORRES M, PADIAL-MOLINA M, AVILA-ORTIZ G, GARCÍA-DELGADO R, CATENA A, GALINDO-MORENO P (2017) Inferior alveolar nerve trajectory, mental foramen location and incidence of mental nerve anterior loop. *Med Oral Patol Oral Cir Bucal*, 22(5): e630-e635.

VON ARX T, FRIEDLI M, SENDI P, LOZANOFF S, BORNSTEIN MM (2013) Location and dimensions of the mental foramen: A radiographic analysis by using cone-beam computed tomography. *J Endod*, 39(12): 1522-1528.

WONG SK, PATIL PG (2018) Measuring anterior loop length of the inferior alveolar nerve to estimate safe zone in implant planning: A CBCT study in a Malaysian population. *J Prosthet Dent*, 120(2): 210-213.

WORTHINGTON P (2004) Injury to the inferior alveolar nerve during implant placement: a formula for protection of the patient and clinician. *Int J Oral Maxillofac Implants*, 19(5): 731-734.

ZHANG X, XU N, WANG H, YU Q (2017) A cone-beam computed tomographic study of apical surgery--related morphological characteristics of the distolingual root in 3-rooted mandibular first molars in a Chinese population. *J Endod,* 43(12): 2020-2024.

ZMYSLOWSKA-POLAKOWSKA E, RADWANSKI M, LEDZION S, LESKI M, ZMYSLOWSKA A, LUKOMSKA-SZYMANSKA M (2019) Evaluation of size and location of a mental foramen in the Polish population using cone-beam computed tomography. *BioMed Res Int*, 2019: 1659476.

Ubiquity and attribution of Haller cells – A CBCT study

Karthikeya Patil[1], C.J. Sanjay[1], Lakshminarayana Kaiyoor Surya[1], V.G. Mahima[1], Nagabhushana Doggalli[1], Vidya Doddawad[2]

[1] Department of Oral Medicine and Radiology, JSS Dental College and Hospital, JSS Academy of Higher Education and Research, Mysore - 570 015, India

[2] Department of Oral Pathology and Microbiology, JSS Dental College and Hospital, JSS Academy of Higher Education and Research, Mysore - 570 015, India

SUMMARY

With the increasing popularity of sinus surgeries and the prolific advances in imaging technology, there is a major inclination towards the in-depth study of the anatomy of paranasal sinuses and the osteomeatal complex. Anatomical variations like deviation of nasal septum, paradoxical middle turbinate, double middle turbinate, and concha bullosa are seen in routine clinical examinations, but variations like Haller cells and Onodi cells require explicit radiological support. CBCT has the unique advantage of obtaining isometric images in all three planes with 3-Dimensional viewing and circumvent the obscurity of images due to superimposition. CBCT enables detection of even miniscule Haller cells along with discernment into the disease process and is a crucial preoperative planning tool. There has been a dearth of studies in the literature in this regard, and our study is a promising attempt to elucidate the significance of Haller cells with respect to surgical aspects.

Key words: Haller cells – Cone Beam Computed Tomography (CBCT) – Sinus surgery

INTRODUCTION

Haller cells were first identified by Albrecht von Haller (1708–1777) in 1765 and were subsequently named after him (Proetz et al., 1953). The Haller cells are now named infraorbital ethmoidal cells as they are an extension of the anterior ethmoidal cells and are located in the medial orbital floor, medial to the infraorbital canal and lateral to the naso-lacrimal duct.

With the increasing popularity of sinus surgeries and the recent advances in imaging technology, there is a major proclivity towards the detailed study of the anatomy of paranasal sinuses and the osteomeatal complex. It is well known that minor but significant anatomical variations can lead to sinusitis and cause inadvertent complications during endonasal surgeries. One of the notable variations is Haller cells. These Haller cells are seen as incidental findings in a computerized tomography examination of the paranasal sinuses.

The position of Haller cells in the medial portion of the orbital floor, lateral to the maxillary infundibulum below the level of the ethmoidal bulla, places them in a key position to disturb the normal pattern of mucociliary flow and predispose to recurrent maxillary sinusitis (Stammberger et

Corresponding author:
Dr Sanjay CJ, MDS. Reader, Department of Oral Medicine and Radiology, JSS Dental College and Hospital, JSS Academy of Higher Education and Research, Mysore - 570 015, India. Phone: +91 9742565566. E-mail: drsanjaycj_dch@jssuni.edu.in

Submitted: August 24, 2022. **Accepted:** September 10, 2022

https://doi.org/10.52083/SEDM6472

al., 1988; Bolger et al., 1991). Haller cells, though often an incidental finding may trigger different actions, are pathologically important due to the obstruction of the mucociliary drainage from the maxillary sinuses leading to sinusitis. Larger cells can also lead to significant orofacial pain. Several radiographic studies have shown a significant relationship between Haller cells' size (greater than 3 mm) and the incidence of maxillary sinusitis (Kantarci et al., 2004). Extensive knowledge guides the endoscopic surgeon in preventing the grave complication of orbital injury. The strategic location of Haller cells in the infraorbital region can lead to damage to the lamina papyrecae if sufficient caution is not taken. Anatomical variations like deviation of nasal septum, paradoxical middle turbinate, double middle turbinate, and concha bullosa are seen in routine clinical examinations, but variations like Haller cells and Onodi cells require explicit radiological support.

To date, there have been only a few studies recognizing and comparing image quality in Cone Beam Computed Tomography (CBCT) scans with that on Multi slice Computed Tomography (Miracle et al., 2009).

Cadaver and clinical studies have provided the principal evidence for the application of CBCT imaging to endoscopic sinus surgery, concluding that both spatial and soft-tissue contrast were sufficient to aid surgical navigation in the Sino nasal cavity (Rafferty et al., 2005). CBCT has the unique advantage of obtaining isometric images in all three planes with 3-Dimensional viewing and circumvent the obscurity of images due to superimposition.

CBCT enables detection of even miniscule Haller cells along with discernment into the disease process and is a crucial preoperative planning tool. In this regard, there has been a dearth of studies in the past, so our study is an endeavor to elucidate the significance of Haller cells with surgical aspects.

MATERIALS AND METHODS

This is an in-vitro study conducted in the Department of Oral Medicine and Radiology, JSS Dental College and Hospital, JSS Academy of Higher Education and Research, Mysuru.

Purposive sampling was used to collect the sample, and sample size was calculated using the formula n= (z2) P(1-P)/d2, where n = sample size, z = statistic for level of confidence, P = expected prevalence, and d = allowable error. This formula assumes P and d are decimal values, but it would also be correct if they were percentages, with the exception that the term (1-P) in the numerator would become (100-P).

An ethical clearance to conduct the study was obtained from the IEC of the JSS Academy of Higher Education and Research (IEC No 27/2021 dated 13-12-2021).

The source of data collection was done in two parts: prospective and retrospective. The archaic CBCT images satisfying the eligibility criteria were procured from the Department of Oral Medicine and Radiology for the retrospective part.

Data were collected prospectively following the CBCT (in house PLANMECA PROMAX 3D MID) procedure of patients who met the eligibility criteria for their own dental treatment needs at the Department of Oral Medicine and Radiology.

The analysis of the images was carried out by software ROMEXIS VIEWER. The images viewed had a 75micrometer voxel size for a better resolution.

Inclusion criteria:

- CBCT images show the complete maxilla extending from the alveolar bone to the orbit (full face scan and 90mm maxilla scan) with superior diagnostic quality.
- Images were obtained for orthodontic procedures, dental implants, and other maxillofacial indications without a history of maxillary trauma or obvious anomalies clinically.
- Images procured for orofacial pain suggestive of chronic sinusitis.

Exclusion criteria:

- Subjects and images of subjects younger than 18 years of age are not involved, as the sinuses are not completely developed.

- Subjects with midfacial anomalies, previous trauma, and surgeries of the midface
- Images which are not of optimum quality
- Presence of artefacts
- Images which do not show the area of interest clearly

Selected CBCT images were evaluated in coronal and axial views for detecting the Haller cell morphology and in parasagittal views for identifying the type of the cells. The visibility, location, laterality, and type of Haller cell were examined by an expert Oral & Maxillofacial Radiologist twice, and an average of the two was considered to avoid intra-examiner variability.

The types of morphology variation of Haller cell were classified as:

- Small < 2mm
- Medium 2 to 4mm
- Large > 4mm in size

Based on the internal arrangement, they were divided into:

- Unilocular
- Multilocular

A mean and standard deviation were employed for the evaluation of continuous data and a percentage proportion for categorical data. Statistical evaluation was considered by using the Chi-square test for categorical data and the student test for continuous data at a 95% confidence interval. P values of less than 0.05 were considered significant. SPSS version 22 was employed for the computation of data.

CBCT images were then analysed for the presence of Haller cells (infraorbital ethmoid cells).

However, there is as yet no general definition of the so-called Haller cell (Bolger et al., 1991). In our study, we followed the definition of Haller cells specified by Simeunovic (2008): “Ethmoid air cells that advance in the orbital floor or the roof of the maxillary sinus, respectively, as far as the vicinity of the maxillary ostium, which may build the lateral wall of the infundibulum.” We did not include cells located in the infundibulum or formations originating from posterior ethmoid cells, which are categorized as Onodi cells.

The Onodi cell first described by Adolf Onodi in 1904 is a posterior ethmoid cell that lies superior to the sphenoid sinus, and is in close proximity to at least one optic nerve or internal carotid artery (ICA). This close proximity of the Onodi cell and ICA is a risk factor for surgical complications (Yoshida et al., 2005).

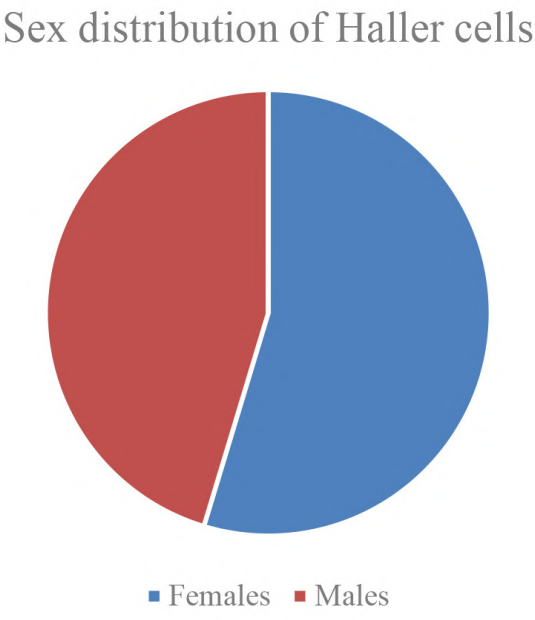

Fig. 1.- Sex distribution of Haller cells.

RESULTS

Out of 139 patients included in our study, 76 (54.6%) were females and 63 (45.4%) were males (Fig. 1), with ages ranging from 20 to 70 years of age with a mean age of 32.3 years.

Haller cells were present in 2 (2.8%) in up to 20yrs of age, 47 (64.5%) in 21-30 years, 6 (8.3%) in 31-40 years, 8 (10.8%) in 41-50, 8 (10.8%) in 51-60 years, 2 (2.8%) in 61-70 years of age group (Table 1, Fig. 2).

Table 1. Age wise distribution of Haller cells.

Years	Males	Females	Total
Up to 20	1	1	2 (2.8%)
21 - 30	21	26	47 (64.5%)
31 - 40	4	2	6 (8.3%)
41 - 50	6	2	8 (10.8%)
51 - 60	2	6	8 (10.8%)
61 - 70	0	2	2 (2.8%)
Total	**34**	**39**	**73**

Haller cells were identified in 73 (52.5%), being unilateral on right side in 24 (17.3%), left side in 25 (17.9%) and bilateral in 24 (17.3%) of the cases (Table 2).

Table 2. Laterality of Haller cells.

Unilateral (Right)	24 (17.3%)
Unilateral (Left)	25 (17.9%)
Bilateral	24 (17.3%)

The pattern of Haller cells was found to be bilateral and unilateral. In certain instances, the locularity varied in the bilateral occurrence of cells which was statistically considered as a separate entity and tabulated.

Unilateral unilocular pattern of Haller cell was more common seen in 22 (22.7%) on right side, 24 (24.8%) on left side, followed by bilateral unilocular in 18 (18.6%) on right side, bilateral unilocular in 17 (17.6%) on left side, bilateral multilocular on right side in 6 (6.2%), bilateral multilocular on left side in 7 (7.2%). The least common type of cells was unilateral multilocular on right side in 2 (2%) and unilateral multilocular on left side in 1 (1%) (Table 3, Fig. 3). The mean diameter of the Haller cells is 4.52+/-2.79 mm.

Table 3. Pattern of Haller cells.

Unilateral Unilocular Right	22 (22.7%)
Unilateral Unilocular Left	24 (24.8%)
Bilateral Unilocular Right	18 (18.6%)
Bilateral Unilocular Left	17 (17.6%)
Bilateral Multilocular Right	6 (6.2%)
Bilateral Multilocular Left	7 (7.2%)
Unilateral Multilocular Right	2 (2%)
Unilateral Multilocular Left	1 (1%)

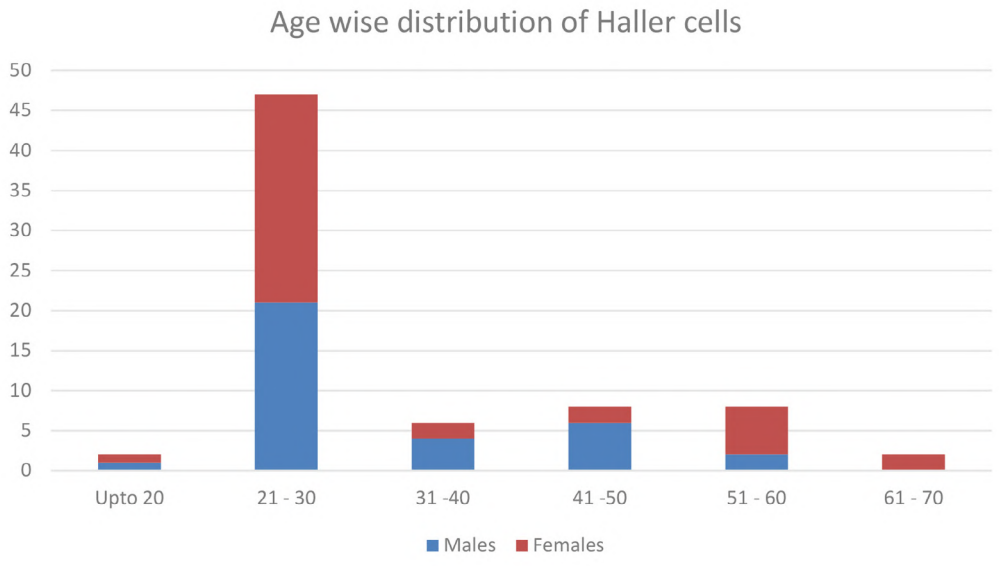

Fig. 2.- Age wise distribution of Haller cells.

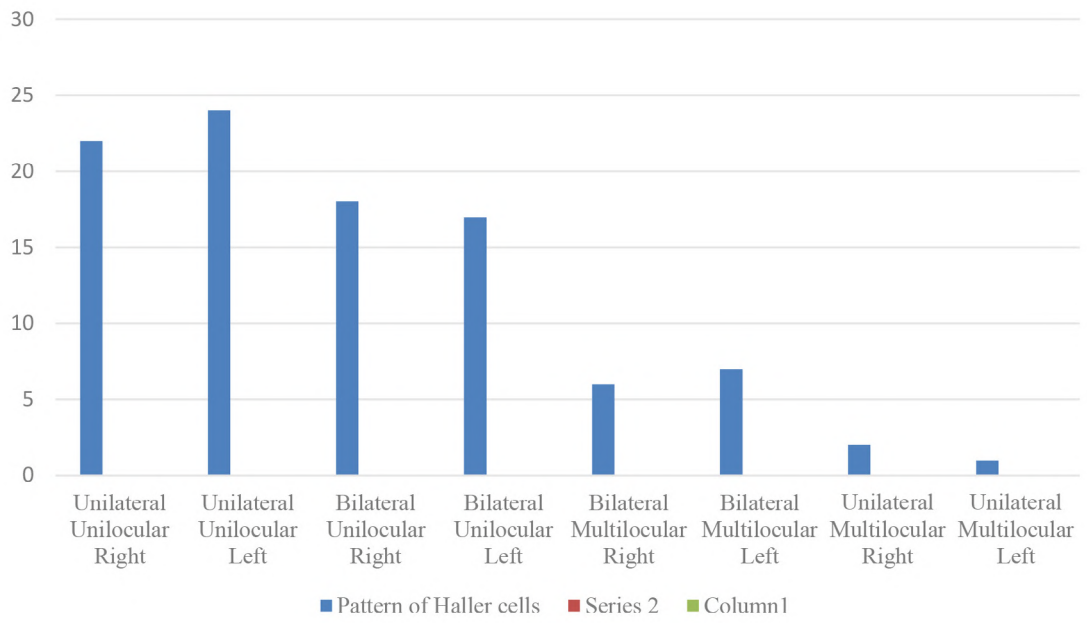

Fig. 3.- Pattern of Haller cells.

DISCUSSION

The ethmoid bone is an intricate bone consisting of a cribriform plate, a median perpendicular ethmoid plate, and two ethmoidal labyrinths. The ethmoidal labyrinths have a varied level of pneumatization, forming the anterior and posterior ethmoidal cells. The variations of ethmoidal cells occur when there is an extension into the surrounding paranasal sinuses. The most important and common variety is the extension into the maxillary sinus, forming the Haller cells.

According to the literature in English, the prevalence of Haller cells is remarkably variable, ranging from 2.7% to 45.1% (Bolger et al., 1991; Perez-Pinas, 2000). This enormous variability in the frequency of Haller cells is probably owing to the inconsistency in the definition of Haller cells. Kennedy and Zinreich (1988) considered Haller cells as ethmoid cells projecting below the ethmoid bulla within the orbital floor in the region of the opening of the maxillary sinus. Bolger et al. (1991) defined Haller cells as any cell located between the ethmoid bulla, the orbital lamina of the ethmoid bone, and the orbital floor. Kainz et al. (1993) recognized Haller cells as cells within the orbital floor.

The variability in the prevalence of Haller cells could also be explained on the basis of the patients' age group and race, and on the imaging techniques used (Rysz et al., 1993).

In our study, we have included the criteria by Mathew et al. (2013), who considered the distinction between the Haller cells and the infraorbital recess of the maxillary sinus (Fig. 4). The prevalence of Haller cells was high in our study population (52.52%). It is comparable to the studies of Mathew et al. (2013). A retrospective study done by Kamdi et al. (2018) revealed a prevalence of 49.5%. The higher incidence of Haller cells in our study is probably due to the advanced technique and interpretation of CBCT.

The CBCT facilitates identification of Haller cells as minute as 1mm, as the slice thickness of the scan is around 0.4 to 0.66 mm. The volumetric analysis of CBCT enables the identification of Haller cells of any size. In contrast, it is not feasible in other radiographs or with multi-slice computed tomography. In our study, we are emphasizing the usefulness of CBCT in the detection and analysis of Haller cells. The higher number of females included in the study could be attributed to a larger proportion of females visiting the department due to increased awareness about dental hygiene and aesthetic purposes. It can also be attributed to willingness for extensive evaluation and treatment.

In our study, the male to female prevalence ratio was 1:1.20. There was no statistical significance between the prevalence of Haller cells in both groups. This was consistent with the results obtained by Kamdi et al. (2018). A study done by Raina et al. (2012) indicated a male-to-female ratio of 1.46:1 for the presence of Haller cells.

The distribution of Haller cells with respect to gender was not statistically significant (Raina et al., 2012). We also noticed a female preponderance in our study, but the ratio was not statistically significant.

The prevalence of Haller cells was the highest (53.25%) in 82 patients in the 21-30 age group, followed by 31 (20.13%) in the 31-40 age group. It is similar to the study done by Kamdi et al. (2018) on 16-25 years of age. The similarities and differences in the occurrence of Haller cells in this age group can be attributed in the maximum number of subjects included in the study.

Our study concluded that the unilateral occurrence of Haller cells was appreciated in 24 on Right side and 25 on Left side, summing up to 49 (35.2%) than in 24 (17.3%) bilateral occurrences. Haller cells were more frequently detected on the left than the right (statistically no significance noted).

Study by Kamdi et al. (2018) showed a preponderance of cells on the right side. The same result was noted by Ahmed et al. (2006) on panoramic radiographs. There is no clinical significance to the locularity of the Haller cells, though we recommend detailed investigation into this aspect.

In the study performed by Alkire et al. (2010), the authors compared the impact of septal deviation, concha bullosa, and Haller cells on the occurrence of rhinosinusitis. They concluded that only the obstruction caused by Haller cells was statistically relevant to the development of this pathologic condition. Septal deviation and concha bullosa are easily detected during routine clinical examinations or diagnostic nasal endoscopies.

The most important presence of Haller cells cannot be detected by any other method except radiologically. Therefore, a study on this aspect is emphasized.

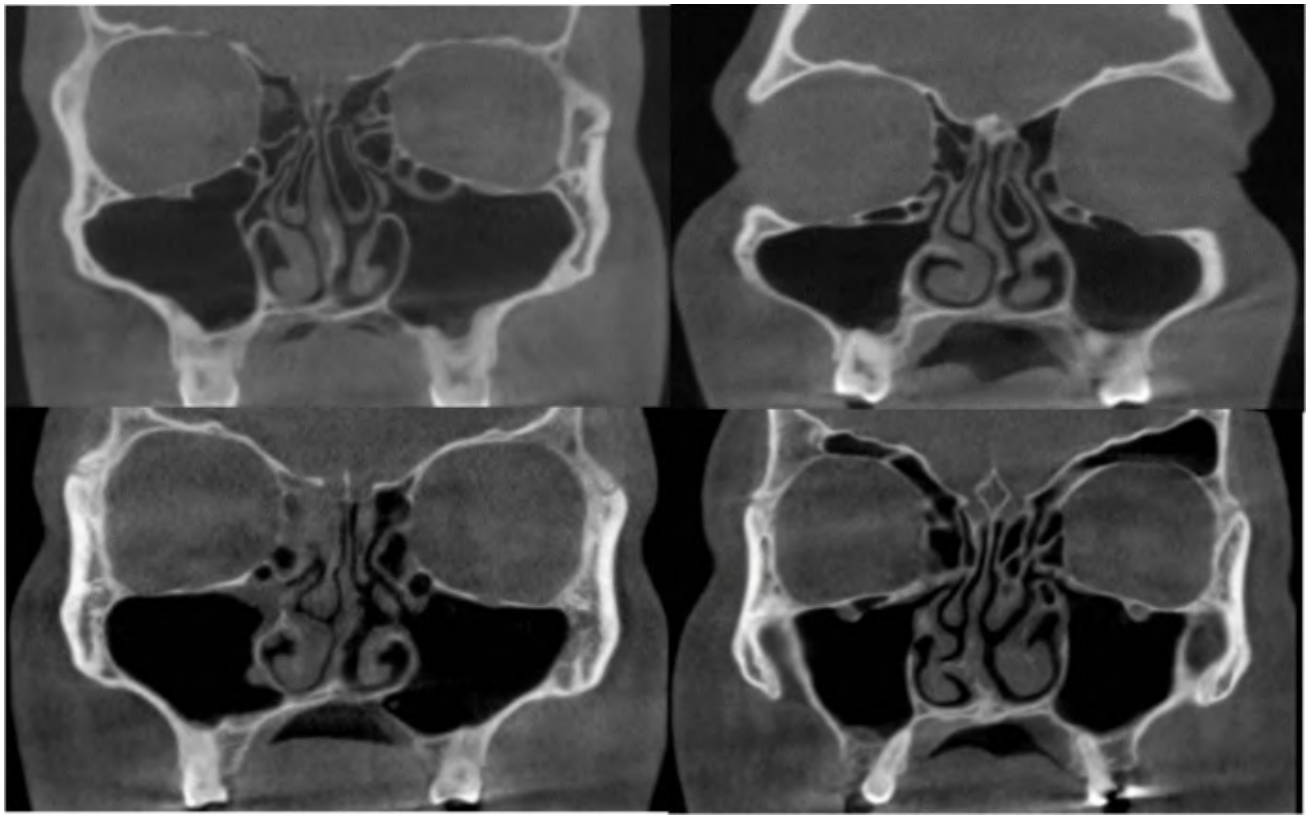

Fig. 4.- Variable presentation of Haller cells in our study on CBCT.

The presence of infraorbital ethmoidal (Haller) cells can increase the risk of orbital injury during ethmoidectomy (Nouraei et al., 2009). Functional Endoscopic Sinus Surgery (FESS) is the primary approach used today for the surgical treatment of chronic sinusitis. Diagnosis of Haller cells, however, is difficult in endoscopy due to their lateral location (Choi, 2020). Failure to recognize the Haller cell also increases the risk of orbital injury during ethmoidectomy (Nouraei et al., 2009). Orbital injury is one of the most dreaded complications of FESS. Lamina papyracea, being a paper-thin bone, is more prone to injury. The close proximity of Haller cells makes adequate knowledge important in such situations. Orbital injury can range from post-operative periorbital oedema, which can be treated conservatively, to injury to the Lateral Rectus muscle causing gaze palsy, which has a grim prognosis.

Hammad and Gomaa (2012) evaluated the role of some anatomical nasal abnormalities (deviated nasal septum, concha bullosa, and Haller cell) in rhinogenic headache, vacuum headache, and pressure headache. They proposed that, as a main cause of referred headache, Haller cells can occupy the infundibulum or be associated with another anatomical variation, such as concha bullosa, and can predispose to sinusitis. In the absence of sinusitis, it might block the sinus drainage pathway, resulting in sinus Mal ventilation, Vacuum headache, and Pressure headache.

CONCLUSION

Haller cells are a clinical entity which, in spite of being a common occurrence, has not been extensively considered. In view of its significant association with the cause of orofacial pain, maxillary sinusitis, a detailed study is a pressing priority. With the advanced techniques of CBCT it is plausible to have a detailed study of Haller cells. Our study is a forthright attempt to illuminate the detailed prevalence of the cells, their laterality, and their association with sinusitis. The study aims at forewarning the surgical personnel to plan intervention and foresee untoward complications.

Notes:

Ethical approval for the procedures performed in studies involving human participants were in conformity with the ethical standards of the institutional and /or national research ethical committee. The study strictly adhered to the 1964 Declaration of Helsinki and later amendments. Informed consent was taken from all individual participants who were included in the study voluntarily.

REFERENCES

AHMAD M, KHURANA N, JABERI J, SAMPAIR C, KUBA RK (2006) Prevalence of infraorbital ethmoid (Haller's) cells on panoramic radiographs. *Oral Surg Oral Med Oral Pathol Oral Radiol Endodontol*, 101(5): 658-661.

ALKIRE BC, BHATTACHARYYA N (2010) An assessment of sinonasal anatomic variants potentially associated with recurrent acute rhinosinusitis. *Laryngoscope*, 120(3): 631-634.

BOLGER WE, PARSONS DS, BUTZIN CA (1991) Paranasal sinus bony anatomic variations and mucosal abnormalities: CT analysis for endoscopic sinus surgery. *Laryngoscope*, 101(1): 56-64.

CHOI JH (2020) Hypoesthesia of midface by isolated Haller's cell mucocele. *Brazil J Otorhinolaryngol*, 86: 516-519.

HAMMAD MS, GOMAA MA (2012) Role of some anatomical nasal abnormalities in rhinogenic headache. *Egypt J Ear Nose Throat Allied Sci*, 13(1): 31-35.

KAINZ J, BRAUN H, GENSER P (1993) Haller's cells: morphologic evaluation and clinico-surgical relevance. *Laryngo-rhino-otologie*, 72(12): 599-604.

KAMDI P, NIMMA V, RAMCHANDANI A, RAMASWAMI E, GOGRI A, UMARJI H (2018) Evaluation of Haller cell on CBCT and its association with maxillary sinus pathologies. *J Indian Acad Oral Med Radiol*, 30(1): 41.

KANTARCI M, KARASEN RM, ALPER F, ONBAS O, OKUR A, KARAMAN A (2004) Remarkable anatomic variations in paranasal sinus region and their clinical importance. *Eur J Radiol*, 50(3): 296-302.

KENNEDY DW, ZINREICH SJ (1988) The functional endoscopic approach to inflammatory sinus disease: current perspectives and technique modifications. *Am J Rhinol*, 2(3): 89-96.

MATHEW R, OMAMI G, HAND A, FELLOWS D, LURIE A (2013) Cone beam CT analysis of Haller cells: prevalence and clinical significance. *Dentomaxillofac Radiol*, 42(9): 20130055.

MIRACLE AC, MUKHERJI SK (2009) Conebeam CT of the head and neck, part 2: clinical applications. *Am J Neuroradiol*, 30(7): 1285-1292.

NOURAEI SAR, ELISAY AR, DIMARCO A, ABDI R, MAJIDI H, MADANI SA, ANDREWS PJ (2009) Variations in paranasal sinus anatomy: implications for the pathophysiology of chronic rhinosinusitis and safety of endoscopic sinus surgery. *J Otolaryngol Head Neck Surg*, 38(1): 32.

PEREZ-PINAS I, SABATE J, CARMONA A, CATALINA-HERRERA CJ, JIMENEZ-CASTELLANOS J (2000) Anatomical variations in the human paranasal sinus region studied by CT. *J Anat*, 197(2): 221-227.

PROETZ AW (1953) Essays on the applied physiology of the nose 2nd ed. Annals Publishing Co., St. Louis.

RAFFERTY MA, SIEWERDSEN JH, CHAN Y, MOSELEY DJ, DALY MJ, JAFFRAY DA, IRISH JC (2005) Investigation of C-arm cone-beam CT-guided surgery of the frontal recess. *Laryngoscope*, 115(12): 2138-2143.

RAINA A, GULEDGUD MV, PATIL K (2012) Infraorbital ethmoid (Haller's) cells: a panoramic radiographic study. *Dentomaxillofac Radiol*, 41(4): 305-308.

RYSZ M, BAKOŃ L (2009) Maxillary sinus anatomy variation and nasal cavity width: structural computed tomography imaging. *Folia Morphol*, 68(4): 260-264.

SIMEUNOVIC G (2008) Über die Hallersche Zelle (Cellula ethmoidalis infraorbitalis) von der Entdeckung bis zur heutigen klinischen Relevanz [Dissertation]. Bern Universität, Med. Fakultät.

STAMMBERGER H, WOLF G (1988) Headaches and sinus disease: the endoscopic approach. *Ann Otol Rhinol Laryngol*, 97(5 suppl): 3-23.

YOSHIDA K, WATAYA T, YAMAGATA S (2005) Mucocoele in a Onodi cell responsible for acute optic neuropathy. *Br J Neurosurg*, 19: 56.

Cadherins and catenins as a novel theoretical mechanism in a polyorchid cadaver

Jack D. Walsh[1A], Ernest F. Talarico, Jr.[2B,3C], Joseph G. Castaneda[3C], Sana M. Wahab[3C], Katelyn M. Paulus[3C], Amy E. Stromberg[3C], Victoria N. Olson[3C], Griffin D. Hall[4D], Paul J. Janus[3C], Nicholas R. Rocco[5E]

[1] Department of Chemistry, [2] Department of Anatomy, [3] Department of Biology, [4] College of Pharmacy, [5] Department of Urology

[A] Georgia Institute of Technology, Atlanta, Georgia, USA

[B] Tan Tao University School of Medicine, Long An Province, Việt Nam

[C] North Park University, Chicago, Illinois, USA

[D] Roosevelt University, Chicago, Illinois, USA

[E] United States Naval Hospital Guam, Agana Heights, Guam, USA

SUMMARY

Polyorchidism is a rare congenital disorder defined as the presence of more than two testicles for which the underlying etiology is unknown. Prior research in this laboratory suggested a new anatomical-functional description for polyorchidism of Type 3 Subgroup B, or supernumerary testis (SNT) attached to the draining epididymis and vas deferens without reproductive potential and SNT located outside the scrotal sac. The purpose of the current investigation was to examine the mechanism underlying the role(s) of cadherins and catenins in the development of polyorchidism using genomic analysis of a cadaveric polyorchid. Formyl Fix Paraffin Embedded tissue samples of a SNT from a 96-year-old polyorchid were prepared using the Accel-NGS 2S Plus DNA Library Kit for whole exome sequencing (*Integrated DNA Technology*, Coralville, IA). Paired end sequencing was carried out using the Illumina NovaSeq 6000 system (*Illumina*, San Diego, CA) using 150 bp reads to an average depth of coverage of 44x. BLAST was used to analyze and compare the SNT sequence to reference genomes in the NCBI database. Sequence analysis of the SNT showed two missense mutations that resulted in single nucleotide variants (SNV) within exons of the N-Cadherin gene (CHD2), NT 23, T to C (Leu 8 to Pro) and NT 2441, A to G (Asn 845 to Ser), respectively. A mutation in the Desmocollin 2 (DSC2) gene was also demonstrated; NT 2393, G to A. The present research suggests a novel biomolecular mechanism based on N-Cad and p120 catenin underlying the development of polyorchidism with application to supernumerary organs in other systems and to metastasis of neoplasms.

Key words: Anatomy – Cadherin – Catenin – Congenital disorder – Genome – Polyorchid – Polyorchidism – Supernumerary – Testes – Testicle

Corresponding author:
Jack D. Walsh. Doctoral Candidate, School of Chemistry and Biochemistry, Georgia Institute of Technology, 901 Atlantic Drive, NW Atlanta, Georgia 30332, USA. E-mail: jwalsh67@gatech.edu
Paul J. Janus, Ed.D. Anatomy and Biology Instructor, Department of Biology, North Park University, 3225 West Foster Avenue, Chicago, Illinois 60625-4895 USA. E-mail: pjjanus@northpark.edu

Submitted: August 2, 2022. **Accepted:** September 20, 2022

https://doi.org/10.52083/TKWN4852

ABBREVIATIONS

Adenine (A)

Adhesion Junction/Adhesion Junctions (AJ/AJs)

Amino Acid (AA)

Cytosine (C)

Epithelial-Cadherin (E-Cad)

Epithelial-to-mesenchymal transition (EMT)

Guanine (G)

Juxtamembrane domain (JMD)

Leucine (Leu)

National Center for Biotechnology Information (NCBI)

N-Cadherin/Cadherin 2 gene (CDH2)

Neural-Cadherin (N-Cad)

Nucleotide (NT)

Phenylalanine (Phe)

Premoridal Germ Cells (PGCs)

Proline (Pro)

Sex-Determining Region Y (SRY)

Single Nucleotide Variants (SNV)

SRY-Box Transcription Factor 9 (SOX9)

Supernumerary Testis/Testes (SNT/SNTs)

Supernumerary Testis/Testes (ST/STs)

Testis-Determining Factor (TDF)

Testis-Specific Enhancer (TESCO)

Thymine (T)

INTRODUCTION

Polyorchidism is a rare congenital disorder where more than two testicles develop. In 1880, the first histological finding of polyorchidism was found, and in 1895, the first clinical case was confirmed (Lane, 1895; Artul and Habib, 2014; Hassan et al., 2008; Hassan et al., 2014). There are fewer than 200 human cases reported in medical literature. In addition, seven documented cases exist in the animal kingdom: two horses, two dogs, two cats, and a hummingbird (Roca-Ferrer et al., 2015; Tamminen et al., 2012; Witt and Bautista, 2011; Aziz et al., 2016; Talarico et al., 2022). In human polyorchids, diagnosis in patients ranges from 4 weeks to 75 years in age with a median age of 17 years (Mathur et al., 2002; Bergholz, 2009; Mittal et al., 2018; Talarico et al., 2022).

Patients with polyorchidism typically do not present with pain or other discomfort on clinical evaluation. However, if pain is present, it is localized to the scrotum/lower abdomen or the region to where the mass is found (Dollard, 2011; Sakamaoto et al., 2007; Mittal et al., 2018; Otero, 2016). Ultrasound and magnetic resonance imaging can differentiate between polyorchidism and paratesticular lesions (i.e., inguinal lipoma, etc.) (Arslanoglu, 2013). Occasionally, there are some additional abnormalities seen in polyorchids that include testicular maldescent (40%), inguinal hernia (30%), testicular torsion (13%), hydrocele (9%), and malignancy (6%) (Mathur et al., 2002; Tonape et al., 2012; Talarico et al., 2022). Furthermore, polyorchidism is associated with an increased risk of testicular cancer (Talarico et al., 2018; Bergholz et al., 2009).

In the majority of polyorchid cases, the supernumerary testis (SNT) or testes (SNTs) are located on the left side with a 3:1 ratio (left > right) (Sheah et al., 2004). SNTs are typically smaller than the two normal testes (Artul and Habib, 2014; Cohen et al., 2017; Talarico et al., 2022). Prior research has shown that inguinal SNTs without reproductive potential tend to be infiltrated with adipose tissue with increased patient age (Talarico et al., 2022). This has led to the suggestion of a novel anatomical-functional classification in polyorchidism, Type 3, Subgroups A and B (Talarico et al., 2022).

The mechanism(s) of polyorchidism is unknown, but it is hypothesized to result from a malfunction or duplication of the gonadal ridge during embryological development, possibly involving molecular or genetic factors that predispose a patient to developing SNTs.

In embryology, the gonadal ridge is the precursor to the gonads. The gonadal ridge forms during the beginning of testicular development, and is derived from intermediate mesoderm. It is known that its formation is initiated by coelomic epithelial cells on the mesonephros (Yang et al., 2018; Avellar et al., 2019). The Wolffian duct is found in the mesonephros, which contributes to the formation of the epididymis, vas deferens, and seminal vesicles (Yang et al., 2018; Avellar et al., 2019).

From a molecular perspective, the cells of male embryos have an X and a Y chromosome. The sex-determining region of the Y chromosome (Yp11) is composed in part of the sex-determining region Y (SRY) gene that encodes for testis-determining factor (TDF) (Cox, 2013; Hoare et al., 2021). In the absence of the SRY gene, the resulting embryo will be female. SRY encodes for the transcription factor that activates the testis-specific enhancer (TESCO) of SRY-Box Transcription factor 9 (SOX9), which is responsible for the differentiation of the Sertoli cells (Fig. 1) (Albrecht et al., 2001). In addition, Sertoli cells are required for testis formation and spermatogenesis. These cells have both endocrine and paracrine roles in spermatogenesis (Iliadou et. al., 2015). Steroidogenic Factor 1 also contributes to the differentiation of Sertoli cells and is encoded by the Nuclear Receptor Subfamily 5 Group A Member 1 (NR5A1) gene (Fig. 1) (Sekido et al., 2008). SOX9 levels are unregulated by SRY. When cellular and tissue levels of SRY and SOX9 reach a sufficient threshold in the genital ridge, SOX9 upregulation causes the development of Sertoli cells (Warr et al., 2012). This initiates morphological changes leading to the development of testicular tissue and incorporation of gametes from the yolk sac in the mature testis (Fig. 1) (Warr et al., 2012).

With reference to Fig. 1 and testicular genesis, it is important to note that the absence of the SRY gene (or presence of an X chromosome instead of a Y chromosome) discussed above differs from Swyer Syndrome (Ostrer, 2019). Swyer syndrome occurs due to mutations of the SRY gene or deletion of the segment of the Y chromosome containing the SRY gene (i.e., SRY gene plus additional gene/ partial gene sequence). In either case, there is no development of Sertoli cells (Fig. 1) and no production of testosterone. The resulting embryo will be phenotypically female with bilateral streak gonads (infertile), but is genetically male. Thus, most of these patients present clinically as "young females" with delayed puberty/amenorrhea (Ostrer, 2019).

Presently, there are several theories regarding the development of polyorchidism. The most widely accepted theory suggests that during development, aspects of mesonephric sections accountable for development of the gonads undergo degeneration or duplication (Yamamoto et al., 2015; Lawrentschuk et al., 2013). When incomplete division occurs, incomplete polyorchidism (i.e., bilobed testicle) is the consequence (Bergholz and Wenke, 2009). *Thus, the question arises, "What molecular or genetic mechanism(s) play roles in the genesis of polyorchids?"*

Is it reasonable to suggest that cadherins (i.e., adhesion proteins) may be involved in polyorchidism? Cadherins are a superfamily of approximately 123 cell adhesion proteins that create linkages to adjacent cells through

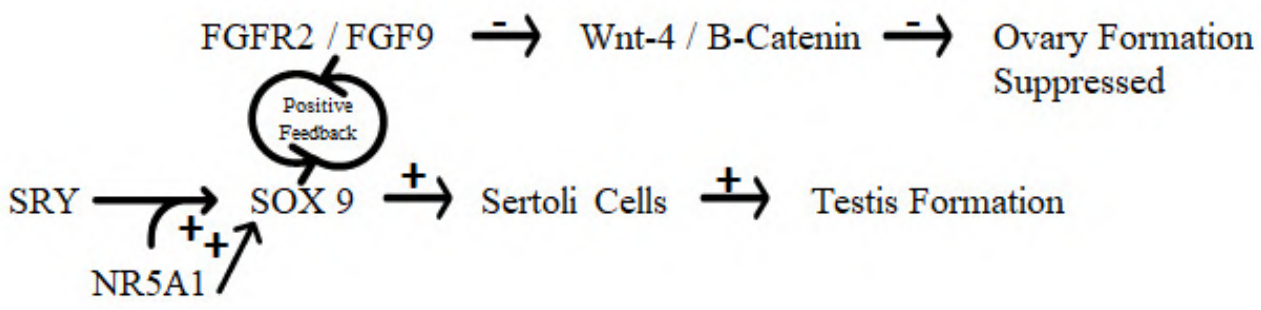

Fig. 1.- Genetic Factors Involved in Testes Development. The Sex-Determining Region Y (SRY) gene encodes for the transcription factor that activates SRY-BOX Transcription Factor 9 (SOX 9). SOX 9 is responsible for the differentiation of the Sertoli cells. Sertoli cells are required for testis formation and spermatogenesis. Nuclear Receptor Subfamily 5 Group A Member 1 (NR5A1) is necessary for functional maturation of Sertoli cells (Kato et al., 2012). The SOX 9 and the positive feedback loop for Fibroblast Growth Factor 9 (FGF9)/ Fibroblast Growth Factor 9 (FGFR2) not only stimulates Sertoli cells but also inhibits β-catenin and Wingless-Type MMTV Integration Site Family Member 4 (WNT-4) which, if uninhibited, would lead to the formation of ovaries. [Abbreviations: Increased expression (+); Decreased expression (-); Sex-Determining Region Y (SRY); SRY-BOX Transcription Factor 9 (SOX 9); Nuclear Receptor Subfamily 5 Group A Member 1 (NR5A1); Fibroblast Growth Factor 9 (FGF9); Fibroblast Growth Factor Receptor 2 (FGFR2); Wingless-Type MMTV Integration Site Family Member 4 (WNT-4)].

extracellular domains (Maître and Heisenberg, 2013). Originally discovered by Masatoshi Takeichi in 1977 (Takeichi, 1977) while studying calcium-dependent cell adhesion in hamster lung tissue samples, cadherins are classified into distinct groups (Table 1). The most studied cadherins are Type I, or classical cadherins, including epithelial-cadherin (E-cadherin, E-Cad) and neural-cadherin (N-cadherin, N-Cad) (Piprek et al., 2019a, 2019b; Piprek et at., 2020).

To achieve cell-to-cell binding, the extracellular regions of cadherin molecules composed of five or six domains (Fig. 2A) connect to opposing domains of cadherin on adjacent cells (Fig. 2B). These extracellular domains are linked to an intracellular domain by a transmembrane region. The intracellular (or cytoplasmic) domain interacts with intracellular p120, β-catenin, α-catenin (Shapiro and Weis, 2009). Then, α-catenin binds to F-actin filaments (Shapiro and Weis, 2009).

Two first extracellular domains (EC1) from either cell come together and attach through homophilic binding, with the recognition and selectivity of the opposing cadherin mediated by the Histidine-Alanine-Valine motif (Piprek et al., 2020). The binding takes place primarily through two interactions (Fig. 2). EC1s of both cadherins interact with conserved tryptophan residues and into conserved hydrophobic pockets of the opposing cadherin in a *trans* configuration, which are then further stabilized when docked. It is proposed that the *trans* configuration is characterized by creating a "zipper confirmation" bringing two cells together through the *trans* attachment of the cadherins. This zipper causes an antagonistic tension to the surface tension of the cell, causing easier cell-cell contact (Maître and Heisenberg, 2013). Additionally, the second extracellular domain (EC2) asymmetrically attaches to EC1 of a lateral partner cadherin through a *cis* configuration, allowing further stabilizing a "cluster" or bundle of cadherins for

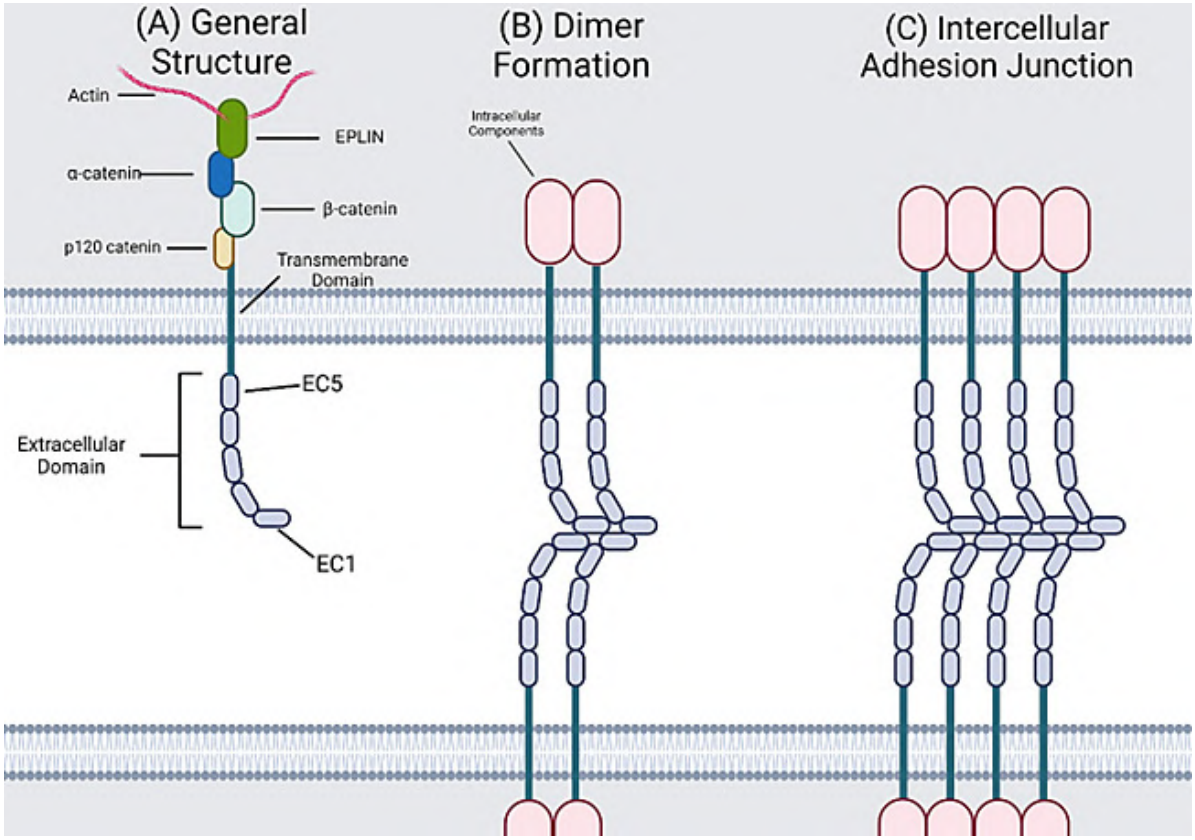

Fig. 2.- General Structure and Interactions of Cadherins. **(A)** General structure of the cadherin protein showing extracellular repeats 1-5 (EC1-EC5) with p120 catenin and beta catenin bound to the intracellular domain, α-catenin bound to β-catenin, and EPLIN facilitating connection between alpha catenin and actin. **(B)** the formation of a cadherin dimer showing to laterally adjacent cadherins interacting with each other and two similar cadherins on opposing molecules in cis conformation. **(C)** Eight cadherins representing a cluster of cadherin complexes forming strong AJs. [Abbreviations: Extracellular repeat (EC); Epithelial Protein Lost In Neoplasm (EPLIN)].

Table 1. Classification of Cadherins, Origins and Associated Systems/Tissues*.

Classification/ Grouping	Cadherin	Origin of Discovery	Associated Tissue
Classical Cadherins			
Type I	E-Cadherin (CDH1)	V79 hamster lung cell line	Various epithelia: lung, immune, salivary, liver, gallbladder, gastrointestinal, endocrine (excluding adrenal), bladder, and reproductive (male & female, excluding ovary)
	N-Cadherin (CDH2)	Neuronal Cells	Neurons (central & peripheral nervous system), cardiac (intercalated discs), thymic epithelium, salivary gland (myoepithelial cells), liver (hepatocytes), gastrointestinal (stomach parietal cells), pituitary (pars intermedia, anterior/posterior lobe), pancreas (islet cells), kidney (proximal tubule), testes (seminiferous epithelium), mammary gland, ovary, oviduct
Type II	P-Cadherin (CDH3)	Mouse embryo, extra-embryonic ectoderm	Placenta, uterine decidua
	R-Cadherin (CDH4)	Chicken retina	Neurons and glial cells
	M-Cadherin (CDH5)	Myogenic mouse cells	Muscle (myoblasts and myotubules)
	T-Cadherin (CDH13)	White adipose tissue	Adipose tissue
	Cadherin 12/BR-Cadherin	Neuronal Cells	Neurons
Desmosomal Cadherins	Desmogliens 1-3	Epidermis	Integument; desmosome containing tissues
	Desmocollins 1-3	Variable tissue origin	Complex stratified tissues
Protocadherins	Pcdh1, Pcdh-2, Pcdh3	Mouse nerve tissue	Neural tissues; neuroblastoma cell lines
ST-Cadherin	HPT-1	Gastrointestinal tract	Liver and intestine; pancreas

*(Amagai and Stanley, 2012; Bornemann and Schmalbruch, 1994; Delva et al., 2009; Gao et al., 2021; Inuzuka et al., 1991; Nose et al., 1986; Pancho et al., 2020; Raya-Sandino et al., 2021; Takeichi, 1977; Yamauchi et al., 2014)

the adhesion process (Fig. 2C) (Harrison et al., 2011). These cadherins contribute to several processes within development, ranging from cell and tissue formation, cancer cell development, as well as helping various signaling pathways (Piprek et al., 2019a, 2019b; Piprek et at., 2020).

E-Cads direct Primordial Germ Cells (PGCs) as they move to the gonadal ridge under controlled expression. Once these cells reach their destination at the gonadal ridge, E-Cad and N-Cad interact heterophillically from the PGCs and the surrounding somatic cells, respectively. In the gonadal ridge, coelomic epithelial cells will undergo the process of epithelial-to-mesenchymal transition (EMT), during which they reduce cadherin expression in favor of less adhesion and promotion of migration (Piprek et al., 2019a, 2019b; Piprek et at., 2020).

The purpose of the present research is to investigate the mechanism underlying the role(s) of cadherins and catenins in the development of polyorchidism using genomic analysis of a cadaveric polyorchid.

MATERIALS AND METHODS

Cadaveric Material

With the consent given from the Anatomical Gift Association of Illinois, the study was conducted on a 96-year-old male cadaver at the Advanced Human Cadaver Laboratory at North Park University (Chicago, Illinois, USA). The anatomical donor was embalmed on October 18, 2019, and prosection began on August 27, 2020. Medical history and hospital records were unavailable. Throughout the study, procedure for care and use were performed in accordance with both state and federal guidelines.

Tissue Preparation

STs and SNTs were excised from the cadaver and placed into trays which were then moved to a labeled tissue cassette. As previously described in Talarico et al. (Talarico et al., 2022), increments of 5 x 5 mm, sagittal sections of the left and right ST and SNTs were obtained using a No. 22 scalpel blade. The samples collected were placed into containers with Formal Fixx (*Thermo Scientific Shandon,* Hampton, NH, USA). After a 24-hour period, each sample was then immersed in a container with 70% EtOH for 72 hours. After, each sample was paraffin embedded, sectioned, and processed at the University of Chicago Molecular Diagnostic Laboratory Center (*University of Chicago*, Chicago, IL, USA), where DNA extraction took place.

DNA Extraction

Formyl Fix Paraffin Embedded (FFPE) samples were prepared using the Accel-NGS 2S Plus DNA Library Kit for whole exome sequencing (*Integrated DNA Technology*, Coralville, IA) according to the manufacturer's protocol. The DNA concentration used to establish the library was a minimum of 500 ng.

Whole Genome Sequencing

Paired end sequencing was carried out using the Illumina NovaSeq 6000 system (*Illumina*, San Diego, CA, USA) using 150 bp reads to an average depth of coverage of 44x (i.e., there were 44 "reads" for each base). Sequencing data was converted into FASTQ format and demultiplexed using the bcl2fastq software from Illumina. Paired end reads were aligned to the GRCh37/hg19 reference genome using the Burrows Wheeler Alignment algorithm (Li, 2013). BAM files were processed and variants called using GATk's Haplotype Caller best practices pipeline, including duplicate reading marking and base quality score recalibration (DePristo et al., 2011).

RESULTS

General Summary

Sequence analysis of the SNT shows two missense mutations that result in single nucleotide variants (SNV) within exons of the N-Cadherin gene (CHD2). A mutation in the Desmocollin 2 (DSC2) gene was also demonstrated. All identified SNVs were translated into amino acid substitutions in the polypeptide sequence.

Genomic Analysis

Thymine to Cytosine

One mutation in the SNT genome occurs at Chr18(GRCh37), exon: 1, NT: 25756964, or NM_001792.4, NT 23, thymine (T) to cytosine

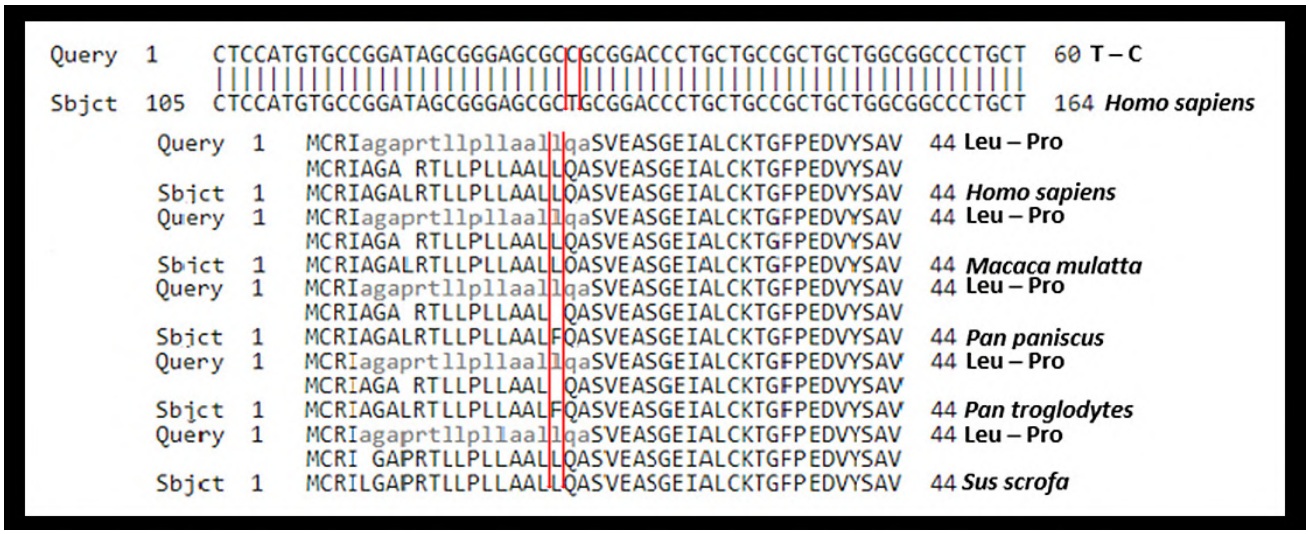

Fig. 3.- Thymine to Cytosine Substitution in the SNT Genome of N-Cadherin. BLAST alignments for SNV NM_001792.4 NT 23 T to C, against Human (homo sapiens: NM_001792.4) as well as AA translation Leu – Pro, against Human (Homo sapiens: AAH36470.1), Rhesus monkey (Macaca mulatta: XM_028838055.1), Bonobo (Pan paniscus: XM_034943719.1), Chimpanzee (Pan troglodytes: XM_523898.6), and Pig (Sus scrofa: XP_020951864.1).

(C) (Walsh et al., 2022a). When translated this nucleotide substitution results in the replacement of leucine (Leu) 8 to proline (Pro) (NP_001783.2) (Walsh et al., 2022a). This data is shown in Fig. 3.

The normal nucleotide sequence for CDH2 in humans against the sequence with the identified SNV, T 23 to C is shown in Fig. 3. Further, the translated AA sequence for Leu-Pro against multiple species N-Cad sequences are compared showing conservation of the normal sequence in all but the sequence for Pig (*Sus scrofa*), which matched the Leu-Pro AA substitution. Blasting of the sequence in the NCBI Database also showed an additional substitution in the sequences for *Pan paniscus* (Bonobo) and *Pan troglodytes* (Chimpanzee), Leu 19 to Phenylalanine (Phe).

Asparagine to Serine

The second mutation found in CDH2 occurs at NM_001308176.1, exon 16, NT 2441, dbSNP: rs2289664 A to G (Walsh et al., 2022b). Translation of this SNV results in the replacement of asparagine (Asn) 845 to serine (Ser) (NP_001295105.1) (Walsh et al., 2022b) (Fig. 4). The alignment of the translation product compared against known species sequences is shown in Fig. 5.

Fig. 4 shows the normal nucleotide sequence against the sequence of the identified SNV from full exome sequencing data compared to multiple species. Conservation of the normal nucleotide sequence is seen differing from the SNV 2441 A to G. Also present is the variation of Bonobo and Chimpanzee with a substation of SNV 852 C to G.

The translated result of the identified SNV resulting in Ser replacing Asn at position 845 (AAH36470.1) is shown in Fig. 5. This substitution is observed to occur in the cytoplasmic region of N-Cad which as shown in Fig. 5 is a conserved sequence across multiple similar species. Shown in the AA translation, the previously indicated variation in Bonobo and Chimpanzee for the NT sequence is synonymous and results in the same AA in the polypeptide.

Desmocollin 2 (DSC2)

Genomic sequencing of the specimen also identified a mutation in DSC2. This mutation occurs at NM_004949.3, Exon: 15, NT: 2393, G to A, dbSNP: rs61731921 (Walsh et al., 2022c). [Sequence alignment is not shown.]

DISCUSSION

Overall Summary of Results

In previous work done in this laboratory, a unique case of tetraorchidism suggested a novel classification of polyorchidism and demonstrated SNTs could be more prevalent due to misdiagnosis as lipomas (Talarico et al., 2022). The purpose of this study was to explore a potential link between cadherins and polyorchidism, because the mechanism underlying the development of polyorchidism is unclear (Bergholz and Wenke, 2009; Artul and Habib, 2014; Cohen et al., 2017). Through full exome sequencing of the SNT, this research discovered two missense mutations within the CDH2 gene (Leu 8 to Pro and Asn 845 to Ser). Since the

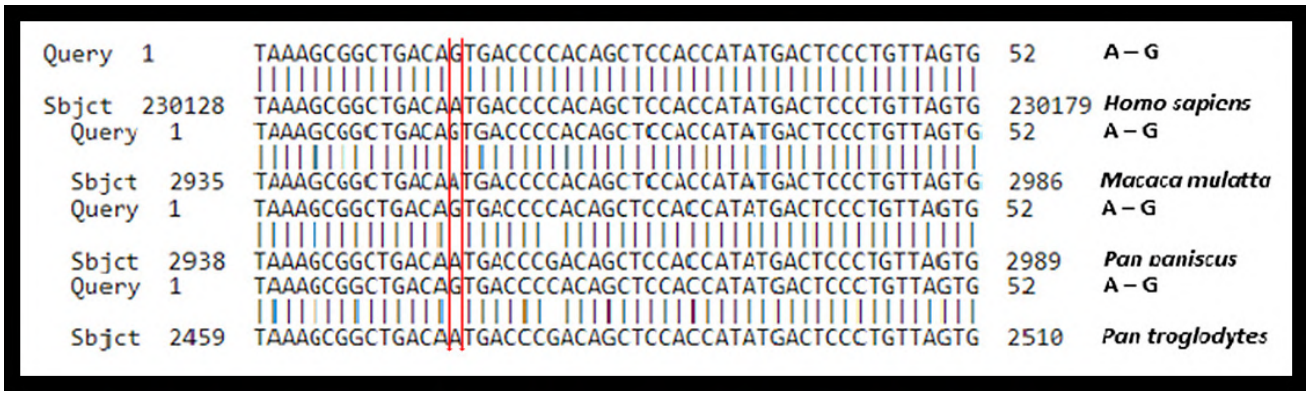

Fig. 4.- Adenine to Guanine Mutation in N-Cadherin of SNT. BLAST alignments for NM_001308176.1 2441 A to G, against Human (Homo sapiens: NG_011959.1, Rhesus monkey (Macaca mulatta: XM_028838057.1, Bonobo (Pan paniscus: XM_034943719.1, and Chimpanzee (Pan troglodytes: XM_016933484.2).

Leu 8 to Pro mutation occurs in the prodomain region of N-Cad, the prodomain region is cleaved off of the cadherin molecule; resulting in the activation of the final product. Due to the prodomains cleavage, it is not present in the final product of the functional protein that is inserted into the cell membrane (Latefi et al., 2009). This mutation does not likely play a role in polyorchidism and will not be addressed. The Asn 845 to Ser mutation occurs in the cytosolic portion of the N-Cad, which could cause improper binding to the p120 catenin. These findings present a *novel* model for the development of polyorchidism building on the gonadal ridge theory. Finally, the current study provides support for the association between cryptorchidism, polyorchidism and cancer.

N-Cadherin and p120 Catenin

As previously stated, full exome sequencing of cadaveric SNT tissue identified two mutations in the CDH2 gene. The first of the N-Cad mutations (Leu-8 > Pro) occurs in the prodomain of the cadherin protein, which is cleaved off during protein maturation in the late Golgi Apparatus (Latefi et al., 2009). Based on this, it is reasonable to suggest that there is little functional change given its absence in the final functional protein structure, as well as its distance from the cleavage site, given the location of the mutation at Leu 8 of the ~130 AA prodomain (Koch et al., 1993).

The second N-Cad mutation (Asn-845 > Ser) is located in the cytosolic domain of the cadherin protein that is a highly conserved sequence of the cadherin protein family (Kister et al., 2001). Specifically, the region referred to as the juxtamembrane domain (JMD). This region of N-Cad and other classical cadherins is responsible for the binding of p120 catenin (Fig. 2) (Kourtidis et al., 2013).

p120 catenin is a member of the catenin family of armadillo repeat (conserved alpha helix repeats) containing proteins that have multiple regulatory functions in Rho GTPase function, nuclear signaling, and regulation/maturation of adhesion junctions (AJs) (Kourtidis et al., 2013). The p120 gene contains 4 alternatively spliced exons and 4 different transcriptional start sites that can produce 64 different isoforms of the p120 protein. Loss of functional p120 can have mild-to-significant effects based on affected tissue types (Hernández-Martínez et al., 2019). p120 is also highly regulated by multiple serine, threonine, and tyrosine sites that can be phosphorylated (Kourtidis et al., 2013; Fukumoto, 2007). Specific functions of each isoform have not been well fully investigated. However, there is a known change in the ratio of p120 isoform expression during EMT (Kourtidis et al., 2013; Zhang et al., 2014).

Celomic epithelial cells of the gonadal ridge proliferate and undergo EMT resulting in the

Fig. 5.- Translation of A to G Mutation in N-Cadherin Changes Asparagine to Serine. BLAST alignment for amino acid sequence of SNV NM_001308176.1 NT 2441 A to G, against Human (Homo sapiens: NP_001295105.1), Rhesus Monkey (Macaca mulatta: XP_014977198.1), Chimpanzee (Pan troglodytes: XP_0716788973.1), Bonobo (Pan paniscus: XP_034799610.1), and pig (Sus scrofa: XP_020951864.1).

formation of the gonadal ridge (Piprek et al., 2020). During this time, alternate expression of p120 catenin results in reduced adhesion in favor of cell motility (Acloque et al., 2009). Based on the mutation (Asn 845 > Ser) found in N-Cad in the present study, it is reasonable to suggest that the potential for p120 to decouple from N-Cad (Fig. 6) results in reduced clustering activity and potential endocytosis yielding a reduction of available N-Cad in the cell membrane. Impairment of cellular adhesion at this stage of gonad development could initiate the detachment between the proliferating somatic cells of the gonadal ridge as they encapsulate migrating PGCs. Therefore, it is reasonable to suggest that reduced adhesion of somatic cells at this stage of gonadal development could result in aberrant division of the gonadal ridge yielding SNTs. Another potential outcome would be the incomplete separation of the gonadal ridge resulting in partial separate development and formation of a bilobed testicle or incomplete polyorchidism (Hekmatnia et al., 2016).

Support of the Proposed Model from Studies on Neoplasms

It has been shown that during EMT, there is a decrease in E-Cad expression. The effects of this are weakened cell AJs which allow for detachment and migration of individual cells. Also seen during EMT is an increase in N-Cad expression (Saénz-de-Santa-María et al., 2020). “N-cadherin expression, which is thought to contribute to a stroma-oriented cellular adhesion profile leading to more motile, invasive and metastatic cell phenotypes.” In cancer, EMT is pivotal to supporting metastasis, chemoresistance, and tumor stemness (i.e., tumor cell ability to proliferate and differentiate) (Loh et al., 2019). Furthermore, elevated levels of soluble N-Cad have been found in the serum of cancer patients, specifically those with cancers of the prostate, breast, or urinary bladder (Cao et al., 2019).

As discussed by Cao et al. (2019), breast cancer, pancreatic cancer, melanoma, multiple myeloma, lung cancer, prostate cancer and squamous cell carcinoma have all been found in connection

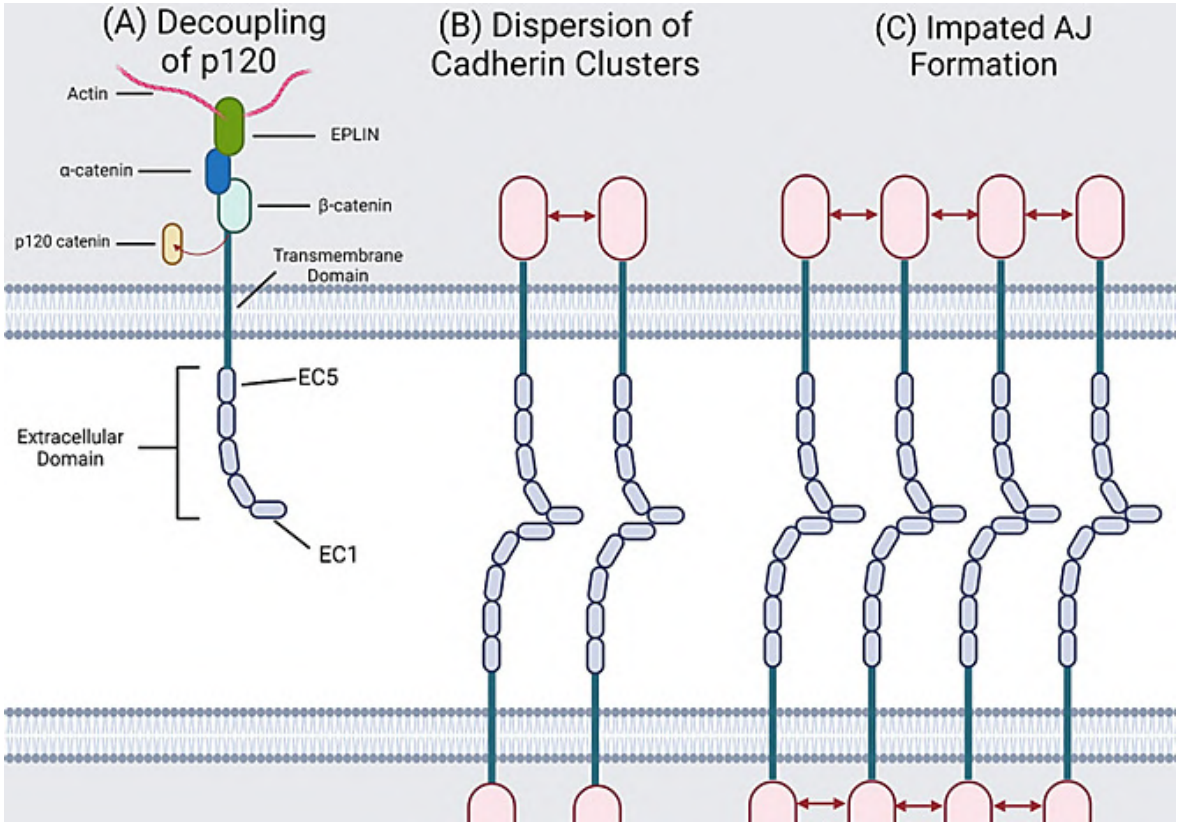

Fig. 6.- Suggested Mechanism for Cadherin in the Genesis of Polyorchidism. **(A)** Decoupling of p120 catenin from adhesion complex due to N-Cad mutation in JMD. **(B)** shows separation of adjacent cadherin dimers due to lack of clustering activity normally facilitated by p120 catenin. **(C)** shows how lack of clustering activity fails to allow the formation of clustered AJs. [Abbreviations: Extracellular Repeat (EC); Epithelial Protein Lost In Neoplasm (EPLIN); Adhesion Junction (AJ); Juxtamembrane domain (JMD)].

to increased expression of N-Cad. When N-Cad expression is increased, collective migration occurs in tumor cells. In contrast, deletion of the intracellular domain, or just the β-catenin binding domain of N-Cad will result in higher incidences of individual migration, or cancer cells detaching and migrating from their cell clusters (Mrozik et al., 2018). β-catenin is one component of the N-Cad protein complex, connecting the transmembrane portion to the actin cytoskeleton. It is plausible that the missense mutation discovered in the present study occurs within the same region of the protein complex, resulting in a similar disruption as deletion of β-catenin.

The *novel* model presented here suggests a relationship between the development of polyorchidism and cancer metastasis based on two criteria. The first supportive evidence comes from the genomic sequencing of a cadaveric SNT that showed a mutation in the cytoplasmic domain of N-Cad. This mutation was located at a point within the sequence where the N-Cad binds to p120 catenin. Because "membrane expression and lateral clustering of N-Cad is dependent upon p120 catenin" (Mrozik et al., 2018), it is reasonable to suggest that the mutation identified in the present work might impact how efficiently N-Cad can provide intercellular adhesion (Fig. 6 and Fig. 7). This investigation suggests that mutant N-Cad affects the binding of p120 (Fig. 6) resulting in abnormal separation of the gonadal ridge and expression of the polyorchid phenotype (Fig. 7). Therefore, using the same reasoning this *novel* mechanism may promote a similar detachment of cells in tumors, resulting in neoplastic migration.

The second supporting evidence for this model is that polyorchids have a higher risk for testicular cancer (Nurfajri et al., 2021; Talarico et al., 2018; Talarico et al., 2022). Prior research done by Mrozik (Mrozik et al., 2018) also reports that aberrant expression of N-Cad is a "well-documented feature of epithelial malignancies". Epithelial cells in the testes, also known as germinal epithelium, exist lining the walls of the seminiferous tubules. One of the many structures that N-Cad is responsible for is the arrangement of the seminiferous epithelium (Piprek et al., 2020). Thus, a loss of adhesive capabilities due to a cytoplasmic mutation of N-Cad in the germinal epithelium could be linked to both testicular cancer and polyorchidism.

Significance of the Current Work

N-Cad has been known to promote cell survival, migration, and invasion relative to progression of neoplasms (Yu et al., 2019). Further, it has been

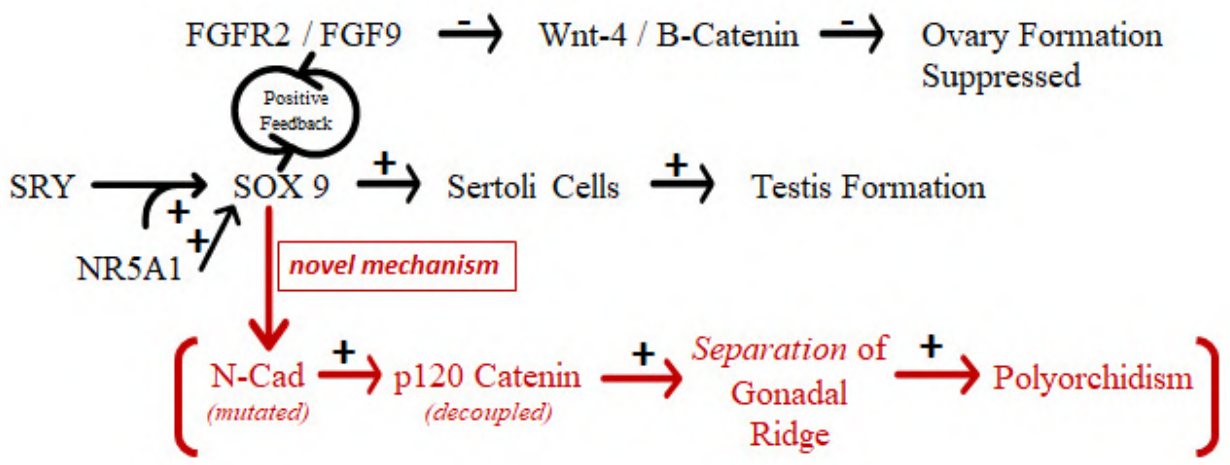

Fig. 7.- Suggested Development of Polyorchidism in Association with Mutated N-Cadherin. The traditional pathways for gonadal development are shown in "black" (also see Fig. 1). In the novel mechanism proposed in this investigation (shown in "dark red"), a mutation in N-Cad can lead to decoupling of p120 catenin causing migration of cells from the gonadal ridge to another location, thus resulting in polyorchidism. [Abbreviations: Increased expression (+); Decreased expression (-); Sex-Determining Region Y (SRY); SRY-BOX Transcription Factor 9 (SOX 9); Nuclear Receptor Subfamily 5 Group A Member 1 (NR5A1); Fibroblast Growth Factor 9 (FGF9); Fibroblast Growth Factor Receptor 2 (FGFR2); Wingless-Type MMTV Integration Site Family Member 4 (WNT-4); N-Cadherin (N-Cad)].

shown that elevated (i.e., expressed) levels of N-Cad from neoplasms are associated with poor prognosis (Mariotti et al., 2007). In prior research done by Mrozik et al. (2018), over-expression of an N-Cad mutant, where the extracellular domain was fused to the anti-binding domain of α-catenin impeded the movement of follower cells. This demonstrates that N-Cad-actin linkage is vital for efficient, collective cell migration. In the novel mechanism presented, a mutation for N-Cad could have the same result. In the gonadal ridge, coelomic epithelial cells undergo EMT where AJ expression is reduced in favor of greater motility. With the mutant N-Cad discovered in this work, impaired binding of p120 catenin likely results in the reduction of AJ binding strength. Thus, it is reasonable to suggest that a decrease in N-Cad clustering fosters an environment for decreased AJ binding strength. This can lead to increased motility of individual cells of the gonadal ridge, resulting in aberrant division and the development of polyorchidism. This same mechanism could apply in some instances of metastatic neoplasms.

Future Work

Genomic analysis of a SNT lead to the discovery of a *novel* N-Cad mutation. Using this N-Cad mutation and known factors involved in testicular genesis, a new molecular model was suggested for the development of polyorchidism. This work lays the foundation for future studies at the molecular and genetic level to further refine all factors and their mechanistic roles in the genesis of this pathology. As suggested by the current work, future studies may also show the application to oncologic models, as well as pathologies in other organ systems.

Additional Findings

An additional finding from genomic sequencing of the male polyorchid in the present work identified a mutation in DCS2. This mutation is known to be associated with arrhythmogenic right ventricular cardiomyopathy, type II. The cause of death of the polyorchid was charted as cardiomyopathy. A survey of the scientific literature did not document any known association between polyorchidism and this mutation in DCS2.

Limitations

The research was conducted on a postmortem, 96-year-old male anatomical donor. Access to the comprehensive medical, social and occupational histories of the donor were not available. It is unknown if the donor was aware of the condition, if he had a family history of polyorchidism or reproductive challenges. Further, secondary to embalming solutions used in this donor and the time from initial embalming, DNA extraction from the STs did not yield a library for analysis. However, the NCBI database allowed the utilization of the BLAST with known, unaltered genomic sequence for unaffected human and animal testes. Lastly, because of the limited number of polyorchids, this study represents the genomic analysis of only one subject.

CONCLUSION

The etiology of polyorchidism is currently unknown, however, the present work establishes a plausible genetic theory based on N-Cad and p120 catenin. This work may apply to the development of supernumerary organs in other systems and in the development and metastasis of neoplasms. Finally, this work establishes a strong foundation for further exploration into the molecular mechanics of cell adhesion as it relates to findings in gross anatomy.

ACKNOWLEDGEMENTS

The authors wish to express their sincere gratitude to the patient and his family, who donated his remains to medical research and education. We also wish to thank the director and staff of Anatomical Gift Association of Illinois (Chicago, Illinois, USA) for their expertise in preparing this anatomical donor's remains for the present study. We also express our sincere appreciation to Daniela Del Gaudio, Director, Molecular Diagnostic Laboratory, Kelly Arndt, Genomics Laboratories Manager, Pricilla Kandikatla, Senior Molecular Genomics Technologist, and the team at the University of Chicago Tissue Processing Center (University of Chicago, Chicago, IL, USA).

NOTES ON CONTRIBUTORS

JACK D. WALSH received his B.S. in Molecular Biology and Biotechnology from North Park University (Chicago IL, USA). Mr. Walsh served in the Biology Department at North Park University, where he participated in many projects to improve the laboratories as well as maintenance of equipment and preparation of laboratory venues for Cell Biology and Genetics. His honors include the Outstanding Senior in Biology Award, and active memberships in the *Tri Beta* Biological Honors Society and the American Society for Cell Biology, and the American Society for Biochemistry and Molecular Biology. Currently, Mr. Walsh is perusing his Doctorate of Philosophy in Chemistry and Biochemistry at the Georgia Institute of Technology (Atlanta, GA, USA).

ERNEST F. TALARICO, JR., serves in the appointments of Adjunct Professor of Anatomy (North Park University, Chicago, IL USA); Visiting Professor of Anatomy and Radiology, Medical Student Academic Adviser, and Research Adviser at Tan Tao University School of Medicine (Long An, Việt Nam). He is a founding member of the medical advisory board and founder of the Center for Medical Education and Research at the new Nam Can Tho University Hospital (Can Tho, Việt Nam). Dr. Talarico is a consultant and lead prosector for the Anatomical Gift Association of Illinois (Chicago, IL USA), and senior research consultant in the Cardiovascular Research Laboratories, Methodist Hospital (Merrillville, IN USA). He created and served as director for the International Human Cadaver Prosection Program, which in 2008 received the award for most outstanding and innovative program in undergraduate and continuing medical education from the AAMC Central Group on Educational Affairs. He is creator of the "Talarico Protocol for Human Gross Anatomy" and is the 2008 recipient of the Partnership Matters Award from the Northwest Indiana Area Health Education Center. In recognition of his work and innovations in anatomical education, in October 2010, Dr. Talarico was inducted as a fellow into the Northwest Indiana Society of Innovators.

JOSEPH G. CASTANEDA is currently a junior, undergraduate student at North Park University (Chicago, IL USA) working on a B.S. in Biomedical Sciences. He has served as a prosector in the human gross anatomy laboratory. Mr. Castaneda created a multi-media presentation focused on aneurysms of brachial plexus that is used to educate other students and prosectors, and he presented this novel education project/research, as well as his prior research on polyorchidism, at the 2022 International Conference of the Human Anatomy and Physiology Society. Mr. Castaneda currently works as a medical scribe, and he continues with his research on multi-media use for student learning in anatomical education. He plans to attend medical school.

SANA M. WAHAB is a 2021 graduate from North Park University (Chicago, IL USA). She graduated with a B.S. in Biomedical Sciences. Ms. Wahab was involved in various academic groups including Women in STEM, the American Medical Student Association, the *Tri Beta* Honor Society, as well as cadaveric exploration groups. She also served as a teaching assistant and supplemental instructor for human anatomy. Ms. Wahab is currently working as a medical transcriptionist and applying to medical school.

KATELYN M. PAULUS is a junior undergraduate student in the Exercise Science program at North Park University (Chicago, IL USA). Her area of concentration is Kinesiology. Ms. Paulus has served in the cadaver prosection laboratory, and she created a multi-media presentation that is used to educate students about the brachial plexus and the innervated muscles. Ms. Paulus has consistently achieved the North Park University Dean's List, while serving as captain of, and leading, the North Park University Dance Team.

AMY E. STROMBERG graduated from North Park University (Chicago, IL USA) in 2021 with a B.S in Biomedical Sciences and a minor in Psychology. She has served as a teaching assistant for anatomy and zoology, and has worked as the animal care coordinator for the zoology laboratory. Ms. Stromberg's prior student research focused on the roles of melanism in urban pigeons. She is currently serves as an emergency medical technician in Chicago and plans to attend medical school.

VICTORIA N. OLSON graduated in 2021 from North Park University (Chicago, IL USA), Summa Cum Laude with a B.A. in Biomedical Sciences and a minor in Chemistry. She served as an anatomy teaching assistant and an undergraduate learning assistant for advanced physiology, as well as Treasurer of the *Tri Beta* Honor Society. Ms. Olson created a human cadaver imaging atlas that has been implemented as a learning tool at North Park University. She is a member of the American Medical Student Association and is currently applying to medical school.

GRIFFIN D. HALL graduated in 2022 with a Bachelor of Arts in Biochemistry from North Park University (Chicago, IL USA). Mr. Hall served as a laboratory assistant, supplemental instruction leader, and teaching assistant for classes such Organic Chemistry, Survey of Organic Chemistry and Biochemistry, and Introduction to Anatomy. Mr. Hall is currently pursuing his Doctor of Pharmacy at Roosevelt University College of Pharmacy (Chicago, IL USA) in the summer of 2022.

PAUL J. JANUS received his Ed.D. in Higher Education and Adult Learning from Walden University (Minneapolis, MN USA). Dr. Janus serves as Assistant Professor of Biology and the Director of Anatomical Research at North Park University (Chicago, IL USA). Dr. Janus also serves as the undergraduate student academic adviser, and he has served as the Laboratory Manager for the Department of Biology.

NICHOLAS R. ROCCO is a doctor of allopathic medicine; graduated from Uniformed Services University of Health Sciences School of Medicine (Bethesda, MD USA). Dr. Rocco has completed extensive training in urology, and he serves as Department Head of Urologic Surgery at United States Naval Hospital Guam (Agana Heights, Guam). Dr. Rocco has completed extensive training in urology at Naval Medical Center San Diego (San Diego, CA USA). He now serves as Department Head of Urologic Surgery at United States Naval Hospital Guam (Agana Heights, Guam.

REFERENCES

ALBRECHT KH, EICHER EM (2001) Evidence that Sry is expressed in pre-Sertoli cells and Sertoli and granulosa cells have a common precursor. *Dev Bio*, 240(1): 92-107.

ACLOQUE H, ADAMS MS, FISHWICK K, BRONNER-FRASER M, NIETO MA (2009) Epithelial-mesenchymal transitions: the importance of changing cell state in development and disease. *J Clin Invest*, 119(6): 1438-1449.

AMAGAI M, STANLEY JR (2012) Desmoglein as a target in skin disease and beyond. *J Invest Dermatol*, 132(3) (Pt2): 776-784.

ARSLANOGLU, A, TUNCEL SA, HAMARAT M (2013) Polyorchidism: Color doppler ultrasonography and magnetic resonance imaging findings. *Clin Imaging*, 37(1): 189-191.

ARTUL S, HABIB G (2014) Polyorchidism: two case reports and a review of the literature. *J Med Case Rep*, 8: 464-468.

AVELLAR MCW, RIBEIRO CM, DIAS-DA-SILVA MR, SILVA EJR (2019) In search of new paradigms for epididymal health and disease: innate immunity, inflammatory mediators, and steroid hormones. *Andrology*, 7(5): 690-702.

AZIZ W, REHMAN KU, RAFIQUE MZ (2016) Doppler ultrasound findings in a patient with primary infertility and triorchidism. *BMJ Case Rep*, 2016: 215346.

BERGHOZ R, WENKE K (2009) Polyorchidism: a meta-analysis. *J Urol*, 182(2): 2422-2427.

BORNEMANN A, SCHMALBRUCH H (1994) Immunocytochemistry of M-cadherin in mature and regenerating rat muscle. *Anat Rec*, 239(2): 119-125.

CAO Z-Q, WANG Z, LENG P (2019) Aberrant N-cadherin expression in cancer. *Biomed Pharmacother*, 118: 109320.

COHEN T, AGARD H, PAREKH N, CLARK C (2017) Management of bilateral undescended bilobed testes and review of the literature. *Urology*, 110: 213-215.

COX T (2013) Sex-determining region Y in mammals. *The Embryo Project Encyclopedia*. Arizona State University, http://embryo.asu.edu/handle/10776/6887.

DELVA E, TUCKER DK, KOWALCZYK AP (2009) The desmosome. *Cold Spring Harb Perspect Biol*, 1(2): a002543.

DEPRISTO MA, BANKS E, POPLIN R, GARIMELLA, KV, MAGUIRE JR, HARTL C, PHILIPPAKIS AA, DEL ANGEL G, RIVAS MA, HANNA M, MCKENNA A, FENNELL TJ, KERNYTSKY AM, SIVACHENKO AY, CIBULSKIS K, GABRIEL SB, ALTSHULER D, DALY MJ (2011) A framework for variation discovery and genotyping using next-generation DNA sequencing data. *Nat Genet,* 43: 491-498.

DOLLARD DJ, FOBIA JB (2011) Extra scrotal spermatocele causing lower abdominal pain: a first case report. *Am J Emerg Med*, 29(3): 358. e7-358.e9.

FUKUMOTO Y, SHINTANI Y, REYNOLDS AB, JOHNSON KR, WHEELOCK MJ (2008) The regulatory or phosphorylation domain of p120 catenin controls E-cadherin dynamics at the plasma membrane. *Exp Cell Res*, 314(1): 52-67.

GUO B, QI M, HUANG S, ZHUO R, ZHANG W, ZHANG Y, XU M, LIU M, GUAN T, LIU Y (2021) Cadherin-12 regulates neurite outgrowth through the PKA/Rac1/Cdc42 pathway in cortical neurons. *Front Cell Dev Biol*, 9: 768970.

HARRISON OJ, JIN X, HONG S, BAHNA F, AHLSEN G, BRASCH J, WU Y, VENDOME J, FELSOVALYI K, HAMPTON CM, TROYANOVSKY SM, SHAPIRO L, HONIG B (2011) The extracellular architecture of adherens junctions revealed by crystal structures of type I cadherins. *Structure*, 19(2): 244-256.

HASSAN A, EL-MOGY MS, MOSTAFA T (2008) Triorchidism: a case report and review of similar conditions. *Andrologia*, 40(4): 265-269.

HASSAN A, ELHANBLY S, EL-MOGY MS, MOSTAFA T (2014) Triorchidism: two case reports. *Andrologia*, 46(9): 1073-1077.

HEKMATNIA F, MOMENI M, HEKMATNIA A, BARADARAN MAHDAVI MM (2016) A bilobed testicle diagnosed with ultrasound in an 18-year-old boy. *J Res Med Sci*, 21: 62.

HERNÁNDEZ-MARTÍNEZ R, RAMKUMAR N, ANDERSON KV (2019) p120-catenin regulates WNT signaling and EMT in the mouse embryo. *Proc Natl Acd Sci USA*, 116(34): 16872-16881.

HOARE BS, KHAN YS (2022) Anatomy, abdomen and pelvis, female internal genitals. In: StatPearls [Internet]. Treasure Island (FL): *StatPearls Publishing*, Available from: https://www.ncbi.nlm.nih.gov/books/NBK554601/.

ILIADOU PK, TSAMETIS C, KAPRARA A, PAPADIMAS I, GOULIS DG (2015) The sertoli cell: novel clinical potentiality. *Hormones (Athens, Greece)*, 14(4): 504-514.

INUZUKA H, REDIES C, TAKEICHI M (1991) Differential expression of R- and N-cadherin in neural and mesodermal tissues during early chicken development. *Development*, 113: 959-967.

KATO T, ESAKI M, AYMAI M, YAYOI I (2012) NR5A1 is required for functional maturation of Sertoli cells during postnatal development. *Reproduction*, 143(5): 663-672.

KISTER AE, ROYTBERG MA, CHOTHIA C, VASILIEV JM, GELFAND IM (2001) The sequence determinants of cadherin molecules. *Protein Sci*, 10(9): 1801-1810.

KOCH AW, FAROOQ A, SHAN W, ZENG L, COLMAN DR, ZHOU MM (2004) Structure of the neural (N-) cadherin prodomain reveals a cadherin extracellular domain-like fold without adhesive characteristics. *Structure*, 12(5): 793-805.

KOURTIDIS A, NGOK SP, ANASTASIADIS PZ (2013) p120 catenin: an essential regulator of cadherin stability, adhesion-induced signaling, and cancer progression. *Prog Mol Biol Transl Sci*, 116: 409-432.

LANE WA (1895) A case of supernumerary testis. *Trans Clin Soc Lond*, 28: 59-60.

LATEFI NS, PEDRAZA L, SCHOHL A, LI Z, RUTHAZER ES (2009) N-cadherin prodomain cleavage regulates synapse formation in vivo. *Dev Neurobiol*, 69(8): 518-529.

LAWRENTSCHUK N, MACGREGOR RJ (2013) Polyorchidism: a case report and review of the literature. *ANZ J Surg*, 74(12): 1130-1132.

LI H (2013) Aligning sequence reads, clone sequences and assembly contigs with BWA-MEM. *ArXiv*, Cornell University, arXiv:1303.3997v2 [q-bio.GN].

LOH CY, CHAI JY, TANG TF, WONG WF, SETHI G, SHANMUGAM MK, CHONG PP, LOOI CY (2019) The e-cadherin and n-cadherin switch in epithelial-to-mesenchymal transition: signaling, therapeutic implications, and challenges. *Cells*, 8(10): 1118.

MAÎTRE JL, HEISENBERG CP (2013) Three functions of cadherins in cell adhesion. *Curr Biol*, 23(14): R626-R633.

MARIOTTI A, PEROTTI A, SESSA C, RÜEGG C (2007) N-cadherin as a therapeutic target in cancer. *Expert Opin Invest Drugs*, 16(4): 451-465.

MATHUR P, PRABHU K, KHAMERSRA HL (2002) Polyorchidism revisited. *Pediatr Surg Int*, 18(5-6): 499-450.

MITTAL PK, ABDALLA AS, CHATTERJEE A, BAUMGARTEN DA, HARRI PA, PATEL J, MORENO CC, GABRIEL H, MILLER FH (2018) Spectrum of extratesticular and testicular pathologic conditions at scrotal MR imaging. *Radiographics*, 38(3): 806-830.

MROZIK KM, BLASCHUK OW, CHEONG CM, ZANNETTINO ACW, VANDYKE K (2018) N-cadherin in cancer metastasis, its emerging role in haematological malignancies and potential as a therapeutic target in cancer. *BMC Cancer*, 18(1): 939 P1-16.

NOSE A, NAGAFUCHUI A, TAKEICHI M (1986) Expressed recombinant cadherins mediate cell sorting in model systems. *Cell*, 54(7): 993-1001.

NURFAJRI DH, PRANOTO D, PRAMOD SV, SAFRIADI F, HERNOWO BS (2021) Polyorchidism and testicular malignancy, what can we learn: A case report. *Urol Case Rep*, 39: 101828.

OSTRER H (2019) Swyer Syndrome. *National Organization for Rare Disorders (NORD)*, available from: https://rarediseases.org/rare-diseases/swyer-syndrome/.

OTERO J, BEN-YAKAR N, ALEMAYEHU B, KOZUSKO SD, BORAO F, VATES III TS (2016) A unique case of intraabdominal polyorchidism: a case study. *Case Rep Urol*, 2016: 2729614.

PANCHO A, AERTS T, MITOSGIANNIS MD, SEUNTJENS E (2020) Protocadherins at the crossroad of signaling pathways. *Front Mol Neurosci*, 13: 117.

PIPREK RP, KOLASA M, PODKOWA D, MALGORZATA K, KUBIAK JZ (2019a) Tissue-specific knockout of E-cadherin (Cdh1) in developing mouse gonads causes germ cell loss. *Reproduction*, 158(2): 147-157.

PIPREK RP, KOLASA M, PODKOWA D, MALGORZATA K, KUBIAK JZ (2019b) N-cadherin is critical for the survival of germ cells, the formation of steroidogenic cells, and the architecture of developing mouse gonads. *Cells*, 8(12): 1610.

PIPREK RP, MALGORZATA K, MIZIA P, KUBIAK JZ (2020) The central role of Cadherins in gonad development, reproduction, and fertility. *Int J Mol Sci*, 21(21): 8264.

RAYA-SANDINO A, LUISSINT AC, KUSTERS DHM, NARAYANAN V, FLEMMING S, GARCIA-HERNANDEZ V, GODSEL LM, GREEN KJ, HAGEN SJ, CONWAY DE, PARKOS CA, NUSRAT A (2021) Regulation of intestinal epithelial intercellular adhesion and barrier function by desmosomal cadherin desmocollin-2. *Mol Biol Cell*, 32(8): 753-768.

ROCA-FERRER J, RODRIGUEZ E, RAMIREZ GA, MORAGAS C, SALA M (2015) A rare case of polyorchidism in a cat with four intra-abdominal testes. *Reprod Domest Animi*, 50(1): 172-176.

SAKAMOTO H, SAITO K, OOHTA M, INOUE K, OGAWA Y, YOSHIDA H (2007) Testicular volume measurement: comparison of ultrasonography, orchidometry, and water displacement. *Urology*, 69(1): 152-157.

SEKIDO R, LOVELL-BADGE R (2008) Sex determination involves synergistic action of SRY and SF1 on a specific Sox9 enhancer. *Nature*, 453(7197): 930-934.

SHEAH K, TEH HS, PEH OH (2004) Supernumerary testicle in a case of polyorchidism. *Ann Acad Med Singap*, 33(3): 368-370.

SHAPIRO L, WEIS WI (2009) Structure and biochemistry of cadherins and catenins. *Cold Spring Harb Perspect Biol*, 1(3): a003053.

TALARICO JR EF, CASTANEDA JG, WAHAB SM, PAULUS KM, WALSH JD, STROMBERG AE, OLSON VN, JANUS PJ, ROCCO NR (2022) An unusual case of quadruple polyorchidism in a human cadaver mimicking bilateral lipoma. *Eur J Anat*, 26(1): 117-131.

TALARICO JR EF, MAS JL, JONES JA (2018) Characterization and radiographic study of stage III testicular cancer in a 31-year-old male patient. *Eur J Anat*, 22(3): 241-256.

TAKEICHI M (1977) Functional correlation between cell adhesive properties and some cell surface proteins. *J Cell Biol,* 75(2 Pt 1): 464-474.

TAMMINEN TM, LEINONEN MR, KACK H, ANDERSSON M (2012) A polyorchid dog. *Reprod Domests Anim*, 47(2): e26-28.

TONAPE T, SINGH G, KOUSHIK P, TUMEPALLI T (2012) Triorchidism: a rare genitourinary abnormality. *J Surg Tech Case Rep*, 4(2): 126-128.

WALSH JD, TALARICO JR EF, JANUS PJ (2022a) Homo sapiens Cadherin 2 (CDH2) In polyorchidism, partial cds Genbank Direct Submission, National Center for Biotechnology Information (Submission SNP No. 2137544389, Local Identifier: CDH2V1).

WALSH JD, TALARICO JR EF, JANUS PJ (2022b) Homo sapiens Cadherin 2 (CDH2) In polyorchidism, partial cds Genbank Direct Submission, National Center for Biotechnology Information (Submission SNP No. 5981325822, Local Identifier: CDH2V2).

WALSH JD, TALARICO JR EF, JANUS PJ (2022c) Homo sapiens Desmocollin 2 In polyorchidism, partial cds Genbank Direct Submission, National Center for Biotechnology Information (Submission SNP No. 5981325823, Local Identifier: DCS2V1).

WARR N, GREENFIELD A (2012) The molecular and cellular basis of gonadal sex reversal in mice and humans. *Wiley Interdiscip Rev Dev Biol*, (4): 559-777.

WITT CC, BAUTISTA E (2011) Triorchidism in a Hummingbird. *Wilson J Ornithol*, 123(3): 632-635.

YAMAUCHI T, IWABU M, OKADA-IWABU M, KADOWAKI T (2014) Adiponectin receptors: a review of their structure, function and how they work. *Best Pract Res Clin Endocrinol Metab*, 28(1): 15-23.

YAMAMOTO T, MATSUDA Y, SHIBAMORI K, MATSUKI M, IWAKI H, YANASE M (2015) Polyorchidism: a case report and review of the literature. *Hinyokika Kiyo*, 61(3): 121-124.

YANG Y, WORKMAN S, WILSON M (2018) The molecular pathways underlying early gonadal development. *J Mol Endocrinol*, 17-0314, doi: 10.1530/JME-17-0314.

YU W, YANG L, LI T, ZHANG Y (2019) Cadherin signaling in cancer: its functions and role as a therapeutic target. *Front Oncol*, 9: 989.

ZHANG Y, ZHAO Y, JIANG G, ZHANG X, ZHAO H, WU J, XU K, WANG E (2014) Impact of p120-catenin isoforms 1A and 3A on epithelial mesenchymal transition of lung cancer cells expressing E-cadherin in different subcellular locations. *PLoS One*, 9(2): e88064.

Myocardial bridge over coronary arteries and myocardial coat lining coronary sinus: clinical implications

Dibakar Borthakur[1], Rajesh Kumar[2], Rima Dada[1]

[1] Department of Anatomy, All India Institute of Medical Sciences, New Delhi
[2] Department of Anatomy, All India Institute of Medical Sciences, Patna

SUMMARY

Myocardial Bridge (MB) on the coronary artery and myocardial coat (MC) on the cardiac veins are usually detected in angiography and cadaveric dissection. Left anterior descending branch (LAD) of the left coronary artery is the most frequent site of MB. Rarely MB is also seen over the right coronary arterial branches. MB has proven association with ischemic heart disease and other critical cardiac consequences like myocardial infarction (MI) (Alegria et al., 2000; Soran et al., 2000). MC, on the other hand has not gained enough attention in previous studies. Large MB can be readily identified in angiograms, but minutes MB can be picked up by newer imaging studies like multidetector computed tomography (MDCT) and optical coherence tomography (OCT) scan (Tiryakioglu and Aliyu, 2020). Cadaveric dissection, however, holds its unique place in direct visualization and studying the macro and micro-anatomical characteristics. To study the prevalence and anatomical attributes of MB and MC in Indian population, ten adult cadaveric hearts (6 male and 4 female) were dissected as part of a routine undergraduate teaching at the Anatomy Department, All India Institute of Medical Sciences, New Delhi, India. MB over the coronary artery and MC over the cardiac vein were identified. Data pertaining to the MB and MC dimensions were measured with a digital vernier calliper. Histology of the MC was carried out to confirm its presence and observe the cyto-architecture pattern. Relevant gross macroscopic and microscopic images were photographed and photomicrographed.

20% of the dissected cadavers revealed MB involving LAD in first heart while LAD and RCA both in second heart with lengths 5 mm, 18 mm and 2 mm respectively. MC was noted over coronary sinus and proximal few millimeters of great and middle cardiac veins. Histological examination revealed cardiac striated muscle in MC with typical cyto- architecture. The mean myocardial muscle index (MMI) of MBs ranged from 1.6 to 21.6. The present study highlights 20% prevalence of MBs in Indian population involving both right and left coronary artery. 10% of the subjects had histologically confirmed MC over cardiac veins. MC over the coronary sinus and other cardiac veins need more elaborate explorative studies to quantify the anatomic properties and to examine the possible association with cardiovascular disease. Nevertheless, anatomic attributes should be kept

Corresponding author:
Dr. Rima Dada, MBBS, M.D., PhD. Lab for Molecular Reproduction and Genetics, Department of Anatomy, All India Institute of Medical Sciences, New Delhi – 110029, India. E-mail: rimadadaaiims20@gmail.com

Submitted: August 28, 2022. **Accepted:** September 23, 2022

https://doi.org/10.52083/YQFO7375

in mind to better appreciate MI in evolution and MI at evaluation in a case with MB.

Key words: Myocardial bridge – Myocardial coat – Myocardial cover – Coronary artery – Coronary sinus

ABBREVIATIONS

CAD – Coronary artery disease

CCTA – Coronary computed tomographic angiography

CS – Coronary sinus

CTA – Computed tomography angiography

IHD – Ischemic heart disease

IVUS – Intravascular ultrasound

LAD – Left anterior descending

LCA – Left coronary artery

MB – Myocardial bridge

MC – Myocardial coat

MDCT – Multidetector computed tomography

MI – Myocardial infarction

MMI – Myocardial muscle index

OCT – Optical coherence tomography

RCA – Right coronary artery

INTRODUCTION

The myocardial bridge is a clinical entity characterized by the presence of a portion of the epicardial coronary artery lying under cover of the myocardium. Ever since its description by Reyman in 1737 and Black in 1805, it has constantly fascinated cardiac physicians and surgeons (Reyman, 1737; Black, 1805; Möhlenkamp et al., 2002). Later, during 1951, Geiringer presented his extensive research findings in autopsy samples. The entity became more vivid after Portmann and Iwig narrated their angiographic observations in 1960 (Geiringer, 1951; Portman, 1960; Ishii et al., 2014). The cardiac muscle fibers running over the coronary artery embedded in the epicardium are conventionally called the "myocardial bridge (MB)". The coronary artery passing under the bridge is termed "tunneled artery". Other terminologies – viz., muscular cardiac bridge, intramural coronary, myocardial loop, mural coronary – are also used synonymously. It is primarily encountered and thought to be more frequent in the anterior interventricular artery (also known as left anterior descending or LAD artery). Other coronary artery branches – e.g., posterior descending, circumflex, right and left marginal and diagonal arteries – are also reported to be affected by MB. The MB covering LAD is a fairly common occurrence, as detected in heart autopsies, and the incidence is as high as 50% (Lujinović et al., 2013). Thus, some authorities believe it to be a normal variant rather than an instance of aberrant anatomy, and it correlates well as majority of such MBs remain asymptomatic. However, in some subjects with MBs, grave clinical consequences like ischemic angina, arrhythmia and acute coronary syndrome have been constantly reported. MBs occurring at special sites such as LAD are also linked with the risk of myocardial infarction (MI) and even sudden death. The overall risk of occurrence of critical cardiac events becomes higher in cases of pre-existing heart disease. Different schools of thought prevail as to whether presence of MBs can lead to critical cardiac events (Alegria et al., 2005; Soran et al., 2000; Michel et al., 2014; Zeina et al., 2007) or whether they are merely an asymptomatic benign anatomic entity (Alegria et al., 2005; Soran et al., 2000; Tiryakioglu et al., 2020; Nasr et al., 2014; Rogers et al., 2017). Coronary artery angiogram is a useful tool for detecting the presence of MBs. However, the reported angiographic detection rate is as low as 5%. The angiographic study utilizes the principle of compression of coronary artery by the MB musculature typically described as 'milking' during the systole. Many times a small muscular bridge of less than 1mm is not detected, as they cannot produce a milking effect large enough to get picked up. Invasive diagnostic methods like intracoronary ultrasound coupled with Doppler can increase the detection rate marginally, but multidetector computed tomography (MDCT) scan is an efficient visualization technique to visualize and detect a MB in a non-invasive manner, whose detection rate is comparable with that of autopsy. It is now well known that the right coronary artery (RCA) and the other unnamed small coronary arteries can also get covered by MB fibres, all of which have the potential for

increasing the preponderance of atherosclerosis and consequent MI. The detection of MB over a large coronary artery is relatively easy in imaging studies, as changes in the blood flow in the burrowing artery distal to the site of MB fibres can be well visualized. With advanced radio- imaging technology, especially coronary computed tomographic angiography (CCTA) and MDCT, data pertaining to the detailed anatomic attributes of MBs in other coronary arteries have been gradually accumulating in literature (Tiryakioglu et al., 2020). Recently, optical coherence tomography (OCT) has emerged as a superior high resolution imaging modality successful for minute MBs not detectable even in intravascular ultrasound (IVUS) and routine angiography (Okamura et al., 2022). It was the gradual understanding of clinical correlation of MB with myocardial ischemia and resultant ischemic heart disease (IHD) that fueled more organized and in-depth research to explore the entity. Because MDCT and other newer techniques can accurately identify and functionally quantify the MB fibers, now it has been possible to guide the clinicians in evaluating a case of IHD or coronary artery disease (CAD) by providing functional correlation between MB fibers and resultant milking effect during systole, and link these data with clinical presentations which might adequately help in instituting prompt and adequate therapy.

The coronary sinus (CS) is a notable structure on the posterior coronary sulcus serving as the predominant terminal pathway of venous drainage of the left ventricle and inter-ventricular septum. A myocardial coat (MC) has been consistently seen over the coronary sinus, which has been attributed to the embryological development of the CS from the left horn of the sinus venosus and a small part of the right atrium. Despite being a more or less consistent structure, detailed study on MC over CS is long overdue in medical literature. The MC not only covers the CS but also wraps around variable adjoining portions of the draining tributaries: viz., middle and great cardiac veins. In up to one fifth of the MCs, it has been described in few different forms like myocardial belts, cuffs, adhesions, etc., which definitely have the potential to behave like a sphincter in the chief draining channel junction with the great cardiac vein (von Ludinghausen et al., 1992). Emphasis has been made on the surgical elimination of the consistent but variable morphological connections existing between left atrial myocardium with CS (Chauvin et al., 2000). A unique atrial macro-entry phenomenon culminating in atrial flutter was identified due to MC over CS, which is subsequently seen to be a direct connection between left atrial myocardium and MC over CS. The route of macro re-entry phenomenon was shown to be through the MC over CS via the left atrium to the interatrial septum, and then retuning back to CS (Olgin et al., 1998). The morphological aspect of MC over CS has to be seen from a different perspective in view of the increasingly performed invasive cardiac procedures through the CS.

MATERIALS AND METHODS

The study was conducted at the All India Institute of Medical Sciences, New Delhi, India, during routine cadaveric dissection for undergraduate medical students. The institutional guidelines for procurement of human cadavers and their use for medical teaching and research were strictly adhered. Relevant ethical clearance and consent from the relatives of the deceased was obtained beforehand. The hearts were dissected out from the middle mediastinum of the embalmed cadavers, which were routinely kept in weak formalin solution. Subsequently, meticulous dissection for the coronary vasculature was carried out keeping in mind the presence of the MBs. The epicardium was carefully stripped off from the underlying myocardium and the epicardial fat and vessels. Proper care was taken not to damage the vascular architectural pattern. Using blunt forceps, the epicardial fat was removed bit by bit and the specimens were cleared off from additional loose connective tissues obscuring the coronary vasculature. The various anatomical attributes of the myocardial bridges and tunneled arteries – viz., location, thickness, length, etc. – were measured using a digital vernier caliper. All cadavers were of voluntary body donors (age ranging from 36 years to 73 years). The death certificates collected at the time of body donation revealed that none of the individuals died of cardiac cause.

RESULTS

Two out of the total 10 dissected cadavers revealed MB over LAD and right ventricular branch of the RCA. Data pertaining to the myocardial bridges and / or tunneled arteries were recorded, and specimens were photographed. MB muscle indexes were calculated as follows: MB muscle index (MMI) = Length of MB in millimeters x Thickness of MB in millimeters.

Case 1:

In the first heart specimen from a male cadaver aged 62 years, MB was noted in the proximal segment of the LAD artery (Fig. 1A). The dimensions of the MB were 5 mm x 3 mm x 0.8 mm in length, breadth and thickness respectively. MMI of the MB was 4. The MB was positioned in the same plane as that of the adjoining myocardium. The left coronary artery (LCA) after originating from the left aortic sinus runs anterior to pulmonary trunk and after sprouting other branches lie for a short distance in the anterior interventricular groove, hooked beneath the MB to reappear in the groove and then turned backwards to the diaphragmatic surface running in the posterior interventricular groove. No other coronary artery or their branches were seen to be afflicted by MBs. The course of both the coronary arteries and their branches appeared normal. The segment of the LCA which was not covered by the MB had an average diameter of 3.35 ± 0.35 mm and the diameter of RCA at origin was of normal caliber (3.86 ± 0.28 mm).

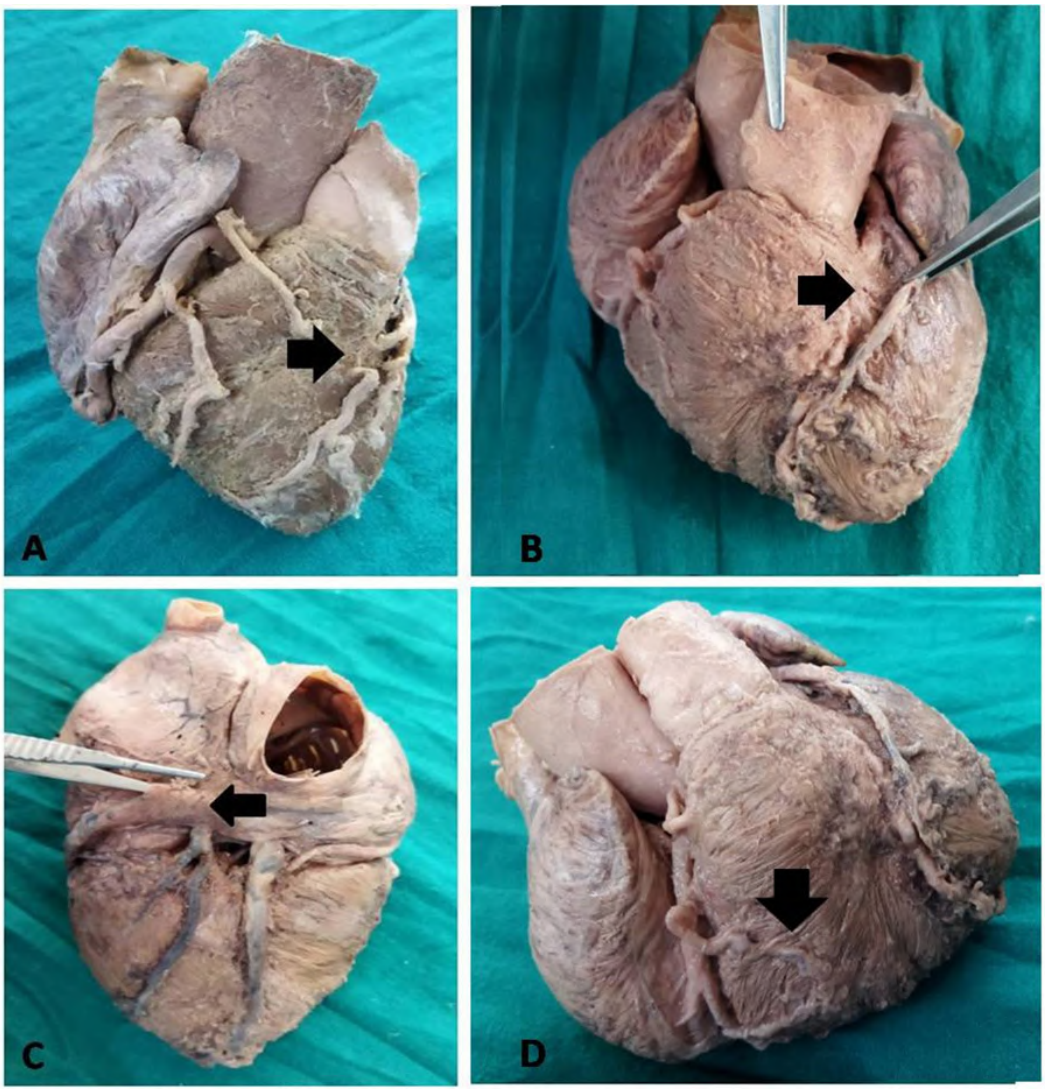

Fig. 1.- A- Myocardial Bridge (MB) over proximal segment of LAD in the first heart specimen; **B**- MB over proximal segment of LAD in the second heart specimen; **C**- MC over the coronary sinus in the second heart specimen; **D**- MB over the right ventricular branch of RCA in the second heart specimen.

Case 2:

In the second heart specimen of the male cadaver aged 57 years, two MBs were noted in the proximal segment of the LAD artery and in the right ventricular branch arising from the RCA just to the left of the anterior coronary sulcus slightly above the inferior border of the heart (Fig. 1B and 1D). The LCA originated normally from the left aortic sinus and runs in the anterior interventricular groove after giving circumflex and diagonal branches. The dimensions of the MB on LAD artery were 18 mm x 4 mm x 1.2 mm in length, breadth and thickness respectively. The MMI of this MB was 21.6. The MB appeared slightly elevated than its adjoining myocardium so that the LAD artery did not appear to be hooking in a deeper plane. The RCA originated from the anterior aortic sinus and after giving the conus and atrial branches it traversed in the anterior coronary sulcus. The second MB was noted over the right ventricular branch of the RCA whose dimensions were 2 mm x 2 mm x 0.8 mm in length, breadth and thickness respectively; and it appeared to be in the plane of the adjoining myocardium. The MMI of this MB was 1.6. The RCA and LCA were of normal caliber (average diameter of RCA at origin was 3.73 ± 0.25 mm; average diameter of main LAC at origin was 4.30 ± 0.32 mm) and had a normal course and branching pattern except the noted MBs.

We also noticed a myocardial coat (MC) over the coronary sinus (CS), extending to the proximal part of the great and the middle cardiac veins in the second cadaveric heart (Fig. 1C). There is mention of MC covering coronary sinus and other large diameter cardiac veins draining into coronary sinus in the literature. The MC extended from the point where the oblique vein of the right atrium drained into the CS till the point at which CS itself drained into right atrium. The proximal portion of the great cardiac vein and middle cardiac veins had similar muscle coat. Histological examination of the same revealed that the CS had a coating of spirally arranged cardiac striated muscle fibers (Fig. 2). Loose areolar tissue with intervened in space between CS wall and MC coat. On gross examination, the MC coat appeared to be in continuity with the cardiac muscle fibers of the left atrium. All the dimensions of MBs (length, breadth and thickness) along with MMIs and dimensions of MC (length, breadth and thickness) have been tabulated (Table 1).

DISCUSSION

The MB results in systolic compression of burrowing coronary arterial segment and is the underlying pathophysiology in myocardial ischemia (Bourassa et al., 2003). In fact, the clinical research did commence on MB due to the increased predilection to myocardial ischemia in subjects harboring MB (Houstiuc et al., 2017; Michel et al., 2014). In the late 20th century, morphologic study involving 642 hearts

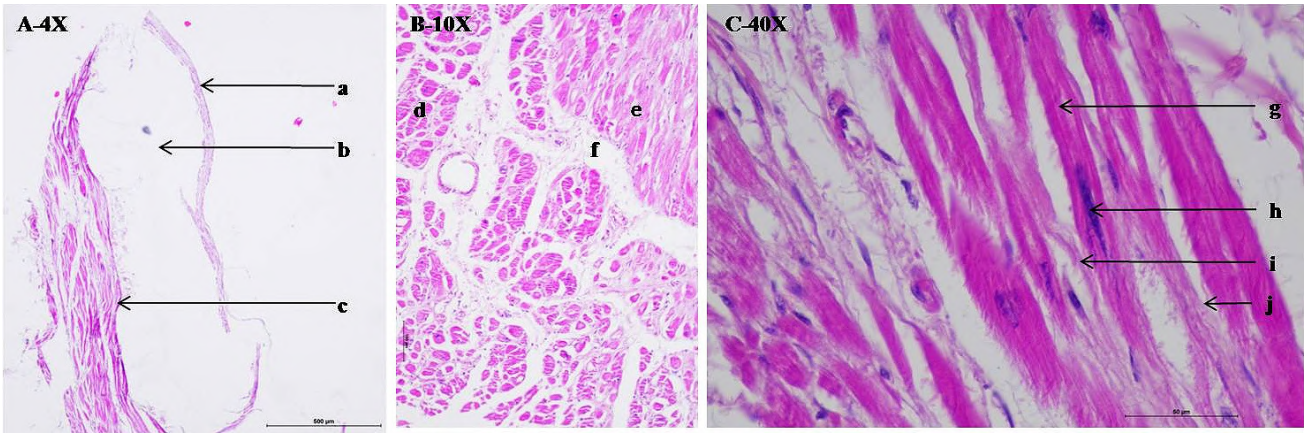

Fig. 2.- Histological features of MC over coronary sinus. **A:** myocardial coat with wall of coronary sinus. Scale bar = 500 µm. **B:** cardiac muscle fibres in transverse and longitudinal section. Scale bar = 200 µm. **C:** characteristic of MC showing branching pattern of muscle fibre, central nucleus and intercalated disc. Scale bar = 50 µm. a- endothelium of the coronary sinus wall, b-adipose tissue between coronary sinus and surrounding cardiac striated muscle coat, c-striated cardiac muscle coat, d-cardiac muscle fibre bundle in a fascicle, e-cardiac muscle fibres seen in longitudinal section, f-perimysium, g-intercalated disc, h-central nucleus of cardiac muscle fibre, i-branching carding muscle fibre, j-endomysium of cardiac muscle.

Table 1. Anatomical parameters of MBs and MC.

	Length (in mm)	Breadth (in mm)	Thickness (in mm)	MMI
MB over LAD (Case 1)	5	3	0.8	4
MB over LAD (Case 2)	18	4	1.2	21.6
MB over branch of RCA (Case 2)	2	2	0.8	1.6
MC over CS	45	6.6	0.2	Not applicable

revealed that the atherosclerosis of the RCA is more extensive than the left in presence of MB, whereas no significant difference was noted between both coronary arteries in absence of MB. Furthermore, atherosclerotic lesions were noted to be more pronounced in the proximal segment of the LAD just preceding the MB with both macroscopic raised lesions and microscopic intimal thickenings. The most frequent segment of the LAD artery with atherosclerotic changes was also the proximal segment irrespective of the presence of any other additional MBs over LAD artery. It was in contrast to the prior observation of the international atherosclerosis project which stated that the RCA had more predilection for atheroma formation (Ishii et al., 1986). One of the two mechanisms by which MB leads to CAD is direct compression on the coronary artery at systole producing decreased coronary blood flow, reduced myocardial perfusion and impeding relaxation of coronaries during diastole. The other operating mechanism is acceleration of the atherosclerotic process at the segment of the artery just proximal to the MB location due to endothelial injury incited by altered hemodynamic processes with retrograde blood flow (Ishikawa et al., 2009). These mechanisms have evolved through the knowledge gathered from cadaveric and imaging studies with regard to their various anatomic attributes. Some of the relevant studies looking at the MB with its different attributes are summarized (Table 2).

A morphological study on MB was done to primarily focus on the MB thickness and the MMI and address its predictive value in context with

Table 2. Myocardial bridges and afflicted arteries across different population groups.

Authors	Study type	Number of specimens	Frequent artery involved	Population group
Bezerra et al., 1989	Cadaveric	90	LAD	Brazilian
Channer et al., 1990	Angiographic	1102	LAC	British
Ferreira et al., 1991	Cadaveric	90	LAD	Brazilian
Lima et al., 2002	Cadaveric	30	LAD	Brazilian
Ballesteros et al., 2008	Cadaveric	86	LAD	Colombian
Bandyopadhyay et al., 2010	Cadaveric	42	LAD	Indian
Saidi et al., 2010	Cadaveric	109	LAD	African
Saini et al., 2012	Cadaveric	100	Posterior interventricular branch of both coronaries	Indian
Lujinovic et al., 2013	Cadaveric	30	LAD	Bosnian
Ashraf et al., 2014	Cadaveric	60	LAD	Arab
*Tiryakioglu et al.,*2019	Angiographic	1	RCA	Nigerian
Zhu et al., 2021	CTA	106	LAD	Diagnosed HOCM cohort of Chinese
Cai et al., 2022	CTA	1	Right coronary artery and total absence of left coronary artery	Chinese
Alexandre et al., 2022	CTA	1	LAD	Portuguese
Bai et al., 2022	CTA	1	LAD	Chinese
Okamura et al., 2022	OCT	1	Only LAD was included	Japanese

CAD and IHD. These parameters are found to be directly correlating with the risk of atheroma formation and subsequent CAD severity in (Ishikawa et al., 2009; Pargaonkar et al., 2018). We noticed that 20 % (2 out of 10 cadavers) of the studied cadavers possess MBs involving both the RCA and the LAD branch of LCA. Comparison of percentage prevalence of myocardial bridge in different studies has been tabulated (Table 3). The average MMI in these two cases was 1.39, which corroborated the existing literature and is significant enough for critical cardiac events. In addition to it, we have also observed a fairly large MB over the coronary sinus, which on gross examination revealed to be coating and might be constricting the sinus at systole. Former studies described similar MC over coronary veins, which were considered a benign finding (Hazirolan et al., 2007; Mohlenkamp et al., 2002). Nonetheless, the observed large MC encircling the coronary sinus in our case might worsen pre-existing the myocardial ischemia due to other causes at the time of systole and might aggravate myocardial ischemia & damage due to myocardial toxicity from ongoing waste product accumulation. It might also create a difficult situation in coronary sinus atrial pacing procedures, when the MC is close to the coronary ostium (Olgin et al., 1998). The histological examination of the segment of the MC over the CS confirmed the presence of myocardium. The MC was external to the epicardium in which the CS was embedded. The MC entirely composed of striated cardiac muscle fibers arranged spirally with characteristic central nuclei, branched muscle fibers and intercalated disc. The earliest extensive report of MC over myocardium along with a proposed classification system is seen in a cadaveric case series of late 1990s (von Ludinghausen et al., 1992). The targeted research to unfold the mystery of MC over CS seems to have been somewhat neglected in comparison to broad and extensive areas of medicine looking at coronary artery MB. The increasing importance of MC over CS can be understood from the cardiac interventions requiring cannulation of CS for drug delivery for retrograde cardioplegia, cardiac pacing and also in instances where coronary artery stenosis hinders the desired access. The same route is now employed for stem cell delivery to revive a degenerated myocardium which suffered recent MI (Kassem et al., 2021; Singh et al., 2005). There is a description of atrial macro-re-entry pathway through the MC over CS in atypical atrial flutter in a patient with obvious structural heart disease (Olgin et al., 1998).

The CAD severity is the net effect of the two mechanisms mentioned above operating simultaneously which is dependent on the

Table 3. Prevalence of MBs in different population groups in angiographic and cadaveric studies.

Authors	Population group	Sample Size	Type of study	Incidence of MB (in percentage)
Geiringer, 1951	British	100	Autopsy	23
Noble et al., 1976	Canadian	5250	Angiographic	0.51
Kramer et al., 1982	American	658	Angiographic	12
Angelini et al., 1983	American	1100	Angiographic	4.5
Wymore et al., 1989	American	64	Angiographic	33
Ferreira et al., 1991	Brazilian	90	Autopsy	55.6
Baptista et al., 1992	American	82	Autopsy	54
Juillière et al., 1995	France	4767	Angiographic	0.82
Harikrishnan et al., 1999	Indian	3200	Angiographic	0.60
Ortale et al., 2001	Brazilian	37	Autopsy	56
Kosiński et al., 2001	Polish	100	Autopsy	41
Podolec et al., 2019	Polish	298556	Angiographic	0.81
Matta et al., 2021	Polish	35813	Angiography	1.42
Claudino et al., 2022	Brazilian	57	Autopsy	40.3

different anatomical dimensions of the MB segment viz. thickness, length, muscle mass etc. whose various properties actually govern it indirectly. We are reporting here two cases of MBs encountered during cadaveric dissections, one of which not only had MBs over the two major coronary arteries but also had fairly large MC over the CS which is a unique situation having tremendous clinical repercussions. Specific correlation between the presence of MB and MC, their anatomical attributes and resultant adverse cardiac event could not be established from the available clinical history. Nevertheless, we should not forget to pay attention to these anatomical attributes while dealing with a patient with IHD; as these have close correlation with the onset, progression and eventual management plan of the CAD patients. Therefore, a large pool of data gathered through newer high resolution, high precision techniques such as MDCT, CCTA or OCT can illuminate more in this relatively grey area of anatomical attributes of myocardial bridge.

CONCLUSIONS

Though not every myocardial bridge (MB) can become determinant of avoidable serious cardiac consequences, some of the MBs obviously have definite proven correlation, which is brought about either by direct coronary arterial compression or by mediating endothelial injury. MB significantly adds to the intimal proliferative lesions combined with subsequent rupture and / or fissure of atheromatous plaques. There can be grave consequences in the form of occurrence of MI in very young age also. Cadaveric anatomic study integrated with the newer more efficient and high-resolution imaging modalities coupled with the clinical research will be able to not only identify the presence of minute MBs but also can quantify its anatomic properties and other attributes. Thus, anatomic parameters should be kept in mind to better appreciate MI in evolution and MI at evaluation in a case with myocardial bridge. Furthermore, it is believed that the finding of MC over CS in one of the 10 cadaveric hearts will ignite anatomist, cardiologist to look for the same in a more inquisitive manner into this less explored entity.

Ethical Approval and Consent to Participate

The study protocol was designed as per the prevailing guideline of the institute on the use of human cadaver for teaching and research and relevant ethical clearance was obtained from donor at the time of whole-body donation.

Availability of data and materials

All data and materials can be procured from first (Dibakar Borthakur) and corresponding (Rima Dada) authors.

Authors Contributions

Dibakar Borthakur and Rajesh Kumar-carried out dissection, staining and wrote the main manuscript, Rima Dada-Reviewed and corrected the final manuscript. All authors reviewed the manuscript.

ACKNOWLEDGEMENTS

The authors also sincerely thank those who donated their bodies to science so that anatomical research could be performed. Results from such research can potentially increase mankind's overall knowledge that can then improve patient care. Therefore, these donors and their families deserve our highest gratitude.

REFERENCES

ALEGRIA JR, HERRMANN J, HOLMES JR DR, LERMAN A, RIHAL CS (2005) Myocardial bridging. *Eur Heart J*, 26(12): 1159-1168.

ALEXANDRE A, VIEIRA P, DIAS-FRIAS A, PEREIRA A, CAMPINAS A, SÁ-COUTO D, BROCHADO B, SÁ I, SILVEIRA J, TORRES S (2022) Myocardial bridging leading to cardiac collapse in a marathon runner. *J Cardiovasc Develop Dis*, 9(7): 200.

ANGELINI P, TRIVELLATO M, DONIS J, LEACHMAN RD (1983) Myocardial bridges: a review. *Prog Cardiovascr Dis*, 26(1): 75-88.

BAI B, MA H, GUO L, YU X, WANG H, LIU Y, YIN H, LIU F, GENG Q (2022) Adenosine-induced myocardial ischemia in a patient with myocardial bridge: a case report. *Heart Mind*, 6(2): 87.

BALLESTEROS LE, RAMIREZ LM (2008) Morphological expression of the left coronary artery: a direct anatomical study. *Folia Morphol*, 67(2): 135-142.

BANDYOPADHYAY M, DAS P, BARAL K, CHAKROBORTY P (2010) Morphological study of myocardial bridge on the coronary arteries. *Ind J Thorac Cardiovasc Surg*, 26(3): 193-197.

BAPTISTA CAC, DIDIO LJA (1992) The relationship between the directions of myocardial bridges and of the branches of the coronary arteries in the human heart. *Surg Radiol Anat*, 14(2): 137-140.

BEAHM E, TERESI L, LUFKIN R, HANAFEE W (1990) MR of the paranasal sinuses. *Surg Radiol Anat*, 12(3): 203-208.

BLACK S (1805) A case of angina pectoris with dissection. *Memoirs Med Soc Lond,* 6: 41.

BOURASSA MG, BUTNARU A, LESPÉRANCE J, TARDIF JC (2003) Symptomatic myocardial bridges: overview of ischemic mechanisms and current diagnostic and treatment strategies. *J Am Coll Cardiol*, 41(3): 351-359.

CAI M (2022) Single coronary artery malformations combined with coronary heart disease, What should we do? *J Clin Res Bioeth*, 13: 445.

CHANNER KS, BUKIS E, HARTNELL G, REES JR (1990) Myocardial bridging of the coronary arteries. *Clin Radiol*, 40(4): 355-359.

CHAUVIN M, SHAH DC, HAÏSSAGUERRE M, MARCELLIN L, BRECHENMACHER C (2000) The anatomic basis of connections between the coronary sinus musculature and the left atrium in humans. *Circulation*, 101(6): 647-652.

CORBAN MT, HUNG OY, ESHTEHARDI P, RASOUL-ARZRUMLY E, MCDANIEL M, MEKONNEN G, TIMMINS LH, LUTZ J, GUYTON RA, SAMADY H (2014) Myocardial bridging: contemporary understanding of pathophysiology with implications for diagnostic and therapeutic strategies. *J Am Coll Cardiol*, 63(22): 2346- 2355.

DOS SANTOS JC, BARRETO JEF, DE SOUSA RCF, DE LIMA FS, OLIVEIRA ADSB (2022) Morphological analysis of myocardial bridges and coronary arterial dominance in northeast Brazil. *Morphologie*, 106(353): 92-97.

FERREIRA AG, TROTTER SE, KÖNIG B, DECOURT LV, FOX K, OLSEN EG (1991) Myocardial bridges: morphological and functional aspects. *Heart*, 66(5): 364-367.

GEIRINGER E (1951) The mural coronary. *Am Heart J*, 41(3): 359-368.

HARIKRISHNAN S, SUNDER KR, THARAKAN J, TITUS T, BHAT A, SIVASANKARAN S, BIMAL F (1999) Clinical and angiographic profile and follow-up of myocardial bridges: a study of 21 cases. *Indian Heart J*, 51(5): 503-507.

HAZIROLAN T, CANYIGIT M, KARCAALTINCABA M, DAGOGLU MG, AKATA D, AYTEMIR K, BESIM A (2007) Myocardial bridging on MDCT. *Am J Roentgenol*, 188(4): 1074-1080.

HOSTIUC S, RUSU MC, HOSTIUC M, NEGOI RI, NEGOI I (2017) Cardiovascular consequences of myocardial bridging: A meta-analysis and meta-regression. *Sci Rep*, 7(1): 1-13.

ISHII T, HOSODA Y, OSAKA T, IMAI T, SHIMADA H, TAKAMI A, YAMADA H (1986) The significance of myocardial bridge upon atherosclerosis in the left anterior descending coronary artery. *J Pathol*, 148(4): 279-291.

ISHII T, ISHIKAWA Y, AKASAKA Y (2014) Myocardial bridge as a structure of "double- edged sword" for the coronary artery. *Ann Vasc Dis*, 7(2): 99-108.

ISHIKAWA Y, AKASAKA Y, SUZUKI K, FUJIWARA M, OGAWA T, YAMAZAKI K, NIINO H, TANAKA M, OGATA K, MORINAGA S, EBIHARA Y (2009) Anatomic properties of myocardial bridge predisposing to myocardial infarction. *Circulation*, 120(5): 376-383.

JUILLIÈRE Y, BERDER V, SUTY-SELTON C, BUFFET P, DANCHIN N, CHERRIE F (1995) Isolated myocardial bridges with angiographic milking of the left anterior descending coronary artery: A long-term follow-up study. *Am Heart J*, 129(4): 663-665.

KASSEM MW, LAKE S, ROBERTS W, SALANDY S, LOUKAS M (2021) Cardiac veins, an anatomical review. *Translat Res Anat*, 23: 100096.

KOSIŃSKI A, GRZYBIAK M (2001) Myocardial bridges in the human heart: morphological aspects. *Folia Morphol*, 60(1): 65-68.

KRAMER JR, KITAZUME H, PROUDFIT WL, SONES FMJ (1982) Clinical significance of isolated coronary bridges: benign and frequent condition involving the left anterior descending artery. *Am Heart J*, 103(2): 283-288.

LIMA VJ, CAVALCANTI JS, TASHIRO T (2002) Myocardial bridges and their relationship to the anterior interventricular branch of the left coronary artery. *Arquivos Brasil Cardiol*, 79: 219-222.

LUJINOVIĆ A, KULENOVIĆ A, KAPUR E, GOJAK R (2013) Morphological aspects of myocardial bridges. *Bosnian J Basic Med Sci*, 13(4): 212.

MATTA A, CANITROT R, NADER V, BLANCO S, CAMPELO-PARADA F, BOUISSET F, RONCALLI J (2021) Left anterior descending myocardial bridge: Angiographic prevalence and its association to atherosclerosis. *Indian Heart J*, 73(4): 429-433.

MÖHLENKAMP S, HORT W, GE J, ERBEL R (2002) Update on myocardial bridging. *Circulation*, 106(20): 2616-2622.

NASR AY (2014) Myocardial bridge and coronary arteries: morphological study and clinical significance. *Folia Morphol*, 73(2): 169-182.

NOBLE J, BOURASSA MG, PETITCLERC R, DYRDA I (1976) Myocardial bridging and milking effect of the left anterior descending coronary artery: Normal variant or obstruction? *Am J Cardiol*, 37(7): 993-999.

OKAMURA A, OKURA H, IWAI S, KYODO A, KAMON D, HASHIMOTO Y, UEDA T, SOEDA T, WATANABE M, SAITO Y (2022) Detection of myocardial bridge by optical coherence tomography. *Int J Cardiovasc Imaging*, 38(5): 1169-1176.

OLGIN JE, JAYACHANDRAN JV, ENGESSTEIN E, GROH W, ZIPES DP (1998) Atrial macroreentry involving the myocardium of the coronary sinus: a unique mechanism for atypical flutter. *J Cardiovasc Electrophysiol*, 9(10): 1094-1099.

ORTALE JR, GABRIEL EA, IOST C, MÁRQUEZ CQ (2001) The anatomy of the coronary sinus and its tributaries. *Surg Radiol Anat*, 23(1): 15-21.

PARGAONKAR V, SCHNITTGER I, ROGERS I, TANAKA S, YAMADA R, KIMURA T, BOYD J, TREMMEL J (2018) Myocardial bridge muscle index (MMI): a marker of disease severity and its relationship with endothelial dysfunction and symptomatic outcome in patients with angina and a hemodynamically significant myocardial bridge. *J Am Coll Cardiol*, 71(11S): A160-A160.

POLACEK P, KRALOVE H (1961) Relation of myocardial bridges and loops on the coronary arteries to coronary occlusions. *Am Heart J*, 61: 44-52.

PORTMAN W, INGRID J (1960) Intramural coronary vessels in the angiogram. *Fortschr Geb Rontgenstr Nuklearmed*, 92: 129-133.

REYMAN HC (1737) Disertatio de vasis cordis propriis. *Med Diss Univ Göttingen,* 7th Sep 1-32.

ROGERS IS, TREMMEL JA, SCHNITTGER I (2017) Myocardial bridges: Overview of diagnosis and management. *Congenit Heart Dis*, 12(5): 619-623.

SAIDI H, ONGETI WK, OGENG'O J (2010) Morphology of human myocardial bridges and association with coronary artery disease. *Afr Health Sci*, 10(3): 242-247.

SINGH JP, HOUSER S, HEIST EK, RUSKIN JN (2005) The coronary venous anatomy: a segmental approach to aid cardiac resynchronization therapy. *J Am Coll Cardiol*, 46(1): 68-74.

SORAN O, PAMIR G, EROL C, KOCAKAVAK C, SABAH I (2000) The incidence and significance of myocardial bridge in a prospectively defined population of patients undergoing coronary angiography for chest pain. *RECON no. 20010062749. Tokai J Exp Clin Med*, 25(2): 57-60.

TIRYAKIOĞLU M, ALIYU MN (2020) Myocardial bridge. *Folia Morphol*, 79(2): 411-414.

VON LÜDINGHAUSEN M, OHMACHI N, BOOT C (1992) Myocardial coverage of the coronary sinus and related veins. *Clin Anat*, 5(1): 1-15.

WYMORE P, YEDLICKA JW, GARCIA-MEDINA V, OLIVARI MT, HUNTER DW, CASTAÑEDA-ZÚÑIGA WR, AMPLATZ K (1989) The incidence of myocardial bridges in heart transplants. *Cardiovasc Intervent Radiol*, 12(4): 202-206.

ZEINA AR, ODEH M, BLINDER J, ROSENSCHEIN U, BARMEIR E (2007) Myocardial bridge: evaluation on MDCT. *Am J Roentgenol*, 188(4): 1069-1073.

ZHU C, WANG S, WANG S, MENG Y, YANG Q, NIE C, SUN H (2021) Prevalence and characteristics of intramural coronary artery in hypertrophic obstructive cardiomyopathy: a coronary computed tomography and invasive angiography study. *Quant Imaging Med Surg*, 11(1): 162-171.

Anatomical study of pulmonary fissures

Alexander Zahariev, Andrés Berke, Santiago Cubas, Ana Villar, Gustavo A. Ugon

Departamento de Anatomía, Facultad de Medicina, Universidad de la República, Montevideo, Uruguay

SUMMARY

The lungs have three main fissures: in the right lung, the oblique and horizontal fissure, and in the left lung the oblique fissure. These can be complete, incomplete or absent. "Classical anatomy" textbooks frequently describe pulmonary fissures as complete, although knowledge of their variations is important both for thoracic surgery and to understand the spread of disease. The objective of this study is to assess the frequency and extension of the main pulmonary fissures, as well as to determine the frequency and location of accessory fissures in cadaveric material.

An observational descriptive study was carried out and consisted of the dissection of 86 ex-situ lungs (43 right and 43 left lungs) of adult corpses from both sexes previously fixed in formaldehyde solution. The presence of complete, incomplete or absent main fissures and the presence of accessory fissures were assessed. For incomplete fissures, the integrity percentage of the fissure was calculated.

In both lungs, incomplete fissures predominated; the oblique fissure of the right lung with a percentage of 65%, the horizontal fissure of 79% and the oblique fissure of the left lung of 58%. Regarding accessory fissures, the overall prevalence was 6%.

The anatomy of pulmonary fissures is highly variable. In our study, incomplete fissures predominated in both lungs. There are differences between the studies regarding the prevalence of the completeness of the fissures because, actually, the literature is not concluding.

Key words: Pulmonary fissures – Right oblique fissure – Right horizontal fissure – Left oblique fissure – Accessory fissures

INTRODUCTION

Classically, the lungs are divided into lobes by three main fissures. There are two main fissures in the right lung: the oblique fissure, which has an anteroinferior direction and divides the inferior lobe from the superior and medium lobes; and the horizontal fissure, which extends from the medium part of the oblique fissure to the anterior aspect of pulmonary hilum, separating the superior lobe from the medium lobe. The left lung consists of two lobes, superior and inferior, separated by the oblique fissure.

These fissures form during embryologic development as a consequence of parenchymal obliteration between bronchopulmonary segments. They have variable depth and they are covered by a double visceral pleura layer in all the extension. Fissures facilitate the movement of the pulmonary lobes, allowing the uniform expansion of the entire lung (Sudikshya et al., 2018).

Variations in fissure were described by Medlar in 1947 through autopsies demonstrating that these can be complete, incomplete, or, less frequently, absent (Medlar., 1947; Sudikshya et al., 2018). When the fissure is complete, lobes remain

Corresponding author:
Alexander Zahariev. Palermo 5819, Montevideo, 11400 Uruguay. Phone: +598 94 667 066. E-mail: alexanderzahariev97@gmail.com

Submitted: August 25, 2022. **Accepted:** September 29, 2022

https://doi.org/10.52083/EKOM2824

attached only in the hilum by the bronchus and pulmonary vessels; when it is incomplete, there exist parenchymal fusion areas between the lobes, and the fissure does not reach the hilum. The presence of incomplete fissures permits to spread benign illnesses, as well as malignant, to the adjacent lobes through parenchymal fusion (Sudikshya et al., 2018).

Regarding thorax surgery, the bibliography demonstrates a higher incidence of postoperative complications when the fissure is incomplete. Therefore, the more incomplete the pulmonary fissures are, the highest the morbidity (West et al., 2020).

Accessory fissures have also been described. The presence of the accessory fissures has imaging importance, which could lead to confusing interpretations and mistaken diagnosis.

The aim of this study is to determine the frequency and extension of the main pulmonary fissures, and to determine the frequency and location of the accessory fissures in cadaveric material.

MATERIALS AND METHODS

An observational descriptive study was carried out and consisted of the dissection of 86 ex-situ lungs (43 right and 43 left lungs) of adult corpses from both sexes previously fixed in formaldehyde solution. Those corpses were all Caucasian between sixty and seventy years old, without any evident pleuropulmonary pathologies. Due to ex-situ dissections, we were not able to identify the sex of each of the samples, and therefore our data do not allow considering differences between males and females. Corpses in which the thorax had been approached and which could have altered the normal pleuropulmonary anatomy were excluded.

The torax was approached through full sternotomy, and cardio-bipulmonary blocks were extracted.

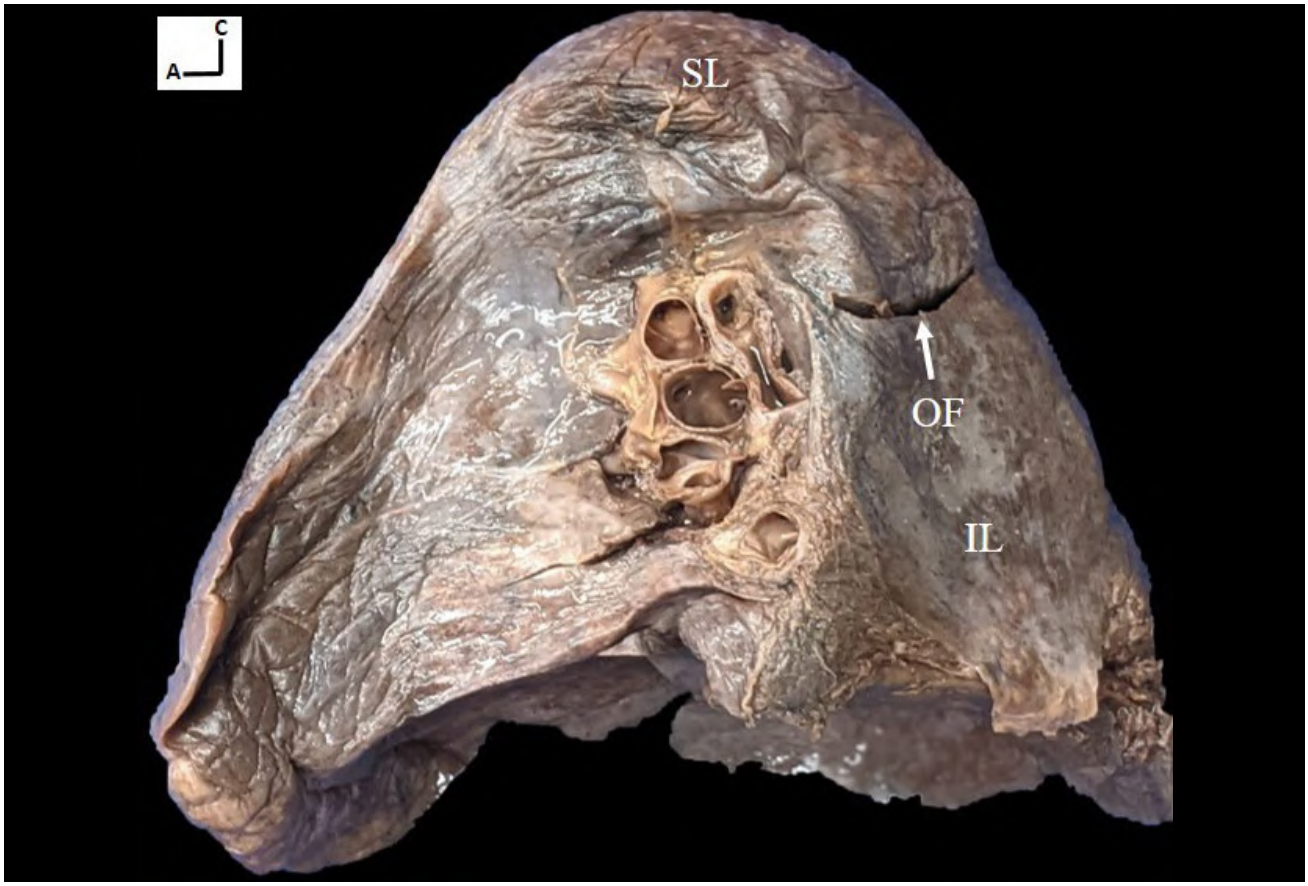

Fig. 1.- Mediastinal surface of the right lung. An incomplete oblique and horizontal fissure is observed; the first portion of the oblique fissure is in the posterosuperior part of the hilium, and in the anterior part of the hilium both fissures are absent. SL: Superior lobe; OF: Oblique fissure; IL: Inferior lobe.

The recorded variables were the following: presence of complete, incomplete or absent main fissures, and presence of accessory fissures.

Incomplete fissures were measured with a measuring tape on the pulmonary surface. Both length and projection of the fissure were measured. Right and left oblique fissure measures were taken from the posterior aspect of the hilum to its anterior aspect, following the path of the fissures. The measure of the horizontal fissure was taken from its origin in the anterior aspect of the oblique fissure to the anterior aspect of the hilium, following the path of the fissure.

In incomplete fissures, the integrity percentage of the fissure was calculated (length/length+projection). Posteriorly, it has been classified into four groups: group 1 (0% - 25%); group 2 (26% - 50%); group 3 (51% - 75%); and group 4 (76% - 99%).

RESULTS

In both lungs (see Figs. 1-3 for morphological details), incomplete fissures were predominant (Table 1). The integrity percentage varies according to the analyzed fissure, obtaining, in the right lung, an average of 81.2% for the oblique fissure; and 47.6% for the horizontal fissure. In the left lung, the average percentage was of 76.2%.

Regarding the accessory fissures, a global prevalence of 6% was obtained (see Figs. 4-6). In the right lung, there were observed 3 superior accessory fissures in the inferior lobe, and, in the left lung, 2 horizontal fissures (Table 1).

DISCUSSION

Many authors have studied pulmonary fissures in cadaveric material, mostly in Indian population (Prakash et al., 2010; Bhimai Devi et al., 2011; Nene et al., 2011; Dutta et al., 2013; Ghosh et al., 2013; Jacob and Pillay, 2013; George et al., 2014;

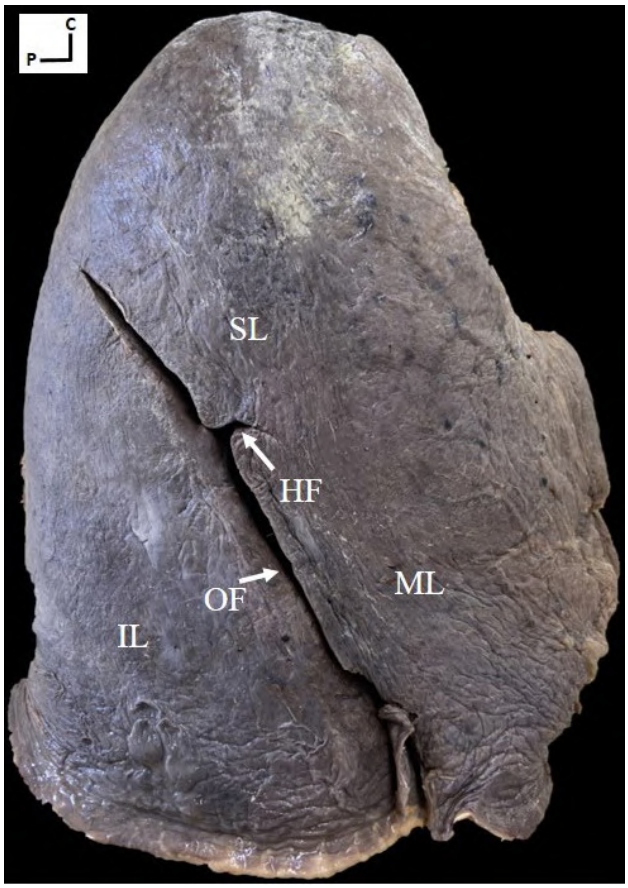

Fig. 2.- Costal surface of the right lung. An incomplete horizontal fissure is observed. SL: Superior lobe; ML; Medium lobe; IL: Inferior lobe; OF: Oblique fissure; HF: Horizontal fissure.

Fig. 3.- Mediastinal surface of the left lung. An incomplete oblique fissure is observed; the first portion of the oblique fissure is in the posterosuperior part of the hilium, and in the anterior part of the hilium the fissure is absent. SL: Superior lobe; OF: Oblique fissure; IL: Inferior lobe.

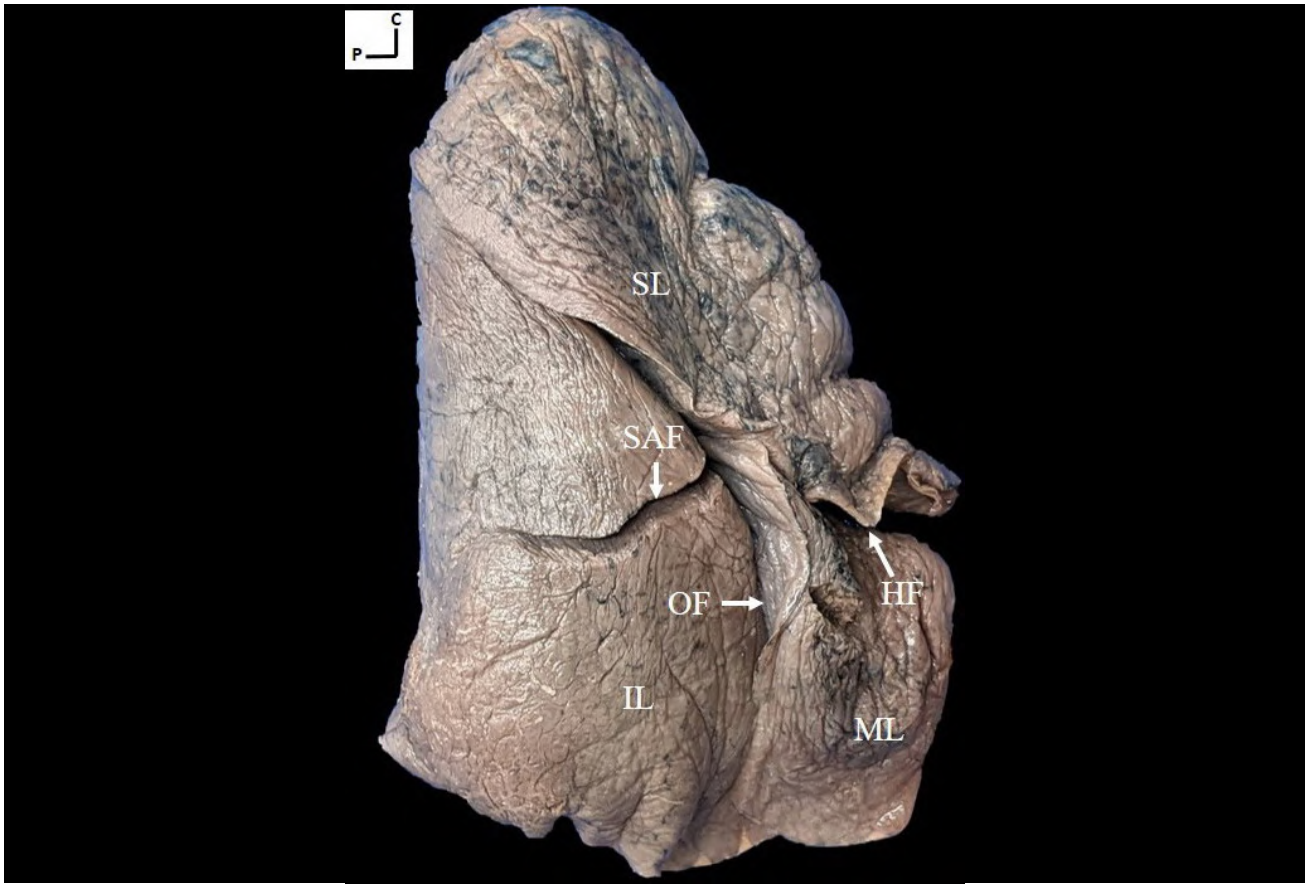

Fig. 4.- Costal surface of the right lung. In the inferior lobe, a superior accessory fissure is observed. SL: Superior lobe; ML; Medium lobe; IL: Inferior lobe; OF: Oblique fissure; HF: Horizontal fissure. SAF: Superior accessory fissure.

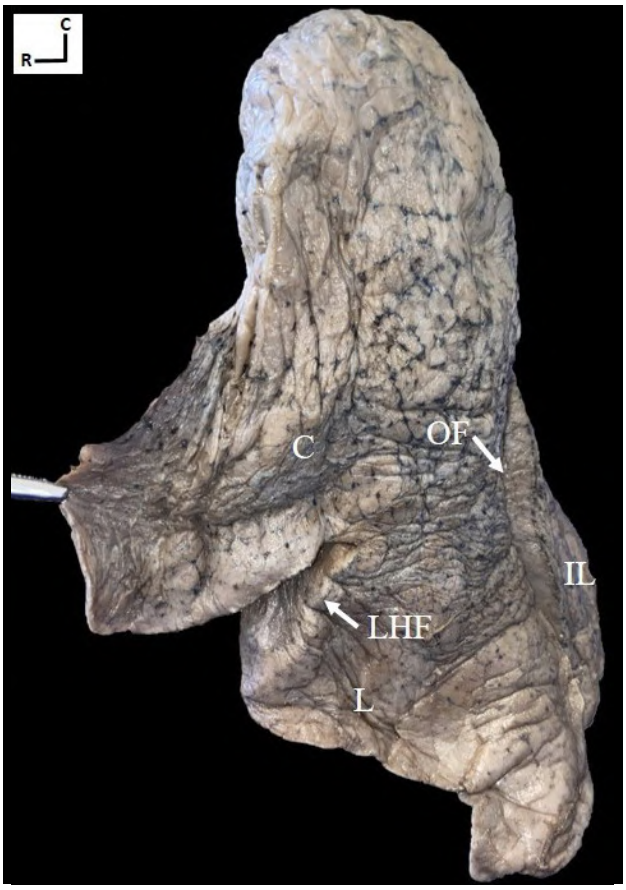

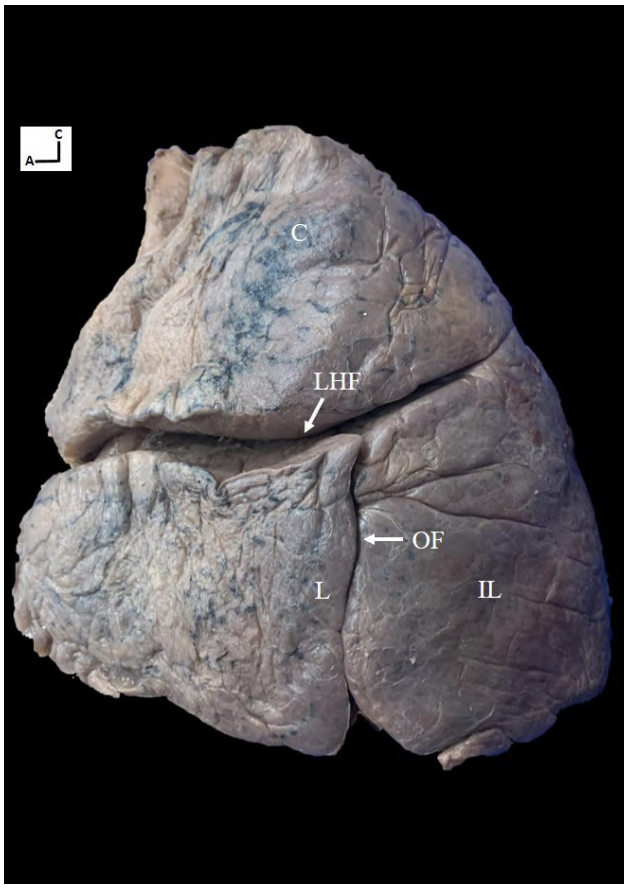

Figs. 5 and 6.- Costal surface of the left lung. In the superior lobe, a horizontal fissure is observed. C: Culmen; L: Lingula; LHF: Left horizontal fissure; OF: Oblique fissure; IL: Inferior lobe.

Table 1. Analyzed variables and results are expressed as absolute frequency and percentual relative frequency.

Right lung			
Oblique fissure	**Nº (%)**	**Horizontal fissure**	**Nº (%)**
Complete fissure	15 (35%)	Complete fissure	9 (21%)
Incomplete fissure	28 (65%)	Incomplete fissure	34 (79%)
Absent fissure	0 (0%)	Absent fissure	0 (0%)
Integrity percentage of fissure	**Nº (%)**	**Integrity percentage of fissure**	**Nº (%)**
0% - 25%	0 (0%)	0% - 25%	4 (11.8%)
26% - 50%	0 (0%)	26% - 50%	17 (50%)
51% - 75%	6 (21.4%)	51% - 75%	10 (29.4%)
76% - 99%	22 (78.6%)	76% - 99%	3 (8.8%)
Average	81.2%	Average	47.6%
Left lung			
Oblique fissure	**Nº (%)**	**Integrity percentage of fissure**	**Nº (%)**
Complete fissure	18 (42%)	0% - 25%	0 (0%)
Incomplete fissure	25 (58%)	26% - 50%	1 (4%)
Absent fissure	0 (0%)	51% - 75%	8 (32%)
		76% - 99%	16 (64%)
		Average	0.762
Accesory fissure			
	Prevalence	**Type of fissure**	
Right lung	3 (7%)	Superior accessory fissure of inferior lobe	
Left lung	2 (4.7%)	Horizontal fissure of superior lobe	

Kaul et al., 2014; Quadros et al., 2014; Magadum et al., 2015; Mamatha et al., 2016; Sudikshya et al., 2018; Jacob et al., 2019) and, to a lesser extent, in European studies (Unver Dogan, 2015; Bostanci et al., 2019; West et al., 2020). The current study is the first cadaveric study of the pulmonary fissures in Uruguayan population.

The anatomy of the pulmonary fissures is highly variable. Differences among the studies concern the prevalence of complete, incomplete and absent fissures (see Table 2). These differences could be attributed to methodological heterogeneity and, probably, ethnicity (West et al., 2020).

Regarding the oblique fissure of the right lung, in the literature there is a higher predominance of complete fissures (Table 2). However, the current study is concordant with the studies by Dutta et al. (2013), Jacob and Pillay (2013), Magadum et al. (2015), Bostanci et al. (2019) and Jacob et al. (2019) in that a predominance of incomplete fissures is observed.

At the same time, the highest prevalence of incomplete oblique fissures was obtained in the current study (65%). The absent fissure was less frequent, even though Magadum et al. (2015) reported a prevalence of 10%.

The horizontal fissure is the most variable of the main fissures (Table 2). Most of the studies observed a predominance of the complete horizontal fissures, even though our current study and six analyzed studies (Prakash et al., 2010; Jacob and Pillay, 2013; Magadum et al., 2015; Bostanci et al., 2019; Jacob et al., 2019; West et al., 2020) reported a predominance of incomplete horizontal fissure with a range between 50% and 83.4%. The horizontal fissure is also the most frequently reported as absent. Ghosh et al. (2013) and Kaul et al. (2014) reported percentages of 47.8% and 40% of absent horizontal fissure, respectively. In the current study we did not report absent horizontal fissure, as in the study by Mamatha et al. (2016).

Table 2. Comparison of the completeness of right oblique fissure and horizontal fissure within the literature. Analyzed variables and results are expressed as absolute frequency and percentual relative frequency.

Authors (year of publication)	Right lung						
	Nº	Oblique fissure			Horizontal fissure		
		Complete	Incomplete	Absent	Complete	Incomplete	Absent
Prakash et al. 2010	28	15 (53.6%)	11 (39.3%)	2 (7.1%)	12 (42.9%)	14 (50%)	2 (7.1%)
Bhimai Devi et al. 2011	22	20 (91%)	2 (9%)	-	16 (72.7%)	4 (18.2%)	2 (9.1%)
Nene et al. 2011	50	46 (92%)	3 (6%)	1 (2%)	39 (78%)	4 (8%)	7 (14%)
Dutta et al. 2013	52	14 (26.9%)	32 (61.5%)	6 (11.5%)	31 (59.6%)	13 (25%)	18 (34.6%)
Ghosh et al. 2013	46	36 (78.2%)	9 (19.6%)	1 (2.2%)	12 (26.1%)	12 (26.1%)	22 (47.8%)
Jacob and Pillay, 2013	30	14 (46.6%)	15 (50%)	1 (3.4%)	3 (10%)	25 (83.4%)	2 (6.6%)
George et al. 2014	65	63 (97%)	2 (3%)	-	40 (61.6%)	23 (35.4%)	2 (3%)
Kaul et al. 2014	50	34 (68%)	12 (24%)	4 (8%)	14 (28%)	16 (32%)	20 (40%)
Quadros et al. 2014	36	34 (94.4%)	2 (5.6%)	-	23 (64%)	9 (25%)	4 (11%)
Magadum et al. 2015	40	12 (30%)	24 (60%)	4 (10%)	14 (35%)	21 (52.5%)	5 (12.5%)
Unver Dogan et al. 2015	210	207 (98.6%)	3 (1.4%)	-	188 (89.5%)	18 (8.6%)	4 (1.9%)
Mamatha et al. 2016	20	17 (85%)	3 (15%)	-	10 (50%)	10 (50%)	-
Sudikshya et al. 2018	50	16 (69.6%)	7 (30.4%)	-	12 (52.2%)	8 (34.8%)	3 (13%)
Bostanci et al. 2019	256	91 (35.5%)	165 (64.5%)	-	70 (27.3%)	175 (68.4%)	11 (4.3%)
Jacob et al. 2019	47	23 (49%)	24 (51%)	-	7 (15%)	33 (70%)	7 (15%)
West et al. 2020	81	52 (64.2%)	29 (35.8%)	-	18 (22.2%)	54 (66.7%)	9 (11.1%)

Concerning the oblique fissure of the left lung, most of the authors obtained a predominance of complete fissure (Table 3). However, in the current study as well as in other analyzed studies (Dutta et al., 2013; Sudikshya et al., 2018; Bostanci et al., 2019; Jacob et al., 2019) a predominance of the 48% and 63% of the incomplete oblique fissures were reported. Bostanci et al. (2019) is the study which includes the highest number of lungs (256), and reports the highest prevalence of incomplete oblique fissure (63%) The left absent oblique fissure is less frequent. Prakash et al. (2010) reported the highest prevalence of absent fissure (10%).

There also exists a wide variety of pulmonary fissures reported in studies using computed tomography (CT). The anatomy of the pulmonary fissures differs from those reported in cadaveric studies. Ozmen et al. (2010) carried out a retrospective study which included 387 CT and observed that the right oblique and horizontal fissures, as well as the left oblique fissures were incomplete in 69.7%, 86.9% and 48.3%, respectively (Ozmen et al., 2010). These results differ from the studies analysed in Tables 2 and 3.

Further studies have demonstrated that preoperative CT is not a completeness predictor of pulmonary fissures in thoracic surgery (Schieman et al., 2011; Kent et al., 2015). This highlights the importance of studying fissure anatomy with cadaveric material. Therefore, we emphasize the value of carrying out more cadaveric studies with a larger population in order to obtain an approximate prevalence of the completeness of the main pulmonary fissures, due to the fact that, actually, the literature is not concluding.

In the current study, the percentage of the pulmonary fissure integrity was calculated in the surface of the lung. This allows us to know how complete the pulmonary fissures are when they are incomplete. In order to do this, we divided it into 4 groups (Table 1), as Ozmen et al. (2010) did in their study using CT. The results of this study and the present one are similar, taking into consideration that there may be differences between both study methods (cadaveric study

Table 3. Comparison of the completeness of left oblique fissure within the literature. Analyzed variables and results are expressed as absolute frequency and percentual relative frequency.

Authors (year of publication)	Left lung			
	Nº	Oblique fissure		
		Complete	Incomplete	Absent
Prakash et al. 2010	28	15 (53.6%)	10 (35.7%)	3 (10.7%)
Bhimai Devi et al. 2011	22	12 (54.5%)	8 (36.4%)	2 (9.1%)
Nene et al. 2011	50	44 (88%)	6 (12%)	-
Dutta et al. 2013	50	22 (44%)	24 (48%)	4 (8%)
Ghosh et al. 2013	36	29 (80.6%)	5 (13.9%)	2 (5.5%)
Jacob & Pillay 2013	18	11 (61.1%)	7 (38.9%)	-
George et al. 2014	73	62 (85%)	11 (15%)	-
Kaul et al. 2014	50	30 (60%)	20 (40%)	-
Quadros et al. 2014	40	39 (97.5%)	1 (2.5%)	-
Magadum et al. 2015	40	20 (50%)	17 (42.5%)	3 (7.5%)
Unver Dogan et al. 2015	210	208 (99%)	2 (1%)	-
Mamatha et al. 2016	20	12 (60%)	7 (35%)	1 (5%)
Sudikshya et al. 2018	50	13 (48.2%)	14 (51.8%)	-
Bostanci et al. 2019	256	95 (37%)	161 (63%)	-
Jacob et al. 2019	49	16 (34%)	29 (62%)	2 (4%)
West et al. 2020	81	66 (81.5%)	13 (16%)	2 (2.5%)

vs in vivo study). In both, right and left oblique fissure completeness predominates in group 4. In the case of the horizontal fissure, the completeness is more heterogeneous among the groups, predominating in group 3 in the study of Ozmen et al. (2010) and in group 2 in the current study.

There are others classifications for the completeness of pulmonary fissures, such as the ones described by Craig and Walker (1997), which classify it into 4 grades. However, this classification is qualitative and do not allow us to characterize the incomplete fissure. Establishing the integrity percentage, as in the current study, will allow us to understand how complete the incomplete pulmonary fissure is, collaborating with thorax surgeons in their surgical plan (West et al., 2020).

Accessory fissures could be the result of the absence of parenchyma fusion in spaces where they would normally fusion. Any factor that alters the parenchyma fusion during the embryologic development is going to cause variations in lobes and pulmonary fissures (Meenakshi et al., 2004). These are generally situated in the limits of bronchopulmonary segments (Sudikshya et al., 2018; West et al., 2020). In the right lung, the most frequent are the following: in the superior lobe, the azygos fissure, which includes the azygos vein and it is called “azygos lobe”; in the inferior lobe, the superior accessory fissure, which separates superior segments from the basal segments; and the inferior accessory fissure, which separates the medial basal segment from the rest of the inferior lobe. In the left lung, the most frequent are the following: in the superior lobe, the horizontal fissure, which separates the lingula from the rest of the lobe; and, in the inferior lobe, the superior accessory fissure, which separates the superior segment from the basal segments (Sudikshya et al., 2018; West et al., 2020).

The accessory fissures found in the current study were the superior accessory fissure of the right inferior lobe, and the left horizontal fissure. In the reviewed bibliography, the superior accessory fissure is reported between 4% and 13.3% (Nene

et al., 2011; Jacob and Pillay, 2013; Bostanci et al., 2019). In the present study, we obtained a similar prevalence (7%). On the other hand, the left horizontal fissure is reported between 4.6% and 27.7%. In our study we obtained a prevalence of 4.7%.

Many authors highlighted the importance of knowledge about their frequency and location of accessory fissures due to the fact it could lead to mistaken interpretations in radiographies and CT. Furthermore, these could also be confused with pathologic process such as lineal atelectasis or pleural scars (Godwin and Tarver, 1985).

At the same time, the presence of accessory fissures can act as a barrier for spread of infection and malignant processes. It also explains the interlobar liquid distribution. Acknowledging their existence is of great importance for the thoracic surgeon in order to carry out a surgical plan for segmentary resections or pulmonary lobectomies (Ghosh et al., 2013).

Lastly, we highlight that a "classical anatomy" textbook lung describes 3 main pulmonary fissures and no accessory fissures. In our study, 18 out of 43 left lungs presented complete pulmonary fissure, as this "classical anatomy" textbook describes; and, in the right lung, only 3 out of 43 had both complete fissures. This should make us think about changing the concept given by "classical anatomy" textbooks; so anatomists, imaging specialist and thoracic surgeons must know that fissures are more variable than textbooks describe.

As for the limitations, we could not value the extension on depth of pulmonary fissures that also has surgical importance. This study was carried out in lungs fixed in formaldehyde, which determines changes that affect measures, however, unavoidable with cadaveric studies.

CONCLUSIONS

The anatomy of pulmonary fissures is highly variable. In our study, incomplete fissures predominated for the 3 main fissures. In the literature, we observed differences between the studies regarding the prevalence of complete, incomplete and absent fissures, as analyzed. For this reason, we emphasize the value of carrying out more cadaveric studies with a larger population in order to obtain an approximate prevalence of the completeness of the main pulmonary fissures, because, actually, the literature is not concluding.

ACKNOWLEDGEMENTS

The authors sincerely thank those who donated their bodies to science so that anatomical research and teaching could be performed. Results from such research can potentially increase scientific knowledge and can improve patient care. Therefore, these donors and their families deserve our highest respect.

REFERENCES

BHIMAI DEVI, NARASINGA RAO B, SUNITHA V (2011) Morphological variations of lung- A cadaveric study in north coastal Andhra Pradesh. *Int J Biol Med Res,* 2(4): 1149-1152.

BOSTANCI K, OZYURTKAN MO, POLAT MO, BATIREL H, LACIN T, YUKSEL M, STAMENOVIC D (2020) Variations in pulmonary fissural anatomy: a medicolegal autopsy study of 256 cases. *ANZ J Surg,* 90(4): 608-611.

DUTTA S, MANDAL L, MANDAL SK, BISWAS J, RAY A, BANDOPADHYAY M (2013) Natural fissures of lung - Anatomical basis of surgical techniques and imaging. *Nat J Med Res,* 3(2): 117-121.

GEORGE BM, NAYAK SB, MARPALLI S (2014) Morphological variations of the lungs: a study conducted on Indian cadavers. *Anat Cell Biol,* 46: 253-258.

GHOSH E, BASU R, DHUR A, ROY A, ROY H, BISWAS A (2013) Variations of fissures and lobes in human lungs-a multicentric cadaveric study from West Bengal, India. *Int J Anat Radiol Surg,* 2(1): 5-8.

GODWIN JD, TARVER RD (1985) Accessory fissures of the lung. *AJR Am J Roentgenol,* 144(1): 39-47.

JACOB S, PILLAY M (2013) Variations in the inter-lobar fissures of lungs obtained from cadavers of South Indian origin. *Int J Morphol,* 31(2): 497-499.

JACOB SM, VENNIYOOR V, PILLAY M (2019) Variations in the morphology of human lungs and its clinical implications. *J Morphol Sci,* 36: 231-236.

KAUL N, SINGH V, SETHI R, KAUL V (2014) Anomalous fissures and lobes of human lungs of North Indian population of western U.P. *J Anat Soc India,* 63: S26-S30.

KENT MS, RIDGE C, O´DELL D, LO P, WHYTE R, GANGADHARAN SP (2015) The accuracy of computed tomography to predict completeness of pulmonary fissures. *Annals ATS,* 12(5): 696-700.

MAGADUM A, DIXIT D, BHIMALLI S (2015) Fissures and lobes of lung – An anatomical study and its clinical significance. *Int J Curr Res Rev,* 7(3): 8-12.

MAMATHA Y, KRISHNA MURTHY C, PRAKASH BS (2016) Study of morphological variations of fissures and lobes of lung. *Int J Anat Res,* 4(1): 1874-1877.

MEDLAR EM (1947) Variations in interlobar fissures. *Am J Roentgenol Radium Ther,* 57(6): 723-725.

MEENAKSHI S, MANJUNATH KY, BALASRUBRAMANYAM V (2004) Morphological variations of the lung fissures and lobes. *Indian J Chest Dis Allied Sci,* 46: 179-182.

NENE AR, GAJENDRA KS, RAMANANDA SARMA MV (2011) Lung lobes and fissures: a morphological study. *Int J Exp Clin Anat,* 5: 32-38.

OZMEN CA, NAZAROGLU H, BAYRAK AH, SENTURK S, AKAY HO (2010) Evaluation of interlobar and accessory pulmonary fissures on 64-row MDCT. *Clin Anat,* 23: 552-558.

PRAKASH, BHARDWAJ AK, SHASHIREKHA M, SUMA HY, KRISHNA GG, SINGH G (2010) Lung morphology: a cadaver study in Indian population. *Ital J Anat Embryol,* 115(3): 235-240.

QUADROS LS, PALANICHAMY R, D ´SOUZA A (2014) Variations in the lobes and fissures of lungs – a study in South Indian lung specimens. *Eur J Anat,* 18(1): 16-20.

SCHIEMAN C, MACGREGOR JH, KELLY E, GRAHAM A, MCFADDEN SP, GELFAND G, GRONDIN SC (2011) Can preoperative computed tomography of the chest predict completeness of the major pulmonary fissure at surgery? *Can J Surg,* 54(4): 252-256.

SUDIKSHYA KC, SHRESTHA P, KUMAR SHAH A, KUMAR JHA A (2018) Variations in human pulmonary fissures and lobes: a study conducted in Nepalese cadavers. *Anat Cell Biol,* 51: 85-92.

UNVER DOGAN N, ILKNUR UYSAL I, DEMIRCI S, HAKAN DOGAN K, KOLCU G (2015) Major anatomic variations of pulmonary fissures and lobes on postmortem examination. *Acta Clin Croat*, 54(2): 201-207.

WEST CT, SLIM N, STEELE D, CHOWDHURY A, BRASSETT C (2021) Are textbook lungs really normal? A cadaveric study on the anatomical and clinical importance of variations in the major lung fissures, and the incomplete right horizontal fissure. *Clin Anat,* 34(3): 387-396.

Structural and functional deficits of the hippocampus in hydrocephalic rats: the role of age at onset and duration of disease

Matthew T. Shokunbi[1,2], Omowumi M. Femi-Akinlosotu[1], Funmilayo E. Olopade[1], Catherine Winiki[1]

[1] *Department of Anatomy, College of Medicine, University of Ibadan, Ibadan, Nigeria*
[2] *Department of Surgery, College of Medicine, University of Ibadan, Ibadan, Nigeria*

SUMMARY

We studied the pyramidal neurons of the hippocampus in neonatal, juvenile and adult rats with hydrocephalus of varying durations and related these changes to their learning and memory. Hydrocephalus was induced in 7-day-old neonates, 4-week-old juvenile and 16-week-old adult Albino rats by intra-cisternal injection 0.02-0.04 ml of 150mg/ml of kaolin in sterile water (150 mg/ml). We studied escape latency and platform crossings with the Morris water maze prior to animal sacrifice at 2 and 4 weeks post induction in neonates and at 4 and 8 weeks post induction in juveniles and adults. We examined pyramidal neurons with cresyl violet and modified Golgi stain and analyzed behavioural scores and pyknotic indices. Statistical significance was determined at $p<0.05$.

The basal dendrites of the pyramidal neurons were reduced in the hydrocephalic groups. In the CA1, the pyknotic index was significantly increased in both groups of hydrocephalic neonates but only in hydrocephalic juveniles and adults sacrificed at 4 weeks. In the CA3 it was increased in hydrocephalic neonates sacrificed at 2 weeks and hydrocephalic juveniles sacrificed at 4 weeks.

The escape latency was greater and the number of platform crossing was lower in the hydrocephalic rats than in their age matched controls. Pyramidal neurons were morphologically altered in hydrocephalus, in association with changes in spatial learning and memory. The CA1 region in young animals was particularly vulnerable. Functional recovery occurs with time and to a greater extent in older animals.

Keywords: Hydrocephalus – Hippocampus – Pyknotic index – Pyramidal neurons – Dendritic arbor

INTRODUCTION

Hydrocephalus is a neurological disorder characterized by enlargement of the brain ventricles due to inadequate passage of cerebrospinal fluid from the source of production within the cerebral ventricles to the area of absorption into the systemic circulation (Rekate, 2008). The pathophysiology of hydrocephalus is multifactorial in nature, with the primary consequences such as direct compression of brain tissue and blood vessels, white matter stretching, edema and reduced cerebral blood flow (McAllister and Chovan, 1998).

Corresponding author:
Matthew Temitayo Shokunbi. Department of Anatomy, College of Medicine, University of Ibadan, Ibadan, Nigeria. Phone: +2348022912220. E-mail: temitayoshokunbi@yahoo.com

Submitted: May 20, 2022. **Accepted:** October 10, 2022

https://doi.org/10.52083/BQJN1298

The hippocampus is the anatomical substrate for learning and memory, functioning in the consolidation of short-term into long term memory. It is microscopically divided into 3 sub-regions (CA1, CA2, CA3), and distinct cellular layers with the pyramidal cells as the principal neurons. However, the CA2 is not well delineated compared to the well-outlined CA1 and CA3 sub-regions. Hippocampal pyramidal neurons connect to neural circuits controlling cognition, memory and motor functions. The expanding ventricular system in hydrocephalus has been shown to compress periventricular structures, and impairment of learning and memory has been reported in hydrocephalic patients and experimental animals (Shim et al., 2003). It is unclear how age at onset and chronicity determine the extent of injury to the hippocampus in hydrocephalus.

We therefore hypothesize that, in hydrocephalus, the alterations in the principal output neurons of the hippocampus and the neurological sequelae will vary with the age of onset and chronicity of the disease. In this study, we examined the population and dendritic architecture of pyramidal neurons of the hippocampus and neurobeviour in neonatal, juvenile and adult hydrocephalic rats following variable periods of hydrocephalus.

MATERIALS AND METHODS

We induced hydrocephalus in neonatal (7 days), juvenile (4 weeks) and adult (16 weeks) rats by intra-cisternal injection of 0.02ml, 0.04ml and 0.06 ml respectively of kaolin suspension (150mg/ml in sterile water). The juvenile and adult rats were induced after anaesthetizing them with intra-peritoneal injection of ketamine/xylazine at 90/10 mg/kg. The control groups received a sham injection into the cisterna magna. All procedures on animal handling conformed to the acceptable guidelines of EU Directive 2010/63/EU for animal experiments (http://ec.europa.eu/environment/chemicals/lab_animals/legislation_en.htm) and the ethical use of animals in research according to the University of Ibadan Animal Care and Use Research Ethics Committee (UI-ACUREC). The rats had free access to water and feed and were weighed twice weekly. They were assessed for the development of hydrocephalus by examination of the head, gait and general grooming with the presence of a dome-shaped head. We sacrificed the animals in batches at 2 (acute) and 4 (intermediate) weeks after induction in the neonates, and at 4 (intermediate) and 8 (chronic) weeks in the juvenile and adult rats.

Behavioural Test: Morris Water Maze Task (MWM)

We examined spatial learning and memory in the rats with the Morris Water Maze (MWM) task (Morris, 1984). Hydrocephalic rats (neonate, juvenile and adult) in their two different timelines and their age-matched controls were tested with a 4-day MWM task of multiple trials (R'Hooge and Deyn, 2001). Six to twelve animals per group were used for the study. Tests were performed in a circular pool (152 cm diameter, 40 cm depth) that was marked north, south, east and west dividing it into four quadrants (Northeast, Northwest, Southeast and Southwest). A hidden platform was fixed in the center of one of the quadrants and submerged 1.0 cm beneath water surface at room temperature. The water was made opaque by adding concentrated milk to prevent the animal from seeing the hidden platform while it is submerged in the water. Each animal underwent nine trials for the training period (three trials per day). For each trial, the rats were placed facing a different direction away from the location of the platform and allowed to swim until they found the underwater platform. If the rat failed to complete the task in 60 seconds, it was guided onto the platform for at least 15 seconds rest before the next trial. The mean of the escape times of the three trials for the three days of training was taken as the escape latency and was compared between control and hydrocephalic rats. On the fourth day, the rats which have undergone the training were tested for memory function by a probe trial in which the hidden platform was removed from the maze. Each animal was place in the maze from any of the four quadrants and allowed to explore the pool for 60 seconds only. The number of times the rats were able to cross the platform location was recorded as a test for memory function while

the duration of time spent in each quadrant was recorded (Nunez, 2008).

Tissue processing

Neonatal rats were perfused transcardially first with normal saline for three minutes to wash out the blood cells and then for 15-20 minutes with 10% neural buffered formalin (NBF) until well fixed, while juvenile and adult rats were anaesthetized with intra-peritoneal injection of ketamine at 90/10 mg/kg before transcardial perfusion with 10% NBF, using pallor of the liver and stiff muscles as an indication of good fixation. The brains were quickly dissected out and fixed in the same solution. After fixation, coronal sections were obtained at the level of the optic chiasma and examined to confirm ventriculomegaly. Hydrocephalus was categorized as mild, moderate or severe according to Olopade et al. (2012). The majority of the neonatal and juvenile rats developed severe hydrocephalus while the adult rats developed mild form of hydrocephalus in both timelines.

Cresyl staining

Sectioned brain tissues (5 µm) were stained with cresyl violet to assess the pyramidal neurons of the hippocampal sub-regions for pyknotic neurons and cell density. These were then viewed with Leica ICC50E light microscope (Switzerland).

Modified Golgi staining

Fixed brain tissues were immersed in potassium dichromate solution (3 g/100 ml of distilled water) stored at room temperature for 5 (neonates) days and 7 days (juvenile and adults respectively) in a dark chamber (solution was replaced every 24 hours). Tissues were then transferred into silver nitrate solution (2 g/100 ml) and stored for 3 days in the dark chamber. The tissues were then infiltrated at 60ºC for 30 minutes, embedded in molten paraffin wax and cooled overnight which was then sectioned at 60 µm thickness. Each section was then transferred in a cassette into a graded series of alcohol (70%, 90%, 100%, 100%) for 3 minutes each and cleared in xylene for 5 minutes. The sections were later mounted on a gelatinized slides, cover-slipped with DPX, air dried and viewed with Leica ICC50E light microscope (Switzerland).

Statistical analysis

We analyzed data by one-way ANOVA using Graphpad Prism Version 6.0 for windows (SanDiego, Califonia USA). Statistical significance was set at $p < 0.05$, for the null hypothesis being true by chance and the confidence interval calculated at 95% level. Photographed sections of the hippocampus were examined and analyzed for pathological changes and neuronal density (using Motic Image Plus 2.0 software).

RESULTS

General observation

The experimental rats (kaolin injection) showed signs of hydrocephalus which included scurfy fur indicating impaired grooming (common to all age groups), unsteady gait and enlarged dome-shaped head in all the age groups. They lost appetite for suckling (neonates) and for their food pellets (juveniles and adults). The rats in the control group were well groomed, with normal head shape and size and they fed well.

Body Weight

The experimental rats (6-14 per group) lost body weight within the first week of kaolin injection, although they gained weight over the following weeks but remained consistently lighter in weight compared to their age-matched controls (7-10 per group). They also had a significantly lower rate of weight gain throughout the study period when compared to their control counterparts (Fig. 1: blue circles and lines depict control groups, while red squares and lines depict hydrocephalic groups).

Morris Water Maze Test

The time taken by each animal to locate the underwater hidden platform, i.e., escape latency, was reduced progressively in all the groups, but not at the same rate. Only the juvenile hydrocephalic rats at 8 weeks post-induction (Hydro Juvenile Chronic) learnt at a significantly slower rate than the other

groups (Fig. 2A). During the probe trial however, the Hydro Neonate Acute group had a significantly fewer number of platform crossings than their age-matched controls (p=0.0421, Fig. 2B).

Gross examination of the brain

Gross examination of the brains in the control group revealed a compact structure with distinct corpus callosum, and the lateral ventricles were slit-like, which cannot be easily distinguished. The gross appearance of the hydrocephalic brains showed enlarged lateral ventricles, a visible aqueduct of Sylvius with thinning of the corpus callosum and cerebral cortex (Fig. 3).

Cresyl Violet

Pyknotic neurons were counted on the cresyl stained sections while the pyknotic index was calculated as the number of pyknotic neurons expressed as a percentage of the total number of pyramidal neurons in the sample frame (Taveira et al., 2012). The cresyl violet staining

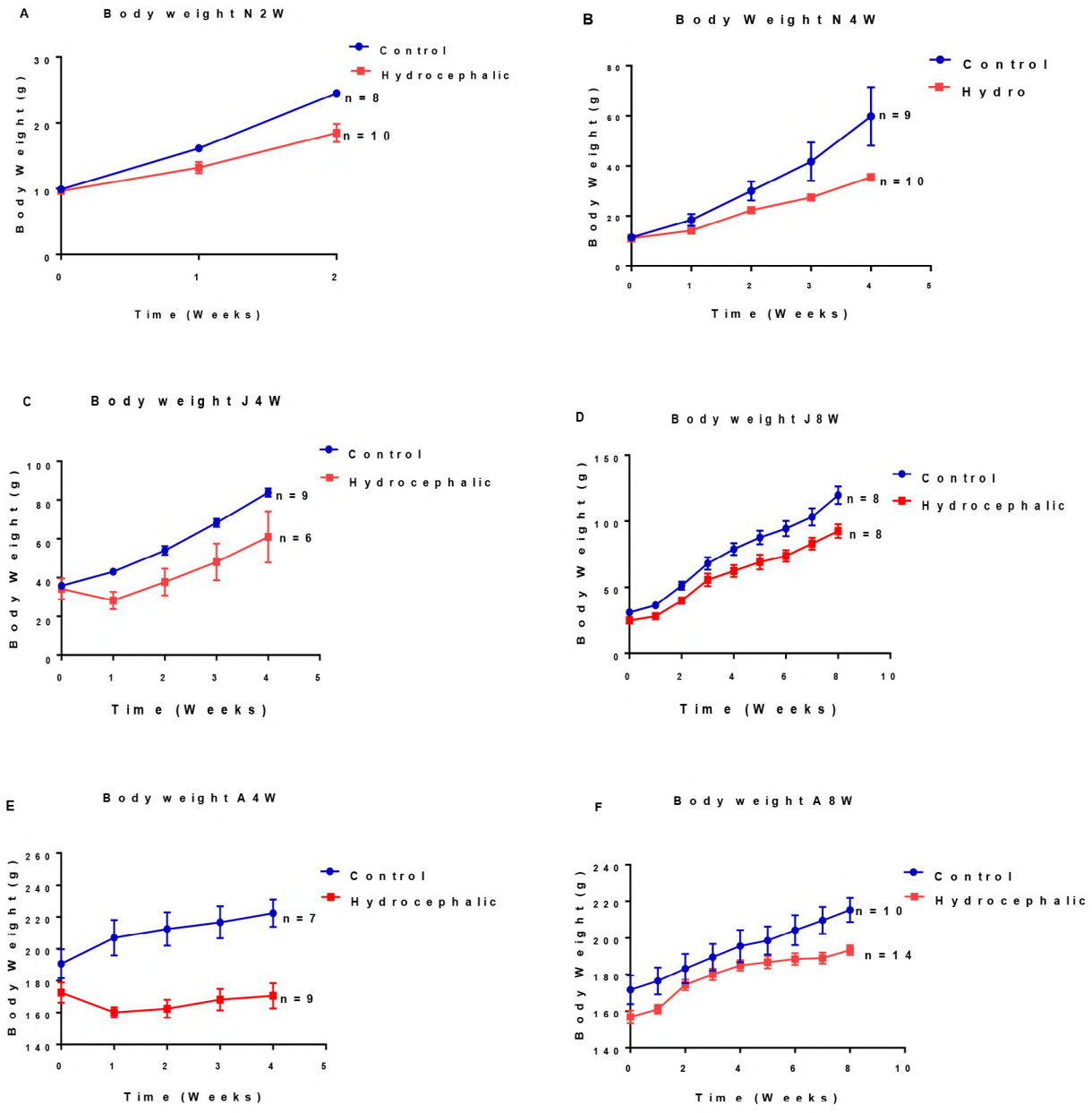

Fig. 1.- Body weight (g) gain of neonatal, juvenile and adult rats over time. **A**: neonates, acute. **B**: neonates, intermediate. **C**: juveniles, intermediate. **D**: juveniles, chronic. **E**: adults, intermediate. **F**: adults, chronic. *p<0.05, **p<0.01

of the hippocampal area of the control rat brains showed neuronal cells, with clearly defined cell bodies and nuclei while the experimental animals showed dark shrunken nuclei and abnormal clumping of heterochromatin, which were considered as pyknotic cells. In all the age groups, the wel-layered structure of the pyramidal layers of the control animals were confirmed with the cresyl violet stain, while the hydrocephalic animals showed varying degrees of disarray of the pyramidal layers (Figs. 4, 5 and 6).

Pyknotic Index

Comparison between the pyknotic index of hydrocephalic and control of each group was analyzed to determine the level of significance of their differences. In the CA1 sub-region, the pyknotic index was significantly higher in neonatal hydrocephalic animals (both acute and intermediate) than in age matched controls. In juveniles and adults, this difference was observed only in those with intermediate hydrocephalus. In the older rats with chronic (8

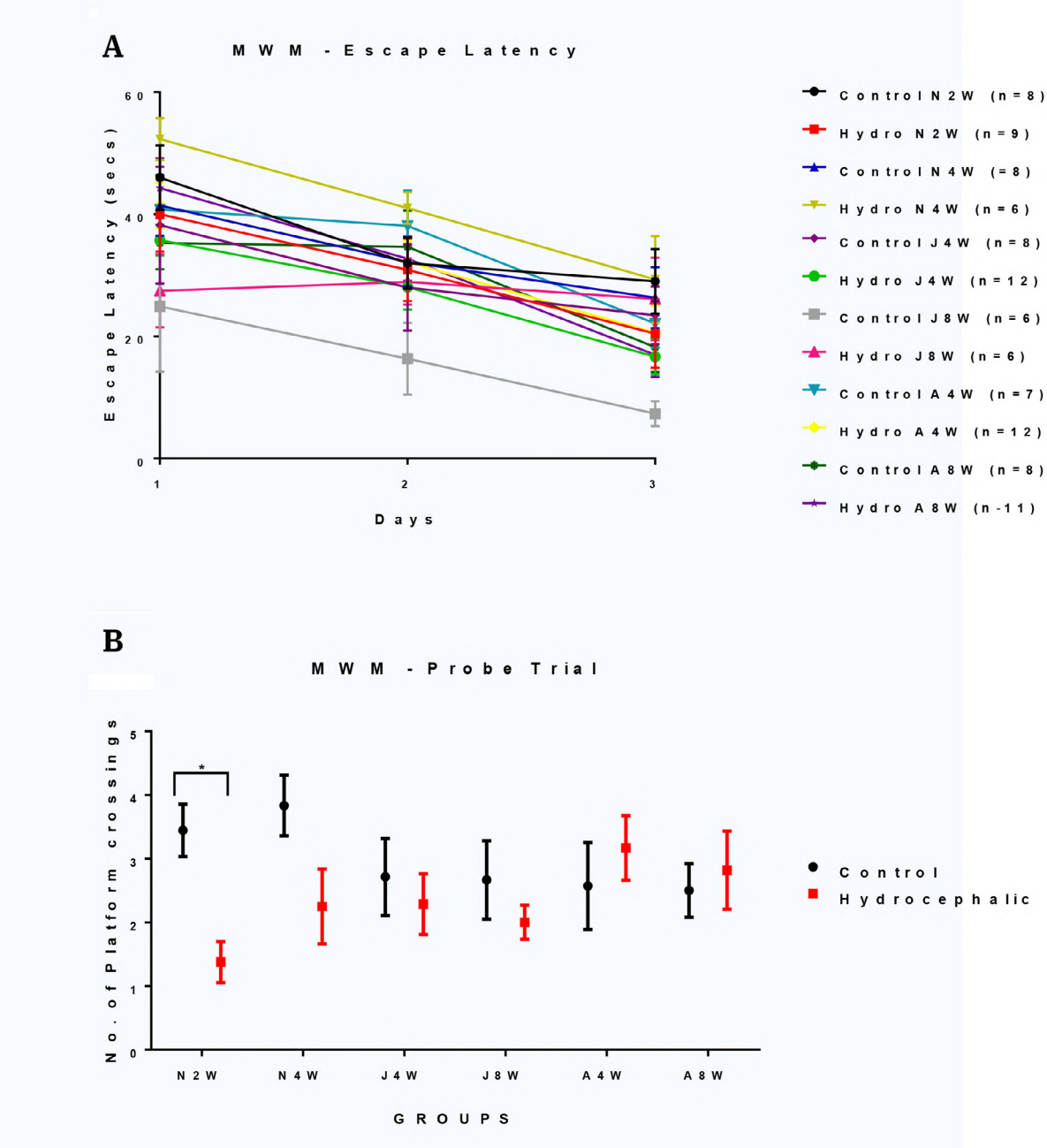

Fig. 2.- Bar chart showing (**A**) Escape latency from platform, (**B**) number of platform crossings during Morris Water Maze Test (N: neonate; J; juvenile; A: adult; W: weeks. *p<0.05

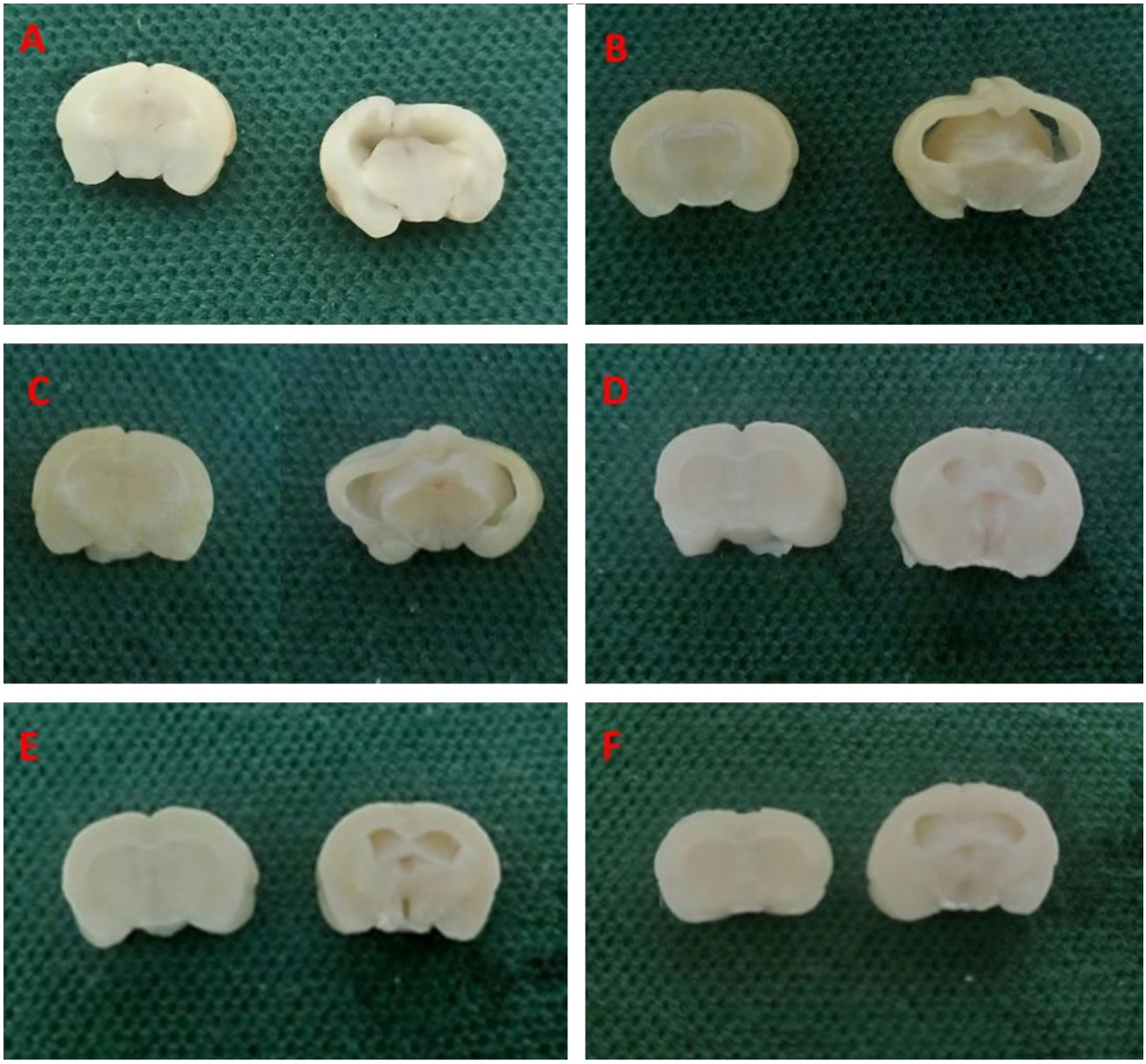

Fig. 3.- Representative gross photographs of dissected rat brains (control and hydrocephalic). The hydrocephalic brains show distended ventricles compared to their age matched controls. **A**: N2W; **B**: N4W; **C**: J4W; **D**: J8W; **E**: A4W; **F**: A8W. (A: adult; N: neonate; J: juvenile; W: weeks).

weeks) hydrocephalus, the differences were not statistically significant.

However, in the CA3 sub-region the pyknotic indices were significantly increased only in neonates with acute hydrocephalus and in juveniles with the chronic form (Table 1).

Neuronal cell density

The total number of neurons (spared and dead cells) in the CA1 and CA3 hippocampal sub-regions was counted per square area using Motic image plus 2.0 to obtain neuronal cell density. Statistical analysis (Table 2) between the hydrocephalic and controls of the CA1 and CA3 sub-region of the hippocampus showed no significant difference in the neuronal cell density among the groups.

Modified Golgi stain

Dendritic arborization of the pyramidal neurons of the hippocampal layers were assessed by the modified Golgi stain. The pyramidal neurons selected for analysis must meet these criteria: (a) completely impregnated, (b) isolated from the other neurons. Well-defined pyramidal neurons with pear-shaped soma were observed in the control animals. Each soma gave rise to a single apical dendrite, which courses through the surface of the hippocampus and divides into

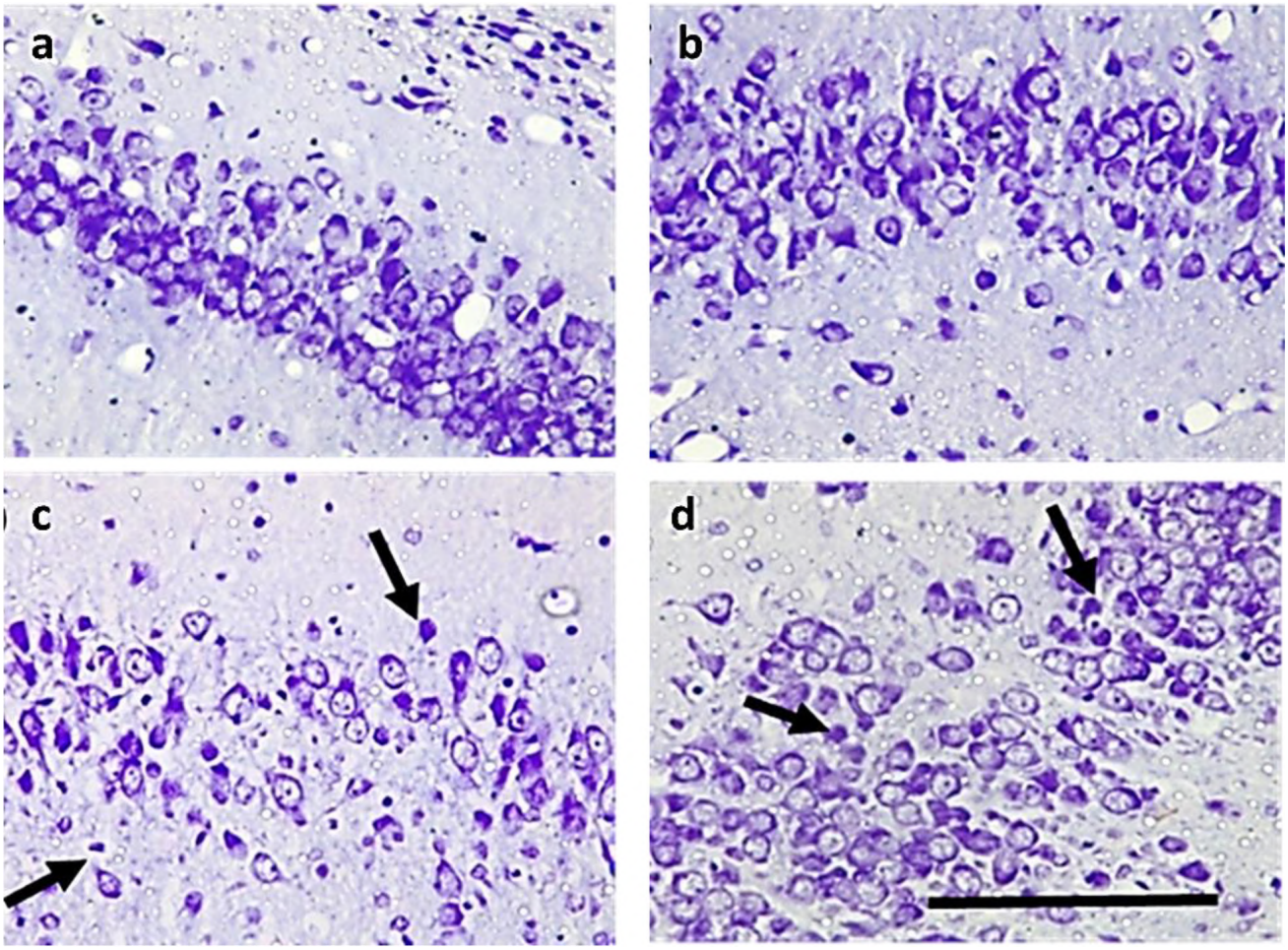

Fig. 4.- Cresyl violet stained CA1 & CA2 subareas of the hippocampus of neonates 2 weeks old (**a-d**). Note the derangement of the layered CA1 and CA2 subareas in the hydrocephalic sections (c,d) and pyknotic neurons (black arrows). (**a, b**: control rats; **c, d**: hydrocephalic rats; a: CA1 control; b: CA2 control. Scale bar: 50 µm).

Table 1. Pyknotic indices of hippocampal CA1 and CA3 subregion.

	CONTROL CA1	HYDROCEPHALIC CA1	CONTROL CA3	HYDROCEPHALIC CA3
GROUPS	(n=4)	(n=4)	(n=4)	(n=4)
N, acute	6.10 ± 1.16	24.50 ± 7.25*	12.55 ± 1.30	23.63 ± 1.26*
N, inter	12.10 ± 1.07	20.85 ± 1.02*	16.60 ± 1.19	22.38 ± 6.75
J, inter	9.68 ± 1.06	22.48 ± 5.28*	14.50 ± 1.22	22.20 ± 2.22*
J, chronic	8.83 ± 0.59	29.50 ± 12.61	13.68 ± 1.10	15.95 ± 3.66
A, inter	6.13 ± 1.11	10.98 ± 1.18*	13.40 ± 0.08	16.35 ± 4.22
A, chronic	8.03 ± 0.53	9.85 ± 1.16	13.13 ± 1.76	15.35 ± 0.84

(N: neonate; J; Juvenile; A: adult; inter: intermediate); *p<0.05

several terminal branches. The hydrocephalic animals demonstrated somatic features similar to that of control. However, major differences were observed in the dendritic branching of the experimental animals (Fig. 7). Although the branching patterns of the apical dendrites were similar to that of control animals, they possess fewer terminal branches.

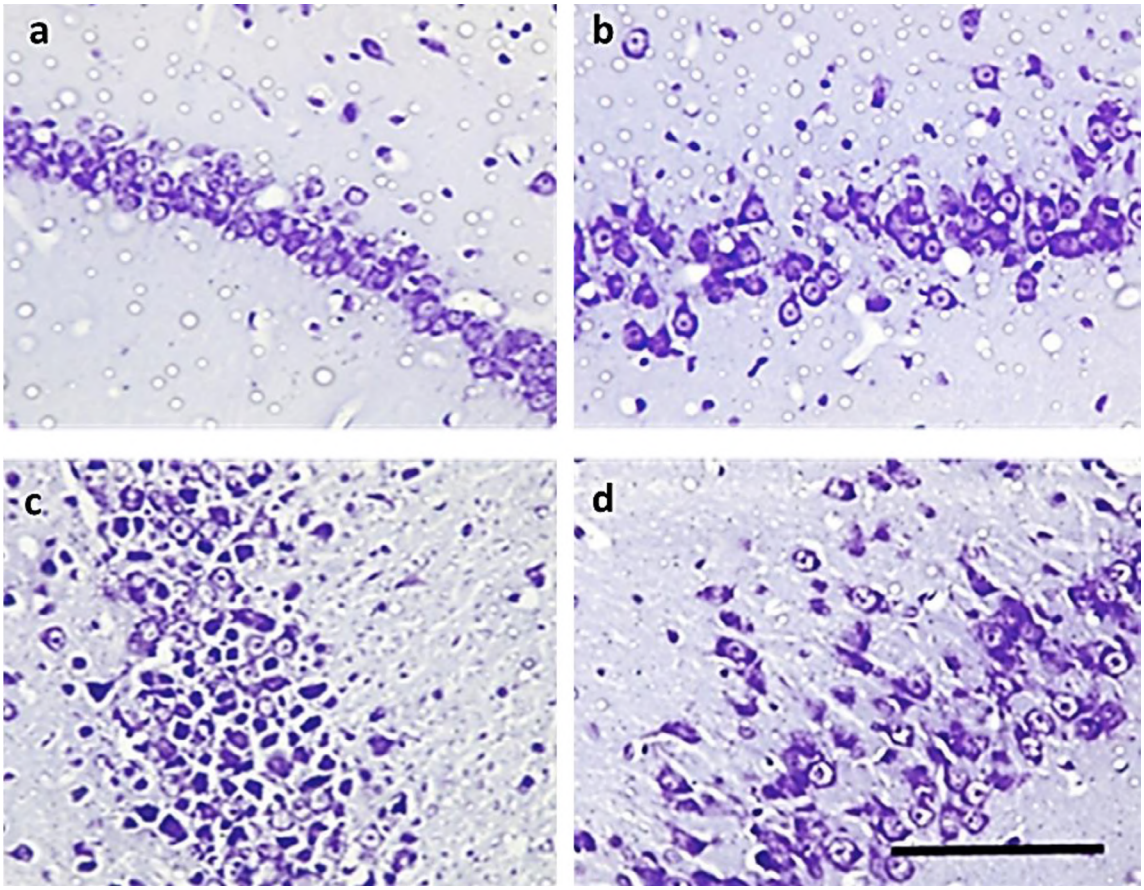

Fig. 5.- Cresyl violet stained hippocampus of juvenile 8 weeks old (**a-d**). Note the derangement of the layered CA1 and CA2 subareas in the hydrocephalic sections (c, d). (**a, b**: control rats; **c, d**: hydrocephalic rats; a: CA1 control; b: CA2 control. Scale bar: 50 µm).

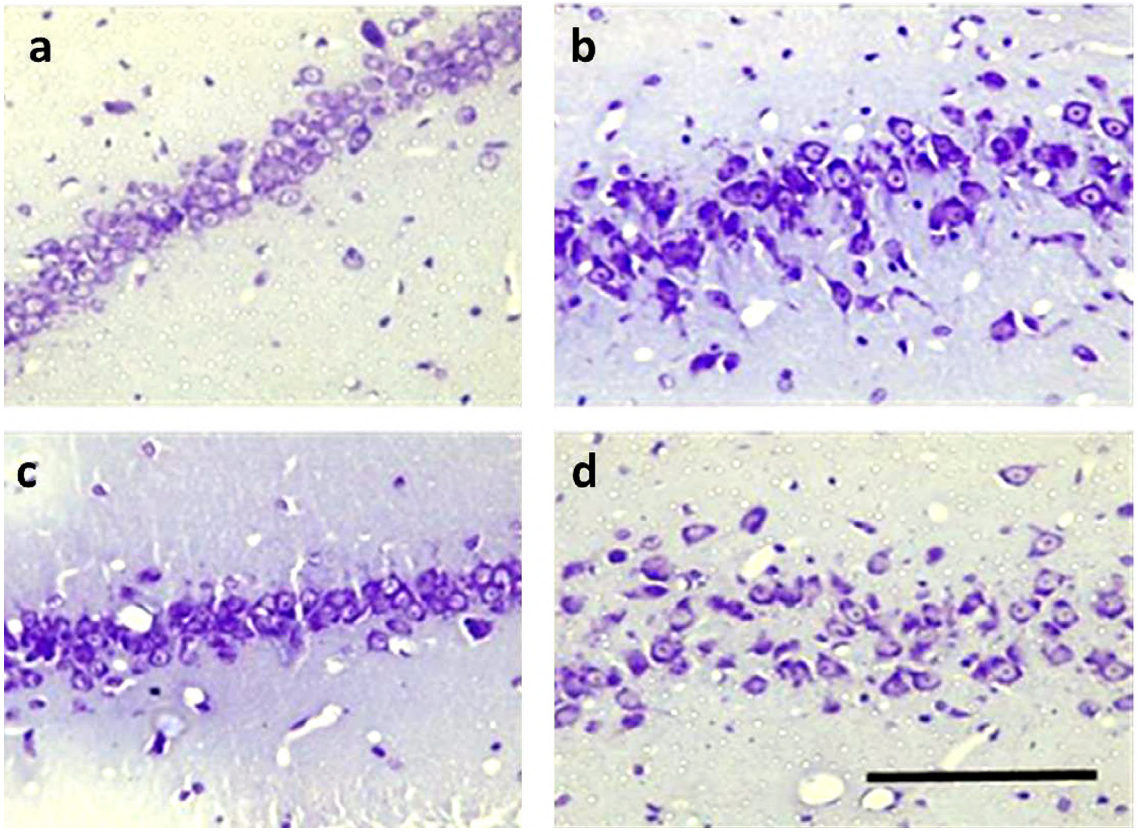

Fig. 6.- Cresyl violet stained hippocampus of adult 4 weeks old rats. Note the dispersed and fewer cells in the CA2 subarea of the hydrocephalic section. (**a**: CA1 control; **c**: CA1 hydrocephalic; **b**: CA2 control; **d**: CA2 hydrocephalic. Scale bar: 50 µm).

Table 2. Neuronal cell density of hippocampal CA1 and CA3 subregions.

	CONTROL CA1	HYDROCEPHALIC CA1	CONTROL CA3	HYDROCEPHALIC CA3
GROUPS	(n=4)	(n=4)	(n=4)	(n=4)
N, acute	41.43 ± 4.56	36.35 ± 2.45	27.65 ± 1.81	25.48 ± 2.93
N, inter	36.05 ± 1.23	39.35 ± 3.71	27.15 ± 0.64	31.75 ± 1.75
J, inter	32.78 ± 2.54	41.13 ± 5.05	31.33 ± 2.18	32.50 ± 1.48
J, chronic	34.25 ± 3.10	33.60 ± 4.60	28.18 ± 1.53	26.20 ± 2.24
A, inter	38.75 ± 2.04	31.83 ± 3.19	26.33 ± 0.78	28.03 ± 2.00
A, chronic	32.00 ± 0.86	37.98 ± 2.30	25.43 ± 0.70	27.48 ± 0.84

(N: neonate; J; Juvenile; A: adult; inter: intermediate); $p > 0.05$ in all subgroups, in comparison to control.

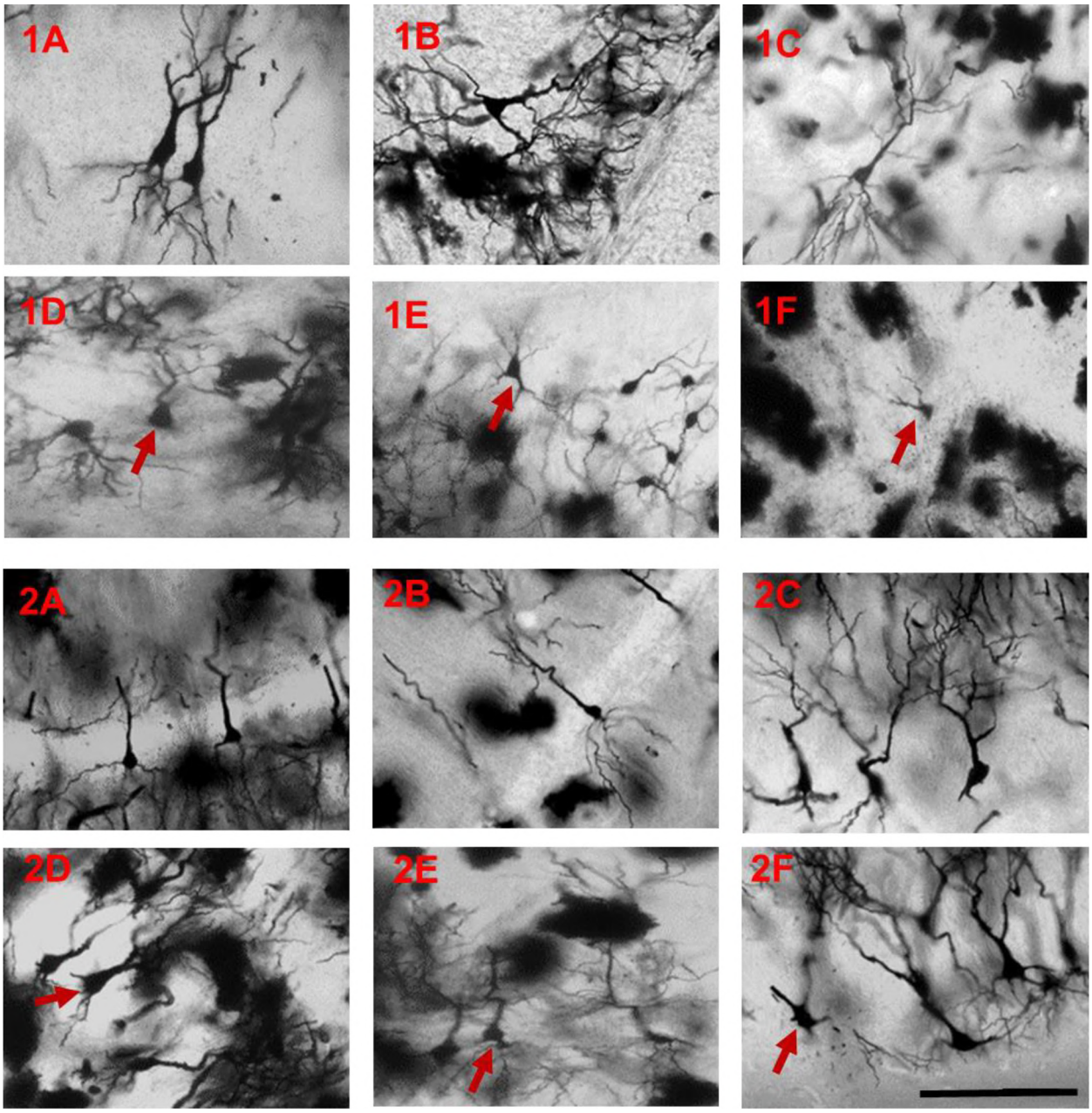

Fig. 7.- Modified Golgi-stained pyramidal cells of the hippocampus of neonates, acute (**1A,1D**); neonate, intermediate (**1B,1E**); juvenile, intermediate (**1C,1F**); juvenile, chronic (**2A,2D**); adult, intermediate; (**2B,2E**) and adult, chronic (**2C,2F**). Note the fewer basal dendrites (red arrows) in the hydrocephalic groups. (1A,1B,1C,2A,2B,2C: control rats; 1D,1E,1F,2D,2E,2F: hydrocephalic rats; Scale bar: 50 µm).

DISCUSSION

In this study, we examined the early, intermediate and long-term changes in the structure of the pyramidal neurons of the hippocampus in relation to learning and memory in hydrocephalic rats at different age groups. We found an age-related vulnerability and a tendency to recovery over time.

We have previously described changes in the density of neurons in the sensorimotor cortex and impaired neurodevelopmental progression in neonatal hydrocephalic mice (Femi-Akinlosotu and Shokunbi, 2020). We showed that in these animals, the pyramidal cells of the sensorimotor cortex suffered diminution of basal dendritic arbor, synaptic spine density and synaptophysin immunostaining (Femi-Akinlosotu et al., 2019). We have also demonstrated that in adult-onset hydrocephalus in this rodent species, the pyramidal layer of the CA1 (but not CA3) region of hippocampus showed increased pyknosis and cells with reduction of dendritic arbor (Shokunbi et al., 2020). In these studies, we provided supportive evidence for significant cellular injury in the sensorimotor and hippocampal cortices for the abnormal neurodevelopmental outcomes in neonatal and adult murine experimental hydrocephalus.

In the present investigation, we explored hydrocephalic neuronal injury further by examining the dendritic arborization of the pyramidal neurons of the CA1 and CA3 regions of the hippocampus at different stages of development in the rat hydrocephalus model, and related our findings to the neurobehavioural status of the animals. Our study revealed the following key findings: a) loss of basal dendrites in pyramidal cells of the hippocampus in all age groups; b) excessive death of pyramidal cells of the CA1 of the hippocampus throughout the neonatal period, but evident only early in the hydrocephalic process in juvenile and adult rats; c) loss of basal dendrites in the early phase of the disease in the CA3 region only in neonates and juveniles; d) relative resistance of the pyramidal cells in CA3 to pyknosis; e) learning and spatial memory were impaired by hydrocephalus. These results indicate a regional gradient in the vulnerability of the pyramidal cells of the hippocampus to hydrocephalus, with the CA1 region showing higher predilection for hydrocephalic injury. They also suggest a greater vulnerability of neonates and juveniles and better recovery in adult rats.

Intra-cisternal injection of kaolin has been an effective method for inducing hydrocephalus in experimental animals producing variable degree of ventricular dilatation (Khan et al., 2006; Del Bigio et al., 2003; Karinna et al., 2012; Olopade and Shokunbi, 2012, Femi-Akinlosotu et al., 2019). In this study, intra-cisternal injection of 150mg of kaolin in 1ml of sterile water successfully induced hydrocephalus in the neonate, juvenile and adult rats, with reduction in mortality rate, probably due to a slower rate of ventricular enlargement (Kondziella et al., 2008). Despite the use of the same volume of kaolin suspension for rats of the same age, the degree of hydrocephalus was variable with substantial ventricular distension often observed in adult rats with chronic hydrocephalus. This is similar to previously reported observations (Brinker et al., 1998; Klinge et al., 2003). Experimental animals showed enlarged dome-shaped head, unsteady gait and poorly groomed fur. These are consistent with findings in previous reports (Ding et al., 2001; Olopade et al., 2012; Olopade and Shokunbi, 2016.). The body weights of the hydrocephalic rats in the three age groups were significantly reduced in the first week post-injection of kaolin. This was followed by a slower rate of gain which was observed among the controls. This has been also previously observed and may likely be due to reduced activity and loss of appetite (Del Bigio, 2001; Olopade and Shokunbi, 2016; Femi-Akinlosotu et al., 2019).

Learning and memory were impaired as revealed in the Morris water maze tasks. The hydrocephalic rats, especially the chronic ones (8 weeks P.I) had significantly higher escape latency, i.e.. they took longer time to locate the hidden platform during the training periods, suggesting impairment in their learning ability. The result of the probe trial showed that the hydrocephalic rats' memories were impaired as the number of crossing made by them were significantly fewer than those of their age-matched controls. These

findings are consistent with earlier studies that also tested rats' performance in multiple days using the Morris Water Maze task (Olopade et al., 2012, 2016; Williams et al., 2014; Chen et al., 2016).

Several previous studies have described increased pyknosis and neuronal dispersal in the hippocampus in hydrocephalic animal brains (Kriebel and McAllister, 2000; Taveira et al., 2012; Chen et al., 2016.) and have related these changes to impaired memory and behavior. However, they did not differentiate the hippocampal subareas, but only examined subarea CA3. Histological staining of the hippocampal pyramidal neurons showed cytoarchitectural distortion of the pyramidal layer of CA1 and CA3 subareas. Dispersed pyramidal neurons and loss of the normal 4-8 rows of pyramidal neurons of the CA1 hippocampal sub-region were observed in hydrocephalic rat brains. These observations had been earlier reported by Chen et al. (2016), where the neurons of the CA1 and CA3 hippocampal sub-regions were altered and dispersed in hydrocephalic rats. Our study revealed that the cytoarchitectural alteration was more pronounced in the neonates and juveniles than in the adults. We observed this across all the groups despite the alteration in the cytoarchitecture of these neurons. However, this is consistent with the report by Chen et al. (2016) that there was no increase in neuronal density of hydrocephalic rats compared to the control rats in both acute and chronic stages of hydrocephalus.

The hippocampus CA1 region is known to be very susceptible to hypoxia and ischemia, and is considered to be an important target for the secondary neuronal injury originating in hydrocephalus (Karinna et al., 2012; Schultz and Engelhardt, 2014). However, other studies have shown neuronal tolerance during hydrocephalus in the CA1 sub-region of hydrocephalic rats, as the CA1 neurons do not show the neuronal degeneration and death such as observed in ischemic brain injury. CA1 sub-region might not be critical in the pathology of hydrocephalus as there was no apparent increase in neuronal death of the hippocampal pyramidal neurons but rather reduction in their connectivity (Ding, 2001; Chen et al., 2016). Nevertheless, dark shrunken neurons, especially at the early hydrocephalic stage have been observed in other studies (Kriebel and McAllister, 2000; Del Bigio, 2003; Cabuk et al., 2011; Taveira et al., 2012; Karinna et al., 2013; Turgut et al., 2018).

Our study revealed that the pyknotic index was significantly increased in the CA1 in the two groups of hydrocephalic neonates, but only in the early (4 weeks) groups of juveniles and adult hydrocephalic rats. The diminished amount of neuronal death observed in the chronic state (8 weeks) can be attributed to a tolerance to the ischemic injury developed during that hydrocephalic insult. Cortical and hippocampal blood flow might have decreased in early hydrocephalus and return to normal in chronic hydrocephalus due to collateral supply (Klinge et al., 2003). Their observations suggest that neuronal tolerance to ischemia might develop in hydrocephalic rats.

The geometry of these pyramidal neurons may influence their propagation and /or integration of their synapses (Piskorowski and Chevaleyre, 2012). Dendritic arborization of hippocampal pyramidal neurons have characteristics morphology, with the apical and basal dendrites of the CA1 pyramidal neurons having a single apical dendrite which may or may not bifurcate from the soma. Several secondary oblique dendrites may also emerge from the apical dendrites. However, the apical dendrite of CA2 neurons bifurcates close to the soma into two or three apical dendrites. The pyramidal neurons of the hippocampus are similar to their counterparts in the forebrain, with extensive apical and short basal dendrites. A typical pyramidal neuron receives tens of thousands of excitatory and inhibitory synaptic inputs (Piskorowski and Chevaleyre, 2012). Alterations in the branching of the neuronal dendritic morphology have essential significance functionally. Our study revealed alterations in the basal dendrites of the pyramidal neurons of the CA1 and CA3 regions of the hydrocephalic rats. Several studies have documented various morphological alterations in the networking of the hippocampal pyramidal neurons (Kirino, 1982; Kawamata et al., 1988; Kriebel and McAllister, 2000; Klinge et al., 2003; Cabuk et al., 2011; Chakraborti et al.,

2012; Piskorowski and Chevaleyre, 2012; Chen et al., 2016). Chakraborti et al. (2012) reported a decrease in the total dendritic length and dendritic spine densities of the CA1 pyramidal neurons of the hydrocephalic hippocampus in young adult mice. They suggested that these changes might reduce excitatory connectivity, which could underlie the learning and memory deficits observed in hydrocephalic states.

CONCLUSION

We have described the acute, intermediate and chronic changes in hippocampal pyramidal neurons in experimental hydrocephalus in neonatal, juvenile and adult rats and the varying effects on learning and memory in these animals. Our results suggest that the CA1 region in young animals is particularly vulnerable, with functional recovery occurring over time and to a greater extent in older animals. These results may have implications for clinical decision making in the management of hydrocephalus.

ACKNOWLEDGEMENTS

The authors acknowledge the assistance of Dr. Folarin, Mr. Osuntade, Mrs. Elizabeth Ogunsola and Mrs. Folashade Adunola towards the processing of the histology sections.

Ethics approval: Approval was obtained from the ethics committee of University of Ibadan, Nigeria. The procedures used in this study adhere to the tenets of the EU Directive 2010/63/EU for animal experiments.

REFERENCES

BRINKER T, BECK H, KLINGE P, KISCHNIK P, OI S, SAMII M (1998) Sinusoidal intrathecal infusion for assessment of CSF dynamics in kaolin-induced hydrocephalus. *Acta Neurochi (Wien)*, 140: 1069-1075.

CABUK B, VOLKAN E, SUHEYLA UYAR BOZKUR T, AYDIN S, SAVAS C (2011) Neuroprotective effect of memantine on hippocampal neurons in infantile rat hydrocephalus. *Turkish Neurosurg*, 21.33: 352-358.

CHAKRABORTI A, ALLEN A, ALLEN B, ROSI S, FIKE JR (2012) cranial irradiation alters dendritic spine density and morphology in the hippocampus. *PLoS ONE*, 7(7): e40844.

DEL BIGIO MR (2001) Pathophysiologic consequences of hydrocephalus. *Neurosurg Clin N Am*, 12/4: 639-649.

DEL BIGIO MR, BRUNI JE (1991) Silicone oil-induced hydrocephalus in the rabbits. *Childs Nervous System*, 7: 79-84.

DEWAN MC, RATTANI A, MEKARY R, GLANCZ LJ, YUNUSA I, BATICULON RE, FIEGGEN G, WELLONS JC, PARK KB, WARF BC (2019) Global hydrocephalus epidermiology and incidence: systematic review and meta-analysis. *J Neurosurg*, 130: 1065-1079.

D'HOOGE R, DE DEYN PP (2001) Applications of the Morris water maze in the study of learning and memory. *Brain Res Rev*, 36(1): 60-90.

FEMI-AKINLOSOTU OM, SHOKUNBI MT, THAJASVARIE N (2019) Dendritic and synaptic degeneration in pyramidal neurons of the sensorimotor cortex in neonatal mice with kaolin-induced hydrocephalus. *Front Neuroanat*, 13: 38. doi.org/10.3389/fnana.2019.00038

FEMI-AKINLOSOTU OM, SHOKUNBI MT (2020) Changes in neuronal density of the sensorimotor cortex and neurodevelopmental behaviour in neonatal mice with kaolin-induced hydrocephalus. *Pediatric Neurosurg*, 55(5): 244-253.

ISAACS AM, RIVA-CAMBRIN J, YAVIN D, HOCKLEY A, PRINGSHEIM TM, JETTE N, LETHEBE BC, LOWERISON M, DRONYK J, HAMILTON MG (2018) Age-specific global epidemiology of hydrocephalus: Systematic review, metanalysis and global birth surveillance. *PLoS ONE*, 13(10): e0204926.

JONES HC, RIVERA KM, HARRIS NG (1995) Learning deficits in congenitally hydrocephalic rats and prevention by early shunt treatment. *Child's Nervous System*, 11: 655-660.

KAWAMATA T, TSUBOKAWA T, KATAYAMA Y (1988) Impaired hippocampal plasticity in experimental chronic hydrocephalus. *Brain Injury*, 2: 19-30.

Khan OH, Enno TL, Del Bigio MR (2006) Brain damage in neonatal rats following kaolin induction of hydrocephalus. *Exp Neurol*, 200: 311-320.

KIRINO T (1982) Delayed neuronal death in the gerbil hippocampus following ischemia. *Brain Res*, 239: 57-69.

KLINGE PM, SAMII A, MUHLENDYCK A, VISNYEI K, MEYER GJ, WALTER GF, SILVERBERG GD, BRINKER T (2003) Cerebral hypoperfusion and delayed hippocampal response after induction of adult kaolin hydrocephalus. *Stroke*, 34: 193-199.

KONDZIELLA D, SONNEWALD U, TULLBERG M, WIKKELSO C (2008) Brain metabolism in adult chronic hydrocephalus. *J Neurochem*, 6(4): 1515-1524.

KRIEBEL RM, MCALLISTER II JP (2000) Pathology of the hippocampus in experimental feline infantile hydrocephalus. *Neurology Rev*, 22: 29-36.

MCALLISTER JP, CHOVAN P (1998) Neonatal hydrocephalus. Mechanisms and consequences. *Neurosurg Clin N Am*, 9: 73-93.

MILANI SIVAGNANAM, NEILANK K JHA (2012) Hydrocephalus: An Overview. Hydrocephalus, intech Europe, ISBN: 978-953-51-0162-8.

MORRIS R (1984) Developments of a water-maze procedure for studying spatial learning in the rat. *J Neurosci Meth*, 11: 47-60.

NUNEZ J (2008) Morris Water Maze experiment. *J Vis Exp*, 19: 897.

OLOPADE FE, SHOKUNBI MT, SIRÉN AL (2012) The relationship between ventricular dilatation, neuropathological and neurobehavioural changes. *Fluids Barriers CNS*, 9(1): 19.

OLOPADE FE, SHOKUNBI MT (2016) Neurobehavioural deficits in progressive experimental hydrocephalus in neonatal rats. *Niger J Physiol Sci*, 31: 105-113.

PISKOROWSKI RA, CHEVALEYRE V (2012) Synaptic integration by different dendritic compartments of hippocampal CA1 and CA2 pyramidal neurons. *Cell Mol Life Sci*, 69: 75-88.

REKATE HL (2008) The definition and classification of hydrocephalus: a personal recommendation to stimulate debate. *Cerebrospinal Fluid Res*, 5: 2.

SCHULTZ C, ENGELHARDT M (2014) Anatomy of the hippocampal formation. *Front Neurol Neurosci*, 34: 6-17.

SHIM I, HA Y, CHUNG JY, LEE HY, YANG KH, CHANG JW (2003) Association of learning and memory with changes in septocholinegic

system in rats with kaolin-induced hydrocephalus. *Neurosurgery*, 53/2: 416-425.

SHOKUNBI MT, OLOPADE FE, FEMI-AKINLOSOTU OM, AJIBOYE EO (2020) Pyramidal cell morphology and cell death in the hippocampus of adult mice with experimentally induced hydrocephalus. *Niger J Paediatr*, 47(4): 298-304.

TAVEIRA KVM, CARRARO KT, CATALAO CHR, DA SILVA LOPES L (2012) Morphological and morphometric analysis of the hippocampus in Wistar rats with experimental hydrocephalus. *Pediatric Neurosurg*, 48: 163-167.

TURGUT M, BAKA M, UYANIKGIL Y (2018) Melatonin attenuates histopathological changes in the hippocampus of infantile rats with kaolin-induced hydrocephalus. *Pediatric Neurosurg*, 53(4): 1-9.

WILLIAMS MT, BRAUN AA, AMOS-KROOHS RM, MCALLISTER JP, LINDQUIST DM, MANGANO FT, VORHEES CV, YUAN W (2014) Kaolin-induced ventriculomegaly at weaning produces long-term learning, memory, and motor deficits in rats. *Int J Dev Neurosci*, 35: 7-15.

Comparative analysis of neurophysiological studies in the diagnosis of bulbar syndrome in patients with Chiari malformation Type 1

Gennady E. Chmutin[1,2], Gayrat M. Kariev[3], Rano O. Ismailova[3], Hanifa M. Khalimova[1,4], Gerald Musa[1], Adam Majer[1], Boris E. Oleinikov[1,2]

[1] Department of Nervous Diseases and Neurosurgery, Peoples' Friendship University of Russia (RUDN University), Moscow, Russia

[2] Federal State Budgetary Institution of Medical Department of Moscow "Morozov Children's City, Clinical Hospital of Medical Department of Moscow", Moscow, Russia

[3] Department of Neurology and Neurosurgery, Republican Specialized Scientific and Practical Medical Center of Neurosurgery, Tashkent, Uzbekistan

[4] Tashkent Medical Academy, Neurology Department, Uzbekistan

SUMMARY

The incidence of bulbar syndrome in craniovertebral junction anomalies is between 12% and 35%. Although the use of evoked potentials intraoperatively and preoperatively has advanced in recent years, their use in predicting the development of neurological deficits remains a challenge. This research explores the predictive significance of evoked potentials in the diagnosis of bulbar syndrome in Chiari 1 anomaly. Data from 39 patients and 30 controls were reviewed**.** Standard multimodal neurophysiological investigations including Brainstem auditory evoked potentials (BAEPs), somatosensory evoked potentials (SSEPs), Nerve Conduction Studies (NCS), and Electromyogram (EMG) were performed. All studies were conducted on the 4-channel complex "Synapsis" (Neurotech, Russia) with computer data processing.

The threshold Nerve conduction velocity (NCV) value was 21.5 m/s. The sensitivity and specificity were 75.5% and 71.2% respectively. The area under the ROC curve (AUC) was 0.96±0.36 (95% CI: 0.89-1.00) and p-value 0.004. The M-response amplitude threshold dividing the study group into high and low-risk groups was 1.01 microV. The sensitivity and specificity were 78.0 and 71.2%, respectively. The BAEPs interpeak intervals III-V and I-V were significantly prolonged (P< 0.05). SSEPs showed a decreased amplitude and reduced NCV (P < 0.01). Glossopharyngeal nerve electroneuromyography is the most informative test. A decrease in M-response amplitude of bulbar muscles and NCV on efferent fibers is highly predictive of the development of bulbar disorders in patients with Chiari 1, even in subclinical cases.

Key words: Chiari malformation Type 1 – Bulbar syndrome – Brainstem auditory evoked potential (BAEP) – Somatosensory evoked potentials (SSEP) – Electroneuromyography (ENMG)

Corresponding author:
Gerald Musa. Department of Nervous Diseases and Neurosurgery, Peoples' Friendship University of Russia (RUDN University), Potapovskaya Roscha 7k2, Moscow, Russia. Phone: +7 9778275213. E-mail: gerryMD@outlook.com - ORCID: 0000-0001-8710-8652

Submitted: August 26, 2022. **Accepted:** October 5, 2022

https://doi.org/10.52083/DAVG1176

INTRODUCTION

The rapid development of modern methods of neuroimaging has led to an increase in the number of patients with diagnosed central nervous system abnormalities (Voronov, 2010; Ismailova, 2020; Levy et al., 1983; Munshi et al., 2000). The modern "gold standard" for diagnosing Chiari malformation is an MRI study. It accurately identifies pathologies of the cranioventral junction, in particular, Chiari malformations, the degree of cerebellar tonsillar ectopia, and the presence of basilar impression (Gushcha et al., 2010; Aronson et al., 1991; Milhorat and Bolognese, 2003). At least a third of Chiari 1 malformations are associated with cervical syringomyelia (OlimjanovnaIsmailova and Kariev, 2020). One of the most dangerous neurological complications of craniovertebral junction abnormalities is bulbar syndrome (Mojaev and Sterlikova, 2009; Sevostiyanov, 2011). The incidence of bulbar syndrome in craniovertebral junction anomalies is between 12 and 35% according to various authors (Aronson et al., 1991; Guo et al., 2007).

Clinical manifestations of the bulbar syndrome in Chiari 1 malformation have been studied by many authors (Sevostiyanov, 2011; Aronson et al., 1991; Møller et al., 1995). Neurophysiological studies have gained popularity in recent years. Their use in intraoperative monitoring during various spinal and cranial surgeries including Chiari 1 surgeries is well studied in the literature (Anderson et al., 2003; Holliday et al., 1985; Moncho et al., 2017; OlimjanovnaIsmailova and Kariev, 2020). Despite their extensive use, whether evoked potentials can be used to predict the development of bulbar disorders in Chiari 1 anomaly is still unclear. Mechanical compression of the brainstem structures by the herniated cerebellar tonsils and abnormalities of CSF dynamics with the formation of a syrinx in the upper cervical region and lower medulla oblongata have been shown to cause local damage to the various tracts and nuclei in the medulla oblongata (OlimjanovnaIsmailova and Kariev, 2020). This causes gross clinical neurological deficits usually picked up on clinical examination. However, in the subclinical cases, evoked potentials have shown promise in making an early diagnosis (Moncho et al., 2017). This research explores the predictive significance of evoked potentials in the diagnosis of bulbar syndrome in Chiari 1 anomaly.

MATERIAL AND METHODS

This was a retrospective study carried out at the Republican Specialized Scientific and Practical Medical Center of Neurosurgery. We analyzed the neurophysiological data of 39 patients with clinical manifestations of the bulbar syndrome in Chiari 1 malformation, who were treated at our institution from 2015 to 2018. The patients' ages ranged from 18 to 65 years, with 11 males and 28 females. These data were compared with data from 30 healthy individuals seen during this period herein called the control group. The standard for determining the degree of cerebellar tonsillar ectopia in Chiari malformation was the Chamberlain line, which runs from the hard palate to opisthion (a point located in the center of the posterior edge of the foramen Magna) (Gushcha et al., 2010; Levy et al., 1983; Milhorat and Bolognese, 2003). Cerebellar tonsillar ectopia more than 5mm below the Chamberlain line was considered significant. In this research, we used the Chamberlain line to determine the presence of the anatomical anomalies of the craniovertebral junction and the degree of cerebellar tonsillar ectopia (Fig. 1).

All patients were investigated according to the multimodal neurophysiological monitoring protocol, including Brainstem auditory evoked potentials (BAEPs), somatosensory evoked potentials (SSEPs), neuro-conduction studies (NCS), and electromyography (EMG) (Isu et al., 1993). All studies were conducted on the 4-channel complex "Synapsis" (Neurotech, Russia) with computer data processing.

Subdermal needle electrodes were used for BAEP recording and were inserted at the vertex to left ear mastoid (Cz/A1); vertex to right ear mastoid (Cz/A2); and vertex to cervical C2 (Cz/Cv2). Stimulation was performed through headphones with 0.1 ms audio clicks with a 20Hz feed frequency and 70dB sound. Filters were set at High Pass/Low Frequency Filter ≥100Hz (-3dB) and Low Pass/High Frequency Filter ≤ 3kHz (-3dB).

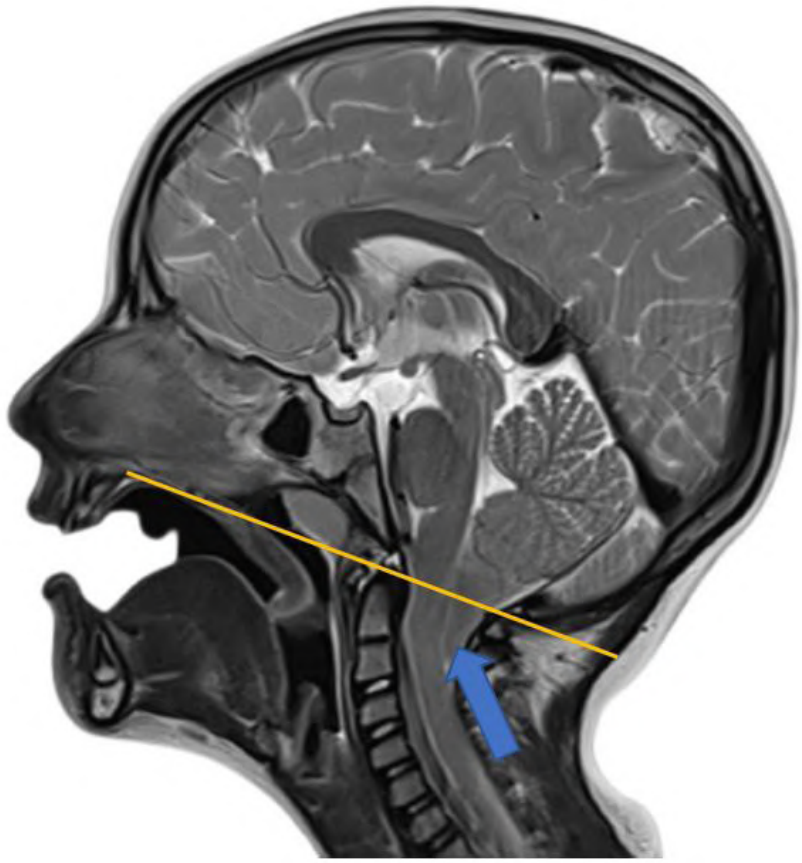

Fig. 1.- MRI showing displacement of the cerebellar tonsils (blue arrow) below Chamberlain's line (orange line) bilaterally.

When recording the SSEPs of the upper limbs, the recording electrodes CP3-Fz or CP3-CP4 for right arm stimulation; CP4-Fz or CP4-CP3 for left-arm stimulation were used. The tests were carried out by electrical stimulation of the median nerve at the wrist level with a current of 15-20 mA and a frequency of 2 Hz.

Lower limb SSEPs were recorded by stimulation of the posterior tibial nerve at the ankle. The traditional derivation of recording is CPz-Fz was used.

The EMG testing was performed on the glossopharyngeal nerve by inserting the recording electrodes in the associated muscles. Where necessary, we analyzed the function of the nerves based on the presence of gross neurological deficits.

Statistical analysis of the data was done using the IBM SPSS Statistics Package version 26. Differences in the distribution of quantitative values were assessed using the student parametric tests. To assess the predictive significance, Receiver operating characteristic (ROC) analysis was used followed by calculation of specificity and sensitivity and area under the ROC curve (AUC).

RESULTS

The BAEPs of all patients with bulbar impairments were analyzed. The data analyzing the latency and amplitude parameters of the study and control groups are presented in Table 1. The latency of the components PIII and PV were moderately prolonged bilaterally compared to the control group. There was a reduction in the amplitudes of peaks III and V. Asymmetric changes in BAEPs were recorded in 76% of the patients examined and a complete absence of PIII and PV components was observed in 24% of cases.

We analyzed SSEP data in 39 Chiari 1 patients with clinical features of the bulbar syndrome. Registration of SSEPs was done by stimulation of the median and tibial nerves in both the study

and control groups. The results of the SSEPs are presented in Table 2. The difference between the control and study group was statistically significant (student t-test *P< 0.05, **P < 0.01). As can be seen from the above data, in the patients with the bulbar syndrome, there was a significant increase in the latency period N13 to 18.4 ms. In the study group, there was a significant decrease in the amplitude of components N13 and N20, mostly bilateral with asymmetry in 61% of the patients.

The peak interval N13-N20 was significantly increased in most patients to 8.0 ms, but the intervals N9- N13 and N9-N20 were only slightly increased relative to normal values. Further, we studied SSEPs, obtained following stimulation of the tibial nerve in Chiari 1 patients with the bulbar syndrome. The data is presented in Table 3.

We identified a significant isolated prolonged N30 latency period to 42.8ms in Chiari 1 patients with the bulbar syndrome, while the latency period of components N22 and P37 were relatively preserved. In these patients, there was a decrease in the amplitude of component N30 to 0.28microV while the amplitude of components N22 and P37 were preserved relative to the control group. A significant increase in the peak interval N30-P37 to 17.8 ms was registered in Chiari 1 patients with the bulbar syndrome with pronounced asymmetry (61%) compared to the control group. However, the peak intervals N22-N30 and N22-P37 showed minor insignificant deviations from the normal.

The Electroneuromyography (ENMG) data was analyzed. The results of MEPs obtained following stimulation of the oculomotor, facial, glossopharyngeal, median, and tibial nerves

Table 1. BAEPs waveforms: Latency period, Peak amplitude, and Peak intervals in the control group (n=30) and Chiari 1 patients with bulbar syndrome (n=39).

Latency period, ms					
	PI.	**PII.**	**PIII.**	**PIV.**	**PV.**
Control Group (n=30)					
Right	1.79± 0.16	2.95 ± 0.18	3.94 ± 0.24	5.06 ± 0.22	5.97 ±0.25
Left	1.72 ± 0.17	2.98 ± 0.19	3.92 ± 0.22	5.13 ± 0.20	6.02± 0.25
Bulbar Syndrome (n=39)					
Right	1.80 ± 0.18	2.98 ± 0.17	4.35 ± 0.25	5.30± 0.21	7.05± 0.22**
Left	1.76± 0.16	3.01 ± 0.20	4.70 ± 0.21**	5.65± 0.19	8.01 ±0.24**

Amplitude, microV			
	PI.	**PIII.**	**PV.**
Control Group (n=30)			
Right	0.286± 0.05	0.262± 0.04	0.368 ±0.06
Left	0.282± 0.04	0.265± 0.06	0.338± 0.08
Bulbar Syndrome (n=39)			
Right	0.348± 0.03	0.050± 0.01**	0.050 ±0.02**
Left	0.340± 0.04	0.180± 0.02*	0.220± 0.04*

Peak intervals			
	PI-PIII.	**PIII-PV.**	**PI-PV.**
Control Group (n=30)			
Right	2.19± 0.16	2.06± 0.18	4.38± 0.22
Left	2.24± 0.18	2.08± 0.22	4.46± 0.24
Bulbar Syndrome (n=39)			
Right	2.36± 0.15	3.96± 0.15**	6.05±0.20*
Left	2.48± 0.17	3.65± 0.20**	6.35±0.21**

are presented in Table 4. The results showed a significant decrease in efferent NCV of the glossopharyngeal nerve in 60% of Chiari 1 patients with bulbar syndrome. In addition to changes in conduction velocity indicators, there was a marked decrease in the amplitude of the M-response of the glossopharyngeal nerve relative to the control group.

The Amplitudes of M-response of the facial and oculomotor nerves showed an insignificant reduction in the study group. Fibrillations were seen in 30% of patients during stimulation of the glossopharyngeal nerve, indicating the involvement of the nuclei. We evaluated the possibility of predicting the development of bulbar syndrome using efferent NCVs of the

Table 2. Median nerve SSEPs: Latent period, Peak amplitude, and Peak intervals in the control group (n=30) and Chiari 1 patients with bulbar syndrome (n=39).

Latency, ms		
	Control Group (n=30)	**Bulbar Syndrome (n=39)**
N9 Peripheral	9.6±0.7	10.1±0.8
N13 Cervical	13.2±0.8	18.4±1.2*
N20 Cortex	18.8±1.0	18.7±1.5
Amplitude microV		
	Control Group (n=30)	**Bulbar Syndrome (n=39)**
N9 Peripheral	5.4±2.5	5.1±2.0
N13 Cervical	2.9±1.3	1.1±0.5**
N20 Cortex	2.8±1.6	1.2±0.4**
Peak intervals, ms		
	Control Group (n=30)	**Bulbar Syndrome (n=39)**
N9-N13	3.5±0.4	3.9±0.5
N13-N20	5.8±0.5	8.0±0.7**
N9-N20	9.2±0.5	9.8±0.6*

Table 3. Tibial nerve SSEPs: Latency period, Peak amplitude, and Peak intervals in the control group (n=30) and Chiari 1 patients with bulbar syndrome (n=39).

Latency, ms		
	Control Group (n=30)	**Bulbar Syndrome (n=39)**
N 22 Lumbar	23.6±1.9	23.9±1.6
N 30 Cervical	30.6±2.5	42.8±1.26**
P37 Cortex	37.5±3.4	38. 4±3.0
Amplitude, microV		
	Control Group (n=30)	**Bulbar Syndrome (n=39)**
N 22 Lumbar	1.3±0.5	1.65±0.3*
N 30 Cervical	0.9±0.3	0.28±0.1**
P37 Cortex	2.6±1.5	2.85±1.6
Peak intervals, ms		
	Control Group (n=30)	**Bulbar Syndrome (n=39)**
N22-N30	7.62±1.14	7.80±1.05
N30-P37	8.05±1.32	17.8±1.52**
N22-P37	15.7±1.65	17.0±1.25

Table 4. ENMG indicators for oculomotor, facial, Glossopharyngeal, and tibial nerves in the control group (n=30) and Chiari 1 patients with bulbar syndrome (n=39).

	Efferent NCV, m/s	Amplitude max, microV	Pathological waves
Control Group (n=30)			
Oculomotor Nerve	29.4±2.2	1080±105.5	-
Facial nerve	39.5±1.8	1235±126.3	-
Glossopharyngeal nerve	42.6±2.0	1860±164.0	-
Median nerve	61.0±1.7	6254±267.0	-
Tibial nerve	49.6±2.1	7125±745.5	-
Bulbar Syndrome (n=39)			
Oculomotor	28.5±2.0	1072±124.8	
Facial nerve	34.1±1.6*	1180±122.0*	+
Glossopharyngeal nerve	20.8±2.6**	788±182.0**	+++
Median nerve	54.5±1.8*	5011±256.5	
Tibial nerve	42.7±1.7	6450±628.5	

glossopharyngeal nerve. Using the ROC analysis method, the graph as shown below was obtained (Fig. 2).

The area under the resulting ROC curve (AUC) was 0.96±0.36 (95% CI: 0.89-1.00), p-value 0.004. The relationship between the amplitude of the M-response of the glossopharyngeal nerve and the presence of bulbar syndrome in patients with Chiari malformation was analyzed. The threshold value of the M- response amplitude separating patients into high and low-risk groups for bulbar syndrome was analyzed using ROC analysis and the results are shown below (Fig. 3).

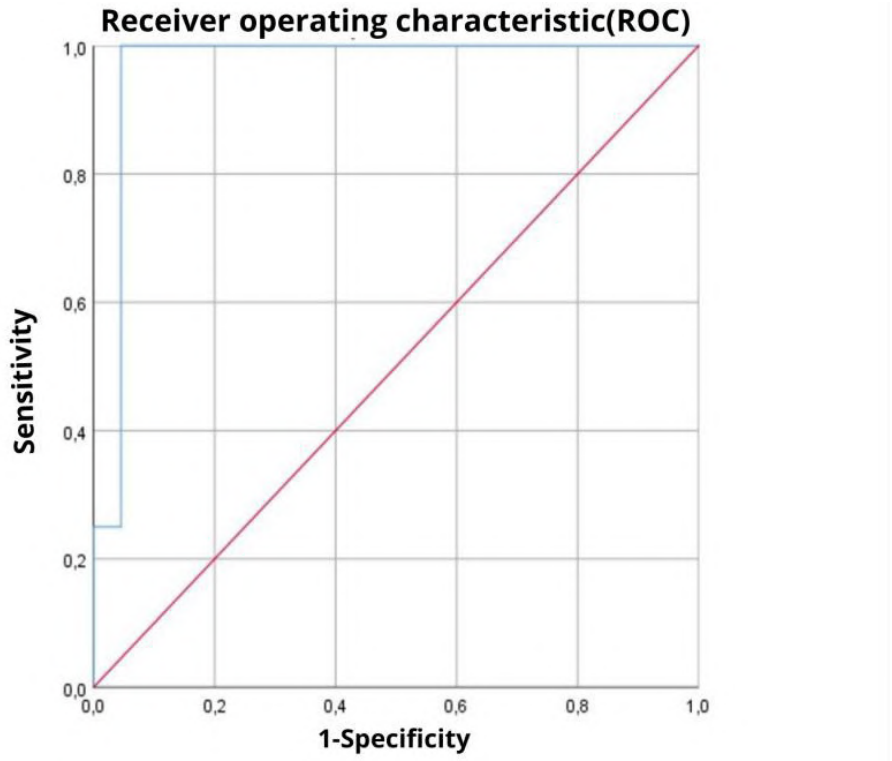

Fig. 2.- ROC curve, assessing the possibility of predicting the development of bulbar syndrome in patients with Chiari type 1, depending on the NCV of the glossopharyngeal nerve.

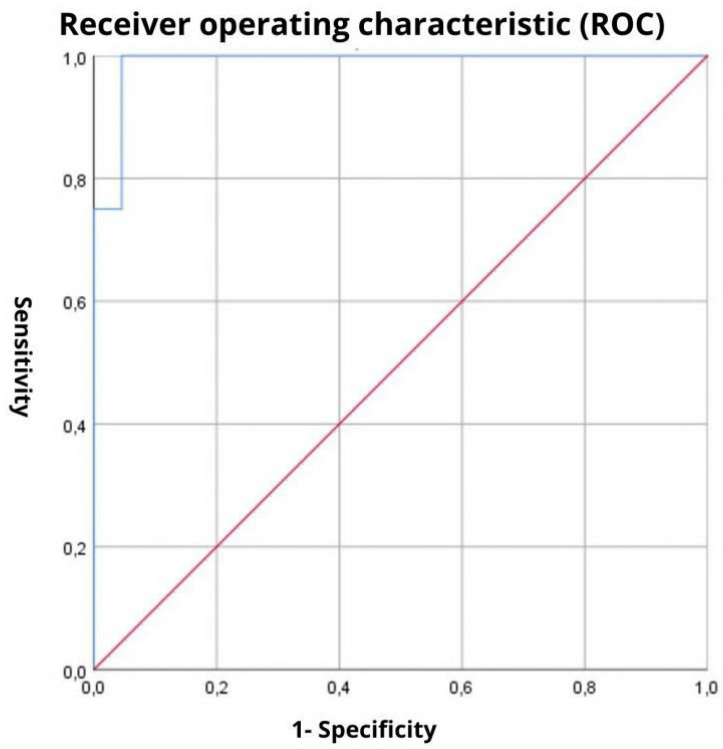

Fig. 3.- ROC curve, outlining the relationship between the development of bulbar syndrome in patients with Chiari 1 and the amplitude of the M-response of the glossopharyngeal nerve.

The resulting ROC curve was characterized by an AUC of 0.98±0.18 (95% CI: 0.95-1.00). There was an inverse relationship between the development of bulbar syndrome and the M-response amplitude p<0,002.

DISCUSSION

The predictive value of BAEPs has been studied extensively in literature with no consensus (Moncho et al., 2017; Holliday et al., 1985). Henriques et al., in their study of 75 patients, concluded that BAEPs are invaluable in the diagnosis, evaluation, and prevention of further morbidity in Chiari patients (Henriques Filho and Pratesi, 2006). The analysis of BAEPs revealed statistically significant changes consistent with conduction abnormalities. The interpeak intervals III-V and I-V were significantly prolonged to almost double in the group with bulbar symptoms compared to the control group. In 24% of patients, interpeak intervals could not be analyzed due to the complete absence of peak III and V components. These changes in BAEPs objectively indicated gross impairment of conductivity at the level of the lower pons and midbrain with clinical manifestations of bulbar syndrome in patients with Chiari 1. These changes were asymmetrical in some cases with dissociated functional involvement of Ponto-mesencephalic structures.

The analysis of SSEPs changes following stimulation of the median and tibial nerves in Chiari 1 patients with clinical manifestations of bulbar syndrome indicated a pronounced slowing of conductivity at the presynaptic level of the medulla oblongata nuclei with decreased nuclear activation. The pronounced slowed conductivity at the pontomedullary level in patients with bulbar disorders was associated with moderate impairment of thalamocortical conduction. This is similar to the results discussed in the literature. The common SSEP abnormalities in Chiari 1 discussed in the literature include a reduction in cortical amplitude from the posterior tibial nerve, a reduction or absence of cervical median nerve potential, and an increased N13-N20 interval (Moncho et al., 2013).

In the analysis of ENMG data obtained from stimulation of the median and tibial nerves, there was a slight reduction of the efferent nerve conduction velocities in the study group compared to healthy individuals. At the same time, the maximum amplitude of the M-response of the median and tibial nerves was practically unchanged compared to the control group. This phenomenon, in our opinion, is associated with the reactive involvement of conductive efferent pathways in Chiari 1 patients with bulbar syndrome with the development of bilateral pyramidal tract involvement. The ENMG was characterized by a pronounced impairment of conductivity at the level of the nuclei of the medulla, often with the involvement of the decussation of the pyramidal pathways. These data allowed us to assess the condition of Chiari 1 patients with bulbar syndrome, even in the subclinical phase of the disease.

The nerve conduction velocity of the glossopharyngeal nerve in the study was the most predictive for bulbar syndrome. In 60% of the patients, the NCV was significantly reduced. It should be noted that the glossopharyngeal NCV was abnormal in patients with mild and subclinical bulbar disorders as well. BAEP and SSEP studies play an important role in incidentally detected Chiari malformation patients and may help to establish objective evidence of subclinical dysfunctions (Moncho et al., 2017). The threshold value of the NCV was 21.5 m/s. Patients with NCV of 21.5 m/s and below had an increased risk of bulbar syndrome, while the risk was lower in patients with NCV values above 21.5 m/s. The sensitivity and specificity of the model at the chosen threshold value were 75.5% and 71.2% respectively. The observed dependence was significant with a p-value of 0.004. The isolated involvement of the glossopharyngeal nerve in Chiari malformation presenting as neuralgia, central sleep apnea, and syncope has been reported in the literature by various authors (Yglesias et al., 1996; Aguiar et al., 2002; Li et al., 2012; Ruiz-Juretschke et al., 2012; Kanpolat et al., 2001). The predictive value of the glossopharyngeal nerve in Chiari 1 malformation with bulbar syndrome has been poorly explored in literature.

The threshold of the M-response amplitude of the glossopharyngeal nerve dividing the study group into high and low-risk groups was 1.01 microV. In patients with M-response 1.01microV and below, the risk of development of decompensated bulbar syndrome was significantly higher than among patients with higher amplitude. The sensitivity and specificity of the model were 78.0 and 71.2%, respectively.

CONCLUSION

The most informative method of determining the risk of development and prognosis of bulbar syndrome in patients with Chiari 1 malformation is Electroneuromyography (ENMG) of the Glossopharyngeal nerve. The decrease in M-response amplitude of bulbar muscles and the decrease in NCV on efferent fibers are highly predictive of the development of bulbar disorders in patients with Chiari 1, regardless of the presence of clinical symptoms.

Ethics Statement

The studies involving human participants were reviewed and approved by Institutional Review Board at the Republican Specialized Scientific and Practical Medical Center of Neurosurgery. The Ethics Committee waived the requirement of written informed consent for participation as this was a retrospective study.

ACKNOWLEDGEMENTS

The publication was carried out with the support of the Peoples Friendship University of Russia (RUDN) Strategic Academic Leadership Program.

REFERENCES

AGUIAR PH, TELLA OI JR, PEREIRA CU, GODINHO F, SIMM R (2002) Chiari type I presenting as left glossopharyngeal neuralgia with cardiac syncope. *Neurosurg Rev,* 25: 99-102.

ANDERSON RCE, DOWLING KC, FELDSTEIN NA, EMERSON RG (2003) Chiari I Malformation: potential role for intraoperative electrophysiologic monitoring. *J Clin Neurophysiol,* 20: 65-72.

ARONSON DD, KAHN R, CANADY A, BOLLINGER R, TOWBIN R (1991) Instability of the cervical spine after decompression in patients who have Arnold-Chiari malformation. *J Bone Joint Surg,* 73: 898-906.

GUO F, WANG M, LONG J, WANG H, SUN H, YANG B, SONG L (2007) Surgical management of Chiari malformation: analysis of 128 cases. *Pediatr Neurosurg,* 43: 375-381.

GUSHCHA OA, SHAKHNOVICH AR, KASHCHEEV AA, ARRESTOV SO, ABUZAID SM (2010) The new mini-invasive technique of surgical treatment of Arnold Chiari anomaly: experimental-clinical study. *Neurosurg J,* 4: 23-38.

HENRIQUES FILHO PSA, PRATESI R (2006) Abnormalities in auditory evoked potentials of 75 patients with Arnold-Chiari malformations types I and II. *Arquivos Neuro-psiquiatria,* 64: 619-623.

HOLLIDAY PO III, PILLSBURY D, KELLY DL JR, DILLARD R (1985) Brain stem auditory evoked potentials in Arnold- Chiari malformation: possible prognostic value and changes with surgical decompression. *Neurosurgery,* 16: 48-53.

ISMAILOVA RO (2020) Evoked brain potentials in the preoperative diagnosis of Type 1 Chiari malformation. *Global J Med Res,* 20: 37-52.

ISU T, SASAKI H, TAKAMURA H, KOBAYASHI N (1993) Foramen magnum decompression with removal of the outer layer of the dura as treatment for syringomyelia occurring with Chiari I malformation. *Neurosurgery,* 33: 845-850.

KANPOLAT Y, UNLU A, SAVAS A, TAN F (2001) Chiari Type I malformation presenting as glossopharyngeal neuralgia: case report. *Neurosurgery,* 48: 226-228.

LEVY WJ, MASON L, HAHN JF (1983) Chiari malformation presenting in adults: a surgical experience in 127 cases. *Neurosurgery,* 12: 377-390.

LI F, YANG Y, LIU Y, LI Q, ZHU S (2012) Glossopharyngeal neuralgia as onset of Chiari type I malformation. *Headache,* 52: 1576-1578.

MILHORAT TH, BOLOGNESE PA (2003) Tailored operative technique for Chiari type I malformation using intraoperative color Doppler ultrasonography. *Neurosurgery,* 53: 899-906.

MOJAEV SV, STERLIKOVA NV (2009) Results of surgical treatment of Chiari I type anomaly of ventrolateral localization. *Ukranian Neurosurg J,* 3: 35-39.

MØLLER AR, JHO HD, YOKOTA M, JANNETTA PJ (1995) Contribution from crossed and uncrossed brainstem structures to the brainstem auditory evoked potentials: a study in humans. *Laryngoscope,* 105: 596-605.

MONCHO D, POCA MA, MINOVES T, FERRÉ A, RAHNAMA K, SAHUQUILLO J (2013) Brainstem auditory evoked potentials and somatosensory evoked potentials in Chiari malformation. *Rev Neurol,* 56: 623- 634.

MONCHO D, POCA MA, MINOVES T, FERRÉ A, CAÑAS V, SAHUQUILLO J (2017) Are evoked potentials clinically useful in the study of patients with Chiari malformation Type 1? *J Neurosurg,* 126: 606-619.

MUNSHI I, FRIM D, STINE-REYES R, WEIR BK, HEKMATPANAH J, BROWN F (2000) Effects of posterior fossa decompression with and without duraplasty on Chiari malformation-associated hydromyelia. *Neurosurgery,* 46: 1384-1389; discussion 1389-1390.

OLIMJANOVNAISMAILOVA R, KARIEV GM (2020) Clinical and neurophysiological features of syringomyelia in patients with Chiari malformation type 1. *J Critical Rev,* 7: 2305-2316.

RUIZ-JURETSCHKE F, GARCÍA-LEAL R, GARCIA-DUQUE S, PANADERO T, ARACIL C (2012) Glossopharyngeal neuralgia in the context of a Chiari type I malformation. *J Clin Neurosci,* 19: 614-616.

SEVOSTIYANOV DV (2011) Malformations of Chiari I type: pathogenesis, diagnostics, surgical treatment (literature review). *Bull Ural Med Acad Sci,* 1: 63-67.

VORONOV VG (2010) Value of MRI and SKT-AG in substantiation of indications for surgical treatment of Chiari type malformation in adults and children. *Neurosurg Neurol Children's Age,* 1: 9-21.

YGLESIAS A, NARBONA J, VANACLOCHA V, ARTIEDA J (1996) Chiari Type I malformation, glossopharyngeal neuralgia and central sleep apn'oea in a child. *Develop Med Child Neurol,* 38: 1126- 1130.

Rats kidney morphological particularities and functions post-treatment with *vernonia amygdalina* extract and low-dose lead acetate

Gabryel G. Akunna[1], L.C. Saalu[1], A. Irozuoke[2], E. Joshua[1]

[1] *Department of Anatomy, Benue State University, Markurdi, Nigeria*

[2] *Department of Anatomy, Baze University, Abuja FCT, Nigeria*

SUMMARY

This study was conducted to evaluate the effect of *Vernonia amygdalina* extract on Pb-induced kidney toxicity in Wistar rats. This investigation was carried out using 25 Wistar rat of both sexes, and the animals were divided into five groups: 5 rats per group. Group A served as the negative control group and was orally gavaged with 5mg/kg body weight of normal saline daily. Group B served as the positive control and was treated with daily intraperitoneal (IP) injection of 8 mg/kg body weight of Pb acetate (Pb). Group C was treated with daily intraperitoneal (IP) injection of 8 mg/kg body weight of Pb along with 20 mg/kg body weight of *Vernonia amygdalina* extract orally. Group D was treated with daily intraperitoneal (IP) injection of 8 mg/kg body weight of Pb along with 40 mg/kg body weight of *Vernonia amygdalina* extract orally. Group 5 was treated with daily intraperitoneal (IP) injection of 8 mg/kg body weight of Pb along with 60 mg/kg body weight of *Vernonia amygdalina* extract orally. All treatments were done for a period of 28 days. The animals were sacrificed on the 29th day by cervical dislocation, then blood was collected by cardiac puncture, and kidneys were collected for histological profile. Lipid peroxidation (MDA), creatinine and urea level were all determined. There was marked elevation in MDA level with a concomitant depletion in urea and creatinine content in the group treated with only Pb when compared with the negative control group. There was a significant increase in proximal tubular area, distal tubular area, glomerular membrane thickness, area, perimeter and feret's diameter and a significant decrease in proximal tubule, distal tubule ratio and cellularity in this group of rats when compared to the negative control. Oxidation and histological changes in the kidneys were successfully prevented by the pre- administration of *Vernonia amygdalina* as evidenced by creatinine and urea and MDA level. These were made evident as the morphological scores across all experimental groups were significantly different from those of the positive control (group 2). Based on the current findings, it can be concluded that *Vernonia amygdalina* successfully minimizes the deleterious effects in kidney function and histological coherence associated with nephrotoxicity by strengthening the antioxidant defense system, suppressing oxidative stress, and mitigating apoptosis.

Key words: *Vernonia amygdalina* – Kidney – Morphology – Toxicity – Oxidative stress

Corresponding author:
Dr G.G. Akunna. Department of Anatomy, Benue State University, Markurdi, Nigeria. E-mail: ggakunna@gmail.com

Submitted: September 9, 2022. **Accepted:** October 8, 2022

https://doi.org/10.52083/ZTZK6810

INTRODUCTION

In the environment, Pb is a common natural element. It is one of the most significant and prevalent environmental contaminants (Joworaski, 1968). Pb can harm humans and other living things by moving up the food chain and harming them. It is one of the environmentally harmful metals and negatively affects the majority of human organs (Duruibe et al., 2007; Alwaleedi, 2016).

Pb poisoning is linked to a variety of physiological, morphological, and biochemical changes, including liver dysfunction (ATSDR, 1993; Elayat and Bakheelf, 2010), hematological diseases, and impairment of renal system functions (Mugahi et al., 2003; Suradkar and Ghodasara, 2009; Alwaleedi, 2016).

Reactive oxygen species (ROS) generation, depletion of intracellular antioxidant reserves and free radical scavengers, and inhibition of antioxidative enzymes are all well-known mechanisms by which heavy metals cause oxidative stress (Shilpi et al., 2014; Jan et al., 2015). Due to ROS damage to lipids, proteins, and DNA, cells under oxidative stress exhibit a variety of dysfunctions (Ercal et al., 2010).

One of the most obvious symptoms of Pb toxicity has been observed to be impaired kidney functions (Chang et al., 1980). Proximal tubular nephropathy, glomerular sclerosis, and interstitial fibrosis are symptoms of Pb-induced nephrotoxicity (Loghman-Adham, 1997; Diamond, 2005).

Enzymuria, low- and high-molecular-weight proteinuria, reduced transfer of organic anions and glucose, and decreased glomerular filtration rate are functional abnormalities in people that have been linked to excessive Pb exposure. A few investigations have revealed the histological signs of renal damage in humans, including interstitial fibrosis, cellular necrosis, and intranuclear inclusion bodies in the proximal tubule (Cramer et al., 1974; Biagini et al., 1977).

Ijeh and Ejike (2011) and Pitot and Dragan (2013) provide extensive documentation of the medicinal benefits of *Vernonia amygdalina* (VA), a shrub growing 2-5 meters tall with petiolate leaves that are around 6 millimeters in diameter and elliptic in form and consumed as a green vegetable in Nigeria.

Due to its bitter flavor, which can be linked to its anti-nutritional components such tannins, alkaloids, glycosides, flavonoids, and saponins, it is commonly referred to as “bitter leaves” (Igile et al., 1994; Johri and Singh, 1997; Ejoh et al., 2007; Ekpo et al., 2007; Eleyinmi et al., 2008).

Nitrogen, phosphorus, calcium, magnesium, sodium, potassium, manganese, copper, and cobalt are the main ions found in VA, along with ascorbic acid and carotenoids (Egedigwe, 2010). (Kupchan et al., 1969; Ayodele, 1999). According to Pitot and Dragan (1996), the plant’s leaves have antibacterial, anti-cancer, antioxidant, antidiabetic, hepatoprotective, hypolipidemic, and anti-fertility characteristics when extracted in water (Innih and Ubhenin, 2021).

Additionally, the abortifacient, antifertility, antimicrobial, antiplatelet and anticoagulant, antimalarial, hepatoprotective, analgesic, anti-inflammatory, anti-pyretic, antimutagenic, and effect on CD4+ cell count (HIV/AIDS) were reported (Pitot and Dragan, 1996). Bitter leaf’s safety had been demonstrated through both solitary administration and administration while in the presence of toxins (Correia et al., 2000; Demirezen and Kadiriye, 2006).

It is known how VA affects kidney toxicity brought on by Pb (Achuba, 2018; Innih and Ubhenin, 2021). On the impact of chronic and sub-Pb poisoning on renal function parameters, there are contrasting studies. According to certain investigations (Afolabi and Oke, 1981; John, 1999; Innih and Ubhenin, 2021), exposure to Pb caused renal hypertrophy and an increase in glomerular filtrate rate (GFR), whilst other studies indicated a decrease in GFR (Khalil-Manesh et al., 1994). According to independent research on low-dose Pb intoxication (Restek-Samarzija and Momcilovic, 1992; Khalil-Manesh et al., 1994), there were no detectable pathological alterations in Pb-intoxicated rats. Given these discrepancies across various research, it is unclear if Pb toxicity can be linked to the length of time and dosage used to induce Pb intoxication.

Additionally, the majority of the research on this area has been mostly on the subjective qualitative approaches of slide interpretation. In cases of toxicity, morphometric and stereological examinations of tissue are extremely effective. There are more techniques for evaluating the total kidney volume and renal function for hypertrophy or shrinking (Almajdub et al., 2008; Abdellatif and Hassan, 2013; Yamashita et al., 2015; Abdurrahman et al., 2018) including stereological technique which involved the exhaustive sectioning of the kidney and then selecting representative sections using systematic uniform random sampling (Nyengaard, 1999).

Relative medullary thickness (RMT) was discovered to have a substantial direct link with the maximum urine concentrating ability of animals. In an investigation on a goat after a nephrectomy, Tejo et al. (2014) reported this link between animal species (Abdellatif and Hassan, 2013). RMT is calculated by comparing the medullary thickness (MT) to the kidney size (KS) of the medulla, measured from the corticomedullary junction to the tip of the papilla (Al-kahtani et al., 2004; Abdurrahman et al., 2018).

This investigation uses morphometry to assess the effects of VA on the kidney of Wistar rats given low doses of Pb in relation to biochemical indicators of kidney function.

MATERIALS AND METHODS

Acquisition of chemicals: Pb

The chemicals used- Lead (Pb) was procured from a laboratory Emole Nigeria limited at high-level makurdi, Benue state.

Acquisition of plant materials

Vernonia amygdalina (Bitter leaf) used in the study was obtained from a farm land close to River Benue at Wurukum, Makurdi-Benue state.

Procurement and maintenance of animals

A total of 25 Wistar rats between 100-150 g of both sexes were obtained from Animal House at College of Health Science, Benue state University, Makurdi. They were fed with normal rat chow for a period of two week for acclimatization.

They were housed in groups of five (5) in plastic constructed cages, in a well-ventilated room at room temperature and fed with normal commercial pellet diet and water. Animal Research Review Panel and Animal Welfare Unit regulations of temperature and lighting systems were maintained with a room temperature of 20-26°C as well as regular light cycles of 12 hours light/dark. All methods and protocols used in the study were observed following established public health guidelines Guide for Care and Use of Laboratory Animals."

Preparation of leaf extracts

The plant samples were washed thoroughly with tap water to remove any form of dirt. The leaves were then air-dried under shade for 14 days at room temperature and pulverized into powder using a blender and stored in airtight plastic containers. One hundred and twenty-five grams (300 g) of the powdered leaves were macerated in separate cold ethanol (Absolute ethanol) and were allowed to stand to at room temperature for 48hour. The mixture was shaken continuously for several times for a uniform mixture and to obtain a maximum extract yield. After the 48 hours, the macerated solution was filtered using a filter paper into a beaker. The filtrate was boiled on a water bath at a temperature of 70°C to separate the ethanol from the crude drug. The crude drug extract was labelled EEVA (ethanolic extract of Vernonia amygdalina) and yield about 61.6g then was transferred into a Petri dish and kept under sun shied to solidify and dry the extract, after which it was kept in a refrigerator at 4°C.

Experimental design

The Wistar rats were separated into 5 different groups containing 5 animals each, labeled A to E. Group A: This group served as the negative control group and was orally gavaged with 5mg/kg body weight of normal saline daily for 5 days.

Group B: This group served as the positive control and was treated with daily intraperitoneal (IP) injection of 8mg/kg body weight of Pb for 28 days (Salem and Salem, 2016).

Group C: This group was treated with daily intraperitoneal (IP) injection of 8mg/kg body weight of Pb along with 20mg/kg body weight of VA extract (Akinyemi, 2016) orally for 28 days.

Group D: This group was treated with daily intraperitoneal (IP) injection of 8mg/kg body weight of Pb along with 40mg/kg body weight of VA extract orally for 28 days.

Group E: This group was treated with daily intraperitoneal (IP) injection of 8mg/kg body weight of Pb along with 60mg/kg body weight of VA extract orally for 28 days.

Animal sacrifice

After 24 hours at the end of the treatment period of 28 days, the animals were sacrificed by cervical decapitation been the 29th day after an overnight fast. Blood samples were collected immediately by cardiac puncture into ETDA tubes and labeled. The blood samples collected were for various biochemical assays. The kidneys also were harvested into labeled containers under cold conditions for histological analysis.

Assessment of biochemical parameters

Experimental Wistar rats were sacrificed, and blood was dispensed into serum separator tubes and then analyzed for biochemical parameters. Kidney urea, creatinine and malondialdehyde (MDA) levels were assayed and analyzed using a standard BS-200E Mindray chemistry Autoanalyzer, PKF Scientific Limited. The urea and creatinine were measured in mg/dl.

Histological and morphometric analysis

Rats were dissected, and the kidneys were taken out and examined for signs of gross pathology. Tissue samples were immediately fixed in 10% formalin, put through an automated tissue processor, and then embedded in paraffin wax for light microscopic inspection. The tissue blocks were then cut into serial sections using the rotary microtome. Following deparaffinization, the sections were stained with hematoxylin and eosin (H&E). Images of each section were captured using a light microscope after the tissue had undergone histological processing. A computerized image analysis system was used for the morphometric study. Hematoxylin and eosin-stained kidney slices were seen in Image J using a digital camera. The morphometric parameters that were measured were as follows: proximal and distal tubule area in square micrometers, nuclear/cytoplasmic ratio of proximal and distal tubule epithelial cells, glomerular membrane thickness (GBM) in micrometers, glomerular area in square micrometers, glomerular cellularity in square micrometers, perimeter in micrometers, Feret's diameter in micrometers, and circularity. At least 50 proximal and distal tubules and glomeruli were counted in every animal. Prior to each study, a spatial calibration using an object micrometer was carried out.

Circularity was determined by the formula: $\frac{(4\pi^{*}\text{area})}{(\text{perimeter}^2)}$

Statistical analysis

Mini tab software (version 17.1.0. cracked) was used for the data analysis. Data were presented as mean ± SEM on bar chart graphs and tables. To compare the biological effects of the treatment, analysis of variance (ANOVA) was used. Values of less than 0.05 were considered statistically significant.

RESULTS

Gross anatomical features

There was no significant change in the body weight, kidney weight and kidney weight and body weight ratio when compared across all group as shown in Table 1.

Biochemical analysis and oxidative makers

Creatinine

The activity level of creatinine in group 2 rats was significantly ($p \leq 0.05$) decreased when compared to Group-1 rats. The rats in Groups 3, 4 and 5 recorded a mean creatinine level when compared to group 2 rats. There were significant ($p \leq 0.05$) increase when compared to group 2 rats. The activity level of Urea in Group

Table 1. Showing the mean ± standard deviation of different gross anatomical features across all group.

	Initial body weight (g)	Final body weight (g)	Body weight difference (%)	Kidney weight (g)	Kidney weight/body weight ratio
Group 1	80.94 ± 6.59	102.56± 9.51	21.62±4.94	1.70 ± 1.30	0.08±0.06
Group 2	106.24± 6.33	128.46± 5.32	22.62±2.02	1.51 ± 0.30	0.08±0.06
Group 3	101.70±13.64	117.60± 14.40	15.9±3.09	1.70 ± 1.01	0.11±0.09
Group 4	101.34±11.15	114.84± 11.76	13.50±4.11	1.82 ± 1.2	0.11±0.06
Group 5	93.62±10.92	107.04± 10.42	13.42±2.09	1.0 ± 0.40	0.13±0.11

Table 2. Showing the mean ± standard deviation of different biochemical analysis and oxidative markers across all groups.

	Creatinine (mg/dl)	Urea (mg/dl)	MDA (nmol/mg pro)
Group 1	0.84 ± 0.04	26.00 ± 1.32	0.64 ± 0.11
Group 2	0.51 ± 0.11*	19.91 ± 1.50*	3.17 ± 0.13*
Group 3	0.85 ± 0.05**	21.88 ± 2.06	1.76 ± 0.50**
Group 4	0.85± 0.09**	22.16 ± 2.37	0.88 ±0.44**
Group 5	0.93 ± 0.12**	21.88 ± 2.06	0.95 ± 0.63**

*and** showed a significance when compared to group 1 and 2 respectively.

2 rats were significantly ($p \leq 0.05$) decreased when compared to group 1 rats. The rats in Groups 3, 4 and 5 recorded a mean urea level that had non-significant ($p > 0.05$) increase when compared to Group-2 rats.

The activity level of lipid peroxidation was significantly ($p \leq 0.05$) increased in Group-2 rats when MDA level was compared to group 1 rats. However, the rats in Groups 3, 4 and 5 recorded a mean MDA level that was significant ($p \leq 0.05$) when compared to Group 2 rats with each.

Histological profile

Macroscopically the kidneys of Group 1 (Fig. 1) appeared to be normal as seen in histological text. The surfaces were granular and there was presence of numerous cortical tissues with corticomedullary closure and devoid of vascular markings. The pyramids were also intact. The kidney surfaces of Group-2 rats (Fig. 2) appear contracted and have a granular surface. The cut surface shows general loss of cortical tissue, corticomedullary demarcation and vascular markings.

The pyramids are small but intact. When Group-2 histomorphology were compared to that of Group 1, there were varying degrees of relatively cellular interstitial nephritis. Areas of dilated tubules alternate with atrophic tubules, rendering a granular appearance to the kidney surface. A large proportion of glomeruli are lost without leaving a trace, which is a characteristic feature.

Level of distortion and disruption of the cytoarchitecture of the renal cortical structure with marked diffuse glomerulonephritis and an enlarged Bowman's space are observed as compared to the control section.

The kidney of Groups 3 to 5 (Figs. 3, 5) also appeared distorted when compared to Group 1. But when you compare them to Group 2 they were better off.

Morphological scores

There was a significant increase in proximal tubular area, distal tubular area, glomerular membrane thickness and a significant ($p \leq 0.05$) decrease in proximal tubule and distal tubule ratio of Group-2 rats when compared to the negative control (Group 1).

The proximal tubular area and distal tubule ratios across all experimental groups were significantly ($p \leq 0.05$) different from those of the positive control (Group 2). For distal tubule area and glomerular membrane thickness,

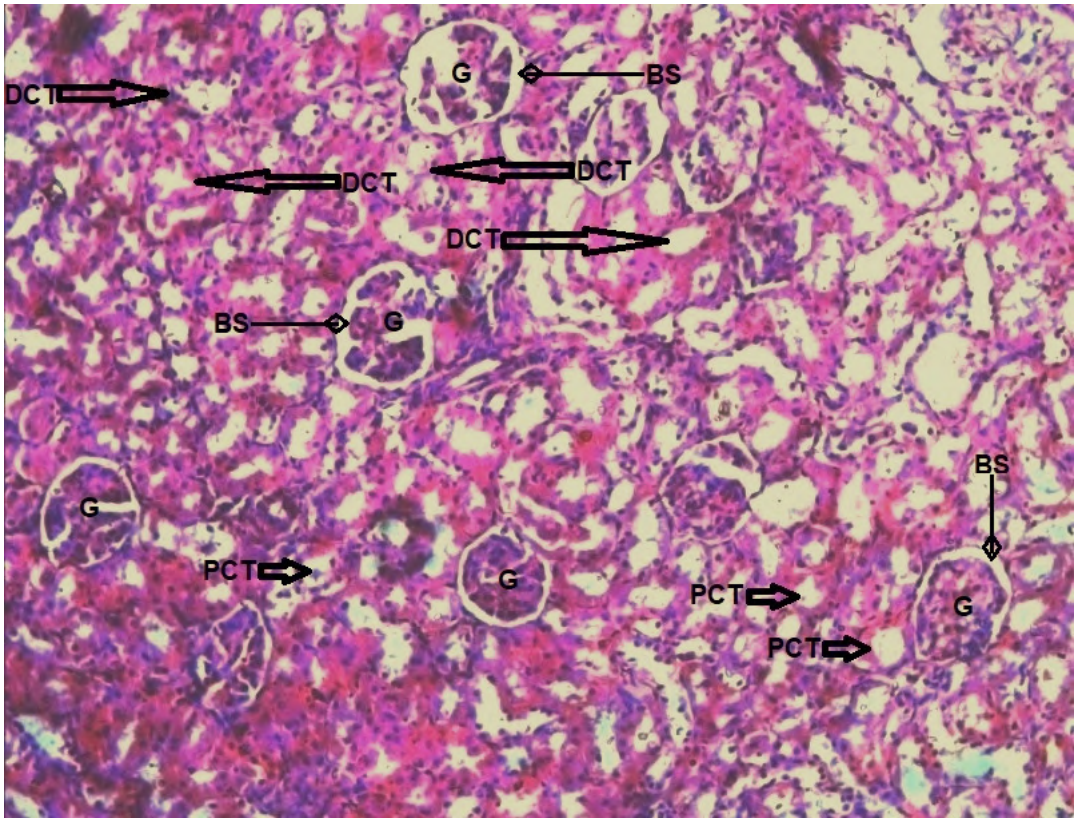

Fig. 1.- Kidney morphology from Group-1 rats (5 ml/kg of normal saline) showing the distal convoluted tubule (DCT), proximal convoluted tubule (PCT), glomerulus (G) and Bowman's space (BS). Magnification: x200. Stain: H&E.

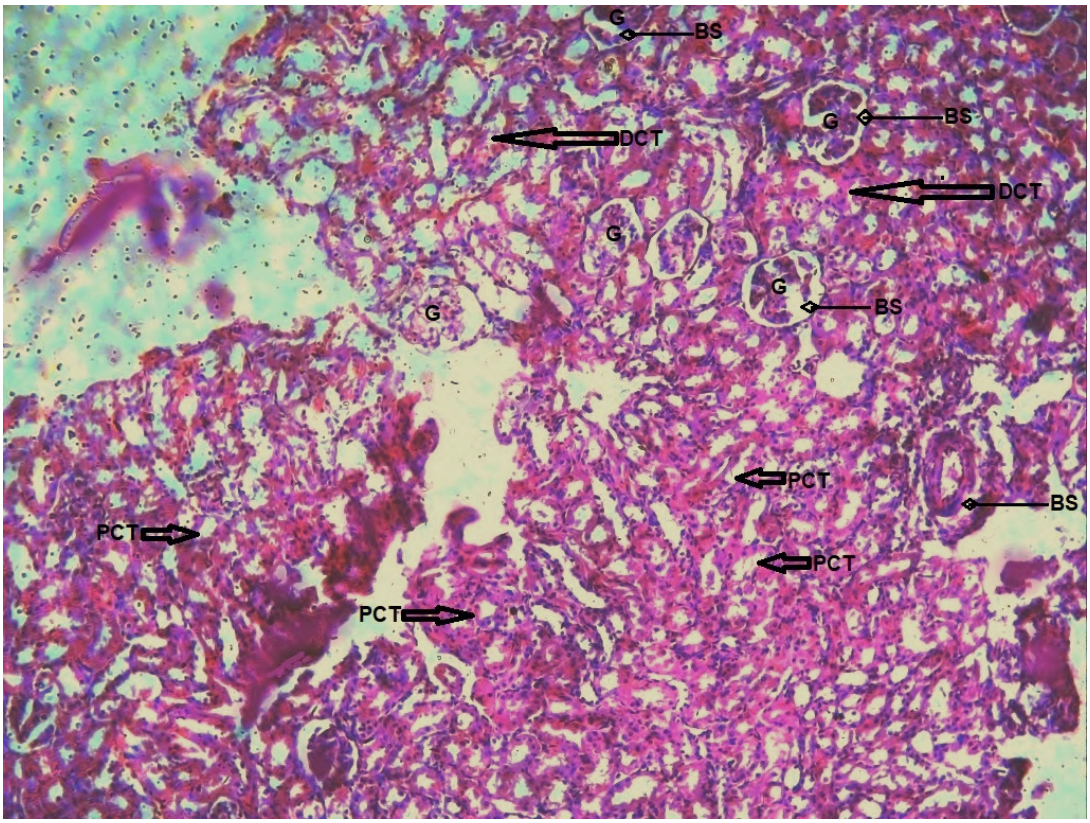

Fig. 2.- Kidney from Group 2 / positive control (20 mg/kg body weight of Pb intraperitoneally) showing the distal convoluted tubule (DCT), proximal convoluted tubule (PCT), glomerulus (G) and Bowman's Space (BS). Magnification: x200. Stain: H&E.

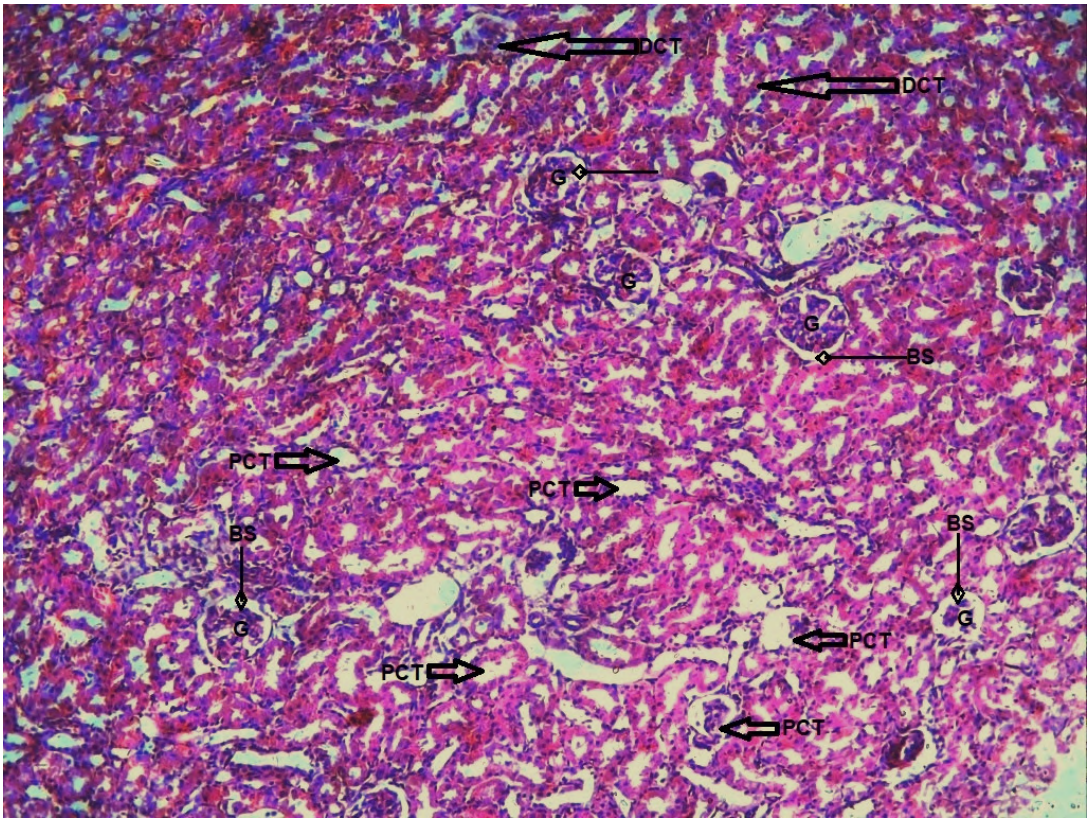

Fig. 3.- Kidney from Group 3 (20 mg/kg body weight of Pb intraperitoneally and 100 mg/kg body weight of *Vernonia amygdalina* extract) showing the distal convoluted tubule (DCT), proximal convoluted tubule (PCT), glomerulus (G) and Bowman's Space (BS). Magnification: x200. Stain: H&E.

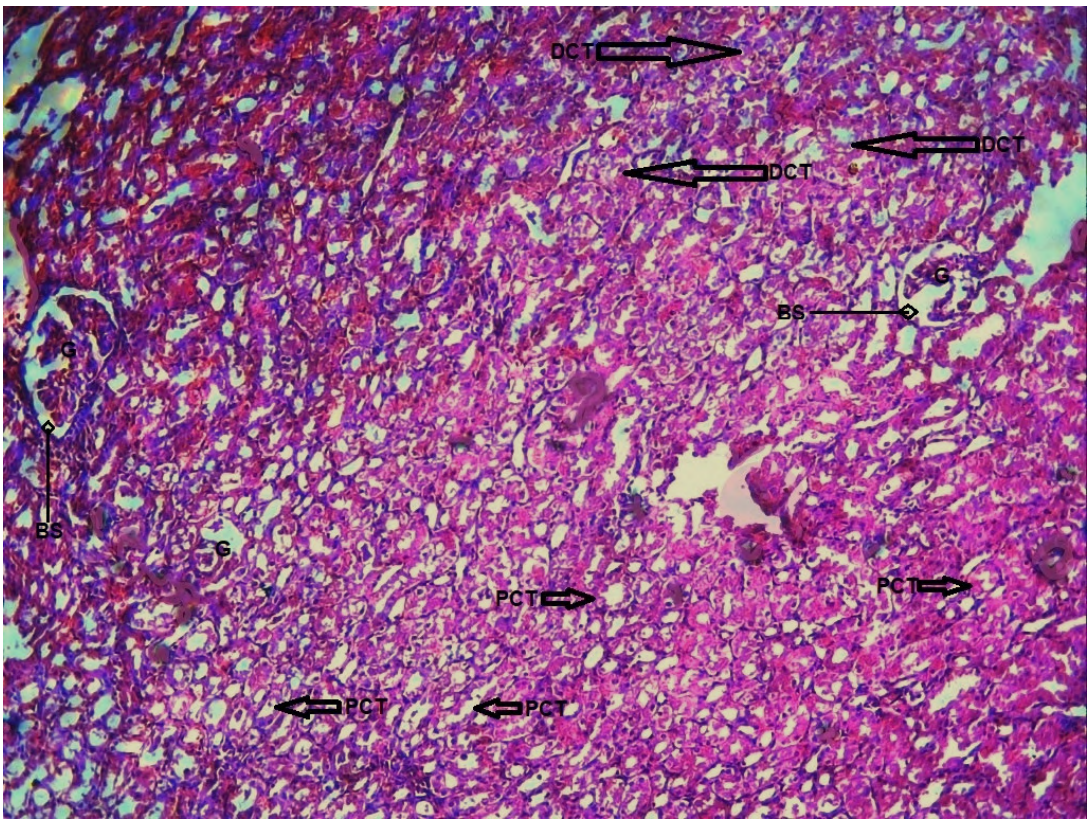

Fig. 4.- Kidney from Group 4 (20 mg/kg body weight of Pb intraperitoneally and 200 mg/kg body weight of *Vernonia amygdalina* extract), showing the distal convoluted tubule (DCT), proximal convoluted tubule (PCT), glomerulus (G) and Bowman's Space (BS). Magnification: x200. Stain: H&E.

only Groups 4 and 5 were significantly ($p \leq 0.05$) different from that of the positive control (Group 2). Also, with proximal tubule ratio only Group 5 was significantly ($p \leq 0.05$) different from that of the positive control (Group 2) (Table 3).

There was a significant ($p \leq 0.05$) increase in area, perimeter and feret's diameter and a significant ($p \leq 0.05$) decrease in cellularity of Group-2 rats when compared to the negative control (group 1).

Although the area, cellularity and feret's diameter in Groups 4 and 5 rats were significantly ($p \leq 0.05$) different from those of the positive control (Group 2), there was no significant ($p \geq 0.05$) difference between the values of area, cellularity and feret's diameter in Group-3 rats when compared to the positive control (Group 1). Group 4 had no significant difference between the perimeter values when compared to the positive control (Group 1) (Table 4).

Table 3. Showing the mean ± standard deviation of some morphological scores across all groups.

Groups	Proximal tubule Area (µm²)	Distal tubule Area (µm²)	Proximal tubule N/C ratio	Distal tubule N/C ratio	Glomerular membrane thickness (µm)
1	1323±103.04	726.40±23.02	0.614±0.11	0.762±0.23	0.72±0.51
2	3634± 132.1**	1214.2±64.1**	0.271±0.13**	0.523±0.16**	0.91±0.71**
3	2131±102.1*	1204.1±89.3	0.292±1.04	0.663±0.31*	0.82±0.21
4	2021±97.1*	946.3±104*	0.262±1.08	0.681±0.41*	0.71±1.04*
5	1783±131.3*	832.6±132.3*	0.562±2.3*	0.625±0.03*	0.63±0.31*

*and** showed a significance when compared to group 1 and 2 respectively.

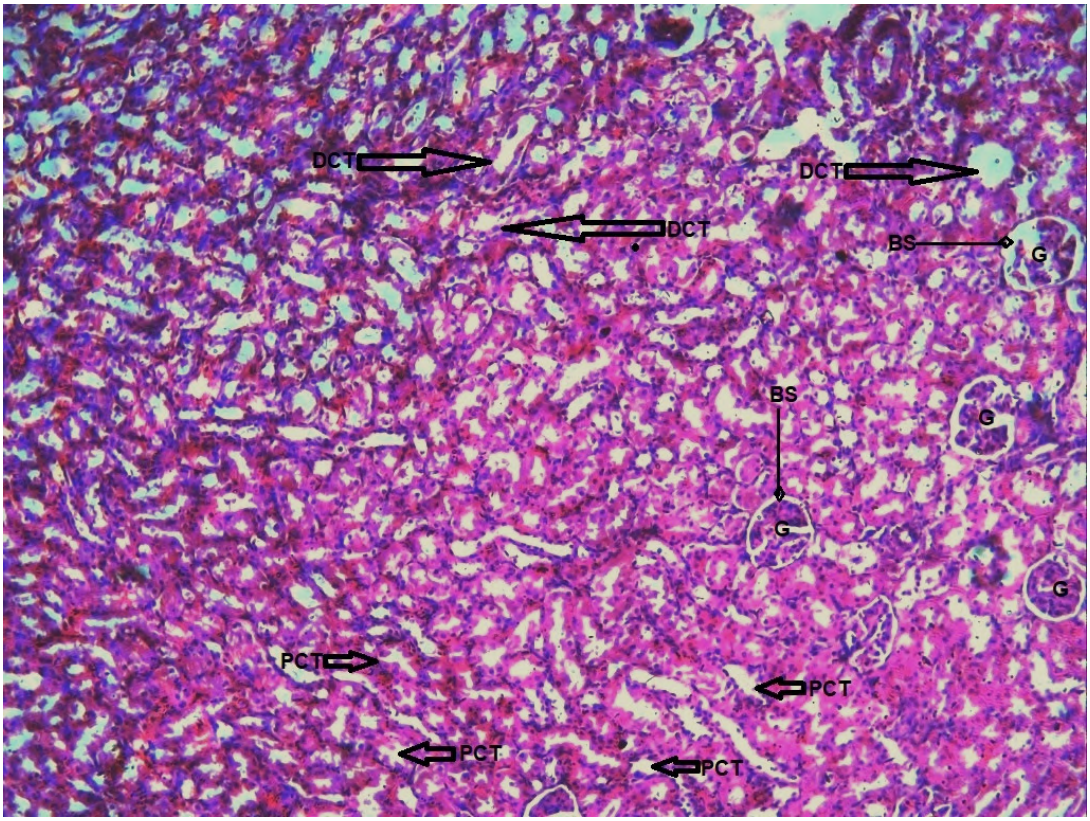

Fig. 5.- Kidney from Group 5 (20 mg/kg body weight of Pb intraperitoneally and 300 mg/kg body weight of *Vernonia amygdalina* extract), showing the distal convoluted tubule (DCT), proximal convoluted tubule (PCT), glomerulus (G) and Bowman's Space (BS). Magnification: x200. Stain: H&E.

Table 4. Showing the mean ± standard deviation of some morphological scores across all groups.

Groups	Area (μm²)	Cellularity (cells/μm²)	Perimeter (μm)	Feret's diameter (μm)	Circularity
1	9321±201.4	0.0092±0.0001	412.3±6.1	130.2±3.1	0.764±0.001
2	12240±140.1**	0.006± 0.0001**	492±21.03**	162.1±1.3**	0723±0.003**
3	11411±110.3	0.007± 0.0002	328±24.3*	151.3±2.8	0721±0.001
4	10121±91.4*	0.008± 0.0001*	472±17.1	142.5±5.7*	0724±0.004
5	91201±124*	0.008± 0.0004*	332±11.5*	129.1±6.2*	0728±0.002

*and** showed a significance when compared to group 1 and 2 respectively.

DISCUSSION

In this study, all groups of rats had a non-significant increase in body weight but not in kidney weight. This finding conflicts with other earlier studies on the impact of Pb on kidney weight (Seddik et al., 2010; Ali et al., 2010). While Flaherty et al. (1986) saw increases in kidney wet weight and dry weight in rats given varied doses of Pb, Goyer (1971) noted an increase in kidney wet weight in rats given a high dose of Pb for prolonged periods of time (Aseth et al., 1995; Teijon et al., 2006). Because of their active growth phase, the rats in this study may have gained weight even in the positive control group (Marija et al., 2004).

In mice, exposure to Pb has been found to increase the generation of reactive oxygen species (ROS), which causes lipid peroxidation and changes to the antioxidant defense mechanisms, leading to oxidative stress (Demirezen and Kadiriye, 2006; Xienia et al., 2000). The byproducts of several degenerative processes in different tissues, known as ROS, damage the cellular components and impair normal metabolism (Foyer and Noctor, 2000). When compared to the positive control, the VA-treated rat groups showed a considerable improvement in their antioxidant system.

The positive impact of antioxidant nutrients through exogenous supplementation of antioxidant molecules may be ascribed to lowering the chance of Pb interacting with important biomolecules and promoting oxidative damage or enhancing the cell's antioxidant defense (Marija et al., 2004). Because flavonoids include numerous hydroxyl groups, which serve as metal chelators by creating a coordination link with Pb, VA may have prevented the accumulation of Pb in the kidney. These biologically active substances may have chelated lead and improved its removal from the body, reducing lead buildup in renal tissue (Sharma et al., 2010; Iwara et al., 2013; Oladele et al., 2021).

Additionally, as compared to the negative control group, animals treated with Pb alone had higher levels of urea and creatine. This is consistent with findings from investigations in rats (Mugahi et al., 2009; Elayat and Bakheelf, 2010), goats (Swarup and Dwivedi, 1992; Haneef et al., 1998), sheep (Mugahi et al., 1998), and goats after oral administration of Pb (Ahmed and Shalaby, 1991).

This could be a symptom of kidney disease and is thought to constitute functional proof of Pb-induced nephrotoxicity (Patterson, 1965; Zook et al., 1972). The increase in serum creatinine level revealed decreased creatinine clearance and a compromise of the glomerular filtration function. Creatinine clearance is a more clinical biomarker of glomerular filtration capacity.

The metabolic byproducts of creatine and amino acids, respectively, are creatinine and urea. They frequently serve as markers of renal function. Due to a decrease in glomerular filtration, damage to functional nephrons can cause a rise in serum creatinine and urea levels (Ellman, 1959; El-Ashmawy et al., 2005). Since serum creatinine and urea cannot be excreted from the blood due to renal failure, their elevated levels indicate glomerular dysfunction (El-Ashmawy et al., 2005). This results in a rise in blood levels and a corresponding decrease in urine. The blood levels of urea and creatinine were raised as a result of this impairment of the renal functions.

In contrast to the negative controls, the rats treated with Pb had lower levels of creatinine and urea in their kidneys, according to the current investigation, whereas Heba et al. (2014) observed

a significant increase in serum creatinine and urea activities. Our findings showed that VA had a nephroprotective effect against Pb-induced nephrotoxicity, as evidenced by improvements in creatinine and urea levels in the pretreated groups.

This might be through its direct action on free radicals of Pb, protecting the kidney from cellular damage by maintaining its membrane integrity. The development of localized tubular necrosis away from the kidney's photomicrograph further supported the pathognomonic symptoms of kidney damage brought on by Pb.

Dystrophic and necrotic processes that manifest as ischemic necrosis of the tubular epithelium and interstitial oedema with connective tissue disorganization complicate pathomorphological processes (Aarabi, 2009; Merets'kyi and Holovata, 2013).

Pb exposure induced increasing glomerular and tubular changes, according to histological studies. These results are consistent with those of earlier studies by Abdel-Moneim et al. (2011), who identified changes in Pb exposure-related kidney histopathology. Heba et al. (2014) previously documented tubular vacuolization, necrosis, and dilation seen in the current research as a result of Pb intoxication. These Pb-induced tubular abnormalities may be the result of hydrolic changes in the renal tissue, which suggests that Pb toxicity leads to a partial breakdown in the transport of ions by tubule cells, resulting in tubular swelling, necrosis, and vacuolization of the tubules.

It should be mentioned that the structure and function of a rat's kidney are comparable to those of a human kidney in the context of the clinical application of the findings of experimental investigations of the effects of Pb on rats. Minor variations are mostly found at the macrostructural level; unlike human kidneys, rats' kidneys only contain one pyramid. The structure of the vascular grid also differs. However, the nephron structure, kidney layer hierarchy, and functioning are comparable to those found in humans.

This closeness has allowed for a number of inferences on the comparability of the pathological changes brought on by Pb in the rat kidney (Prus et al., 2020). When compared to rats in Group 1, rats in Group 2 had larger glomeruli, irregularly thickened glomerular basement membrane, and neutrophil cell infiltration.

There was a considerable Pb-induced apoptotic reaction in the renal glomerular tissue, as evidenced by the reduction in the number of cells in the glomerular area.

According to Kohn et al. (2002), the damage to glomerular cells may be significantly influenced by mitochondrial dysfunction. Barnes et al. (2020) also made this observation. This is the first morphometric investigation of rat kidneys in this experimental setting that we are aware of.

This finding offers proof that the compromised function observed in rats exposed to Pb may be related to renal morphological alterations. We noted a decrease in the content of urea and creatine. It is sufficient to state that this research has provided quantitative microscopic morphometry on the effects of VA on kidney damage caused by Pb in a rat model.

ACKNOWLEDGEMENTS

The author will like to thank the entire technical staff of the department of Anatomy, Benue State University for the timely assistant that was provided in the course of this project.

REFERENCES

AARABI B, SIMARD J (2009) Traumatic brain injury. *Curr Opin Crit Care*, 15(6): 548-553.

ABDELLATIF AM, HASSAN Y (2013) Effects of uninephrectomy on morphological and histological measurements of the remnant kidney in a goat (*Capra hircus*) model. *J Phys Pharm Adv*, 3(3): 94-102.

ABDEL-MONEIM E, DKHIL MA, AL-QURAISHY S (2011) The potential role of flaxseed oil on Pb induced kidney injure in adult male Albino rats. *Afr J Biotechnol*, 10(8): 1436-1451.

ABDULKADIR A, MBAJIORGU EF, NYIRENDA T (2018) Effects of concurrent chloroquine and ethanol administration on the rat kidney morphology. *Pan Afr Med J*, 29: 49.

ACHUBA FI (2018) Role of bitter leaf (*Vernonia amygdalina*) extract in prevention of renal toxicity induced by crude petroleum contaminated diets in rats. *Int J Vet Sci Med*, 6(2): 172-177.

AFOLABI OA, OKE OL (1981) Preliminary studies on the nutritive value of some cereal-like grains. *Nutr Rep Int*, 24: 389-394.

AHMED YF, SHALABY SA (1991) Clinicopathological and histopathological studies on chronic Pb intoxication in male Barki sheep. *Afr J Agric Sci*, 18: 19-37.

ALI MA, AWAL MA, MOSTOFA M, ISLAM MA, GHOSH A (2010) Effects of selenium and vitamin B6 with their combination in Pb induced toxicities in long Evans rats. *Bangl J Vet Med*, 8: 63-73.

AKINYEMI T (2016) Effect of bitter leaf (*Vernonia amygdalina*) saponin-rich extract on streptozotocin-induced diabetes in Wistar rats. Masters Thesis. http://196.220.128.81:8080/xmlui/handle/123456789/3453

AL-KAHTANI MA, ZULETA C, CAVIEDES-VIDAL E, GARLAND JR T (2004) Kidney mass and relative medullary thickness of rodents in relation to habitat, body size and phylogeny. *Physiol Biochem Zool*, 77(3): 346-365.

ALMAJDUB M, MAGNIER L, JUILLARD L, JANIER M (2008) Kidney volume quantification using contrast-enhanced in vivo X-ray micro-CT in mice. *Contrast Media Mol Imaging*, 3(3): 120-126.

ALWALEEDI SA (2016) Hematobiochemical changes induced by Pb intoxication in male and female albino mice. *Natl J Physiol Pharm Pharmacol*, 6: 46-51.

ASETH J, JACOBSEN D, ANDERSEN O, WICKSTROM E (1995) Treatment of mercury and Pb poisoning with dimercaptosuccinic acid (DMSA) and sodium dimercapto-propanesulfonate (DMPS). A review. *Analyst*, 120: 853.

AGENCY FOR TOXIC SUBSTANCES AND DISEASE REGISTRY (ATSDR) (1993) Toxicological Profile for Pb (1993) Update. Prepared by Clement International Corporation under contact no. 205-88-060 for ATSDR. Atlanta, GA: US Public Health Services.

AYODELE MS (1999) Karyomorphological studies in some Nigerian species of Vernonia SCHREB. (Asteraceae) with different growth forms. *Feddes Repert*, 110: 541-553.

BARNES P, YEBOAH JK, GBEDEMA W, SAAHENE RO, AMOANI B (2020) Ameliorative effect of *Vernonia amygdalina* plant extract on heavy metal-induced liver and kidney dysfunction in rats. *Adv Pharmacol Pharmac Sci*, 2020: 2976905.

BIAGINI G, CAUDARELIA R, VANGELISTA (1977) Renal morphological and functional modification in chronic Pb poisoning. In: Brown SS (ed). *Clinical chemistry and chemical toxicology of metals*. Elsevier/North-Holland Biomedical Press, pp 123-126.

CHANG LW, WADE PR, OLSON MN (1980) Ultrastructural changes in renal proximal tubules after tetraethyle Pb intoxication. *Environ Res*, 23: 208.

CORREIA PM, OLIVEIRA E, OLIVEIRA PV (2000) Simultaneous determination of Cd and Pb in foodstuffs by electro-thermal atomic absorption spectrometry. *Anal Chim Acta*, 405: 205-211.

CRAMER K, GOYER RA, JAGENBURG R (1974). Renal ultrastructure, renal function and parameters of Pb toxicity in workers with different periods of Pb exposure. *Br J Ind Med*, 31: 113-127.

DEMIREZEN D, KADIRIYE U (2006) Comparative study of trace elements in certain fish, meat and meat production. *Meat Sci*, 74: 255-260.

DIAMOND GL (2005) Risk assessment of nephrotoxic metals. In: Tarloff J, Lash L (eds). *The toxicology of the kidney*. London: CRC Press, pp 1099-1132.

DURUIBE JO, OGWUEGBU MC, EGWURUGWU JN (2007) Heavy metal pollution and human biotoxic effects. *Int J Phys Sci*, 2: 112-118.

EGEDIGWE CA (2010) Effect of dietary incorporation of *Vernonia amygdalina* and *Vernonia colorata* on blood lipid profile and relative organ weights in albino rats. MSc., Dissertation, Dept. Biochem., MOUAU, Nigeria.

EJOH RA, NKONGA DV, INOCENT G, MOSES MC (2007) Nutritional components of some nonconventional leafy vegetables consumed in Cameroon. *Pak J Nutr*, 6: 712-717.

EKPO A, ESEYIN OA, IKPEME AO, EDOHO EJ (2007) Studies on some biochemical effects of Vernonia amygdalina in rats. *Asia J Biochem*, 2: 193-197.

EL-ASHMAWY IM, EL-NAHAS AF, SALAMA OM (2005) Protective effect of volatile oil, alcoholic and aqueous extracts of Origanum majorana on Pb toxicity in mice. *Basic Clin Pharmacol Toxicol*, 97: 238-243.

ELAYAT W, BAKHEELF MS (2010) Effects of chronic Pb toxicity on liver and kidney functions. *J Med Lab Sci*, 1: 29-36.

ELEYINMI AF, SPORNS P, BRESSLER DC (2008) Nutritional composition of Gongrone malatifolium and Vernonia amygdalina. *Nutr Food Sci*, 38: 99-109.

ELLMAN GL (1959) Tissue sulfhydryl groups. *Arch Biochem Biophys*, 82: 70-77.

ERCAL N, GURER OH, AKYIN BN (2010) Toxic metals and oxidative stress part I: mechanisms involved in metal-induced oxidative damage. *Curr Topics Med Chem*, 1: 529-539.

FOYER CH, NOCTOR G (2000) Oxygen processing in photosynthesis: regulation and signaling. *New Phytol*, 146: 359-388.

HANEEF SS, SWARUP D, DWIVEDI SK, DASH PK (1998) Effects of concurrent exposure to Pb and cadmium on renal function in goats. *Small Rum Res*, 28: 257-261.

HEBA M, ABDOU, MOHAMED A. HASSAN (2014) Protective role of omega-3 polyunsaturated fatty acid against pb-induced toxicity in liver and kidney of female rats. *BioMed Res Int*, 2014: 435857.

IGILE GO, OLESZEK W, JURZYSTA M, BURDA S, FAFUNSO M (1994) Flavonoids from Vernonia amygdalina and their antioxidant activities. *J Agri Food Chem*, 42: 2445-2448.

IJEH II, EJIKE CE (2011) Current perspectives on the medicinal potentials of Vernonia amygdalina. *Del J Med Plants Res*, 5: 1051-1061.

INNIH SO, UBHENIN AE (2021) The protective effect of vernonia amygdalina in Pb-induced nephrotoxicity in Wistar rats. *Niger J Exp Clin Biosci*, 9: 227-233.

IWARA, IA, OUT EA, EFIONG E. IGILE GO, MGBEJE BAI, EBONG PE (2013) Evaluation of the nephroprotective effect of combine extract of vernonia amygdalina and moringa oleifera in diabetic induced kidney injury in albino Wistar rats. *Sch J App Med Sci*, 1(6): 881-886.

JAN A, AZAM M, SIDDIQUI K, ALI A, CHOI I, HAQ Q (2015) Heavy metals and human health: mechanistic insight into toxicity and counter defense system of antioxidants. *Int J Mol Sci*, 16(12): 29592-29630.

JOHN JB (1999) Estimating plasma in pH. In: Bray John J (ed). *Lecture Notes on Human Physiology*, 4th ed. Lecture Note Series, Blackwell Scientific Publications Lecture Notes, Wiley, New York, United States, p 610.

JOHRI RK, SINGH C (1997) Medicinal uses of Vernonia species. *J Med Aromat Plant Sci*, 19: 744-752.

JOWORASKI Z (1968) Stable and radioactive Pb in environment and human body. Warsaw: Nuclear Energy Information Center, Review Report, 29. pp 17-30.

KHALIL-MANESH F, TARTAGLIA-ERLER J, GONICK HC (1994) Experimental model of Pb nephropathy. IV. Correlation between renal functional changes and hematological indices of Pb toxicity. *J Trace Elem Electrolytes Health Dis*, 8: 13-19.

KOHN S, FRADIS M, BEN-DAVID J, ZIDAN J, ROBINSON E (2002) Nephrotoxicity of combined treatment with cisplatin and gentamicin in the guinea pig: glomerular injury findings. *Ultrastruct Pathol*, 26(6): 371-382.

KUPCHAN SM, HEMINGWAY RJ, KARIM A, WERMER D (1969) Tumour inhibitors XLVII vernodalin and vernomygdin, two new cytotoxic sesquiterpene lactones from Vernonia amygdalina Del. *J Organic Chem*, 34: 3908-3911.

LOGHMAN-ADHAM M (1997) Renal effects of environmental and occupational Pb exposure. *Environ Health Perspect*, 105: 928-939.

MARIJA V, PIASEK M, BLANUSA M, SARIC M, JURESA D, KOSTIAL K (2004) Succimer treatment and calcium supplementation reduce tissue Pb in suckling rats. *J Appl Toxicol*, 24: 123-128.

MERETS'KYÏ VM, HOLOVATA TK (2013) Morphological changes in internal organs of animals in different periods of craniocerebral trauma on background of diabetes mellitus. *Klin Khir,* 4: 73-75.

MUGAHI MN, HEIDARI Z, SAGHEB HM, BARBARESTANI M (2003) Effects of chronic Pb intoxication on blood indices of male adult rat. *DARU*, 11: 147-151.

NYENGAARD JR (1999) Stereologic methods and their application in kidney research. *J Am Soc Nephrol*, 10(5): 1100-1123.

OLADELE, JO, OYELEKE OM, OLOWOOKERE BD, BABATOPE OD, OLANIYAN MD, AKINDOLIE BO, OLADELE OT (2021) Bitter leaf (Vernonia amygdalina) modulates nitrobenzene-induced renal damage in rats via suppression of oxido-inflammatory activities. *Serbian J Exp Clin Res*, 22(4): 317-324.

PATTERSON C (1965) Contaminated and natural Pb in environments of man. *Arch Environ Health*, 11: 344-360.

PITOT CH, DRAGAN PY (1996) Chemical carcinogenesis. In: Casarett and Doull's (eds). *Toxicology: The Basic Science of Poisons*, 5th edn. McGraw-Hill, New York, pp 201-260.

PRUS R, POKOTYLO P, LOGASH M, ZVIR T (2020) Morphological particularities and morphometry of rats' kidneys under the effect of experimental mild traumatic brain injury. *Folia Morphol*, 80(2): 310-316.

RESTEK-SAMARZIJA N, MOMCILOVIC B (1992) Late changes in renal function after Pb poisoning and chelation therapy-article in Czech. *Arh Hig RadaToksikol*, 43: 321-328.

SALEM NA, SALEM EA (2016) Protective antioxidant efficiency of garlic against lead-induced renal and testicular toxicity in adult male rats. *J Heavy Met Toxicity Dis*, 1: 3.

SEDDIK L, BAH TM, AOUES A, BENDERDOUR M, SLIMANI M (2010) Dried leaf extract protects against Pb-induced neurotoxicity in Wistar rats. *Eur J Sci Res*, 42: 139-151.

SHARMA V, SHARMA A, KANSAL (2010) The effect of oral administration of Allium sativum extracts on Pb nitrate induced toxicity in male mice. *Food Chem Toxicol*, 48(3): 928-936.

SHILPI G, SHILPI S, SHARMA S (2014) Tolerance against heavy metal toxicity in cyanobacteria: role of antioxidant defense system. *Int J Pharm Pharmac Sci*, 7(2): 916.

SURADKAR SG, GHODASARA DJ, VIHOL P, PATEL J, JAISWAL V, PRAJAPATI KS (2009) Haemato-biochemical alterations induced by Pb toxicity in Wistar rats. *Vet World*, 2: 429-431.

SWARUP D, DWIVEDI SK (1992) Changes in blood and cerebrospinal fluid indices in experimental Pb toxicity in goats. *Ind J Animal Sci*, 62: 928-931.

TEIJON C, OLMO R, BLANCO D, ROMERO A, TEIJON JM (2006) Low doses of Pb: effects on reproduction and development in rats. *Biol Trace Elem Res*, 111: 151-165.

TEJO RIQUELME PA, DIAZ ISENRATH GB, ANDINO N, BORGHI CE (2014) Renal intraspecific variation along an aridity gradient detected by new renal indices in a desert herbivorous rodent. *J Exp Zool*, 321(6): 348-356.

XIENIA U, FOOTE GC, VAN S, DEVREOTES PN, ALEXANDER S, ALEXANDER H (2000) Differential developmental expression and cell type specificity of Dictyostelium catalases and their response to oxidative stress and UV light. *Biochim Biophys Acta*, 1492: 295-310.

YAMASHITA SR, ATZINGEN AC, IARED W, BEZERRA ASA, AMMIRATI AL, CANZIANI MEF, D'IPPOLITO G (2015) Value of renal cortical thickness as a predictor of renal function impairment in chronic renal disease patients. *Radiol Bras*, 48(1): 12-16.

ZOOK BC, CARPENTER JL, ROBERTS RM (1972) Pb poisoning in dogs: occurrence, source, clinical pathology, and electroencephalography. *Am J Vet Res*, 33: 891-902.

Significance of foetal autopsy in diagnosis of VACTERL association

J.P. Jessy[1], Rajesh Kumar[2], Anupriya Kaur[3], Kanchan Kapoor[4], Mahesh Sharma[4], Amandeep Kaur[5]

[1] *Department of Anatomy, All India Institute of Medical Sciences, New Delhi, India*
[2] *Department of Anatomy, All India Institute of Medical Sciences, Patna, India*
[3] *Department of Paediatrics, PGIMER, Chandigarh, India*
[4] *Department of Anatomy, GMCH Chandigarh, India*
[5] *Department of Anatomy, AIIMS, Guwahati, India*

SUMMARY

VACTERL association occurs in 1 in 10000-40000 live births and is associated with vertebral defects, anal atresia, cardiac malformations, tracheoesophageal fistula, renal dysplasia and limb defects. A 19-week-old male foetus with antenatal diagnosis of foetal hydronephrosis on antenatal ultrasound in the left kidney was medically terminated and brought for foetal autopsy. No other malformation was reported on antenatal scan. On autopsy, facial abnormalities, upper and lower limb defects, coronal vertebral clefts and imperforate anus with a two vessel-umbilical cord were found. Both environmental and genetic factors are considered to be responsible for this association. The present case illustrates the importance of foetal autopsy for making a definitive diagnosis in the missed sonographic findings like anal atresia and absence of upper- and lower-limb bones.

Key words: VACTERL association – Malformation – Atresia – Dysplasia

INTRODUCTION

VACTERL association refers to statistically non-random co-occurrence of a group of congenital malformations. VACTERL stands for Vertebral defects, Anal atresia, Cardiac malformations, Tracheoesophageal fistula (TEF) with oesophageal atresia, Radial/Renal dysplasia, Limb defects. Various possible explanations considered for the occurrence of these malformations in a non-random fashion are: (1) chronic teratogenic influence throughout the period of embryogenesis; (2) an inaugural malformation which secondarily disturbs development of other anatomical structures –the so-called malformation sequence or cascade; (3) disturbances in molecular pathways or mutations of single genes; (4) disturbances in the developmental process that is essential to all systems affected (Stevenson et al., 2013).

Various environmental agents form a plausible explanation for induction of the malformation during the first trimester. Early gestational exposure to drugs like thalidomide for long term affects multiple anatomical systems like craniofacial, cardiac, and gastrointestinal structures other than the limb abnormalities. Other predisposing factors include maternal

Corresponding author:
Dr Jessy J.P. Assistant Professor, Department of Anatomy, First Floor, Academic block, All India Institute of Medical Sciences, New Delhi – 110029 India. Mobile: +918427990925. E-mail: jesjp07@gmail.com

Submitted: July 5, 2022. **Accepted:** September 3, 2022

https://doi.org/10.52083/WINX3037

diabetes, which causes oxidative stress, mitochondrial dysfunction and disturbance in key development pathways (Stevenson et al., 2013).

CASE REPORT

A 19-week-old male foetus with antenatal diagnosis of foetal hydronephrosis on antenatal ultrasound in the left kidney was medically terminated and brought for foetal autopsy. No other malformation was reported on antenatal scan. The mother was a 25-year-old primigravida with history of treatment for thyroid disorder for 3-4 months of pregnancy. The mother did not have any other significant medical history or any other history of drug intake. Informed consent was taken from the parents before performing the autopsy.

Fig. 1.- Showing bilateral meromelia and absent thumb (medial four digits are shown by red arrows), facial features - mild retrognathia (white arrow) with bilateral low set ears (yellow arrow).

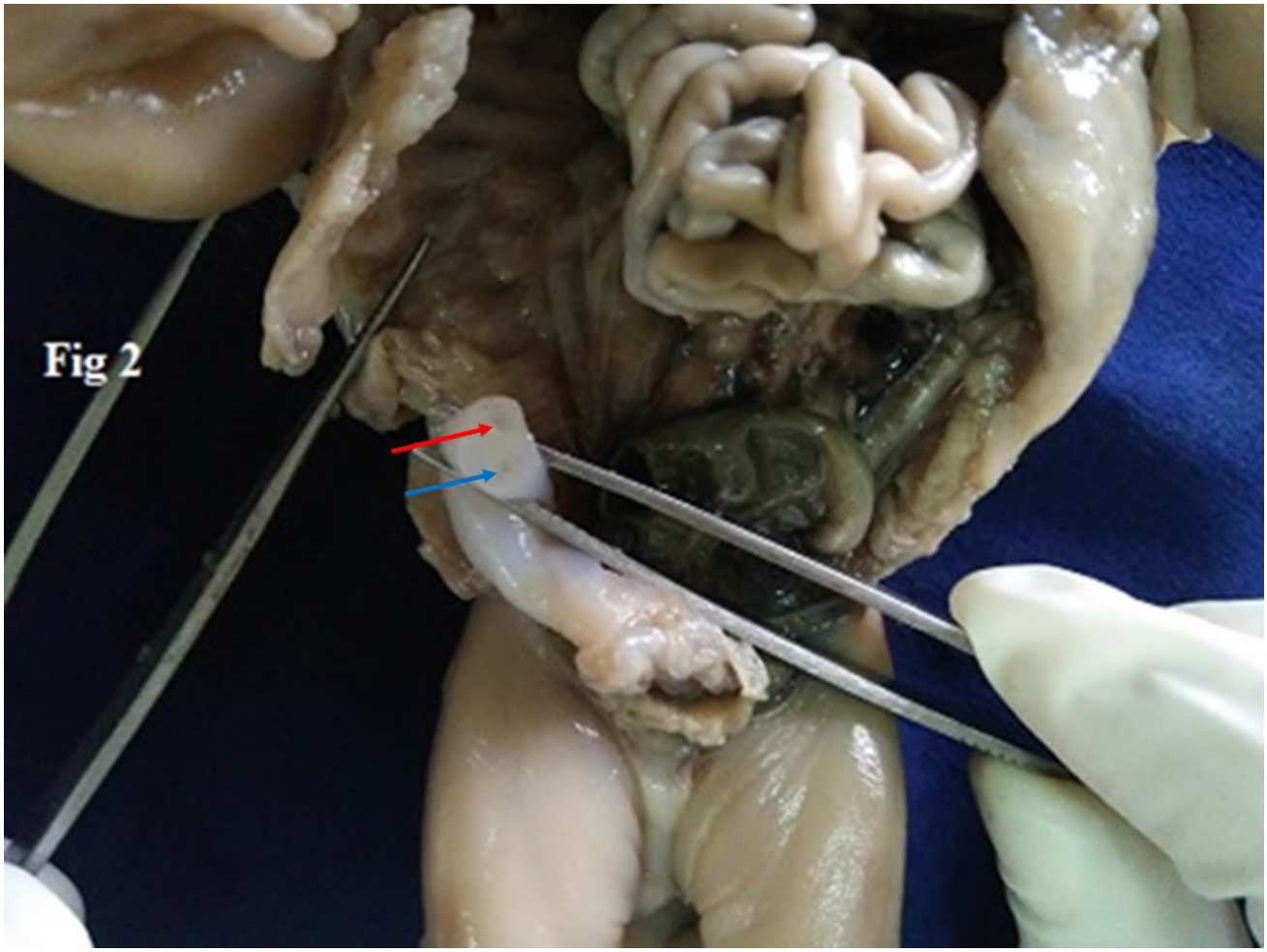

Fig. 2.- Showing 2 vessels umbilical cord (umbilical vein by red arrow and umbilical artery by blue arrow).

On further investigation, external examination showed that the 19-week-old male foetus had bilateral meromelia with absent thumb (Fig. 1). The umbilical cord consisted of 2 vessels (one umbilical artery and one umbilical vein) (Fig. 2). There was also absence of anal opening: a 1x1-cm depression was present in the anorectal region (Fig. 3). Facial features showed mild retrognathia with bilateral low set ears. Post-termination skeletal survey showed (Fig. 4) bilateral absence of radius, absence of left fibula and coronal clefts in multiple thoracic vertebrae. On internal examination, the gastrointestinal system showed blindly-ending large intestine distended with meconium (Fig. 5). The urinary system was normal. Tracheoesophageal fistula was not detected and there was no cardiac malformation.

DISCUSSION

The incidence of VACTERL association is estimated to be approximately 1 in 10,000 to 1 in 40,000 live-born infants (Jangle et al., 2014). VACTERL association is a term applied to sporadic, non-random association of specific birth defects (Stevenson et al., 2013). However, there is also strong clinical and genetic evidence for causal heterogeneity in patients with VACTERL association (Solomon et al., 2011). There should be at least three out of the following six findings for confirmed diagnosis of VACTERL association (Jangle et al., 2014).

V- Vertebral anomalies: hypoplastic (small) vertebrae or hemivertebra (where only one half of the bone is formed). About 70% of patients with VACTERL association will have vertebral anomalies.

Fig. 3.- Showing absence of anal opening, 1x1 cm depression (white arrow) present in the anorectal region.

Fig. 4.- Showing bilateral absence of radius (white arrow), absence of left fibula (yellow arrow) and coronal clefts in multiple thoracic vertebrae (red arrows).

A- Anal atresia or imperforate anus is seen in about 55% of patients with VACTERL association.

C- Cardiovascular anomalies: these are present in up to three-quarters of patients with VACTERL association and the most common are ventricular septal defects, atrial septal defects and Tetralogy of Fallot.

T-E- Tracheoesophageal fistula: oesophageal atresia with tracheoesophageal fistula (TE fistula) is seen in about 70% of patients with VACTERL association.

R- Renal (Kidney): renal defects are seen in half the patients with malformation of one or both kidneys or obstructive uropathy.

Limb defects: limb defects are seen in up to 70%, which include absent or displaced thumbs, polydactyly, syndactyly and forearm (including radial aplasia) and leg defects.

Various authors have found a variable number of anomalies in patients with this association. Some of the recent reports with anomalies found by different authors have been tabulated (Table 1). Cardiac malformations have been reported in approximately 40-80% of patients with VACTERL association, while tracheo-oesophageal fistula have been found in 50-80% of cases (Weaver et al., 1986; Solomon et al., 2010). In this case report, tracheal-oesophageal fistula and cardiac anomalies were not present. The exact cause of the presence of particular anomalies associated with VACTERL has not been clearly found yet. It has been referred to various genetic or developmental defects during different stages of the embryo (Kim et al., 2001a, b). Familial clustering has also been

seen in variable number of cases (Solomon et al., 2010).

Since there are no major genes for this condition, and also its phenotypes are too heterogeneous to be defined as a syndrome, it is still referred to as an 'association'. Previous studies have observed that 90% of the patients diagnosed with VACTERL association had three or fewer phenotypes (referred to as VACTERL-like association) and <1% of patients had all six anomalies (Chen et al., 2016). It has been observed that multiple embryological processes are disturbed in the genesis of VACTERL malformations. Abnormal timing of molecular oscillator known as segmentation clock results in mal-segmentation of the vertebrae. Mesodermal proliferation and migration, epithelial-mesenchymal interactions and programmed cell death are observed to be involved in atresia of the oesophagus and anus. Failure to lay down, condense or chondrify the anlage of the radius is involved in radial aplasia. Failure of development of ureteric bud or primary failure of the metanephric mesenchyme in the early five week results in renal agenesis and the abnormal development of mesonephros/ mesonephric duct leads to lower urinary defects.

Fig. 5.- Internal examination: gastrointestinal system showing blindly ending large intestine distended with meconium.

Table 1. Various malformations found in patients with VACTERL association.

Authors	Anomalies found in VACTERL
Walsh et al., 2001	All six anomalies
Komura et al., 2007	All six anomalies
Harris et al., 2009	Abdominal wall hernia, imperforate anus, vestibular fistula, absent right rib, vertebral anomalies, tethered cord, syringomyelia, cardiac anomalies, absence of tracheoesophageal fistula
Salati et al., 2010	Anomalies involving cardiac, skeletal (vertebrae, limb) and renal system
Shah et al., 2004	All six anomalies with Prune Belly syndrome
Obeidat et al., 2019	Imperforate anus, tracheoesophageal fistula, esophageal atresia, and left renal agenesis with unicornuate uterus
Tongsong et al., 2001	All six anomalies
Cunningham et al., 2013	No statistically significant association between CHD severity and the presence or absence of other VACTERL component features, specifically anorectal malformation or tracheo-esophageal fistula; CHD presence also did not correlate with the presence of tracheo-esophageal fistula or anorectal malformation
Yang et al., 2019	Multiple airway abnormalities including bridging bronchus, airway malacia, and complete tracheal rings with VACTERL
Pariza et al., 2021	Scoliosis, imperforate anus, common truncus arteriosus, tracheoesophageal fistula, polycystic kidneys, with short right ureter, lower limb hypoplasia, micrognathia, hygroma, duodenal atresia, and cloacal malformation, with an aberrant omphalomesenteric duct
Puvabanditsin et al., 2016	Vertebral anomalies, anal and urethral atresia, esophageal atresia with tracheoesophageal fistula (TEF), renal agenesis, pulmonary hypoplasia, genital and sacral appendages, and a single umbilical artery
Chen et al., 2013	Small cerebellum, ventricular septal defect, single umbilical artery, scoliosis, right club hand, radial aplasia, renal agenesis and imperforate anus.
Nakaya et al., 2017	Non-functioning right kidney with VUR, hemidiaphragmatic eventration, ventricular septal defect (VSD) with tetralogy of Fallot, cryptorchidism, and hyperdactylia
Pelluard-Nehmé et al., 2007	Single umbilical artery, dextroposition of heart, Butterfly-shaped vertebrae, hemivertebrae, fused cervical vertebrae, left diaphragmatic hernia, anal imperforation, hypospadias and amelia of left upper limb
Endoh et al., 2008	VACTERL association with a cleft hand
Ünal et al., 2008	VACTERL association, arachnoid cyst in sylvian fissure and corpus callosum agenesis

The common cardiac anomalies in VACTERL association are ventricular and atrial septal defects and Tetralogy of Fallot occurring due to abnormal development of the cardiac septa, results in cardiac malformation (Stevenson et al., 2013). The thoracic vertebrae are most commonly affected, followed by cardiac, tracheoesophageal structures and forearm bones followed by anorectal structures in the end (Stevenson et al., 2013).

The ZIC3 gene has been shown to cause X-linked VACTERL association. Various types of ZIC3 mutations have been reported to be responsible for both VACTERL or VACTERL-like association. Anal atresia is present in most patients with ZIC3 mutations; vertebral anomalies are not commonly observed and demonstrated phenotypic variability (Chen et al., 2016). Mitochondrial dysfunction is one of the aetiological factors of VACTERL association but seen in small proportion of affected individuals (Siebel et al., 2013). SHH gene plays a significant factor, as the key inductive signal in patterning of the ventral neural tube, the anterior-posterior limb axis and the ventral somites. In humans, SHH mutation has been observed to cause more severe VACTERL phenotypes (Chen et al., 2016).

Prenatal and postnatal growth deficiency, laryngeal stenosis, ear anomaly, large fontanels, lower limb defects, rib anomalies, external genital defects, single umbilical artery (SUA), and tethered cord are less frequently seen with VACTERL association (Yang et al., 2019). The present case presented with intestinal and lower

limb abnormalities, which is a rare association. In the present case, because of the presence of limb defects, coronal vertebral clefts and imperforate anus, we label this constellation of birth defects as VACTERL association and can be because of the A3243G point mutation in mtDNA (Damian et al., 1996). The present case also highlights the importance of doing foetal autopsies, as some anomalies in our case were missed on antenatal scan and the exact diagnosis of VACTERL was possible only after the autopsy.

Genetic counselling was provided to the affected couple, as in 90% of the cases this association is sporadic with minimal risk of recurrence. However, in 10% of the cases it is seen that first-degree relatives are affected with either isolated or multiple components of VACTERL association. Hence, review of the family members for features of VACTERL was advised along with focus on polyhydramnios, absent gastric bubble and single umbilical vessel on antenatal scan in subsequent pregnancies.

CONCLUSION

VACTERL is a relatively common congenital malformation syndrome. However certain features of VACTERL association, such as anorectal malformation and tracheoesophageal fistula are often missed during prenatal imaging. Hence, foetal autopsy contributes significantly to the diagnosis of VACTERL association.

Limitation- Karyotyping and other genetic analysis were carried out neither in reported case nor in family or close relatives. Genetic analysis should be done in these types of cases to explore the genetic basis in detail.

ACKNOWLEDGEMENTS

Authors acknowledge the family for giving consent to carry out this study for the benefit of scientific world. Results from such research can potentially increase mankind's overall knowledge that can then improve patient care. Therefore, the family deserves our highest gratitude.

REFERENCES

CHEN CP, CHANG TY, CHEN YY, CHERN SR, SU JW, WANG W (2013) VACTERL association with hydrocephalus in a fetus conceived by in vitro fertilization and embryo transfer. *Taiwanese J Obstet Gynecol*, 52(4): 575-579.

CHEN Y, LIU Z, CHEN J, ZUO Y, LIU S, CHEN W, LIU G, QIU G, GIAMPIETRO PF, WU N, WU Z (2016) The genetic landscape and clinical implications of vertebral anomalies in VACTERL association. *J Med Genet*, 53(7): 431-437.

CUNNINGHAM BK, HADLEY DW, HANNOUSH H, MELTZER AC, NIFORATOS N, PINEDA-ALVAREZ D, SACHDEV V, WARREN-MORA N, SOLOMON BD (2013) Analysis of cardiac anomalies in VACTERL association. *Birth Defects Res A Clin Mol Teratol*, 97(12): 792-797.

DAMIAN MS, SEIBEL P, SCHACHENMAYR W, REICHMANN H, DORNDORF W (1996) VACTERL with the mitochondrial np 3243 point mutation. *Am J Med Genet*, 62(4): 398-403.

ENDOH N, IGAWA HH, SUGIHARA T (2003) VACTERL association with a cleft hand. *Congenital Anomalies*, 43(3): 180-183.

HARRIS K, DORN C, BLOOM B (2009) Lumbocostovertebral syndrome with associated VACTERL anomaly: a neonatal case report. *J Perinatol*, 29(12): 826-827.

JANGLE SH, GINDODIA KR, SIDDIQUI MM (2014) A case report of VACTERL association and management of its renal component. *Int J Health Sci Res*, 4: 305-309.

KIM JH, KIM PCW, HUI CC (2001a) The VACTERL association: lessons from the Sonic hedgehog pathway. *Clin Genet*, 59(5): 306-315.

KIM PC, MO R, HUI CC (2001b) Murine models of VACTERL syndrome: Role of sonic hedgehog signaling pathway. *J Pediat Surg*, 36(2): 381-384.

KOMURA M, KANAMORI Y, SUGIYAMA M, TOMONAGA T, SUZUKI K, HASHIZUME K, GOISHI K (2007) A female infant who had both complete VACTERL association and MURCS association: report of a case. *Surg Today*, 37(10): 878-880.

NAKAYA T, HYUGA T, TANAKA Y, KAWAI S, NAKAI H, NIKI T, TANAKA A (2017) Renal dysplasia characterized by prominent cartilaginous metaplasia lesions in VACTERL association: A case report. *Medicine (Baltimore)*, 96(15): e6499.

OBEIDAT RA, ALESHAWI AJ, TASHTUSH NA, ALSARAWI H (2019) Unicornuate uterus with a rudimentary non-communicating cavitary horn in association with VACTERL association: case report. *BMC Women's Health*, 19(1): 1-5.

PARIZA PC, STAVARACHE I, DUMITRU VA, MUNTEANU O, GEORGESCU TA, VARLAS V, BOHÎLȚEA RE (2021) VACTERL association in a fetus with multiple congenital malformations–Case report. *J Med Life*, 14(6): 862.

PELLUARD-NEHMÉ F, BAUDET C, CARLES D, ALBERTI EM, DELRUE MA, LACOMBE D (2007) A new case of VACTERL association with unilateral amelia of upper limb. *Clin Dysmorphol*, 16(3): 185-187.

PUVABANDITSIN S, VAN GURP J, FEBRUARY M, KHALIL M, MAYNE J, AI MCCONNELL J, MEHTA R (2016) VATER/VACTERL association and caudal regression with Xq25-q27. 3 microdeletion: A case report. *Fetal Pediat Pathol*, 35(2): 133-141.

SALATI SA, RABAH SM (2010) VACTERL association. *Online J Health Allied Sci*, 9(2).

SHAH D, SHARMA S, FARIDI MMA, MISHRA K (2004) VACTERL association with Prune-Belly syndrome. *Indian Pediat*, 41(8): 845-847.

SIEBEL S, SOLOMON BD (2013) Mitochondrial factors and VACTERL association-related congenital malformations. *Mol Syndromol*, 4(1-2): 63-73.

SOLOMON BD (2011) Vacterl/Vater association. *Orphanet J Rare Dis*, 6(1): 56.

SOLOMON BD, PINEDA-ALVAREZ DE, RAAM MS, CUMMINGS DA (2010a) Evidence for inheritance in patients with VACTERL association. *Human Genet*, 127(6): 731-733.

SOLOMON BD, PINEDA□ALVAREZ DE, RAAM MS, BOUS SM, KEATON AA, VÉLEZ JI, CUMMINGS DA (2010b) Analysis of component findings in 79 patients diagnosed with VACTERL association. *Am J Med Genet A*, 152(9): 2236-2244.

STEVENSON RE, HUNTER AGW (2013) Considering the embryopathogenesis of VACTERL association. *Mol Syndromol*, 4(1-2): 7-15.

TONGSONG T, CHANPRAPAPH P, KHUNAMORNPONG S (2001) Prenatal diagnosis of VACTERL association: a case report. *J Med Assoc Thailand*, 84(1): 143-148.

ÜNAL S, KIBAR AE, ÖZAYDIN E, KARADAG N, BALCI S (2008) A new case of VACTERL association with congenital arachnoid cyst. *Clin Dysmorphol*, 17(3): 221-222.

WALSH LE, VANCE GH, WEAVER DD (2001) Distal 13q deletion syndrome and the VACTERL association: case report, literature review, and possible implications. *Am J Med Genet*, 98(2): 137-144.

WEAVER DD, MAPSTONE CL, YU PL (1986) The VATER association: Analysis of 46 patients. *Am J Dis Children*, 140(30): 225-229.

YANG L, LI S, ZHONG L, QIU L, XIE L, CHEN L (2019) VACTERL association complicated with multiple airway abnormalities: A case report. *Medicine (Baltimore)*, 98(42): e17413.

The electron microscope on the eve of its first centenary

Pedro J. Mestres Ventura

Institute of Anatomy and Cell Biology, Laboratory of Electron Microscopy, Medical School, University of Saarland, Homburg Saar, Germany

SUMMARY

In a few years' time, the electron microscope will be 100 years old. The ideas leading to the invention of the instrument emerged in Berlin between 1928 and 1933. Ernst Ruska is the undisputed inventor of the transmission electron microscope. In the mid-1930s, scientists from several European countries and especially from the United States, France, Canada and Japan became interested in contributing to the new technology. Ernst Ruska was awarded the 1986 Nobel Prize in Physics for his invention.

Key words: History of electron microscope – Ernst Ruska – Electromagnetic lenses – Transmission electron microscope – Scanning electron microscope

PREAMBLE

In a few years' time, the first centenary of the birth of an instrument and the science associated with it, will be celebrated: the electron microscope and electron microscopy. As in the case of the optical microscope, invented by the Dutchman Zacharias Janssen in 1590 (the attribution of the invention of the optical microscope to Janssen is based on a letter from William Borelius, a Dutch physician and childhood friend of Janssen). According to this letter, Zacharias Janssen and his father, Hans Martens, invented the microscope in 1590 and shared its discovery with Albert VII, Archduke of Austria (https://www.mundomicroscopio.com/primer-microscopio/). The electron microscope has made it possible to visualize structures smaller than 200 nm, which is the resolution limit of a conventional optical microscope. The electron microscope has had an immense impact in many research fields, such as materials, chemistry, biology and medicine, geology, etc. – to name but a few.

This article is dedicated to the acknowledgement of the scientists who made this invention possible and to recall some of the circumstances under which it occurred.

INTRODUCTION

I would like to begin with some general aspects of the instrument: the electron microscope. The resolution of a microscope – the minimum separation between points distinguishable by observation - is limited by the wavelength of the radiation used to make the image. Thus, electron microscopes have a much higher resolution capacity than optical or photonic microscopes, because the wavelength of electrons is many

Corresponding author:
Pedro J. Mestres-Ventura, PhD, MD. Prof. Emeritus. Department of Anatomy and Cell Biology, Bld. 61, Faculty of Medicine, Saarland University, D-66421 Homburg Saar, Germany. Phone: +34 644217127. E-mail: pedro.mestres@uks.eu

Submitted: September 25, 2022. **Accepted:** October 10, 2022

https://doi.org/10.52083/KOSC8456

times shorter than that of light. While the best conventional optical microscopes can reach about one-fifth of a micron (1 micron = 1 thousandth of a millimeter), however rarely approach this limit, electron microscopes easily achieve a resolution hundreds of times higher – to the order of a millimicron (one thousandth of a micron, equivalent to ten Angstrom units) - and that without reaching the theoretical limit.

Basically, in a transmission electron microscope, a beam of high-voltage electrons is directed from a cathode to an anode, through a column or tube under a very high vacuum, where the beam passes through the sample and various magnetic or electric fields which act as lenses, until they hit a luminescent screen where the image is formed. The final magnification obtained is a function of the focal lengths and the position of the lenses along the trajectory of the electron beam, in the same way as in an optical microscope. In electron microscopes, the focal lengths are modified electronically and the positions of the lenses are fixed, while in the light microscope the opposite is the case. However, the results correspond as both are based on the same optical theory. The invention was an almost natural further development of cathode ray technology and oscilloscopes.

CATHODE RAY TUBES AND OSCILLOSCOPES

Probably the first of these devices was the glass tube invented by Geissler in 1850, which contained a rarefied gas and in which an electrical current induced the emittance of characteristic lighting, as in the later-developed neon tubes. Throughout the second half of the 19th century, cathode ray tubes were further developed. For example, William Crookes' cathode ray tube (1875), where cathode rays were deflected by the influence of a magnetic field and produced images by impacting a phosphorescent screen (for Crookes ray tube see: https://global.britannica.com/biography/William-Crookes).

Later Ferdinand Braun (1897) built a tube in which cathode rays could be deflected both horizontally and vertically (Martin, 1986). In the same year, J.J. Thomson (Strutt, 1942) discovered the first subatomic particle, for which the Irish physicist George Johnston Stoney proposed the term "electron" (Encyclopaedia Britannica, 1910). At this point we must mention Emil Wiechert, a German physicist born in East Prussia who worked at the University of Königsberg. Wiechert discovered at the same time as J.J. Thomson (commonly known as the discoverer) the particle now called the "electron", which he named "Teilchen" (particle). In April 1896, at a conference at the Königsberg Physical and Economic Society, he reported the existence of a particle whose mass had to be significantly smaller than that of the hydrogen atom. On January 7, 1897, he reported at a conference in the same scientific society that he had detected the particle and determined that its mass was approximately 2,000 to 4,000 times smaller than that of the hydrogen atom. In September 1897 he announced the exact values of the particle mass. Thomson's lecture at the Royal Society took place on April 30, l 1897. The scientific activities at Königsberg were obviously unknown in London.

From the end of the 19th century until well into the 20th century, the search for cathode ray tubes and oscilloscopes continued, as these devices were very important in the electricity-producing industry. The Braun tube was improved by creating a vacuum inside to facilitate the circulation of lightning.

Undoubtedly, the development most relevant to our topic was made by Hans Busch, who constructed and precisely measured the parameters of the first electromagnetic lens (Busch 1912, 1926). Busch (1884-1973) studied physics in Berlin and Göttingen, where he received his doctorate. In 1922, he joined the University of Jena where he became a professor and where he developed electronic optics and electronic lenses.

Another important scientist in our context was the Hungarian Dennis Gabor (1900-1979). Early in his career, Gabor analyzed the properties of high-voltage power transmission lines using cathode ray oscilloscopes, which sparked his interest in electron optics. Gabor's research on the basic processes of the oscilloscope contributed to the development of other devices, such as television tubes. In 1921,

he joined the Department of Electrotechnics at the Berlin-Charlottenburg Technical University (TU-Berlin), and, after completing his doctorate in 1927 (on the recording of activity in electrical circuits with the high-speed cathode ray oscilloscope), he joined the Siemens physics laboratory. He had to leave Germany in 1933 due to his Jewish origins. In 1971, he received the Nobel Prize in Physics for the invention of holography, with which he tried to correct electronic optical aberrations. Many of Gabor's discoveries were very useful to Knoll and Ruska in connection with the electron microscope.

As has become clear from the above, Berlin was leading in physics and electronics in the 1920s and – seen from today's perspective – it is surprising that the idea of conceiving and building a microscope did not spark earlier. This all the more so, in view of the fact that this was closely related to the work being carried out on oscillographs.

ERNST RUSKA AND THE ELECTRON MICROSCOPE

Ernst Ruska is indisputably considered to be the inventor and builder of the first electron microscope, even if that first instrument was nothing more than a proof of principle (Fig. 1). On March 5, 1931, the microscope was publicly presented by Ruska and his tutor, Max Knoll.

Fig. 1.- Ernst Ruska standing next to the column of a Siemens model 1A electron microscope in the 1950s (https://www.biografiasyvidas.com/biografia/r/ruska.htm)

The coverage in German press and radio was remarkable and extensive, even if it was incorrectly reported that Ruska came from Leipzig. He, in fact, was born in Heidelberg in 1906 (see Kalendarblatt Deutsche Welle 9. Mars 1931). The instrument was a prototype with little ability of magnifying the image projected. However, it was the basis for the development of the electron microscope as understood today.

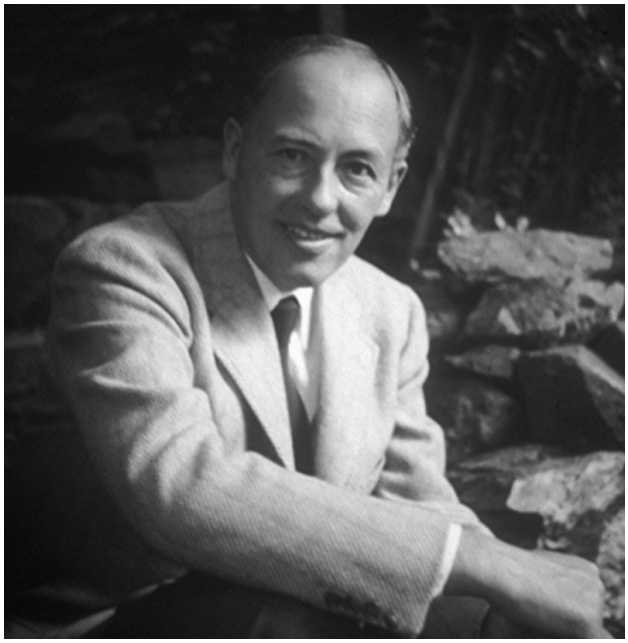

Fig. 2.- Max Knoll, Ruska's doctoral supervisor in Berlin (https://www.goodreads.com/author/show/4289817.Max_Knoll).

At the age of 19, Ruska began studying physics and electrical engineering in Munich. In 1927, the family moved to Berlin where he continued his studies, specializing in high voltage electrical devices and attending the course held by Professor Adolf Matthias at the TU Berlin. At the end of the summer semester of 1928, Professor Matthias set up a working group to develop a high-speed oscilloscope for measuring electrical processes in power plants and high-voltage lines. The management of the group was entrusted to Dr. Max Knoll (Fig. 2). The youngest students in the group were Bodo von Borries and Ernst Ruska. The working atmosphere within the group was excellent, as Max Knoll practiced the philosophy of teamwork, something uncommon at that time in Germany.

Ruska was commissioned to work in the field of high vacuum and related techniques, but also with examination of cathode ray tubes and their behavior under the influence of electromagnetic coils with the aim of making the electron beam as thin as possible. Hans Busch had already shown that the behaviour of a magnetic coil (lens) with electron beams was the same as a glass lens with photon beams (Busch 1927).

Based on Busch's studies, Ruska built an electromagnetic lens in the course of his work in the group with which he obtained images of the hole of an aperture disc ("Lochblende"). These were obviously the first images obtained with electrons (Ruska, 1929).

His diploma thesis (graduation paper) was devoted to electrostatic lenses, as an alternative to electromagnetic lenses, proving in the end that the latter were far superior to the former (Ruska, 1930). He presented his diploma thesis on December 23, 1930. Then the problem of finding a job arose.

The country's economic situation had badly deteriorated and there was practically no chance of finding a job either in industry or at university. Following his parents' wishes, Ernst Ruska decided to pursue a doctorate at the TU Berlin (Technical University): a job – but without a salary.

By 1929 Ruska had already shown that images could be perfectly focused with one coil. The next question was whether the image could be further enhanced by the addition of a second coil. He did indeed succeed in constructing something new: a prototype electron microscope, equipped with new lenses. In April 1931, he experimentally proved that electrons considerably surpassed the resolution provided by the optical microscope. Ruska received his doctorate from the TU-Berlin in August 1933, and the microscope he then built has to be regarded as the first electron microscope in the history (Fig. 3).

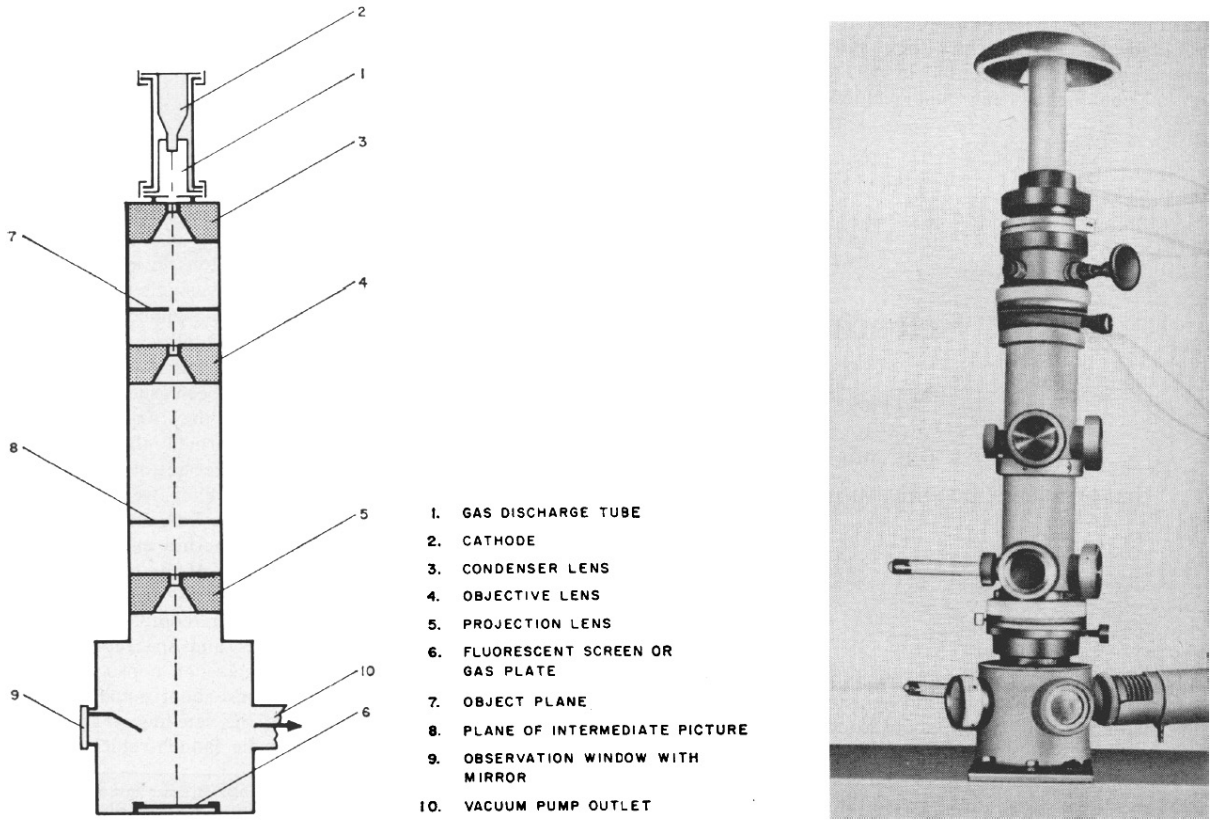

Fig. 3.- Transmission electron microscope designed by E. Ruska in the early 1930's. On the left is a technical drawing of the instrument. On the right an image produced by the instrument. Both images taken from an article by Freundlich (1963) with permission of the Science (AAAS) journal.

On the basis of studies by Busch (1927), Ruska and his instructor Knoll were convinced that – due to the thin mass of the electron – the electron microscope must provide images of an object or sample at much higher magnification than possible with an optical microscope. In his speech at the Nobel Prize (1986), Ruska explained that they had not known de Broglie's theories (1924) until well into 1931, despite the fact that they had been confirmed experimentally by Davisson, physics Nobel Prize winner of 1927. At that time, German universities were subject to severe economic constraints that affected, among other things, the acquisition of bibliography.

De Broglie's theories – not shared by everyone at first – worried Ruska at first because they included an unknown wave ("Materialwelle"). However, when he applied de Broglie's equations, he saw his own predictions widely confirmed, as these equations ultimately confirmed or agreed with the ideas and work hypothesis which Ruska and other scientists had formulated earlier.

Being unaware of the mutual bibliographies, de Broglie published in 1950 the work entitled "Optique eletronique et corpusculaire", in which he did not cite the fundamental works of Brüche and Scherzer (1934) or Busch and Brüche (1937) and von Ardenne (1940), nor of the English scientist Myers (1939). It is, however, interesting to note that all of them had been cited by the Frenchman Paul Chanson (1947) in his doctoral dissertation (for all these citations see Hawkes, 2004). In view of these bilateral omissions and unawareness, it is obvious that de Broglie and his ideas did not influence the development of geometric electronic optics, a concept elaborated by German scientists (Hawkes, 2004).

THE SERIAL CONSTRUCTION OF THE TRANSMISSION ELECTRON MICROSCOPE (TEM)

In order to achieve higher magnifications, electromagnetic lenses had to be improved. Ruska had already described solutions for this in his course work of 1929 and also dealt with the subject in his diploma work (1930) and doctoral thesis (1933). The solutions basically consisted of surrounding the coils with an iron cover, which considerably reduced the focal length of the lenses. Together with his colleague and friend Bodo von Borries, also a doctoral student as himself at the TU Berlin, they patented these solutions (Borries, B von, Ruska, E, 1932). It should be noted that von Borries (Fig. 4) was a key figure in the technical and industrial development of the electron microscope and that, in his younger years, he unfortunately did not receive the recognition he deserved (Gelderblom, 2020).

Fig. 4.- Bodo von Borries (1905-1956). DGE historical images (https://www.dge-homepage.de).

In the light of his new findings, Ruska decided to build a new electron microscope with greater magnification capacity. Unfortunately, funding was lacking; not only did he not have a salary but also the university was not able to finance either the building materials nor the necessary work. In April 1932, Max Knoll left the university and moved to the Telefunken company in Berlin, dedicating himself exclusively to the development of television. The vacant position was filled by Prof. Matthias with von Borries, who thus became the head of the laboratory and the work program of the group essentially remained unchanged.

Fig. 5.- Electron microscope built by E. Ruska in 1938 and rebuilt in 1980 (Source: Wikipedia)

In the fall of 1933, Ruska's situation improved markedly thanks to the personal recommendation of Max von Laue, the 1914 Nobel Laureate in Physics, who helped him to get a scholarship with resources for himself (salary) and the necessary materials. This enabled him to build a second electron microscope in just over three months, with construction completed in November 1933.

Nonetheless, Ruska's stay at the university could not be extended and he decided to accept a position at the company *Fernsehen* AG in Berlin. The 2nd device he had built, capable of 12.000-fold magnification, was left at the university where it was used with great success by students of the department (Fig. 5).

Although busy with industrial work, Ruska and von Borries continued to their search for funds to enable serial production of the microscope. Their unlucky streak ended thanks to the mediation of Helmut Ruska, Ernst's younger brother, who was an attending physician in the Department of Internal Medicine at the Charity Hospital in Berlin. Helmut had been an avid supporter of the electron microscope from the very beginning. He believed strongly in the future of the instrument, especially in the area of infectious diseases and biomedicine.

Helmut convinced his superior, Professor Dr. Richard Siebeck – a very influential and prestigious medical doctor and professor – of the value of the new instrument. Professor Siebeck wrote a document evaluating and supporting the scientific project of the electron microscope in which he openly motivated the companies Siemens (Berlin) and Carl Zeiss (Jena) to take an interest in the invention. However, the two companies could not reach a collaboration agreement and, ultimately Siemens took sole charge of the project. Bodo von Borries, Ruska and his brother Helmut negotiated with Siemens and the result was the creation of the "Laboratorium für Übermikroskopie" (Hyper-microscopy laboratory) in Berlin-Spandau, under the direction of von Borries, who had already been part of the Siemens workforce since 1934.

By the end of 1938, two other units of a third Ruska model were built, which were, however, still considered experimental. These instruments already had several lenses (condenser, lenses with pole pieces, projector, etc.) and important additional electronic equipment (vacuum lock to change the sample and photographic plates, etc.), and reached 30.000-fold magnification. The two microscopes were made available to Helmut Ruska for training and for the development of sample preparation techniques. Being a physician, he, of course, was mainly interested in bio-medical samples and was the first person world-wide to photograph virus particles (Fig. 6) (Ruska H, von Borries, Ruska E, 1940; Borries B von, 1949).

By the autumn of 1943, more than 40 microscopes had been built and put into service. One of these, with the production number 26, went to the renowned Professor Arne Tiselius' laboratory at Uppsala University (Gelderblom and Krüger, 2014). The chemical and metallurgical industries acquired many microscopes from Siemens. On the advice of Hitler's private doctors, the Central Government Chancellery in Berlin also acquired three of them for biological weapon research (Gelderblom, 2020).

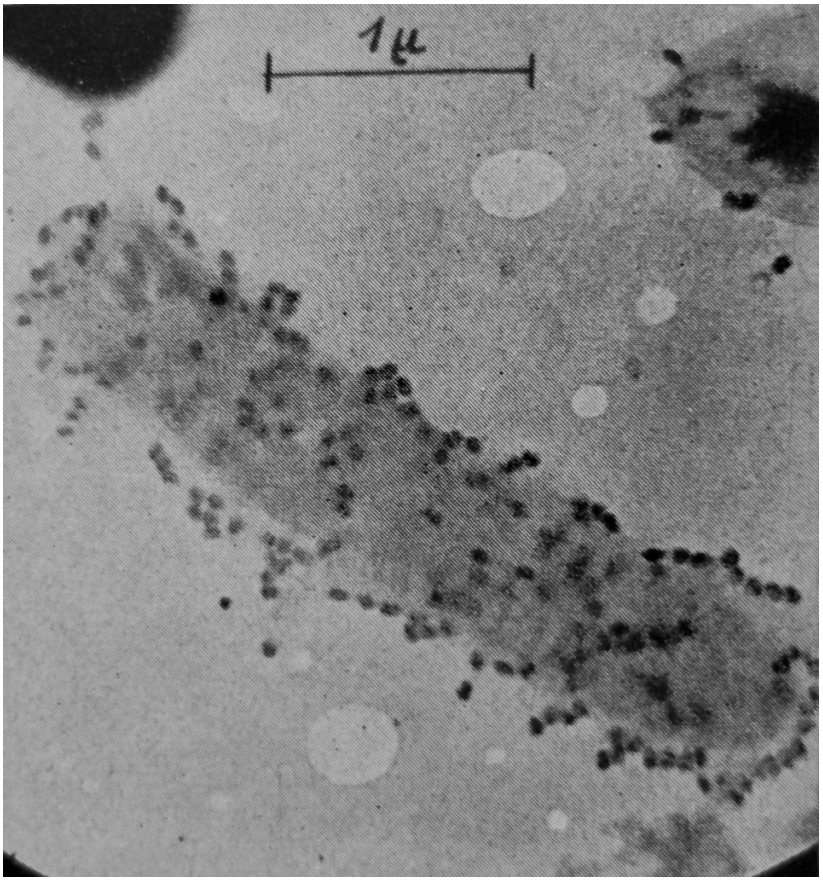

Fig. 6.- Bacteriophages (black dots) on the outer surface of a Proteus bacterium (in grey). Image (Figure 191) from "Die Übermikroskopie" by Bodo von Borries (1949) from a paper by Helmut Ruska (1941) entitled "Über ein neues, bei der Bakteriophagen Lyse auftretendes Formelement" Naturwiss, 29: 367-368.

Siemens launched an "Application and Teaching Laboratory", equipped with 4 microscopes and led by Helmut Ruska, where external scientists and potential clients could do internships. Studies with biological and medical objects were very difficult at that time, as there were no appropriate preparation techniques available to prepare objects for examination under the extreme conditions inside an electron microscope (vacuum, electronic rays, heating of the sample, etc.).

Towards the end of the war, the Siemens microscope factory was destroyed in a bombing raid and the three architects of the electron microscope, Ernst and Helmut Ruska and Bodo von Borries separated, ending a cooperation that had been so fruitful.

After the war, Ernst Ruska remained in West Berlin and immediately set about rebuilding the Siemens' laboratory and workshops to resume the manufacturing of electron microscopes. Thousands of devices were produced and ones such as those in the Elmiskop 1A and 101 series, became legendary as they enjoyed a well-deserved reputation for excellent performance and high reliability (Fig. 7). Siemens surprisingly stopped the production of electron microscopes in the late 1960s – an incomprehensible step in view of the fact that Siemens was a veritable leader in the world market.

OTHER RESEARCH AND MANUFACTURING LOCATIONS OF ELECTRON MICROSCOPES IN BERLIN

Apart from the TU Berlin and Siemens there were two further electron microscopy research and development sites in Berlin:

1) AEG (Allgemeine Elektrizität Gesellschaft = General Electricity Company, since 1929 with the participation of General Electric Company, United States)

and

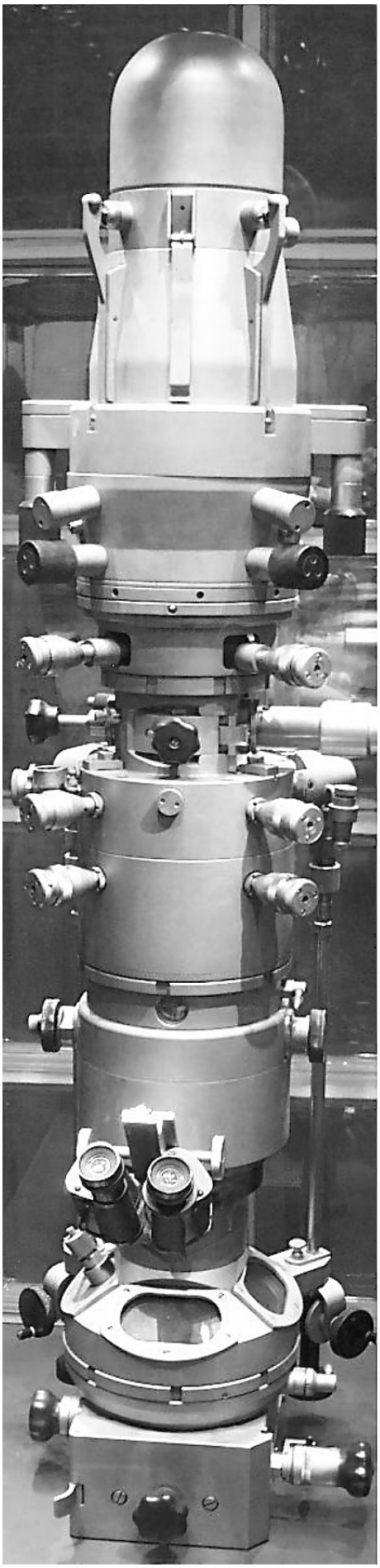

Fig. 7.- Image of the column of an electron microscope Siemens model Elmiskop 1 A (Source: Wikipedia).

2) "Forschungslaboratorium für Elektrophysik" (Electro-Physics Research Laboratory), privately owned by Baron Manfred von Ardenne, who was already the founder and director at the age of 21.

1) On April 1, 1928, AEG set up a research center ("AEG-Forschungsinstitut") in Berlin-Reinickendorf, under the direction of the physicist Carl Ramsauer (1879-1955), which operated until mid-1945. Ramsauer, a professor of physics at the Technical University of Danzig, arrived in Berlin accompanied by some of his assistants. One of them, Ernst Brüche (1900-1985), made a very important contribution to the development of the electron microscope at AEG. In 1940 AEG donated its first transmission electron microscope to the Robert Koch Institute; it had been built by Hans Mahl (1909-1988) and Hans Boersch (1909-1986), Brüche's two assistants.

From the very beginning, the two major companies, Siemens and AEG, were embroiled in a fierce struggle for dominance in the field of electron microscopy. Siemens gave its scientists almost unlimited support to win the fight for prestige; this fight included struggling for patents, product promotion strategies and marketing, in a free-market framework rather than under a totalitarian wartime regiment (Müller, 2009).

After the war, Brüche succeeded Ramsauer in the management of the laboratory and, in 1947, with the support of AEG and Carl Zeiss (Jena), he moved to the city of Mosbach (Baden). The company name was changed to "*Süddeutschen Laboratorien zur Entwicklung und Herstellung von Elektronenmikroskope"*, abbreviated SDL (English: Laboratories of South Germany for the development and manufacture of electron microscopes). AEG dropped out of the company in 1953, leaving only Carl Zeiss, who then decided to relocate the production of electron microscopes to its headquarters in Oberkochen, about 160 km southeast of Mosbach.

In 1949, Carl Zeiss launched a new model of electron microscope, the EM8, equipped with

electromagnetic lenses. This was followed in 1956 by the model EM9, the first electron microscope in the world equipped with a photographic device with automatic control for photographic exposition time; a true novelty.

At the end of the Second World War, the activities in electron microscopy in Germany, both in academia and industry, were soon revived and a framework for a dialogue between the various parties involved had to be created. In February 1949 von Borries took the initiative by organizing a meeting in Düsseldorf (Germany) which, at the same time, was the founding act of the *Deutsche Gesellschaft für Elektronenmikroskopie* (German Society for Electron Microscopy), known by the abbreviation DGE and of which Ernst Ruska was the first president and von Borries its first secretary (Schimmel, 1996). In 1999, the 50th anniversary of the DGE was celebrated in Dortmund (Germany); I had the honor to be the president of the society at the time. On this occasion, Professor Lenz (Tübingen) published a brilliant article on the scientific activities of the congresses organized by the DGE during the first 50 years of its existence, documenting the scientific activities and progress in electron microscopy that took place in the divided, and later reunified, Germany (Lenz, 1999).

Prof. Brüche, on the other hand, left Zeiss, but remained in Mosbach, where in 1951 he founded the Arbeitsgemeinschaft für Elektronenoptik e.V. (AEO = Working Group on Electron Optics), an organization dedicated to teaching and advising scientists and technicians at university and in industry. From 1988 to 1998 the author of this article was president of this organization, which still exists today.

2) The other center in Berlin where electron microscopes were developed was the laboratory of Baron Manfred von Ardenne, set up in 1928 on his estate in Berlin-Lichterfelde. The von Ardennes belonged to a noble family originally from Hamburg. His grandfather Armand von Ardenne and his grandmother Elisabeth von Plotho divorced, which caused a great scandal throughout the country. The novelist Theodor Fontane knew Manfred von Ardenne's grandmother personally and this family history inspired him to write his famous novel Effi Briest (1896). The house of von Ardenne in Berlin, now known as Villa-Folke-Bernadotte, was – and still is – surrounded by a large park with room for additional buildings. Von Ardenne funded his research privately, as at a very young age he already had more than a hundred patents in the field of radio, telecommunications, and television, which yielded him invaluable profits.

Siemens hired von Ardenne in 1936 to investigate whether electron beams in scanning mode could correct the chromatic aberration of the lenses in the transmission electron microscope. Von Ardenne fulfilled the contract within two years by constructing the first scanning transmission electron microscope (STEM) in history. He also implemented it as a conventional scanning microscope, creating an electron beam of approx. 4 nm in diameter: a quite extraordinary achievement for the period (von Ardenne, 1938a). In 1937 he – curiously – patented the instrument in England (von Ardennne, 1938b). In 1941 the Prussian Academy of Sciences awarded him the Silver Leibnitz Medal for these discoveries, together with Ernst Ruska, von Borries, Brüche, Boersch and Mahl, who had also contributed very important work in the field of electron microscopy (Müller, 2009). Unfortunately, von Ardenne's instruments and devices were destroyed in an air raid in 1944.

After the war, von Ardenne accepted an offer from the Soviet Union; here he made a very important contribution to the nuclear program but did not continue his research in the field of electron microscopy. The scanning electron microscope was forgotten for a few years, until research was resumed in the 1940s, then however outside Germany.

SIEMENS PATENTS AND CONFLICTS OVER PRIORITY IN THE INVENTION OF THE ELECTRON MICROSCOPE

Max Knoll, Ernst Ruska and Bodo von Borries had worked at the TU Berlin since 1928, but, at that time, Siemens had had no industrial or commercial interest in electron microscopy; it even seems that there were agreements to transfer commercial space in this field to AEG - something

of dubious legality. However, the head of Siemens' electronics department, the physicist Reinhold Rüdenberg, was apparently well informed of all activities related to electron microscopy in other laboratories in Berlin.

At that time, members of universities very rarely patented ideas or even new constructions. So, when, on June 4, 1931, in Prof. Carl Cranz's famous colloquium in Berlin, Max Knoll presented Ruska's research and the experimental demonstration of Busch's theories, those innovations were not protected by patents (Gorkom et al., 2018a). The intellectual satisfaction of the scientist was considered paramount to possible industrial and commercial interests.

Rüdenberg's assistant, Max Steenbeck, is known to have attended the conference and subsequently informed his superior (Gorkom et al., 2018a). Rüdenberg was a highly skilled physicist and understood the significance of Knoll's presentation. In the same year, 1931, he inconspicuously patented the idea of the electron microscope

Siemens allowed ideas to be patented even if they were in a very early stage and without any experimental verification or prototype device supporting them. In the following months Rüdenberg filed up to 8 more patents on the electron microscope, a term or name he did not invent. Obviously, since Rüdenberg was an employee, Rüdenberg's patents belonged to Siemens.

From 1937 onwards, laws were enacted in Germany to prevent Jews from gaining access to public administration jobs, universities, and large corporations. Rüdenberg, who was Jewish, was able to emigrate to the United States with the generous help of Siemens.

When Knoll and Ruska first published their work on the electron microscope, Rüdenberg had already filed his patent, which is why he claimed recognition as the inventor of the device. Rüdenberg brought the dispute before the US courts. A Boston court ruled against him. During the hearing of the case, Judge Charles Wyzanski of the District Court in Boston (Massachusetts) asked Rüdenberg if he could present any kind of apparatus or construction in support of his theory or idea, to which Rüdenberg replied with a laconic: "No". In his ruling, Judge Wyzanski even took Rüdenberg's family circumstances into account, which gave another dimension to the problem. Here is part of the verdict:

"What happened in 1930 and 1931 can now be told. In the fall of 1930 Professor Rudenberg's younger son was stricken with infantile paralysis. The father, deeply concerned about that illness, learned that doctors knew that it was carried by a virus of poliomyelitis, but a virus so small that it could not be studied under the lens of any existing microscope or any microscope which would depend for its operation upon light waves. The trough between light waves was so much larger than the virus that observations were impossible. Thereupon Professor Rudenberg set himself to devise a new type of microscope. First, he thought of an X-ray microscope. This proved impractical. And finally, he hit upon a microscope based upon electronic principles. (...). In accordance with what was his usual practice, Professor Rudenberg merely drew certain sketches of this invention. He did not embody it in any material apparatus".

Nevertheless, the issue was pursued further; Rüdenberg's descendants continued to sue and make their claims public years after his death.

As already mentioned, Siemens was not interested in the new invention until, among other reasons, it received support from the famous Professor Siebeck. Siemens then unilaterally annulled the previous agreements with AEG, opening a new front of conflict between the two companies.

DEVELOPMENT AND CONSTRUCTION OF ELECTRON MICROSCOPES OUTSIDE GERMANY

It was probably Brussels where the work of Ruska and Knoll first found immediate resonance. A Hungarian scientist, Ladislaus Laszlo Marton, who was a member of a research group led by Professor Henriot of the Faculty of Science at the Free University of Brussels (ULB), was encouraged by his superior to build an electron microscope like Ruska's. Construction was completed by the end of 1932 and the results published in

Flemish in 1933. The following year he built a second, improved, microscope. Marton contacted biologists at his university who provided him with plant samples (*Intermediate Drosera*) from which he obtained images with the electron microscope, which was a world premiere. In addition, he introduced for the first time the fixation of a biological sample for electron microscopy with osmic acid, publishing it in a short note in the journal Nature (Marton, 1934). In the fall of 1934, he built a third microscope (Marton, 1934, 1935, Van Dyck, 1996).

Marton corresponded with Ruska and even visited him in Berlin in late June 1934, on his return journey from a visit to his homeland, Hungary, with his wife Claire. During this visit, he also met Professor Brüche (AEG) and Max Knoll (*Fernsehen* AG) and showed the three of them his images of biological objects, which was a source of surprise and admiration (Gorkom et al., 2018). With the publication of in Physical Review (1934), Marton became known in American scientific circles, demonstrating, for the first time, the possibility of examining biological specimens with an electron microscope.

Significant changes were taking place in neighbouring Germany in those years, which is why Marton decided to emigrate to the United States.

The development of electron microscopy received a major boost in the mid-1930s in the United States when Radio Corporation of America (RCA) decided to develop the instrument and make it a commercially-viable product. In 1938 Vladimir Zworykin, head of RCA's electronic research, hired Marton, who built the RCA Model A, an extremely costly device and difficult to operate. Zworykin could not convince Marton to modify and simplify the microscope.

Zworykin then brought in physics students from the University of Toronto who had built a microscope in the course of a doctoral dissertation (Watson, 1993). In 1935 Eli F. Burton was the director of the Physics Department at the University of Toronto. He became interested in electron optics, probably influenced in this by his friend W.H. Kohl, an emigrated German physicist. Under Burton's leadership, the undergraduates James Hiller and Albert Probus built the first TEM in North America in 1938, equipping it with electromagnetic lenses. The device they built at RCA, called "B", was far superior to model "A" and became the workhorse of the pioneers in the field of electron microscopy in the USA, especially in biological applications.

As, during World War II, scientists on both sides of the Atlantic were completely isolated from each other, electron microscopy in the USA evolved with different characteristics to those in Europe. One such aspect is related to biological and medical research.

The RCA company employed a fellow of the National Research Council (NRC), Thomas Anderson, who established many of the methods for sample preparation (mostly biological) and image interpretation. He maintained close relationships with the University of Pennsylvania and the Institute of the Rockefeller Foundation. It was precisely in the latter that renowned researchers in the field of biology worked, such as Albert Claude, George Palade, Christian de Duve, Keith Porter, among many others. They recognised the exceptional potential of the new technique. In view of these activities, the Rockefeller Foundation strongly supported RCA in the ongoing development and construction of electron microscopes (Rasmussen, 1997).

The problem of preserving samples, especially biological ones, which at the time was only partially resolved in Germany, remained a matter of central importance, especially in the United States (von Borries, 1949; Pease, 1960). On the one hand, there was an urgent need to obtain exquisite preservation of the biological samples, and on the other hand, to cut them as thinly as possible so that the electrons could pass through them, allowing the formation of an interpretable image.

During World War II and well into the 1950s, considerable progress was made in the United States in terms of preparation techniques, which led to fundamental discoveries in cell biology; the basis of what we know today as molecular biology (see attached Table 1).

Table 1. Fundamental discoveries in cell biology.

Decade	Discoveries and biomedical applications	Investigators
1930	Invention and construction of the first TEM First STEM/SEM First images of bacteria and virus (TEM)	Ruska and Knoll von Ardenne Helmut Ruska
1940	First images of whole cells (uncut) TEM Treatise on electron microscopy (*Übermikroskopie*)	Porter, Claude and Fuhrman von Borries
1950	Inner membrane of mitochondria (TEM) Endoplasmic reticulum (TEM) First images of chemical synapses (TEM) Golgi apparatus (TEM) Lysosome (cell fractionation and TEM) Muscle sliding filament theory	Palade Palade and Palay Palade and Palay Dalton and Felix de Duve Huxley
1960	First description of the centrosome (TEM) Animal chromosomes (TEM) First immunohistochemical labelling with ferritin (TEM) Low temperature preparation of biological specimens (TEM) New scanning electron microscopes (SEM)	Bernard and de Harven Ris Singer and Schick Fernández-Morán Oatley and his group at the Cambridge University (UK)
1970	SEM wide application of in cytology, embryology, neuroanatomy, etc.	Revel, Boyde, Meller, Mestres, and others
1980--	Cryo-electron microscopy Cryo-electron tomography	Dubochet, Studer and others Baumeister, Briggs, and others

TEM: Transmission Electron Microscope, STEM: Scanning Transmission Electron Microscope, SEM: Scanning Electron Microscope.

In those years, interest in electron microscopy also emerged strongly in other countries, such as England, France, the Netherlands, Sweden, Hungary, the former Czechoslovakia, Japan (Gorkom et al. 2018a, 2018b), and Switzerland (Günter, 1990). Unfortunately, this topic is beyond the scope of this article.

Before the course of the war turned against Germany, Siemens promoted the use of the electron microscope among researchers and users, following similar business strategies to those of the RCA in the United States. But, as already mentioned, scientific communication was very restricted, so that developments in Germany on the one hand, and in the allied countries, United States and England on the other, took place independently of each other. In fact, from the very beginning, the concepts developed along completely different lines: in Berlin research was based on the cathode ray tube technology and Hans Busch's lenses theory while the American and English physicists' work took a different direction. After de Broglie had formulated his corpuscular-wave theory and it had been confirmed by American and English scientists in 1927, they recognized the possibility of developing some kind of electronic lens. Although they approached the challenge from a different angle, they, in the end, reached the same conclusions as Hans Busch four years previously. The "North Atlantic" connection, as it were, explains the reason for the widespread belief that the design of the electron microscope began with de Broglie, when in fact this was not so.

THE SCANNING ELECTRON MICROSCOPE

The scanning electron microscope works on a different principle from that of the transmission one. With the scanning electron microscope, the

electron beam's impact on the sample induces the emission of secondary electrons, retro-dispersed electrons and X-rays, among other signals, which can be captured and processed into images using specific detectors. For example, secondary electrons originate very close to the surface of the sample, producing images of the object with topographical and 3D information.

Max Knoll published a paper in 1935 in which he described how an electron beam could be used to obtain an image of the surface of electronic components (Knoll was researching in the field of television). This first device does not qualify as a microscope, as it was not equipped with lenses. However, Knoll developed the idea of obtaining images of a surface point-by-point (magnetic deflection of the electron beam = scanning), which were then combined to a single image. Years later, Siemens commissioned von Ardenne to build the first "Raster-Elektronenmikroskop" (scanning electron microscope), but the seminal idea for such an instrument was obviously Knoll's.

At the end of the war, this line of research was not continued in Germany, but in the USA the opposite happened. In the early 1940s, Zworykin, working at the RCA laboratories, built a scanning electron microscope based on the principles of Knoll's device, but with the addition of lenses and a scanning unit, such as those used in television. Zworykin's device had shortcomings, for example in terms of the vacuum system, and RCA decided not to continue with the project. The idea of a scanning microscope was discredited, and the scientific community was very sceptical that a useful instrument could ever be built.

In the late 1940s, in spite of the prevailing skepticism among scientists, Sir Charles Oatley (Fig. 8), of the Engineering Laboratories at Cambridge University, considered it worthwhile to undertake a further attempt at constructing a fully-functioning scanning electron microscope (McMullan, 1995). Many technical components developed in Oatley's laboratory during the years that followed (new lenses, new vacuum systems, other electron sources, new detectors for each of the signals emitted by the samples, etc.) have enabled the construction of a scanning microscope accepted by the scientific

Fig. 8.- Sir Charles Oatley (1904-1996) (Source: Wikipedia).

community. Oatley went to great lengths to convince microscope manufacturers and, in 1962 the Cambridge Instruments Company built the famous "Stereoscan" (Fig. 9), based on the prototypes designed by Oatley and his co-workers (Stewart and Snelling, 1965).

The first Cambridge device (1964) was sent to the United States and was delivered to the company Dupont. The two instruments of the following year remained in England (North Wales and Leeds Universities) and a third went to the *Institut für Medizinische Physik* (Medical Physic) of the University of Münster-NRW (Germany), led by Professor Gerhard Pfefferkorn (Fig. 10). He had been von Ardenne's assistant in younger years and had just experienced the birth of the scanning microscope in Berlin (McMullan, 1995). The fact that one of the first Cambridge microscopes was delivered to Pfefferkorn's institute can be interpreted as a gesture of recognition of both the person and the research work done years earlier in Berlin, which had been continued post-war in Münster (Westphalia) together with Professor Ludwig Reimer (Reimer and Pfefferkorn, 1977).

The new instrument had an extraordinary impact not only on the materials sciences, but also on biology and medicine. Anatomists, embryologists, cytologists, etc. were stunned to see the images that could be obtained with the different signals. The two decades of the 70's and

80's can be considered as the golden age of scanning microscopy in the field of bio-medicine, especially in the United States, where, accompanied by specialized conferences and symposia, most of the world-wide activity in this field was concentrated. Since 1968, annual symposia have been held by Dr. Om Johari, a scientist at IITRI (Illinois Institute of Technology and Research Institute, Chicago), who has published a series of annual volumes entitled "Scanning Electron Microscopy". Similar symposia were organized in Germany and Austria by Prof. Pfefferkorn as chairman of the group EDO (Elektronenmikroskopische Direktabbildung und Analyse von Oberflächen = Electron microscopic direct imaging and analysis of surfaces) of the DGE. The scientific contributions presented were published in the series "*Beiträge zur Direktabbildung von Oberflächen* (BEDO)" (1968-69 till 1996).

Concurrent to these advances, specimen preparation techniques also progressed considerably. This was of fundamental importance, particularly in the fields of biology and medicine (Mestres and Stumpf, 1978; Meller, 1981).

Fig. 10.- Professor G. Pfefferkorn, Director of the Institute of Medical Physics at the University of Münster NRW (Source: private photo).

At one point the relevance of scanning electron microscopy seemed to be diminishing. However, two innovations changed the situation. The first was the invention of the environmental scanning

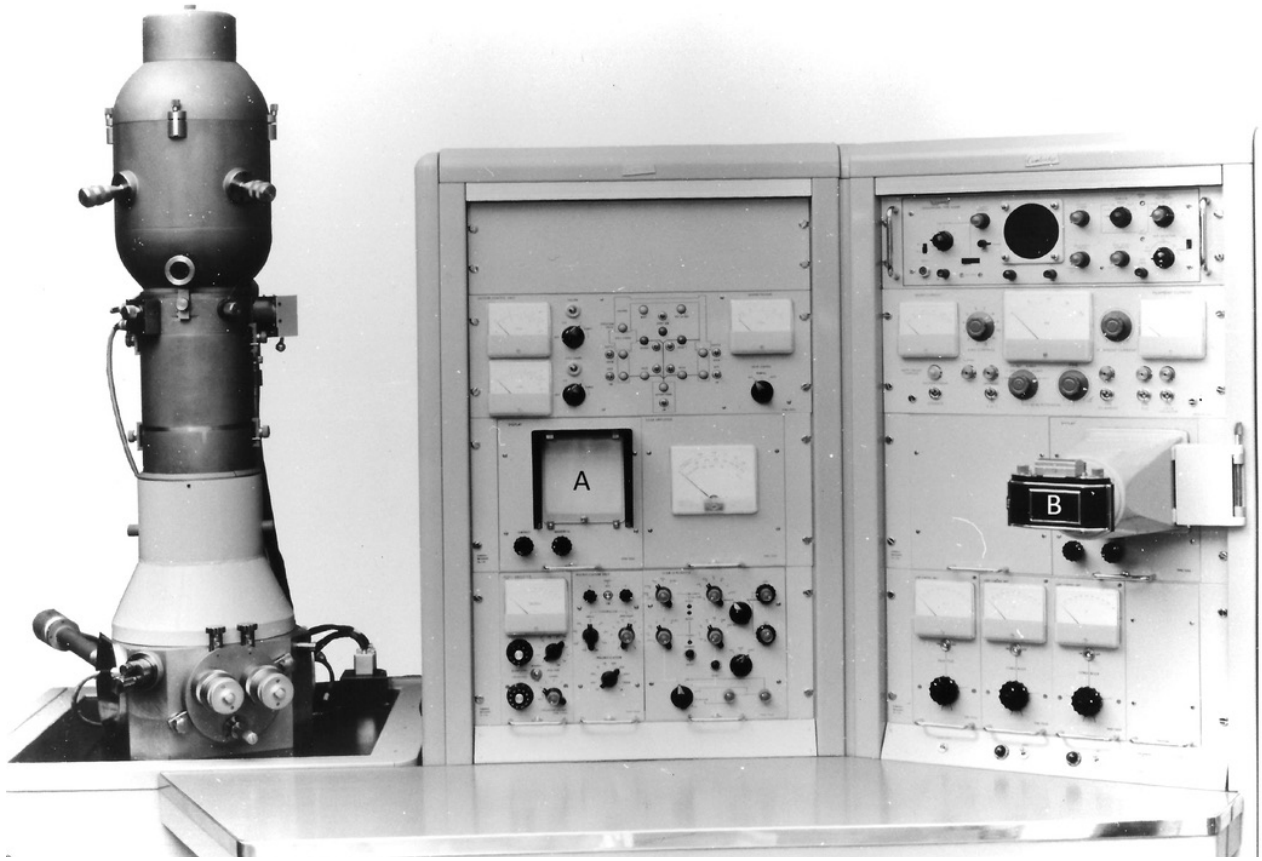

Fig. 9.- "Stereoscan MK1" scanning electron microscope from Cambridge Instruments. A: Screen, B: Camera (Source: Wikimedia Commons archive)

electron microscope, known as the ESEM (environmental scanning electron microscope) (Danilatos, 1988, Mestres et al., 2011), and the second is known as the SEM block-face (Denk and Horstmann, 2004).

Among many other applications, ESEM permits the examination of hydrated samples as well as samples that do not conduct electricity.

Block-face microscopy mainly uses the back-scattered electron (BSE) signal to obtain images of the surface of the block where the tissues are embedded. After each cut, the surface of the block - not the section - is photographed. High resolution 3D reconstructions can then be obtained by combining the images (Kubota et al., 2018). In addition, in the case of biopsies and clinical samples, not only are reconstructions possible but also large areas of the samples can be examined (Núñez-López et al., 2018).

THE ELECTRON MICROSCOPE AND THE NOBEL PRIZES

In 1974, Albert Claude, George E. Palade, and Christian de Duve were awarded the Nobel Prize in Physiology or Medicine for their development of cell fractionation and the application of electron microscopy to biology. It was the first major recognition that electron microscopy received.

Surprisingly enough, neither the invention of the device nor the achievements of those involved in its development had been acknowledged previously. As already implied above, the conflicts between the various research groups in Berlin and the instrument manufacturers were very noisy and unpleasant. It can be assumed that, in this environment of conflict, the Nobel Committee was unwilling – or even unable – to act.

The passage of time seems to have made things easier and in 1986 came a more favorable time: the Nobel Prize in Physics was awarded to Ernst Ruska (1/2) for the invention of the transmission electron microscope and to Gerd Binning (1 / 4) and Henrich Rohrer (1/4), for the discovery of the tunnel effect. The latter is of great importance in the so-called high-resolution microscopy in which the tunnel and atomic force microscopes find wide application. The Swedish Academy of Sciences said the award was given to Ruska: "for his fundamental work in electron optics, and for the design of the first electron microscope" (1986).

Many are of the opinion that other scientists such as Bodo von Borries, Martin Freundlich and even Helmut Ruska deserved recognition for their important contribution to the development of electron microscopy. They were indeed deeply involved in the process but, unfortunately, the evaluation of scientific merits is a difficult task which can leave individuals bereft of their

Fig. 11.- Humberto Fernández Morán (https://www.biografiasyvidas.com/biografia/f/fernandez_moran.htm)

rightful acknowledgement. In this sense it is worth remembering Newton's phrase: "If I have seen further, it is by standing on the shoulders of giants" (Newton, 1675, quoted by Gelderblom, 2020).

More recently, the electron microscopy has been recognized by the Royal Swedish Academy of Sciences. The Nobel Prizes Committee awarded the 2017 Nobel Prize in Chemistry to Jacques Dubochet, Joachim Frank and Richard Henderson, the main pioneers of Cryo-Electron Microscopy (Brzezinski, 2017).

The term "Cryo" refers to the conservation of biological samples using cold. In the early 1950's, it was clear that chemical fixation, the

most widely used method, caused artifacts, with the result that cells fixed with chemical agents did not exactly match living cells. For this reason, and parallel to improvements in chemical fixation techniques, there has been intense research on cryo-techniques since the early 1950s. Humberto Fernández-Morán, who was born in Venezuela 1924 and died in Sweden in 1999 (Fig. 11), was probably the first to propose the freezing of cells at low temperatures, thus avoiding artifacts produced by chemical fixation, leaving the cellular and molecular structures immobilized by the cold in their last moment of vitality (Fernandez-Morán, 1960, 1972; Padrón, 2001). Since then, this type of preparation has come a long way, as has the capability of electron microscopes to examine frozen sections. This is the technological frame in which the methods of cryo electron microscopy (cryo-EM) (Dubochet, 1988 and others) and cryo-electron tomography (cryo-ET) have been developed to the current level of perfection (Baumeister, 2016, 2021; Briggs, 2013 and others).

ACKNOWLEDGEMENTS

The author acknowledges the generous support received of Dr. Hans Gelderblom (RKI, Berlin) and Mrs. Ann Soether for linguistic revision of the text. I would like to express my fond memories of all who have accompanied me in electron microscopy particularly in my laboratories at Ruhr University in Bochum and at the University of Saarland in Homburg.

REFERENCES

BÄUERLAIN FJB, BAUMEISTER W (2021) Towards visual proteomics at high resolution: *J Mol Biol*, 433: 167187.

BECK M, BAUMEISTER W (2016) Cryo-electron tomography: can it reveal the molecular sociology of cells in atomic detail? *Trends Cell Biol,* 26: 825-837.

BRZEZINSKI P (2017) The development of cryo-electron microscopy. Scientific background on the Nobel Prize in Chemistry 2017. The Royal Swedish Academy of Sciences (www.kva.se).

BRIGGS JAG (2013) Structural biology in situ—the potential of subtomogram averaging. *Curr Opin Struct Biol,* 23(2): 261-267.

BUSCH H (1912) Eine einfache Ableitung der vollständigen Theorie des Oszillographen. *Physikalische Zeitschrift*, 13: 615-623. Verlag S. Hirzel, Leipzig.

BUSCH H (1926) Berechnung der Bahn von Kathodenstrahlen im axialsymmetrischen elektromagnetischen Felde. *Annalen der Physik*, 81(25): 974-993.

BUSCH H (1927) Über die Wirkungsweise der Konzentrierungsspule bei der Braunschen Rohre. *Arch Elektrotech*, 18: 583-594.

DANILATOS GD (1988) Foundations of environmental scanning electron microscopy. *Avd Electron Electron Phys*, 71: 109-250.

DAVISSON C, GERMER LH (1927) The scattering of electrons by a single crystal of nickel. *Nature*, 119: 558-560.

DE BROGLIE L (1924) XXXV. A tentative theory of light quanta, The London, Edinburgh, and Dublin Philosophical Magazine and Journal of Science, 47: 278, 446-458, doi: 10.1080/14786442408634378.

DENK W, HORSTMANN H (2004) The serial block-face scanning electron microscopy to reconstruct three-dimensional tissue nanostructure. *PLoS Biol*, 2(11): e 329.

DUBOCHET J, ADRIAN M, CHANG J-J, HOMO J-C, LEPAULT J, MCDOWALL AW, SCHULTZ P (1988) Cryo-electron microscopy of vitrified specimens. *Q Rev Biophys,* 21: 129-228.

ELECTRON (1910) In: Encyclopedia Britannica. 11th edition. Volume 9. London, pp 237.

FERNANDEZ-MORAN H (1960) Low-temperature preparation techniques for electron microscopy of biological specimens based on rapid freezing with liquid helium II. *Ann NY Acad Sci*, 85: 689-713.

FERNANDEZ-MORAN H (1972) Electron microscopy: A glimpse into the Future. *Ann NY Acad Sci*, 195: 376-389.

FREUNDLICH MM (1963) Origin of the electron microscope. *Science,* 142 (3589): 185-188.

GELDERBLOM H (2020) Bodo von Borries (1905-1956): Herforder und Friederizianer – ein Pionier der Elektronenmikroskopie. Historisches Jahrbuch für den Kreis Herford, Band 27, pp 154-199.

GELDERBLOM H, KRÜGER DH (2014) Helmut Ruska (1908-1973): His role in the evolution of electron microscopy in the life sciences, and specially in virology. *Adv Imag Electron Physics*, 182: 1-94.

GORKOM VAN J, with cooperation of Dirk van Delft and Ton van Helvoot (2018a) Chapter 1: The early electron microscopes: a critical study. *Avd Imaging Electron Physics*, 205: 2-137.

GORKOM VAN J, with cooperation of Dirk van Delft and Ton van Helvoot (2018b) Chapter 2: The early electron microscopes: incubation. *Avd Imag Electron Physics*, 208: 43-128.

GÜNTER JR (1990) History of Electron Microscopy in Switzerland. Birkhäuser Verlag. Basel, Boston Berlin.

HAWKES P (2004) Recent advances in electron optics and electron microscopy. Annales de la Fondation Louis de Broglie, Vol. 19, Hors Serie 1, pp 837-855.

KNOLL M (1935) Auflade Potential und sekundäre Emission elektronenbestrahlter Körper. *Z tech Phys*, 16: 467-475.

KUBOTA Y, SOHN J, KAWAGUCHI Y (2018) Large volume electron microscopy and neural microcircuit analysis. *Front Neural Circuits*, 12: 98.

LENZ F (1999) 50 Jahre Deutsche Gesellschaft für Elektronenmikroskopie. Nr. 18, pp 15-18 (http://dge-homepage.de/zeitschrift.html).

MARTIN A (1986) Cathode ray tubes for industrial and military applications. Adv Electronics Electron Physics, Volume 67, Academic Press, p 183.

MARTON L (1934) Electron microscopy of biological objects. *Nature*, 133: 911.

MARTON L (1934) Electron microscopy of biological objects. *Phys Rev*, 46: 527.

MARTON L (1935) La microscopie electronique des objects biologiques. *Bull Acad Royale de Belgique*. Part I, 20: 439 (1934), Part II, 21: 553 (1935), Part III, 21: 606.

MCMULLAN D (1995) Scanning Electron Microscopy (1928-1965). *Scanning*, 17(3): 175-185.

MELLER K (1981) General Methods in Scanning Electron Microscopy of the Nervous System. In: Heym Ch, Forssmann W-G (Eds). *Techniques in Neuroanatomical Research*. Springer Verlag. Chapter 4, pp 55-70.

MESTRES P, PÜTZ N, GARCIA GÓMEZ DE LAS HERAS S, GARCÍA POBLETE E, MORGUET A, LAUE M (2011) The surface topography of the choroid plexus. Environmental, low and high vacuum scanning electron microscopy. *Ann Anat*, 193(3): 197-204.

MESTRES P, STUMPF W (1978) Scanning Electron Microscope Studies of the Brain Ventricular Surfaces. Ed. Scanning Electron microscopy Inc. AMF O'Hare, Illinois (USA).

MÜLLER F (2009) The birth of a modern instrument and its development during World War II. Electron Microscopy in Germany 1930s to 1945. In: Maas A, Hooijmaijers H (Eds). *Scientific Research in World War II*. Routledge, New York / London, pp 121-146.

NEWTON I (1675) Letter from Sir Isaac Newton to Robert Hooke. Historical Society of Pennsylvania. *Retrieved 7 June 2018*.

NOBEL PRIZE IN PHYSICS (1986). https://www.nobelprize.org/prizes/physics/

NÚÑEZ-LÓPEZ T, DEL ROSARIO-HERNÁNDEZ G, LOPEZ-GOMEZ L, MESTRES-VENTURA P (2018) Specimen preparation for "block face" scanning electron microscopy (BFSEM). An energy dispersive X-Ray spectroscopy study. *Eur J Anat*, 22(6): 471-481.

PADRÓN R (2001) Contribution of Humberto Fernández-Morán to the electron microscopy. *Acta Microscópica*, 10(1): 54-56.

PEASE DC (1960) Histological Techniques for Electron Microscopy. Academic Press, New York and London.

REIMER L, PFEFFERKORN G (1977) Rasterelektronenmikroskopie. Springer Verlag, Berlin, Heidelberg, New York.

RUDENBERG VS. CLARK. 72 Federal Supplement 381 (1947) p. 384.

RÜDENBERG R (1953) German patent 889 660, Anordnung zur Beeinflussung des Verlaufs von Elektronenstrahlen durch elektrisch geladene Feldblenden, priority date of 31 May 1931, published 14 September 1953.

RUSKA E (1929) Über eine Berechnungsmethode des Kathodenstrahloszillographen auf Grund der experimentell gefundenen Abhängigkeit des Schreibfleckdurchmessers von der Stellung der Konzentrierspule. Studienarbeit TU-Berlin, Lehrstuhl für Hochspannungstechnik, presented on 10. 05.1929.

RUSKA E (1930) Untersuchung elektrostatischer Sammelvorrichtungen als Ersatz der magnetischen Konzentrierspulen bei Kathodenstrahl-Oszillographen. Coursework Start 18. Juli 1930 at the Hochspannunglaboratorium of the TU-Berlín (supervisor Prof. Dr. A. Matthias). Finished and presented on 23. 12. 1930; 90 pages.

RUSKA E (1933) "Über ein magnetisches Objektiv für das Elektronenmikroskop"._Doctoral thesis at the TU-Berlin (supervisor Prof. Dr. A. Matthias) 31. 08. 1933; Z. Phys. 89: 90-128 (1934).

RUSKA E (1987) Das Entstehen des Elektronenmikroskops und der Elektronenmikroskopie. *Phys Bl*, 43(7): 271-281 (Lecture Nobel Prize 1986; (https://www.nobelprize.org/prizes/physics/1986/ruska/lecture/).

RUSKA H, VON BORRIES B, RUSKA E (1940) Die Bedeutung der Übermikroskopie für die Virusforschung. *Arch ges Virusforsch*, 1: 155-169.

STEWART ADG, SNELLING MA (1965) A new scanning electron microscope. Proc. 3rd Europ. Conf. Electron Microsc. Prague, pp 55-56.

STRUTT RJ, BARON RAYLEIGH (1942) The Life of J.J. Thomson. Cambridge University Press, Cambridge.

VAN DYCK D (1996) Electron Microscopy in Belgium. *Adv Imaging Electron Physics*, 96: 67-78.

VON ARDENNE M (1937) Improvements in electron microscopes. British patent nº 511204, convention date (Germany) 18 Feb 1937.

VON ARDENNE M (1938a) Das Elektronen-Rastermikroskop. Theoretische Grundlagen. *Z Phys*, 109: 553-572.

VON ARDENNE M (1938b) Das Elektronen-Rastermikroskop. Praktische Ausführung. *Z tech Phys*, 19: 407-416.

VON BORRIES B (1949) Die Übermikroskopie. Einführung, Untersuchung ihre Grenzen und Abriss ihrer Ergebnisse. Verlag Dr. Werner Senger, Berlin.

VON BORRIES B, RUSKA E (1932) Magnetische Sammellinse kurzer Feldlänge. German patent specification Nr. 680284, Patent applied for on March 17, 1932, granted on August 3, 1939.

WATSON JHL (1993) In the beginning there were electrons. *Microscopy Today*, 1(1): 10-10.

Mixed reality model for learning and teaching in anatomy using peer assisted learning approach

Asif Ali[1,2], Najma Baseer[3], Zilli Huma[3], Yasar M. Yousafzai[1], Inayat Shah[3], Asad Zia[4], Mohammed Alorini[5], Nick Sethia[6]

[1] Institute of Pathology and Diagnostic Medicine, Khyber Medical University, Peshawar, Pakistan

[2] Gulf Medical University, Ajman, UAE.

[3] Institute Basic Medical Sciences, Khyber Medical University, Peshawar, Pakistan

[4] Public Health Reference Laboratory, Khyber Medical University, Peshawar, Pakistan

[5] Department of Basic Medical Sciences, Unaizah College of Medicine and Medical Sciences, Qassim University, Unaizah, Kingdom of Saudi Arabia

[6] Chief Executive Officer, MCORPUS SPRL Belgium

SUMMARY

The objective of this study was to evaluate the effectiveness of mixed reality models in anatomy teaching and learning at Kirkpatrick's level I, using Peer Assisted Learning approach. This study was based on a single group, post-test study design and was carried out at three affiliated medical schools of Khyber Medical University, Peshawar, over four months. A total of 97 first- and second-year medical students from three medical schools were enrolled. All students received a basic introduction to the use of Hololens (Microsoft), the mixed-reality simulator-based course on the anatomy of the heart and liver via peer-assisted learning (PAL) method. Student satisfaction was evaluated at Kirkpatrick Level I of program evaluation using a validated and structured PAL questionnaire.

Most students agreed or strongly agreed to the effectiveness of questions (mean ± SD 4.3±0.2, percentage 86±4.4%). There was no difference between the satisfaction scores of male and female students (p=0.34), whereas a slight difference was seen between 2nd- and 1st-year students' satisfaction scores (88% versus 85%, p=0.03). There was also a statistically significant difference of perceptions between different medical schools' students' scores (p=.000). Students appear to be satisfied with the use of the mixed reality model for learning anatomy. A randomized trial to directly compare the satisfaction levels between traditional methods and mixed-reality model may be conducted and the effects of mixed-reality models on learning should be assessed.

Key words: Anatomy – Kirkpatrick model – Mixed-reality – Peer-assisted learning

INTRODUCTION

Anatomy has long been considered a cornerstone of not only the basic medical sciences but

Corresponding author:
Dr. Najma Baseer. Associate Professor Anatomy, Institute of Basic Medical Sciences, Khyber Medical University, Peshawar, Pakistan. Phone: +92915892873. E-mail: drnajma.ibms@kmu.edu.pk

Submitted: June 21, 2022. **Accepted:** September 8, 2022

https://doi.org/10.52083/TRAD3516

also for the surgical and allied specialties (McLachlan and Patten, 2006; Losco et al., 2017). The implications of anatomical education are manifold; therefore, the lack of anatomical knowledge may result in serious clinical complications due to its significant association to clinical practice (Losco et al., 2017). Thus, strong anatomy knowledge underpins good clinical practice (Collins, 2008; Losco et al., 2017). Anatomy teaching in undergraduate medical schools has traditionally relied upon didactic teaching, cadaver dissection, tutorials, plastic models, and 2-dimensional photographs (McLachlan and Patten, 2006). The complexity of the human body requires powerful tools to know the relationship of organs (Ali and Evans, 2013; Birbara et al., 2020; Shazad et al., 2021). Many alternative tools and approaches such as dissection versus prosection and the use of radiographic material instead of human specimens are being questioned for their effectiveness in anatomy education (McLachlan and Patten, 2006; Lochner et al., 2016).

The popularity of anatomy e-learning tools is on the rise, with the traditional methods being side-lined (Singh and Kharb, 2013). This rise may be attributed to increasing interest of the students in the electronic learning tools (Van Nuland and Rogers, 2016; Losco et al., 2017). Nowadays, more emphasis is given to the applied sciences, as a result of which less time is allocated to basic sciences education including anatomy in a medical curriculum (Vasan, 2003). This change calls for those teaching tools that are more informative, appealing, and less time-consuming, such as computer-assisted learning tools (Collins, 2008). Similarly, simulation tools and imaging techniques such as radiography and computed-assisted teaching methods have also been used (Sugand et al., 2010; Griksaitis et al., 2012; Knobe et al., 2012). Lately, a mixture of advanced 3-dimensional digitalized models and virtual reality is emerging as a novel substitute to conventional anatomy teaching. These models merge the real world with the virtual one, thus connecting the two in the best possible authentic way (Dutta, 2016; Vasilevski and Birt, 2020; Young et al., 2020). One such form of virtual reality is the mixed reality that combines the real world with virtual reality in 3-D models, and is visualized on hologram using specialized lenses (Dutta, 2016). Mixed reality encompasses a continuum of virtuality, ranging from augmented reality to a completely virtual environment (Milgram and Kishino, 1994; Farshid et al., 2018).

With these advancements, it is critical to determine their impact on educational standards, as the cognitive effort required during the e-learning process may differ significantly from the one needed using the conventional tools (Dutta, 2016). The efficacy of any anatomy teaching tool can be gauged by assessing the extent to which the recall and retention of knowledge are acquired (Losco et al., 2017). For such assessments, Hammick et al. (2010) recommended the program evaluation tools such as Kirkpatrick's levels to gauge their degree of effectiveness hierarchically (Kirkpatrick, 1998; Rajeev , 2009; Losco et al., 2017). Hence, it would be interesting to evaluate the immediate impact of the mixed reality model on anatomy education.

A recent paradigm shift has been observed in educational philosophies, with more emphasis being given to student-centered learning rather than a teacher-centered approach (Harve and Yip, 2013; Lochner et al., 2016). Furthermore, novel learning approaches such as Problem Peer Assisted Learning (PAL) have also been introduced into medical didactic practices (Yiou and Goodenough, 2006; Ali and Evans, 2013). PAL involves students assisting the learning and teaching process with a small group of peers (Fuchs et al., 1997; Nnodim, 1997). It not only develops pedagogic literacy among the students but has proven to be more satisfying and rewarding (Ali and Evans, 2013). Although PAL has long been practiced informally (Dent and Harden, 2009), its inclusion into formal medical education is still anticipated (Ali and Evans, 2013). Since the question of which teaching and learning method fits best to the novel tools remains to be answered, this study aims at determining the immediate impact of this novel mixed reality model on anatomy education using the PAL approach. This evaluation will correspond to level I (satisfaction) of the Kirkpatrick model of program evaluation, with an anticipation that in future such tools

may be utilized in acquiring as well as enhancing the knowledge, understanding, and application of anatomical knowledge to common medical problems.

METHODS

It was a multi-center, post-test design study conducted at Khyber Medical University (KMU), Peshawar, Pakistan, as a joint venture with MCORPUS-SPRL (Belgium). The study was conducted in collaboration with three affiliated medical schools of KMU (hereafter: medical school A, B, and C). Ethical approval was taken from the ethics board of KMU's and the medical colleges involved.

For sampling, all 150 1st and 2nd year students belonging to three medical schools were invited to participate in the study, of which 64.66% (97/150) students participated. First- and second-year MBBS students from medical school A and B (n=44/50 and 34/50, respectively) and only first-year MBBS students from medical school C (n=19/25) participated in the study. Of the 44 students from medical school A, 20 were from the first year while 24 were from the second year. While out of 34 students of medical school B, 17 each from first and second year took part in the study. The second-year students of medical school C were on the preparatory leave for final term exam. These students had undergone the same medical entrance exam before getting enrolled into their respective medical schools. Written consent was acquired from the participating students. Students were ensured that their inclusion or exclusion in this study would have no bearing on their academic score.

Before the start of the study, all the students and trainers were provided with personal logins into the mixed-reality platforms. The study comprised of two phases. Phase I and Phase II. Each of these phases further consisted of three sessions.

Phase I: During the **first session of phase 1**, five KMU faculty members (facilitators) were introduced to the mixed-reality gadget "Hololens" MCORPUS-SPRL (Brussels Area Belgium) and its components**.** Hololens is an advanced mixed-reality gear used to contextually visualize the augmented human body organs in 360° view for more advanced learning. The Hololens was operated by the hand and finger movements controlled in a navigation-pane-like fashion. With Hololens goggles the human body organs could be visualized in a three-dimensional interface, which could then be displayed on screen for other learners, thus allowing a shared learning experience. **Second session** was a hands-on session, in which the facilitators individually manipulated Hololens and its software to get familiarized with 3D anatomy of liver, heart, brain, and eye. During the **third session**, the facilitators developed comprehensive lesson plans for the anatomy of heart and liver. This was meant to avoid inconsistencies in the PAL sessions that were to be carried out in small groups of medical students.

Phase II: In second phase, the facilitators had hands-on interactive sessions with the students. These sessions were carried out separately within the setting of the respective medical schools. All the participating students had already learnt the gross anatomy of the liver and heart during a single problem-based learning (PBL) session of two hours for each topic. This phase also consisted of three sessions. During the **first session**, the facilitators introduced Hololens and the fundamentals of mixed reality to the participants. This was followed by a practical session on Hololens, where students were briefed about its handling. The goggles were worn by facilitator and the 3D-anatomy of eye and brain were visually displayed on the projector screen. The **second session** was carried out in a peer-assisted learning setting. Although these students were already aware of the small group teaching methods such as PBL, PAL was relatively new to them. Students were briefed about the norms of the PAL and were split randomly into 4-5 groups of 5-6 students each. Students belonging to year 1 and 2 were grouped separately. For year one, the PAL sessions were based on heart anatomy while for year 2 the students learned liver anatomy. The first student from each group was taught by the facilitator. Later, each student was asked to wear the Hololens gear, operate it independently, guide and discuss the topic with their subsequent group

member as peer tutor in a same way as they had learned from their preceding group member as peer tutee. So, basically, all the students had both experiences of being a tutor initially followed by a tutee later in the session. This peer tutor-tutee interaction was intended to provide step-by-step instructions to the tutee to learn anatomy using Hololens. The rest of the PAL sessions continued in such a fashion.

During the **third session**, each participant filled the PAL questionnaire to evaluate the effectiveness of the intervention using level 1 of the Kirkpatrick model and gauge the productivity of PAL approach. The PAL questionnaire was a five-point Likert scale questionnaire with a total of 28 items (Ali and Evans, 2013). The questionnaire was contextualized to inquire about the use of a mixed reality model for learning anatomy using PAL approach. It was divided into four parts with four questions as a peer group, six as peer tutor and tutee each, while 12 questions were on evaluation and feedback on PAL sessions. Students were not only unaware of this division; they had not taken part in any similar type of evaluation or responded to a questionnaire of similar sort in the past. The questionnaire also contained two open-ended questions inquiring about the strengths and the weaknesses of the whole learning experience. The students responded to all the questions mentioned in the PAL questionnaire.

Data analysis

The data analysis was carried out using Microsoft Excel version 16.16.27 and IBMS SPSS version 22 (USA). The questionnaire data were analyzed for each item using frequency distribution. The variables which were presented in terms of mean values proportions and percentages included (1) the number of students in total and from each medical school, (2) the gender-wise distribution and (3) the satisfaction level of students as per the PAL questionnaire. These stats also contained mean values with standard deviation. The pair-wise comparison between the responses of three medical schools was carried out using analysis of variance (ANOVA) followed by Post-Hoc Tukey test. Moreover, a heat-mapping concept was used to analyze the responses of the participants. On a heat map, red indicated the lowest while the green shade indicated the highest level of responses. The item-wise analysis of participants' responses was carried out using an approach suggested by Zamalia (2009). On a scale of 1 to 5, a score of 2.5 or less was defined as a negative response while a score of 3.5 and above was defined as a positive response. Scores between 2.5 and 3.5 were considered neutral. For item-wise analysis, since the data was continuous in nature therefore, mean values with standard deviations were used. Since the degree of agreement on the items of Likert questionnaire was categorized into five categories ranging from totally disagree to totally agree, median and IQR values were computed. $p \leq 0.05$ was considered significant.

RESULTS

In this study, 97 medical students participated of which 64.9% were first-year medical students while 35.1% belonged to second year. The great majority of students were female (71.1%).

Frequency statistics of satisfaction level (Kirkpatrick Level 1)

The perceptions of the students regarding the mixed-reality model and PAL sessions were evaluated at four different states, i.e., as a peer group, as a tutor, as a tutee, and a final section of evaluation and feedback. The mean percentage satisfaction level for all the responses was 86.42%±4.46. Overall, the highest level of agreement was observed for item D11 (I enjoyed the session), with all the participants rating it in agreement (N=97, 100%). It was followed by item B6 (Every undergraduate student should be given the opportunity to use this model for learning) and item D5 (Topics selected were relevant to medical education) (97.94% for each item). Interestingly, item A4 (It is more informative than the traditional lecture system) earned the lowest proportion of affirmative response with 70% of the participants rating in its favor, while 21.65% gave neutral response (Fig. 1).

The item-wise analysis of participants' responses was also carried out. For all the items, a positive trend was observed with the great majority of them getting rated above 3.5. The most

positive trend was observed for item D11 and B6, with mean values of 4.65±0.48 and 4.65±0.56 respectively. The lowest positive trend was witnessed for the item which asked whether this session improved students' analytical abilities through discussion in peers (4.04±0.75). This was followed by the item "It is more informative than traditional lecture system" (4.05±1.03) (Table 1).

As a **peer group**, the participants rated item A2 (I found it an interactive way of learning and understanding) the highest (4.49±0.56) while item A4 (It is more informative than traditional lecture system) was rated the lowest (4.05±1.03). Item B6 (Every undergraduate student should be given the opportunity to use this model for learning) received the most positive rating not only as a **peer tutor**, while item B3 (It increased my presentation skills) received the least positive rating (4.08±0.89). As a **tutee** item C1 (I was clear about the topic we discussed) got the maximum grading (4.42±0.64), while item C4 (My analytical ability was improved through discussion in peers) had the lowest (4.04±0.75). Among the items belonging to **the evaluation and feedback section**, item D11 (I enjoyed the session) was rated highest (4.65±0.48), while item D3 (I learned more than I would have done on a conventional course) showed the least positive trend (4.08±0.94). Collectively, the students showed the lowest degree of satisfaction as tutees (83.78%, mean 4.19±0.39) while their experience as Peer group received the highest degree of satisfaction (87%) and a most positive rating (4.35 ±0.45) (Table 1).

Degree of agreement on the items of Likert questionnaire

For frequency distribution across all medical colleges, the data were pooled together and heat maps were generated (Fig. 2). Red indicates the lowest and green indicate the highest level of responses. Very few participants responded in the "strongly disagree" and "disagree" category (Fig.

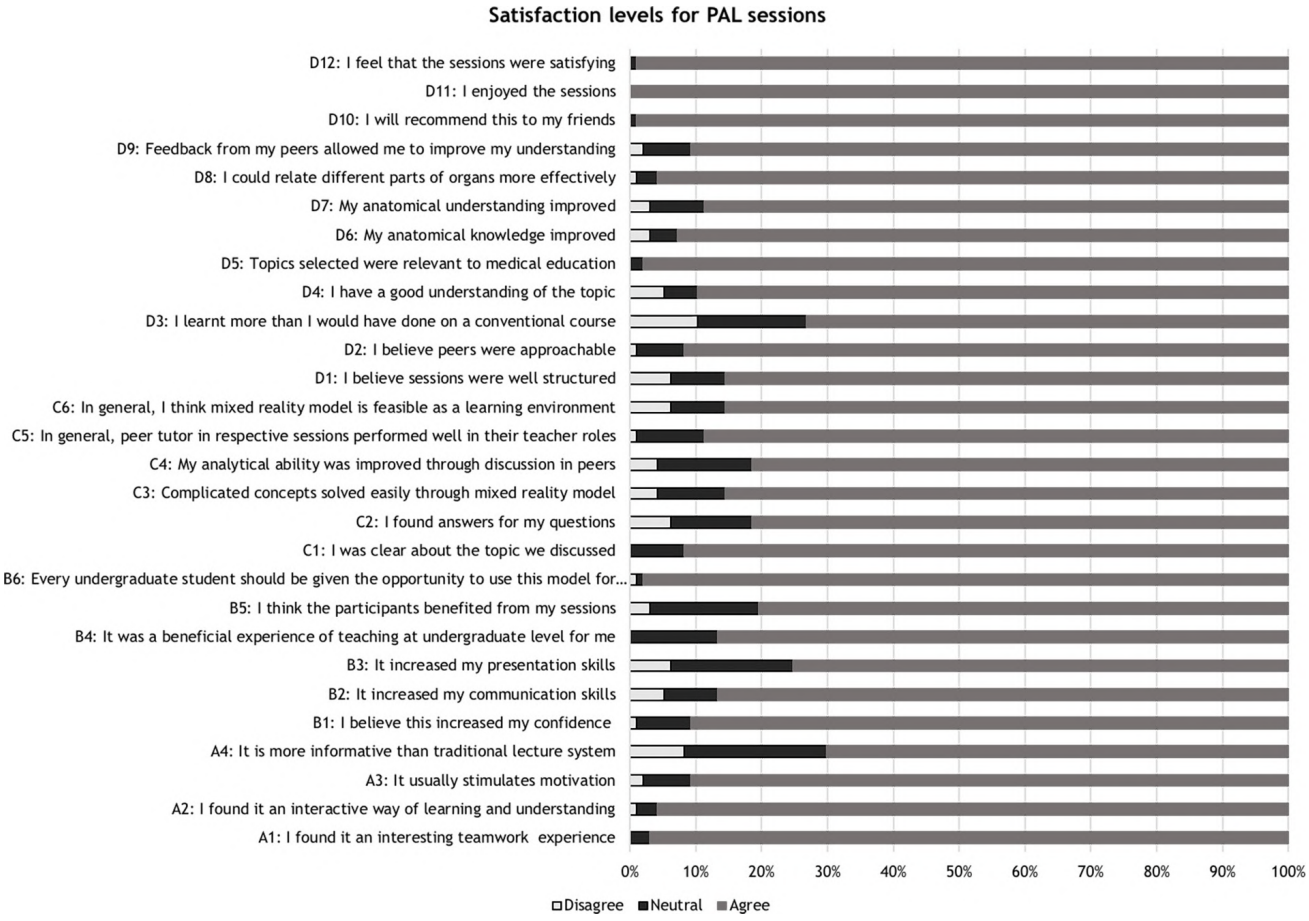

Fig. 1.- Satisfaction level of all the participants in terms of PAL questionnaire.

Table 1. Item wise analysis of PAL questionnaire showing the mean values ± standard deviation for each item.

	As a peer Group	**Mean** ± SD
A1	I found it an interesting teamwork experience	4.49±0.56
A2	I found it an interactive way of learning and understanding	4.56±0.69
A3	It usually stimulates motivation	4.31±0.74
A4	It is more informative than traditional lecture system	4.05±1.03
	As a peer tutor	
B1	I believe this increased my confidence	4.36±0.64
B2	It increased my communication skills	4.24±0.82
B3	It increased my presentation skills	4.08±0.89
B4	It was a beneficial experience of teaching at undergraduate level for me	4.34±0.69
B5	I think the participants benefited from my sessions	4.16±0.81
B6	Every undergraduate student should be given the opportunity to use this model for learning	4.65±0.56
	As a Tutee	
C1	I was clear about the topic we discussed	4.42±0.64
C2	I found answers for my questions	4.10±0.85
C3	Complicated concepts solved easily through mixed reality model	4.16±0.85
C4	My analytical ability was improved through discussion in peers	4.04±0.75
C5	In general, peer tutor in respective sessions performed well in their teacher roles	4.24±0.65
C6	In general, I think mixed reality model is feasible as a learning environment	4.16±0.82
	Evaluation and feedback	
D1	I believe sessions were well structured	4.21±0.82
D2	I believe peers were approachable	4.32±0.64
D3	I learnt more than I would have done on a conventional course	4.08±0.94
D4	I have a good understanding of the topic	4.13±0.78
D5	Topics selected were relevant to medical education	4.52±0.62
D6	My anatomical knowledge improved	4.45±0.66
D7	My anatomical understanding improved	4.34±0.72
D8	I could relate different parts of organs more effectively	4.51±0.63
D9	Feedback from my peers allowed me to improve my understanding	4.32±0.65
D10	I will recommend this to my friends	4.56±0.63
D11	I enjoyed the sessions	4.65±0.48
D12	I feel that the sessions were satisfying	4.53±0.52

2). The median ± IQR of responses to questions in the "strongly agree" category for first-year students in Medical school A was 11±4.75 while for second-year it was 12±3.75. Similarly, for first and second-year students of medical school B, the median and IQR were computed to be 11.50±5.5 and 7.2±3, respectively. Since only first-year students of medical school C took part in the project, their median and IQR values were 5.50±4.75. Interestingly, the median responses were consistently zero across all medical schools for the strongly disagree category. When the data from all medical schools were pooled together, the median and IQR values for the "strongly agree" category were found to be 42±18 while for the "agree" category it was 43±11.

The PAL questionnaire also contained two open-ended questions inquiring about the strength and a suggestion regarding this novel experience. Although the responses were not assessed qualitatively, some of the students made interesting comments and recommendations.

Question	Strongly Disagree	Disagree	Not Sure	Agree	Strongly Agree
A1	0	0	3	41	53
A2	0	1	3	33	60
A3	1	1	7	46	42
A4	2	6	21	26	42
B1	0	1	8	43	45
B2	0	5	8	43	41
B3	0	6	18	39	38
B4	0	0	13	40	45
B5	0	3	16	46	32
B6	0	1	1	29	66
C1	0	0	8	40	49
C2	0	6	12	45	34
C3	2	2	10	47	36
C4	0	4	14	55	25
C5	0	1	10	47	39
C6	2	4	8	51	32
D1	0	6	8	48	35
D2	0	1	7	49	41
D3	0	10	16	38	35
D4	0	5	5	56	31
D5	0	0	2	35	61
D6	1	2	4	46	45
D7	0	2	8	40	46
D8	0	1	3	36	57
D9	0	2	7	48	40
D10	0	0	1	32	64
D11	0	0	0	34	63
D12	0	0	1	43	53

Fig. 2.- Heat-map of responses from all three medical schools, where shades in red indicate disagreement while those in orange are neutral responses.

In the strengths section, one of the students commented that he/she was able to appreciate those anatomical structures which were difficult to study through 2D. Another student stated that "*It improved our confidence level and increased our presentation skills*" while some students found it interesting and enjoyable. As far as the recommendations were concerned, one of the students suggested that "*Histological features should be included*", while the other stated that *"More labeling should be added".* One of the students found Goggles a bit heavy.

Relationship of gender and year of study with mixed reality satisfaction

The mean level of satisfaction for mixed reality model among males was 85.84% compared to 86.66% among females, with no significant difference between genders ($p=0.34$, independent sample t-test). However, the year of the study was significantly associated with satisfaction level, with second-year students showing significantly more satisfaction (88%) than first-year students (85%) (p=0.03).

Relationship of medical schools with mixed reality satisfaction

The level of satisfaction for the mixed reality model also differed significantly among the medical schools (p=0.000, ANOVA). Pairwise comparisons in post-hoc revealed that there was no statistically significant difference between medical school A and B (p=1.00). However, there was a statistically significant difference between medical schools A (87%) and C (80%) (p=0.000) and medical school B (88%) and C (80%) (p=0.000).

DISCUSSION

The 21st century has shown an explosive advancement in the medical field. Because of continual update and discovery of newer

treatments and diagnostic testing, there is an increased burden on the new generation doctors to constantly learn and enhance their skills (McLachlan and Patten, 2006). This has added an immense cognitive load on medical students to not only remember but also apply knowledge learned in their initial years of medical school later to their work place. This study of ours was an effort to evaluate whether innovative teaching and learning strategies can be of some assistance to the students facing the aforementioned challenges (Yousafzai et al., 2018). Interestingly, these approaches are not new, as the advanced techniques employed in other fields, such as simulators used by the aviation industry, are now being used to simulate real surgeries for doctors. Still, it is quite challenging to develop engaging learning environments that are user-friendly and support the learning requirements of professional students (Salem et al., 2020). Advances in simulation technology, however, have led to a paradigm shift where learners have reportedly enjoyed their learning through these gadgets. Similarly in our study, the high level of satisfaction seen indicates the acceptability of the tool for learning anatomy. Although some students rated the traditional lecture system better than the new innovative approach as novel strategies take a while to be accepted and implemented (Ali and Evans, 2013), a great majority of them (~70%) regarded the mixed reality mode of teaching as more informative than the traditional methods. This was supported by a study on the undergraduate pharmacy students (Salem et al., 2020). The novelty of the idea and the fun element of a gaming modality may be one of the reasons for the higher acceptance by the students (~86%) as the PAL questionnaire item "I enjoyed the session" received a 100% positive response. A review published in 2017, suggested computer-assisted learning (CAL) as a partial replacement of dissection to enhance student learning, though total replacement still requires more in-depth studies (Losco et al., 2017). Birbara et al. (2020) carried out a pilot study on anatomy students and their tutors by comparing their perceptions regarding the use of less and more immersive virtual reality methods. Although, the students found virtual-reality-based methods engaging, some experienced these methods mentally taxing. Conversely, in our study, 97% of the students regarded mixed reality as an interesting experience that every undergraduate student should undergo. A similar observation was made when the educational efficacy of the virtual-reality skull model was compared with that of cadaveric skulls and atlases, where participants found the VR model as efficient as the cadaveric skull and more effective than the 2D atlases (Chen et al., 2020).

Apart from a novel teaching tool, we also tested the effectiveness of PAL approach, which is regarded as an interactive student-centered learning method (Ali and Evans, 2013). PAL or even (near-) peer teaching programs have proven to enhance all three learning domains (Bulte et al., 2007; Secomb, 2008). PAL approach was used to inculcate not only a collaborative approach among students but we also wanted to determine whether the PAL would befit mixed reality model, which was evident as the students expressed maximum satisfaction as a peer group. A qualitative study carried out to assess the experience and motivation of the lab tutors showed similar results (Bugaj et al., 2019). The students displayed great passion and motivation as peer teachers owing to the likelihood of developing their skills and knowledge simultaneously.

Although a great majority of our study participants were female (71%), we did not see any gender predisposition (p=0.34). A similar observation was made on university students regarding the adoption of augmented reality (Cabero-Almenara et al., 2019). These results were interesting in a way that they negated the ideology of the gender-based digital divide (Hohlfeld et al., 2013), and advocated the concept of gender equality in technology literacy (Felnhofer et al., 2012). Interestingly, second-year students showed a greater degree of satisfaction as compared to first-year students (p=0.03). This may be attributed either to their higher cognitive ability as compared to their junior peers, or more self-confidence owing to the greater amount of time spent within the same academic environment. Since this was a preliminary study, we further intend to undertake a randomized

trial to directly compare the satisfaction levels between traditional methods and mixed-reality model and to assess the in-depth effects of mixed-reality models on learning, skills, and behavior of the medical students.

CONCLUSION

In the present study, the students appear satisfied with the mixed reality model using the PAL approach as learning and teaching tool. This not only complements the existing body of knowledge by signifying the importance of new innovations in anatomy education, but also shows higher satisfaction and acceptance by the students towards the novel methods. Such new innovative methods would need time to develop and therefore should undergo continuous evaluation by using higher levels of the Kirkpatrick model of program evaluation.

ACKNOWLEDGEMENTS

The authors wish thank to MCORPUS SPRL Belgium for providing the Hololens gears. We are grateful to Prof. Dr. Ijaz Khattak, Prof. Muhammad Noor Wazir, Prof. Dr. Tariq Mufti, Dr. Iqbal Wahid, Dr. Naheed Mahsood, and Dr. Mahrukh Ikram Shah for their continuous support throughout this project.

REFERENCES

ALI A, EVANS P (2013) Multi-resource peer assisted learning in postgraduate setting : a pilot study. *J Coll Physicians Surg Pak*, 23(4): 251-256.

BIRBARA NS, SAMMUT C, PATHER N (2020) Virtual reality in anatomy: A pilot study evaluating different delivery modalities. *Anat Sci Educ,* 13(4): 445-457.

BUGAJ TJ, BLOHM M, SCHMID C, KOEHL N, HUBER J, HUHN D, HERZOG W, KRAUTTER M, NIKENDEI C (2019) Peer-assisted learning (PAL): skills lab tutors' experiences and motivation. *BMC Med Educ,* 19(1): 1-14.

BULTE C, BETTS A, GAMER K, DUMING S (2007) Student teaching: views of student near-peer teachers and learners. *Med teach,* 29(6): 583-590.

CABERO-ALMENARA J, FEMANDEZ-BATANERO JM, BARROSO-OSUNA J (2019) Adoption of augmented reality technology by university students. *Heliyon,* 5(5): p. e01597.

CHEN S, ZHU J, CHENG C, PAN Z, LIU L, DU J, SHEN X, SHEN Z, ZHU H, LIU J, YANG H, MA C, PAN H (2020) Can virtual reality improve traditional anatomy education programmes? A mixed-methods study on the use of a 3D skull model. *BMC Med Educ,* 20(1): 1-10.

COLLINS JP (2008) Modern approaches to teaching and learning anatomy. *Br Med J,* 337.

DENT JA, HARDEN RM (2009) A practical guide for medical teachers. Third. Elsevier Churchill Livingstone.

DUTTA K (2016) Augmented Reality for E-Learning', in Aachen, Germany: Seminar Augmented Reality, Mobile & Wearable.

FARSHID M, PASCHEN J, ERIKSSON T, KIETZMANN J (2018) Go boldly!: Explore augmented reality (AR), virtual reality (VR), and mixed reality (MR) for business. *Bus Horiz,* 61(5): 657-663.

FELNHOFER A, KOTHGASSNER OD, BEUTL L, HLAVACS H, KRYSPIN-EXNER I, (2012) Is virtual reality made for men only? Exploring gender differences in the sense of presenc. Proceedings of the International Society on presence research, 103-112.

FUCHS D, FUCHS LS, MATHES G, SIMMONS DC (1997) Peer-assisted learning strategies: Making classrooms more responsive to diversity. *Am Educ Res J,* 34(1): 174-206.

GSAITIS MJ, SAWDON MA, FINN GM (2012) Ultrasound and cadaveric prosections as methods for teaching cardiac anatomy: A comparative study. *Anat Sci Educ,* 5(1): 20-26.

HAMMICK M, DORNAN T, STEINERT Y (2010) Conducting a best evidence systematic review. Part 1: From idea to data coding. BEME Guide No. 13. *Med Teach,* 32(1): 3-15.

HARVE KS, YIP GW (2013) The Use of E-Learning in contingency planning for Anatomy Education. *Anatom Physiol,* 3(1): 4172.

HOHLFELD TN, RITZHAUPT AD, BARRON AE (2013) Are gender differences in perceived and demonstrated technology literacy significant? It depends on the model. *Educ Technol Res Dev,* 61(4): 639-663.

KIRKPATRICK DL (1998) Evaluating Training Programs: The Four Levels. Falletta SV (edit). Berrett-Koehler Publishers, San Francisco, CA.

KNOBE M, CAROW JB, RUESSELER M, LEU B, SIMON M, BECKERS S, GHASSEMI A, SONMEZ T, PAPE HC (2012) Arthroscopy or ultrasound in undergraduate anatomy education: a randomized cross-over controlled trial. *BMC Med Educ,* 12(1): 85.

LOCHNER L, WIESER H, WALDBOTH S, MISCHO-KELLING M (2016) Combining traditional anatomy lectures with e-learning activities : how do students perceive their learning experience. *Int J Med Educ,* 7: 69-74.

LOSCO CD, GRANT WD, ARMSON A, MEYER A, WALKER B, LOSCO CD, GRANT W, ARMSON A, MEYER AJ (2017) Effective methods of teaching and learning in anatomy as a basic science : A BEME systematic review : BEME guide no. 44. *Med Teach,* 39(3): 234-243.

MAHMUD Z (2009) Identification of learners' attitudes toward statistics based on classification of discriminant function. *WSEAS Trans Inf Sci Appl,* 6(8): 1259-1268.

MCLACHLAN JC, PATTEN D (2006) Anatomy teaching: Ghosts of the past, present and future. *Med Educ,* 40(3): 243-253.

MILGRAM P, KISHINO F (1994) A taxonomy of mixed reality visual displays. *IEICE Trans Inf Syst,* 77(12): 1-15.

NNODIM JO (1997) A controlled trial of peer-teaching in practical gross anatomy. *Clin Anat,* 10(2): 112-117.

RAJEEV P, MADAN MS, JAYARAJAN K (2009) Revisiting Kirkpatrick's model-an evaluation of an academic training course. *Curr Sci,* 96(2): 272-276.

SALEM S, COOPER J, SCHNEIDER J, CROFT H, MUNR I (2020) Student acceptance of using augmented reality applications for learning in pharmacy: a pilot study. *Pharm,* 8(3): 122.

SECOMB J (2008) A systematic review of peer teaching and learning in clinical education. *J Clin Nurs,*17(6): 703-716.

SHAHZAD M, ALI A, SHAH I, AYAZ K, JAMIL B, SALAM A (2021) An observational study to assess satisfaction with multi-resource peer assisted learning among postgraduate research students. *Rawal Med J,* 46(3): 690-694.

SINGH V, KHARB P (2013) A paradigm shift from teaching to learning gross anatomy: Meta-analysis of implications for instructional methods. *J Anat Soc India,* 62(1): 84-89.

SUGAND K, ABRAHAMS P, KHURANA A (2010) The anatomy of anatomy: a review for its modernization. *Anat Sci Educ,* 3(2): 83-93.

VAN NULAND SE, ROGERS KA (2016) The anatomy of E-Learning tools: Does software usability influence learning outcomes. *Anat Sci Educ,* 9(4): 378-390.

VASAN NS (2003) Management and delivery of the gross anatomy curriculum with decreased course time: the importance of structured teaching activities. *Med Educ,* 37(5): 479-480.

VASILEVSKI N, BIRT J (2020) Analysing construction student experiences of mobile mixed reality enhanced learning in virtual and augmented reality environments. *Res Learn Technol,* 28(1063519): 1-23.

YIOU R, GOODENOUGH D (2006) Applying problem-based learning to the teaching of anatomy: the example of Harvard Medical School. *Surg Radiol Anat,* 28(2): 189-194.

YOUNG GW, STEHLE S, WALSH B, TIRI E (2020) Exploring virtual reality in the higher education classroom: Using VR to build knowledge and understanding. *J Univers Comput Sci,* 26(8): 904-928.

YOUSAFZAI Y, BASEER N, FATIMA S, ALI A, SHAH I (2018) Changes in learning style preferences of postgraduates after entering a new learning environment. *J Ayub Med Coll Abbottabad*, 30(3): 386-391.

European Journal of Anatomy